

MODULAR PROGRAM DEVELOPMENT
FOR VEHICLE CRASH SIMULATION, VOL. 2,
PLASTIC HINGE EXPERIMENTS

Prepared by:

W. J. Anderson, College of Engineering
I. K. McIvor, College of Engineering
B. S. Kimball, College of Engineering

Of:

The University of Michigan
Ann Arbor, Michigan 48109

For:

National Highway Traffic Safety Administration
U.S. Department of Transportation
Trans Point Building
2100 Second Street S.W.
Washington, D.C. 20590

Under:

Contract No. DOT-HS-4-00855

November 30, 1976

Technical Report Documentation Page

1. Report No.		2. Government Accession No.		3. Recipient's Catalog No.	
4. Title and Subtitle Modular Program Development for Vehicle Crash Simulation; Vol. 2. Plastic Hinge Experiments.				5. Report Date November 30, 1976	
				6. Performing Organization Code	
7. Author(s) W. J. Anderson I. K. McIvor B. S. Kimball				8. Performing Organization Report No. UM-HSRI-76-4-2	
9. Performing Organization Name and Address University of Michigan, College of Engineering, Ann Arbor, Michigan 48109				10. Work Unit No. (TRAIS)	
				11. Contract or Grant No. DOT-HS-4-00855	
12. Sponsoring Agency Name and Address National Highway Traffic Safety Admini- stration; Department of Transportation, Washington, D.C. 20590				13. Type of Report and Period Covered Final Report 3/74 to 11/76	
				14. Sponsoring Agency Code	
15. Supplementary Notes					
16. Abstract A large number of full-scale automotive box and channel beams have been tested to observe the formation of plastic hinges. The purpose of the testing was to establish a data bank for moment-angle and force-extension properties of various hinges as a basis for computer simulation of crushing of automobile frames. Some 88 tests were made for extensional, bending and torsional hinges in thin walled tubes. Results are in the form of figures of the load-deflection relationship and tables of parameters used to model the hinge behavior through analytical expressions. In addition, several buckling and combined-load tests were carried out to verify the theory and the computer code which were developed concurrently.					
17. Key Words			18. Distribution Statement		
19. Security Classif. (of this report)		20. Security Classif. (of this page)		21. No. of Pages	22. Price

Form DOT F 1700.7 (8-72)

Reproduction of completed page authorized

TABLE OF CONTENTS

	Page
1. INTRODUCTION	1
2. HINGE TESTS	
2.1 Extensional Hinge	4
2.2 Bending Hinge	7
2.3 Torsional Hinge	12
3. INTERACTION TESTS	
3.1 Buckling	16
3.2 Combined Loading	21
3.3 Comparison of Predicted and Experimental Results	24
4. DETERMINATION OF HINGE PARAMETERS AND SCALING LAWS	
4.1 Introduction	37
4.2 Determination of Hinge Parameters	38
4.3 Scaling Laws	41
5. CONCLUSIONS	44
6. APPENDIX A: TABLES	45
7. APPENDIX B: HINGE DATA BANK	54

TABLES

	Page
1. Code for Approximate Wall Thickness	47
2. Run Log and Hinge Parameters	48-51
3. Scale Factors for Scaling Laws	52
4. Geometric Parameters for Scaling Laws	53

FIGURES

	Page
1. Extensional hinge specimen.	5
2. Eccentric axial loading on extensional channel specimen.	5
3. Failure mode of box section in tension.	6
4. Four point bending fixture with small channel specimen installed, prior to test.	8
5. Bending fixture with moderate size box beam near end of test.	8
6. Bending hinge specimen.	7
7. Channel section after bending about strong axis. (First View).	10
8. Channel section after bending about strong axis. (Second View).	10
9. Channel section after bending about weak axis. Free edge in tension.	11
10. Square box section after bending test.	11
11. Torsional hinge in thin walled box beam.	14
12. Torsional hinge in thin walled channel beam.	14
13. Torsional hinge formation in a channel specimen.	13
14. Buckling Test.	16
15. Elastic deformation prior to hinge formation.	17
16. Load-deflection curve for a box beam in buckling.	18
17. Load-deflection relation for a channel column in buckling.	19
18. Load-deflection relation for a channel beam column in buckling.	20

FIGURES (continued)

	Page
19. Eccentric cantilever.	21
20. Dimensions of combined load fixture.	22
21. Orientation of hinge line for box beam under combined bending and torsion.	24
22. Load-displacement relation for a channel beam under combined loading.	25
23. Load-displacement relation for a box beam under combined loading.	26
24. Channel cross-section column in buckling. 5° offset. CB3010UM.	32
25. Channel cross-section column in buckling. CB4015TM.	33
26. Load-deflection for a box cross-section column in buckling. BB3020UM.	34
27. Combined loading test. CC3015RM.	35
28. Combined loading test. BC3020RM.	36

1. INTRODUCTION

This volume describes experiments on the formation of plastic hinges in thin-walled, full scale automotive box and channel beams. A major goal was to accumulate a data bank for moment-angle and force-extension properties of various hinges as a basis for computer simulation of crushing of automobile frames. Some 88 tests were made for extensional, bending and torsional hinges and the data bank is now available. In addition, buckling tests and combined loading tests were carried out to verify the theory and computer code which have concurrently been developed.

The hinges studied here are all localized, large deformation of thin-walled tubes. The hinge has a characteristic length of $2h$, where h is the larger cross-sectional dimension. One might call the mechanism involved "plastic crippling", although in some cases there is substantial elastic deformation of the cross-section before ultimate load occurs. The tests for extensional hinges play two roles. In the small deformation region, they provide uniaxial material properties: Young's modulus, yield strength and ultimate strength. At larger deformation, the extensional hinge formed in a manner similar to "necking down" of a conventional tensile test specimen, and this behavior, involving three-dimensional distortion of the tube is considered a hinge. The bending experiments were designed to produce a hinge by a pure moment applied about a principal axis

of the cross-section, with separate experiments for the "strong" and "weak" axes. Torsional hinges were produced by a pure couple, with a center of rotation at the specimen's geometric center.

Each thin-walled specimen was internally supported by a pair of close-fitting plugs. These internal plugs:

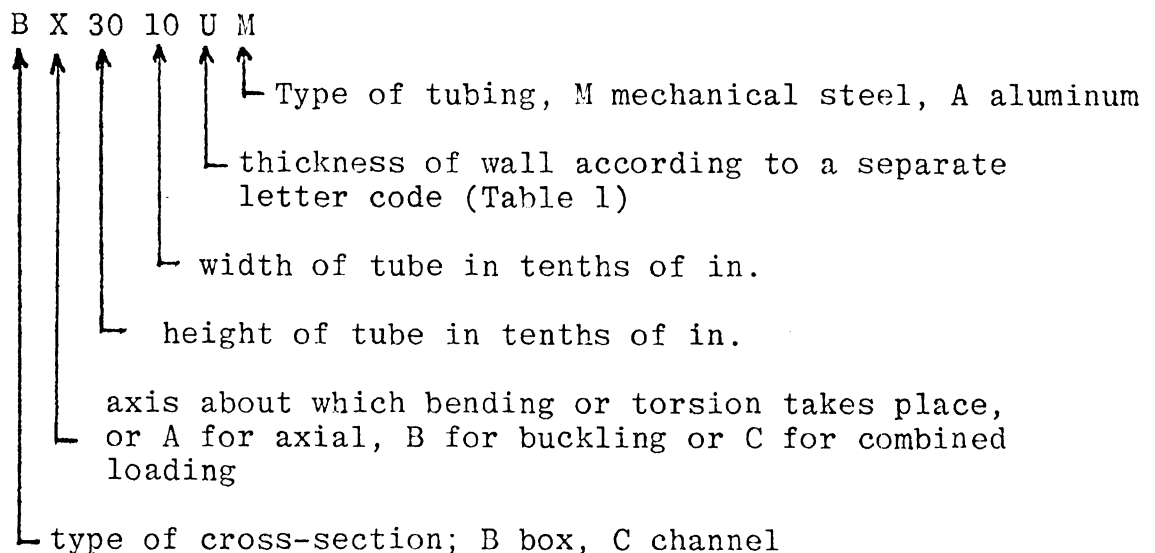
- 1) prevented collapse of the cross-section at the grips of the fixtures
- 2) confined the hinge to a local region
- 3) centered the hinge along the specimen length for ease of observation and to maintain symmetry for the bending tests.

At first, when short internal plugs were used, it was found that the hinge would not localize until late in the loading process after the entire length of the specimen had become plastic. This was due to a uniform stress field. Investigation of actual automobile accidents show many localized hinges and no uniform bending or twisting. Because of this, the concept of extending the internal plugs away from the grip region to locate the hinge was conceived. The plugs were placed to allow a free-standing thin-walled tube for a distance of $2-1/2h$ in the center of the specimen.

Each of the experiments was displacement-controlled to prevent collapse of the specimen during softening regions of loading. Softening occurred in a marked manner in the bending and torsion tests due to collapse of the tube cross-section.

A total of 88 hinge tests, 3 buckling tests, and 2 combined tests were carried out. Of the hinge tests, 22 were extensional, 42 were bending, and 24 were torsional. Of these same 88 hinge tests, 70 involved steel specimens and 18 involved aluminum. These were the only materials tested. The steel was automotive grade 1018 low-carbon steel. The aluminum was 6063, extruded, in a T52 condition. The extension tests gave steel ultimate strengths of approximately 61000 psi and aluminum ultimate strengths near 25,000 psi.

An 8-character title is given for each experiment according to the following scheme:



The axis system is independently defined so that the x axis is the major principal axis ($I_{xx} \geq I_{yy}$). This makes the distinction between height and width in the above code irrelevant; height is taken to be the larger of the two numbers except for the case of bending about the "weak" Y axis (retaining the physical meaning of height and width of the bending specimen as it is actually tested in the bending fixture.) The title of each experiment

is carried in all descriptions of the experiment and is automatically entered by the computer on each plot so that there can be no mixup of cases by human error.

Because of the large number of tests, it was important to automatically store, reduce and plot the data. The primary storage method was punched cards. Computer data reduction was done with a series of programs which terminated in tabular data and in Calcomp plots of moment-angle and force-displacements relations. All hinge data is presented in terms of moment (force) versus half hinge angle (half-displacement) because the half-angle (half-displacement) is the relevant quantity for an interior hinge in The University of Michigan computer simulation.

Each test was carried to displacements as large as practical. The bending hinge half angles typically exceeded 45°. Torsional tests were carried to 90°. Extensional tests were carried to fracture of the specimen. Buckling tests were continued until interference between specimen and machine occurred, and combined loading tests were carried to the maximum machine stroke.

1.1 EXTENSIONAL HINGE

Extensional hinge tests were done for steel and aluminum thin-walled beams in a Tinius Olsen 360,000 lb Universal Test Machine. The specimen dimensions are shown in Fig. 1, where the specimen length, unsupported section length and the gage length for the dial gage are all related to the greater cross-sectional dimension h .

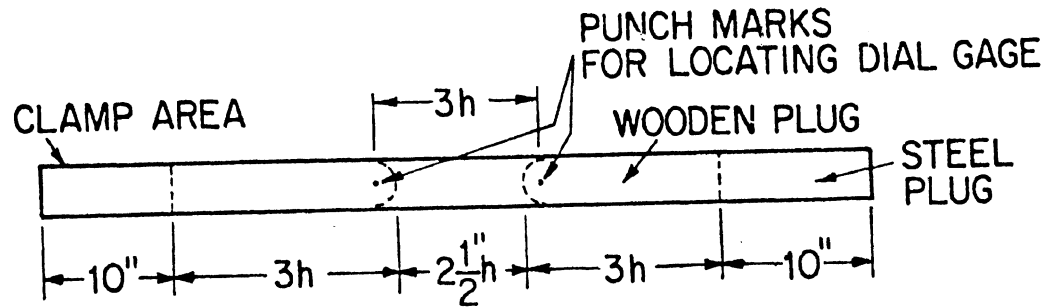


Fig. 1. Extensional hinge specimen.

The plugs used were at first designed to be entirely wood, but were changed to steel within the grip area. It was found that the wedging action of serrated grips in the test machine caused very large compressive stresses on the cross-section within the grips.

The instrumentation consisted of a dial gage mounted in a special fixture located by punch marks at the geometric centerline of the tube cross section in the unsupported area. Some extraneous elastic deformation was measured in the case of channel specimens because of the eccentric positioning of the load on the specimen (Fig. 2). This elastic effect was removed from the

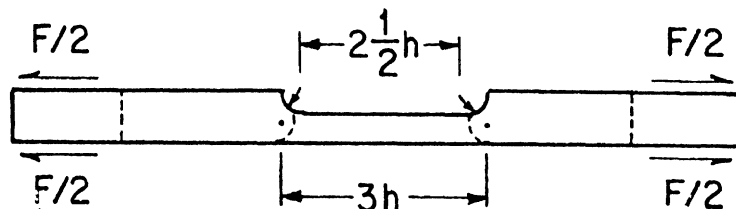


Fig. 2. Eccentric axial loading on extensional channel specimen.

experimental data by accounting for the distance between the axial load and the elastic axis, as well as the offset between dial gage position (on the geometric axis) and the elastic axis.

The tests proceeded generally as expected. The specimens first deformed elastically, followed by a plastic material deformation and then by a nonlinear collapse of the cross-section in a "necking" mode. This consisted typically of the cross-section becoming smaller, i.e. the walls moving inward toward the axis. Failure of the specimen was often a crack appearing on the welded face of the tube, in a v-shaped pattern. (Fig. 3). Before this fracture occurred, Luder's lines (slip lines) could be seen converging in an x shape at this point.

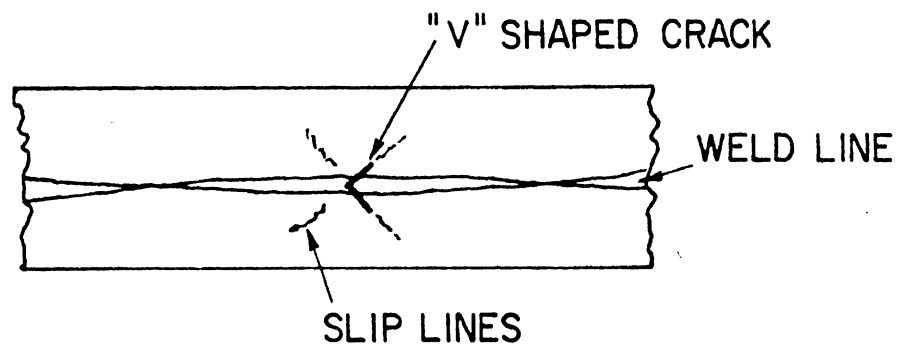


Fig. 3. Failure mode of box section in tension.

Results for all extensional hinge tests are given in Appendix B. In each case, the small strain region is first given in a separate figure in order to recover material properties and a figure for moderate strain follows.

1.2 BENDING HINGE

All of the bending tests were carried out in a specially made four-point loading fixture installed in a 120,000 lb capacity Tinius Olsen Universal Testing Machine, (Figures 4 & 5). Because of the weight of the fixture, it was placed in a hanging, rather than an upright configuration, i.e., this fixture is upside down from a smaller fixture used for 1" tubing used in 1974.

A total of 42 bending tests were carried out, including bending about both strong and weak principal axes. Each specimen tested was 6' long and used wooden internal plugs to support the cross-section at the point of load application and to localize the hinge in the center of the fixture to retain overall symmetry. In all cases, an unsupported section $2\frac{1}{2}h$ at the center of the span was maintained (Fig. 6).

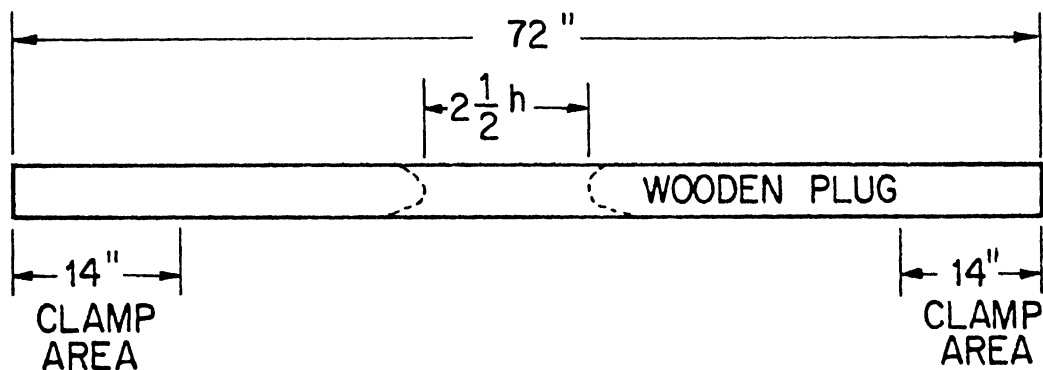


Fig. 6. Bending hinge specimen.

Two major problems had to be overcome in the course of the experiment. The first was the distortion of the entire fixture when bending of a channel about the strong axis was attempted. This particular test causes a large side force, due to the

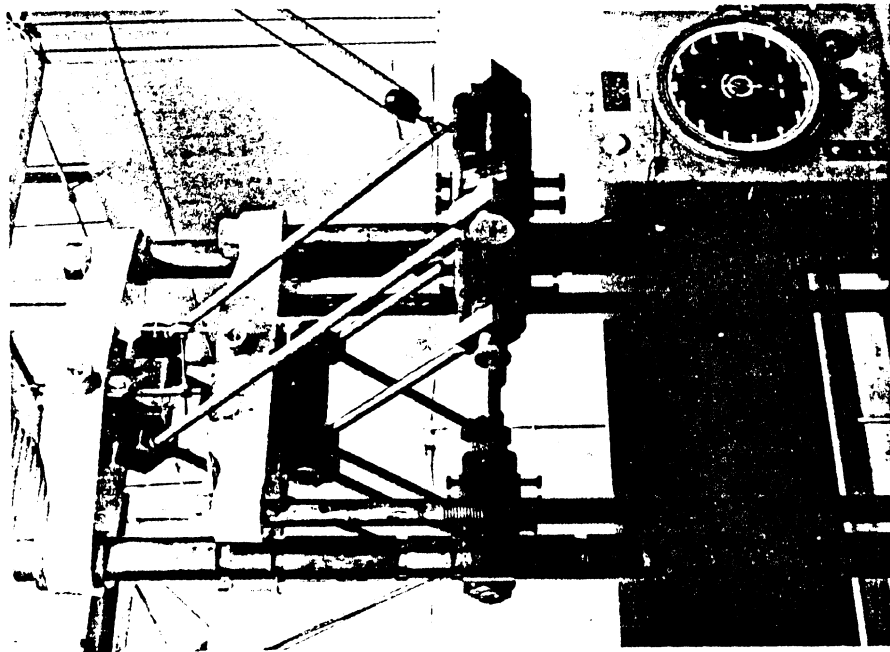


Fig. 4. Four point bending fixture with small channel specimen installed, prior to test.

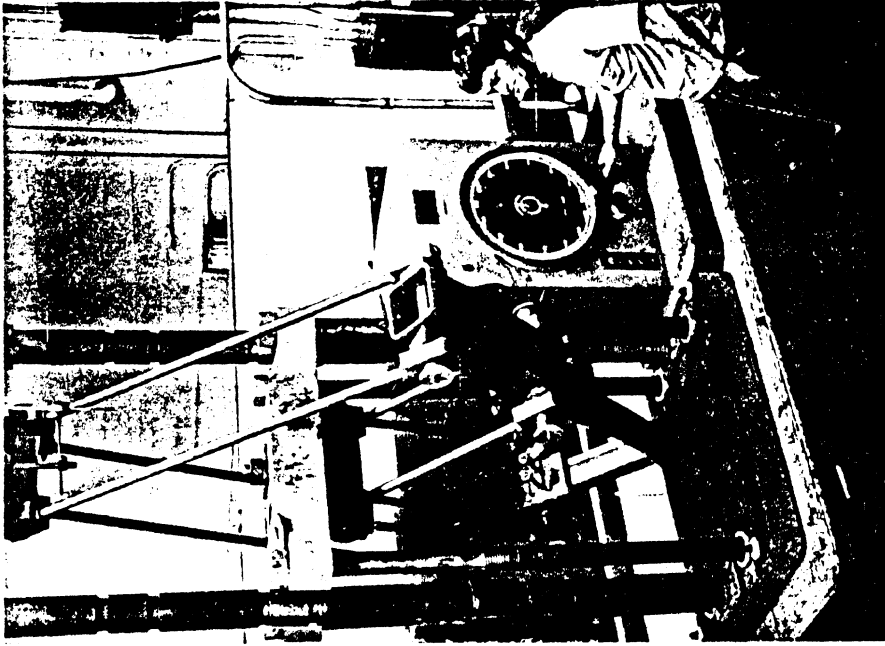


Fig. 5. Bending fixture with moderate size box beam near end of test.

unsymmetric nature of the hinge (Figures 7 & 8). The solution was to eliminate any slack in the system by tightening up fixture bearings and by installing specimens more perfectly; this procedure worked well enough to allow testing of the largest channels which could be installed. A second problem was development of a gravitational correction to the data. The weight of the fixtures provided a dead load on the specimen which was not negligible for the smaller specimens. After weighing and measuring all fixture members carefully, the computer program for reducing beam bending data was modified to include a gravitational correction. This was not a trivial piece of statics to work out; there are 10 correction terms that modify the moment obtained from the live load.

The weak axis bending tests for channel could have put the free edge of the cross-section in tension or in compression. To obtain a "cleaner" description of the problem and to be less sensitive to specimen imperfections (which affect crippling), it was decided to test with the free edge in tension, as in Fig. 9. An additional case was tested with the free edge in compression, and its characteristics were similar, but with more rapid collapse in the large deflection region.

Bending tests for the box sections were well behaved and exhibited the expected pattern of linear elastic behavior, followed by some material softening, and then by large-scale collapse of the cross-section and rapid softening. Fig. 10 shows a square box section after testing.

Results for all bending hinge tests are given in Appendix B. Tests were typically carried out to plastic half-angles near 45°.



Fig. 7. Channel section after bending about strong axis. (First view).

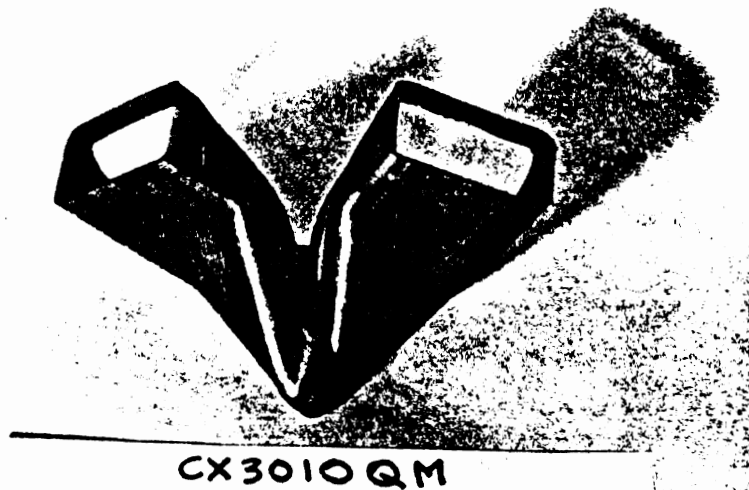
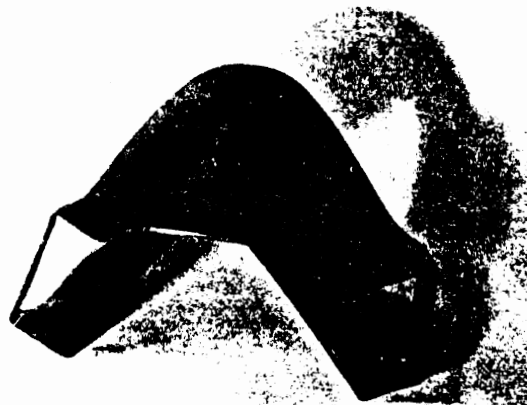


Fig. 8. Channel section after bending about strong axis. (Second view).



CY1540TM

Fig. 9. Channel section after bending about weak axis. Free edge in tension.



BX3030PM

Fig. 10. Square box section after bending test.

1.3 TORSIONAL HINGE

Torsional hinge tests were carried out in a 120,000 in. lb. capacity Riehle torsional test machine. Special fixtures were used to grip the ends of the beams to apply the force uniformly over the clamped ends. A total of 24 steel and aluminum specimens were tested. Each had dimensions identical to the extensional specimens, except that the plug inserts for torsion were entirely wood. The shearing motion did not crush the end section, therefore the steel insert was not required. Most tests were carried out to 180° total rotation, since it was little addition trouble to proceed beyond 90° once the test was underway. (It is realized that few automotive accidents will cause torsional hinges as large as 180°.)

An interesting fundamental problem which had to be resolved at the outset of channel torsional tests concerned the appropriate axis about which to twist the beam to very large rotations. At first, it was assumed that the elastic shear center would be used, and one specimen was so tested. Although this axis has a unique and useful meaning in the small deflection range, one test convinces the researcher that the center of twist is meaningless at very large rotations, and indeed causes extremely large shear forces--almost enough to throw the torsion machine off its pedestal! One concludes that the best axis to use for very large rotations, if one wishes to emphasize plastic, torsional effects, is the geometric center of the cross-section. If this is used, a full 180° rotation causes what one normally expects to see in a pure twisting situation. Furthermore,

ultimate torque about this axis is substantially lower than about the shear center or the centroidal (area "center of gravity") axis. Torsional effects are masked by extraneous shearing effects in the latter two cases.

Failure of the specimens was rather predictable. The box sections twist into a taffy-like mode as seen in Fig. 11. The hinge is rather local, often initiating near one internal plug, but not extending as far as the second plug. (If the hinge had been "captured" between the plugs, the hinge would have been considered constrained and the plug spacing of $2-1/2h$ would have been opened to allow a longer unsupported section.) The channel sections folded as in Fig. 12. This hinge did not have axial symmetry or skew symmetry, but rather was always eccentric. A first fold line was dominant in the process (Fig. 13) and was followed by two secondary fold lines.

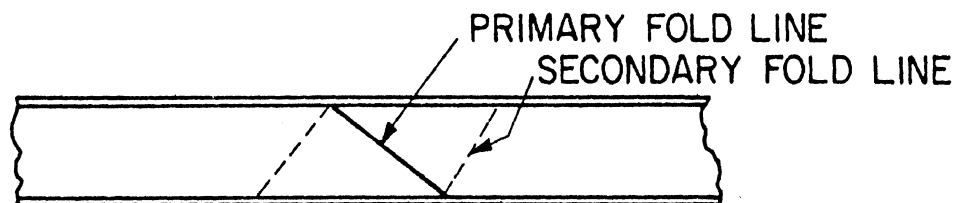
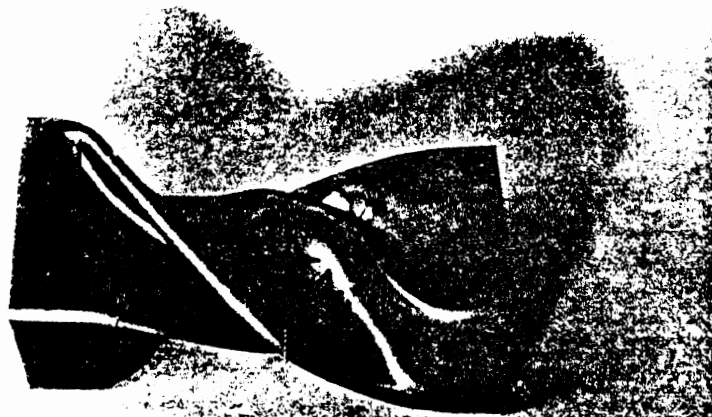


Fig. 13. Torsional hinge formation in a channel specimen.

Tests for several of the aluminum torsional specimens were terminated prematurely because of cracks at stress concentrations where the wall thickness had been machined to the proper amount.



BZ4030TM

Fig. 11. Torsional hinge in thin walled box beam.



CZ3015UM

Fig. 12. Torsional hinge in thin walled channel beam.

It is interesting that the aluminum was more brittle than the low carbon steel and was much more sensitive to cracking.

Results for the torsional tests are presented in Appendix B.

3. INTERACTION TESTS

3.1 BUCKLING TEST

In order to verify the simulation program, the case of buckling was studied. Buckling tests must be done on specimens with carefully controlled imperfections because the accompanying theory does not handle the bifurcation buckling of a perfect structure. The specimens were therefore tested in compression with an initial angle of inclination of 5° from the vertical, and with rigidly fixed ends. The test used the Tinius Olsen 120,000 lb Universal Test Machine (Fig. 14).

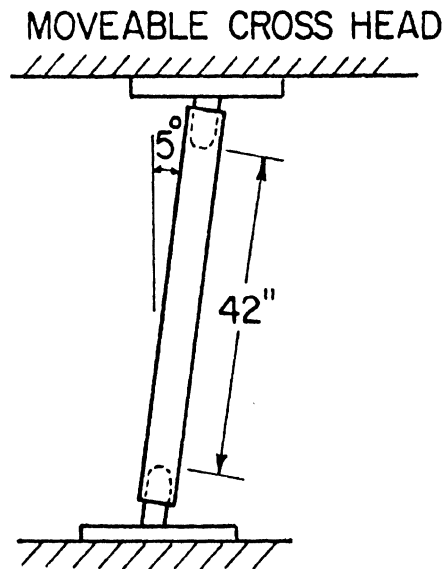


Fig. 14. Buckling test.

Three specimens were tested, a 3" x 2" x 0.1185" box section, a 3" x 1" x 0.1185" channel section and a 4" x 1-1/2" x 0.1135" channel. It was anticipated that each of the specimens would buckle with hinges at the upper and lower ends and a third in the middle. This was not the case for the stiffer two sections, as can be seen from a sketch of elastic deformation prior to buckling (Fig. 15).

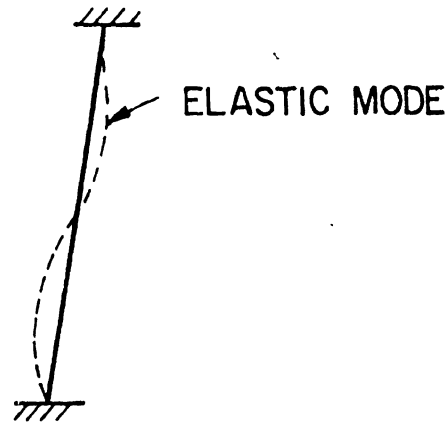


Fig. 15. Elastic deformation prior to hinge formation.

In fact, the elastic mode which existed prior to buckling (and which was clearly visible during the test) had zero moment at the middle of the beam, and the interior hinge formed some distance from the middle, perhaps at 40% of the length. The smaller channel section, however, was relatively weak in bending compared to axial stiffness, and exhibited symmetric elastic deformation before buckling with an eventual hinge closer to the center of the beam. Load-deflection curves are given in Figures 16 to 18, with sketches of the location of the hinges.

In retrospect, because of the high axial stiffness of the members, it is felt that the 5° axial imperfection was not large enough. The problem was that the beams were so stiff in the axial direction that relatively minor changes in elasticity of the supports had major effects on the results. In short, the situation is experimentally imperfection sensitive, as well as theoretically difficult to model.

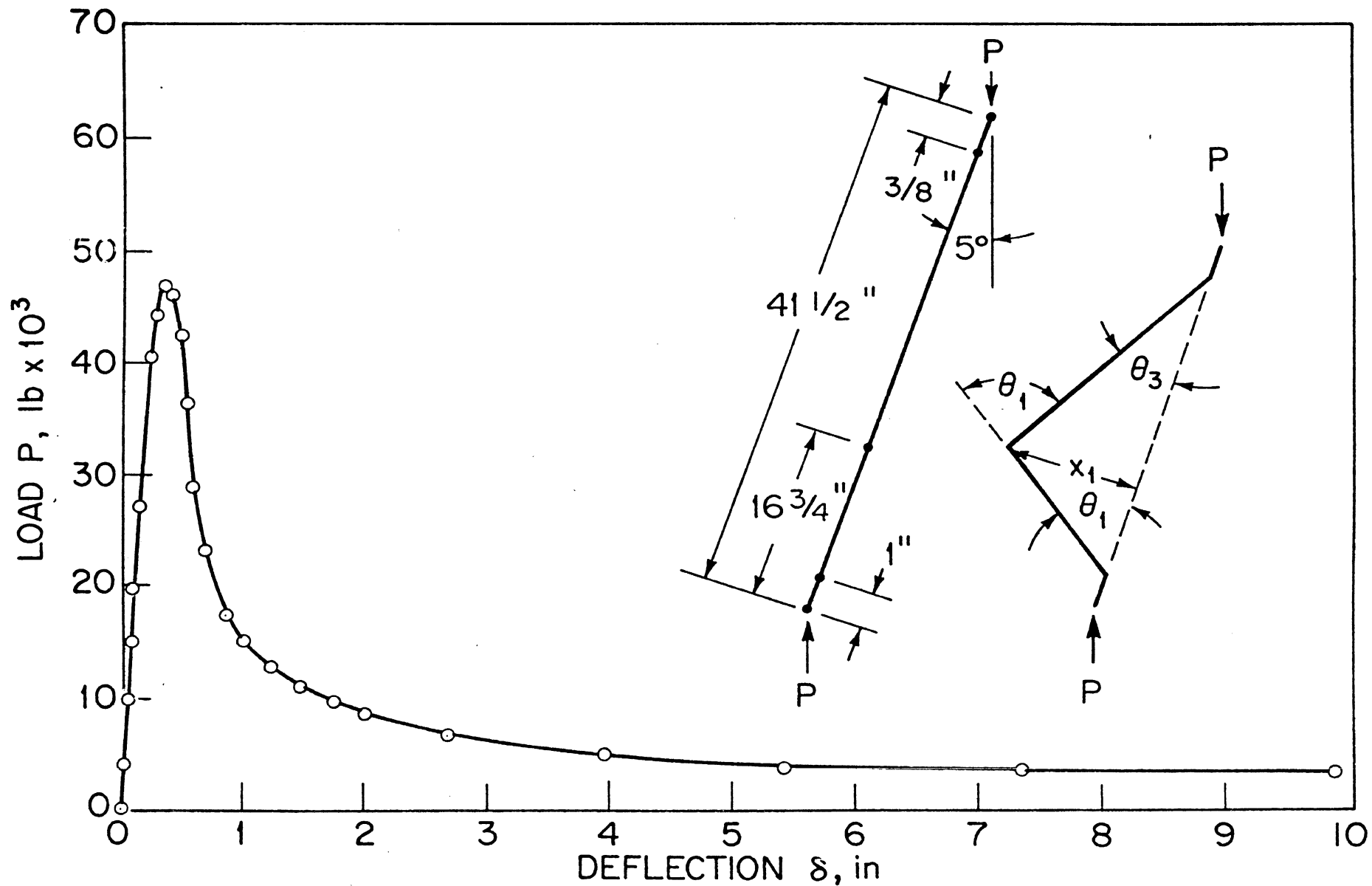


Fig. 16. Load-deflection curve for a box beam in buckling. BB 3020UM

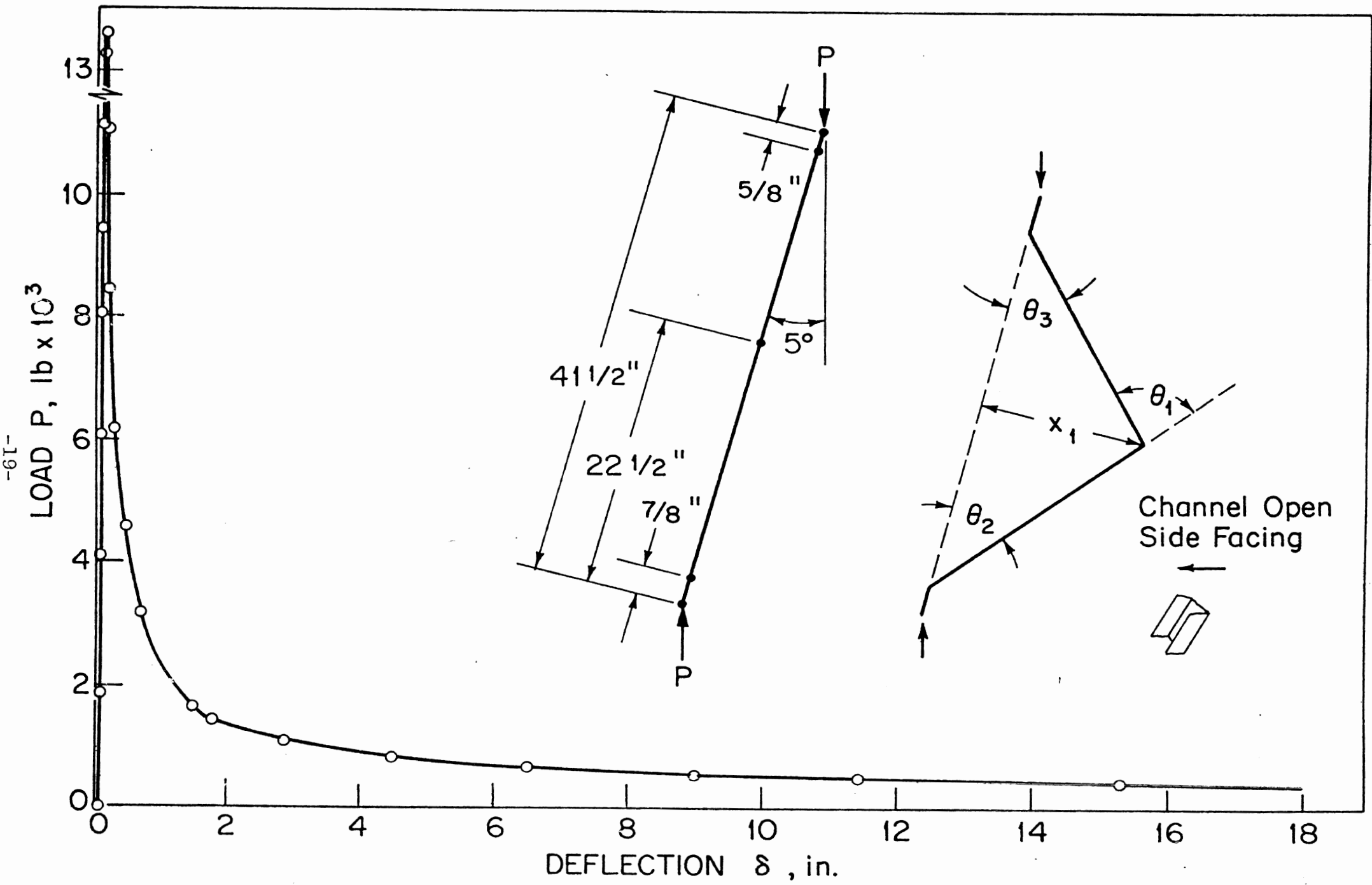


Fig. 17. Load-deflection relation for a channel column in buckling. CB 3010UM

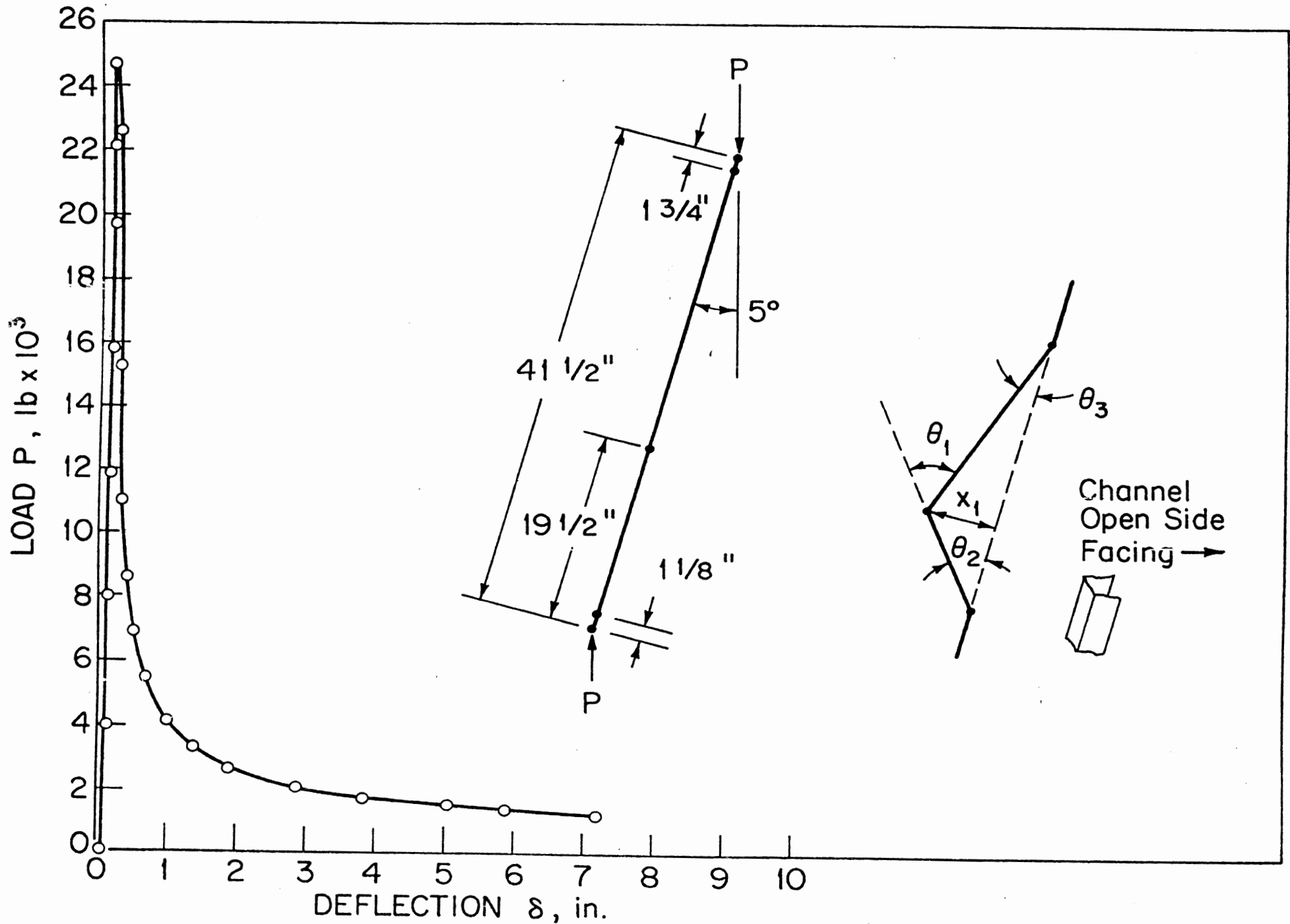


Fig. 18. Load-deflection relation for a channel beam-column in buckling. CR 4015TM

are given in Fig. 20. The cable extends from a point directly

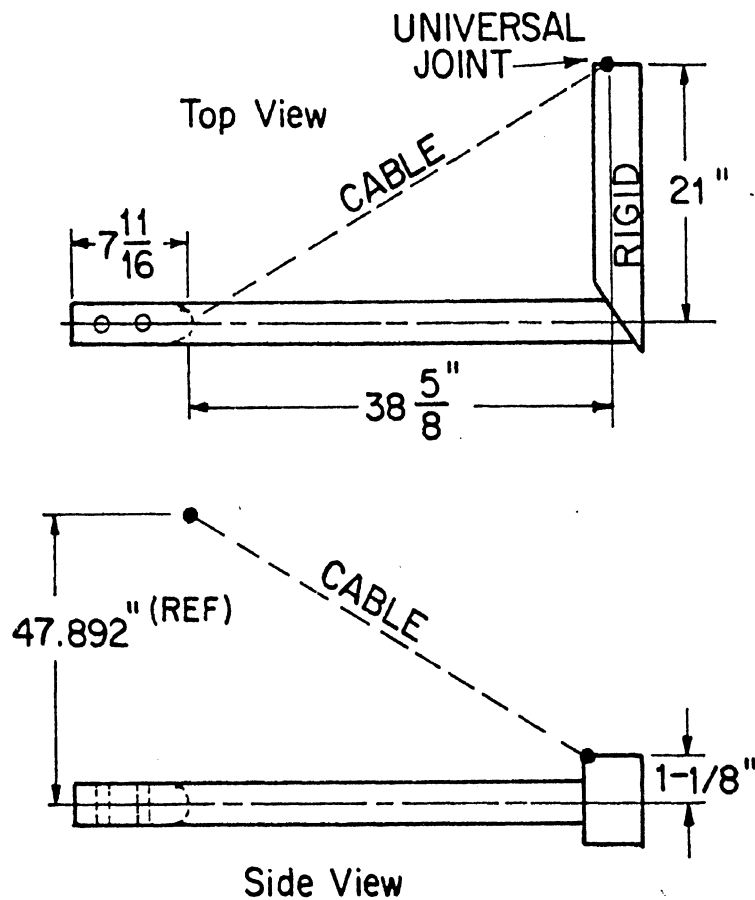


Fig. 20. Dimensions of combined load fixture.

over the root section, and has a length of $64 \frac{3}{16}$ inches from pivot to pivot. The universal joint at the tip of the rigid bar is $1 \frac{1}{8}$ inches above the centerline of the specimen.

The cable used was made from a pair of cables previously used in 1975 for a smaller scale combined load study. In the current test, the cables were put in series (end-to-end) to give the required length. The spring constant was 2913 lb/in, measured from universal joint to universal joint.

Steel plugs were used to support the root cross-section and the tip cross-section. These plugs were taken from the tensile experiment. The cross section along the entire length of the beam was unsupported. The hinge was anticipated to form at the root.

Results are in the form of load-deflection curves and in observations of the hinge formation. The channel specimen (Fig. 22) was extremely flexible and underwent large elastic torsional motion about the beam axis (perhaps 45°) before any plastic effects were apparent. This causes little trouble in the overall test, since the theory to be confirmed includes large elastic deformation. It did, however, require almost $2/3$ of the available stroke of the crosshead just to traverse the elastic region and did not allow the test to proceed as far as hoped into the plastic region. The load was relatively low during the entire test. Hinge formation was unexpected in that a minor hinge formed at the tip of the beam prior to the hinge at the root! Also, because of the almost 90° rotation of the beam tip at that point, the tip hinge was a bending hinge about the strong axis. A root hinge formed thereafter and dominated at higher loads. The small amount of hinging at the tip is felt to be a very delicate phenomenon and is certainly a burden for a theoretical model to predict.

The box section (Fig. 23) has a load-deflection relation similar to that for a beam in pure bending. A rather high ultimate load was reached, with rapid drop in load as a hinge formed at

the root of the specimen. The shape of the hinge resembled a bending hinge, but with a fold line perpendicular to the projection of the cable axis (Fig. 21). After data analysis, it became apparent that the beam had carried higher bending moments in combined loading than was possible for the beam in pure bending and that there was some favorable interference between the two modes of failure. The significance of this effect is

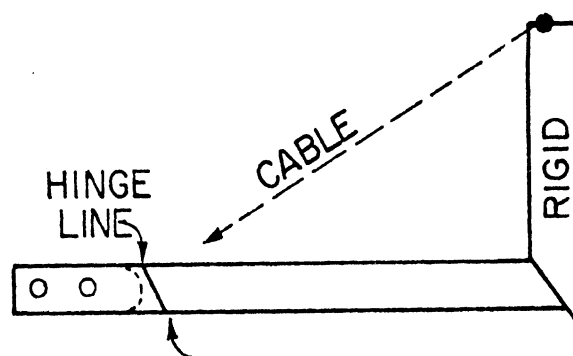


Fig. 21. Orientation of hinge line for box beam under combined bending and torsion.

not fully known at this time, but for this particular beam cross-section, seems to favor a Tresca type, rather than a von Mises type of load interaction curve (yield surface).

3.3 COMPARISON OF SIMULATION AND EXPERIMENTAL RESULTS

For each of the three buckling tests and two combined load experiments, the simulation program was exercised using the material properties and hinge data obtained in the test program. As discussed above the buckling tests were designed with a five degree offset to eliminate bifurcation. Our first simulation predicted failure by uniform axial plastic flow over the entire column. An analytical solution using Euler beam theory confirmed

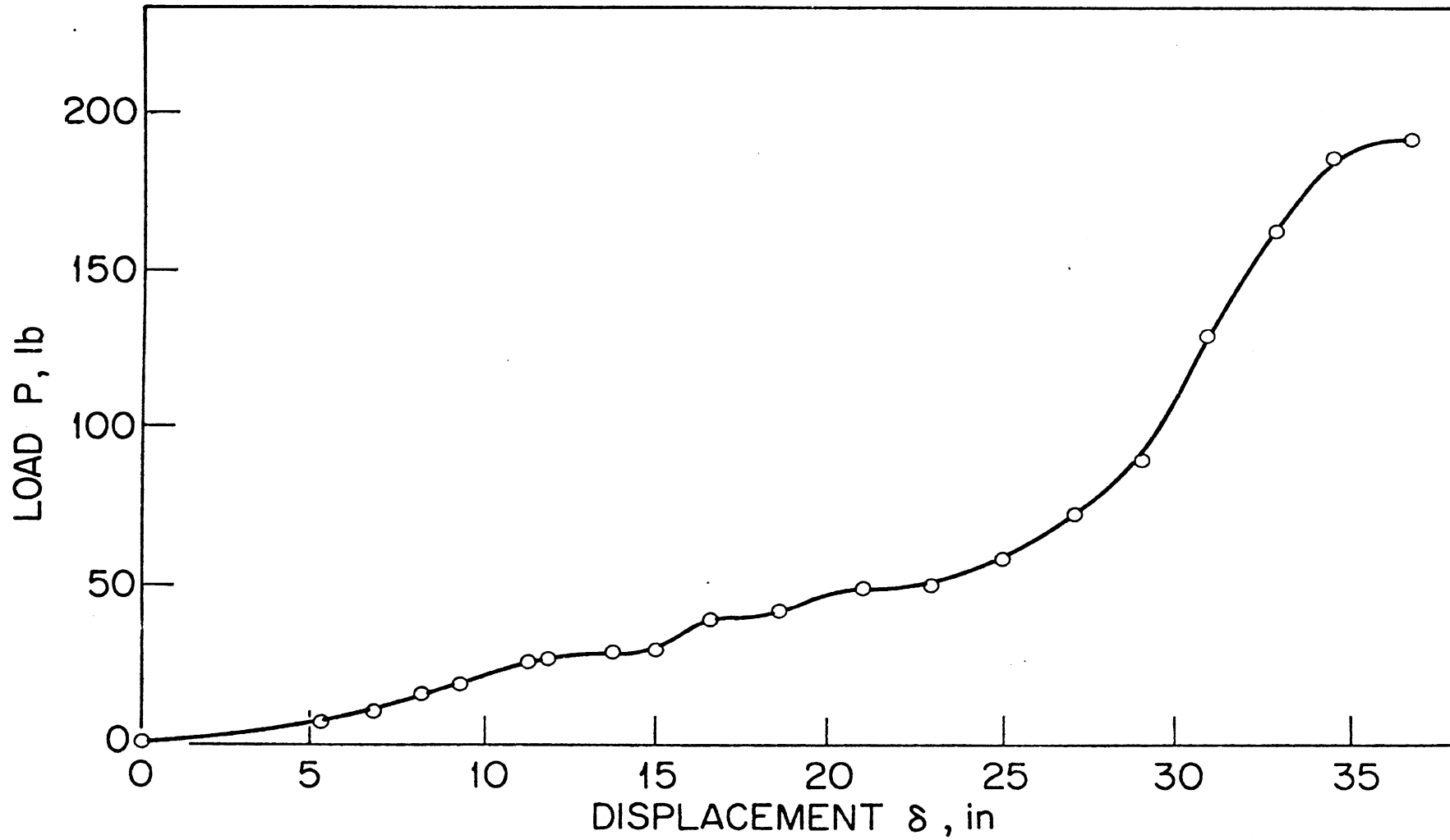


Fig. 22. Load-displacement relation for a channel beam under combined loading. CC 3015RM

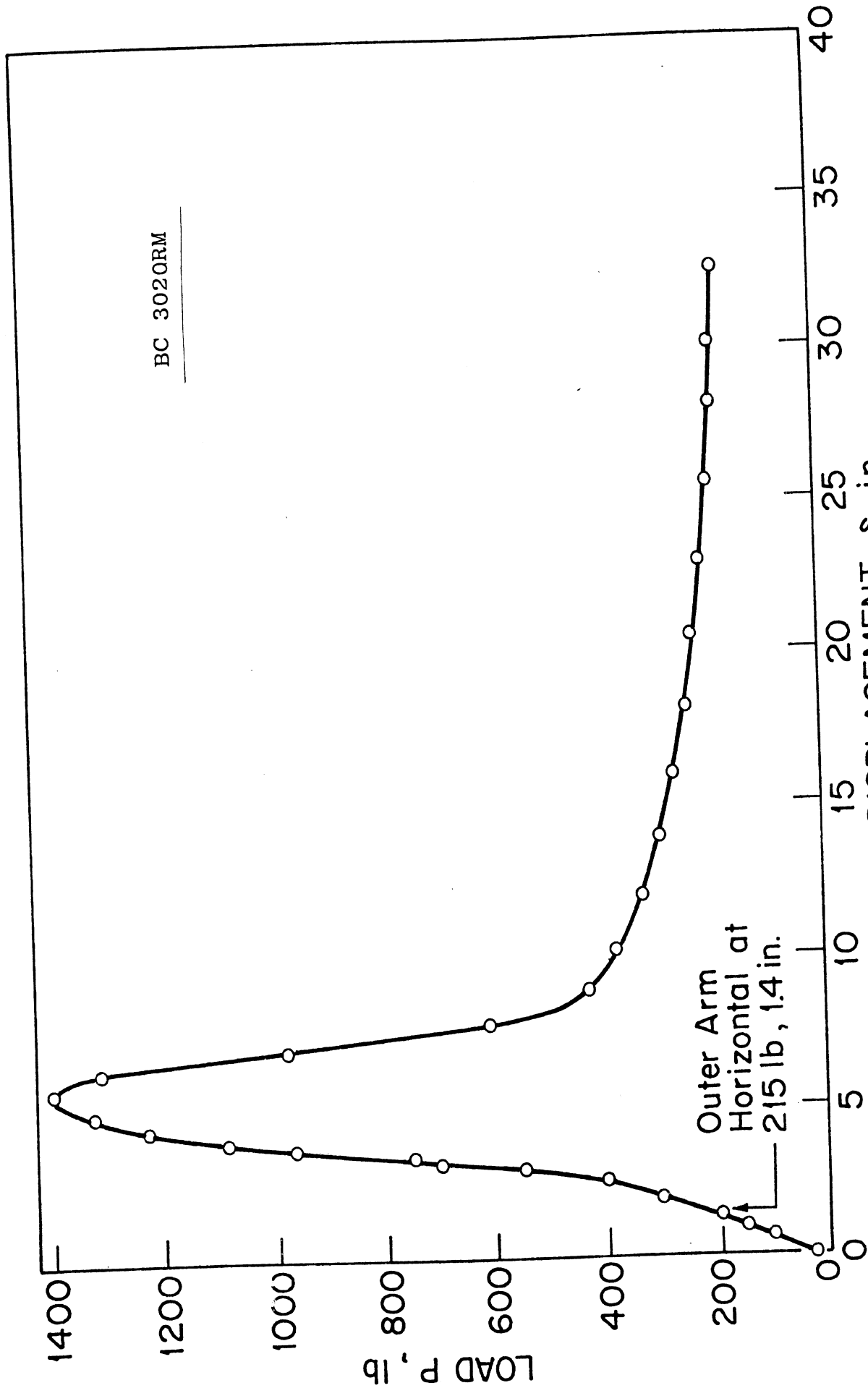


Fig. 23. Load-displacement relation for a box beam under combined loading.

the simulation prediction, i.e. the 5° offset did not introduce any bending prior to overall yielding. Thus the experimental behavior is due to initial imperfections in the specimen itself, and the experiment, despite our offset design, is imperfection sensitive.

To model this an initial deviation from straightness was assumed. The column was taken as two straight line segments rotated from the straight configuration by an angle θ_0 . The simulation results for the channel sections for θ_0 equal to one degree are shown in Figs. 24 and 25. The peak loads were about 20% high, but the qualitative behavior is quite good. The cross section collapse in the experiment is more rapid, but the simulation shows similar behavior. Closer quantitative agreement could be obtained by increasing the initial imperfection. Since the actual imperfections are unknown and our straight-line model is rather crude, increased quantitative agreement is not particularly significant. We believe the results shown indicate that the simulation is predicting the basic physical behavior of the systems.

The results for the box section shown in Figure 26 are not as satisfactory. For an initial imperfection of one degree, the peak load is about 12% high. Both the collapse of the cross section is much sharper in the experiment than in the simulation. To see if the discrepancy is due to elasticity of the base support, it was modeled by a spring and the simulation exercised for two values of stiffness that bracket the low deflection. It is clear from the results that the support elasticity is not a significant factor.

The main difference between the box and channel section is the bending stiffness of the box is much larger compared to the axial stiffness than in the channel section. Thus the actual bending moments at yield may be more sensitive to the elastic displacements. An analysis of the simulation indicates that the bending moment remained in the hardening region until about 2 inches of crush, i.e. plastic rotations were accumulating much slower in the simulation than in the test. This is primarily due to the relatively small value of the moment at initial yield. The test shows that in the small deflection range the actual axial stiffness is considerably less than predicted. The greater test displacement implies a greater magnification of the initial imperfection. Because of the large bending stiffness this could give a much more rapid accumulation of plastic rotation at yield. We have not been able to identify the source of the reduced stiffness in the experiment, although reduction of theoretical axial stiffness is a common experimental problem. Whether this reduction can account for the discrepancy is speculative, but should be explored before definitive conclusions can be reached.

A comparison of predicted and experimental results for the combined load channel test is shown in Fig. 27. In the simulation the initial deflections due to gravity were neglected. The origin of the simulation was taken at the point the outer arm was observed level in the experiment. This is not exactly correct since at this point in the experiment the system is not in an

unstressed state. Due to the small torsional stiffness the system underwent large elastic deformations before the onset of plasticity. Yielding did not occur until about 30 inches of displacement.

Simulation results and experiment are in quite good agreement. During the nonlinear elastic range the simulation is too stiff. It should be noted however that only a single element was used to model the 40 inch specimen. The onset of yielding and the maximum plastic collapse load were accurately predicted.

The results for the box combined load are shown in Fig. 28. Although the initial and final behavior compares favorably, there are marked discrepancies between the test and the simulation. Because of these discrepancies, gravitation was accounted for in the simulation. It did not have a significant effect on the discrepancy. It is interesting to note, however, that in the simulation the outer arm was horizontal at a force of 50 lbs. compared to the force of 200 lbs. observed in the experiment. The peak load in the test was 1400 lbs. compared to 600 lbs. predicted by the simulation.

The large loads obtained in the experiment appear to indicate a favorable interaction under combined loads that is not accounted for in the simulation. In some respects, however, the test results are anomolous in the sense that this interaction appears significant in the small deformation range prior to any noticeable plastic collapse of the cross section. For example the linearity of the test results indicate initial yielding at a load of about 1100 lbs. At this load the bending moment at the root of the cantilever is 42,300 in-lbs. or 55% greater than the initial yield moment in bending of 27,300 in-lbs. In fact the ultimate moment in bending is only 31,100 in-lbs. Thus the discrepancy between the experiment and the simulation is not associated with the local deformation theory itself, but rather with the initial yield surface. On the basis of previous experience with the plastic analysis of beams this is an unexpected result. Thus the test result may indicate a new phenomenon that can occur for some range of cross sections. A definitive conclusion, however, requires the collaboration of additional tests.

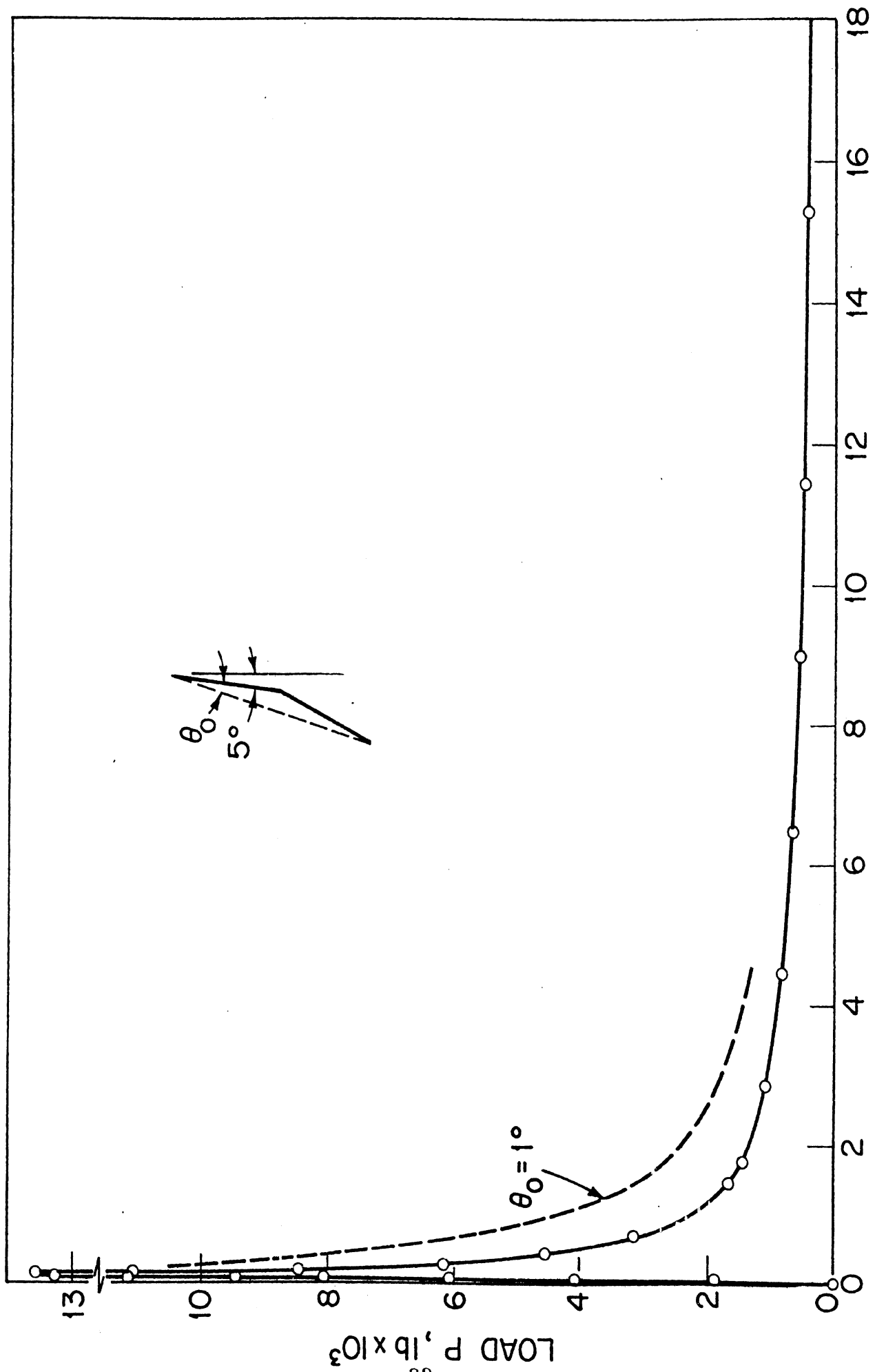


Fig. 24. Channel Cross-section column in buckling. 5° offset. CB3010UM

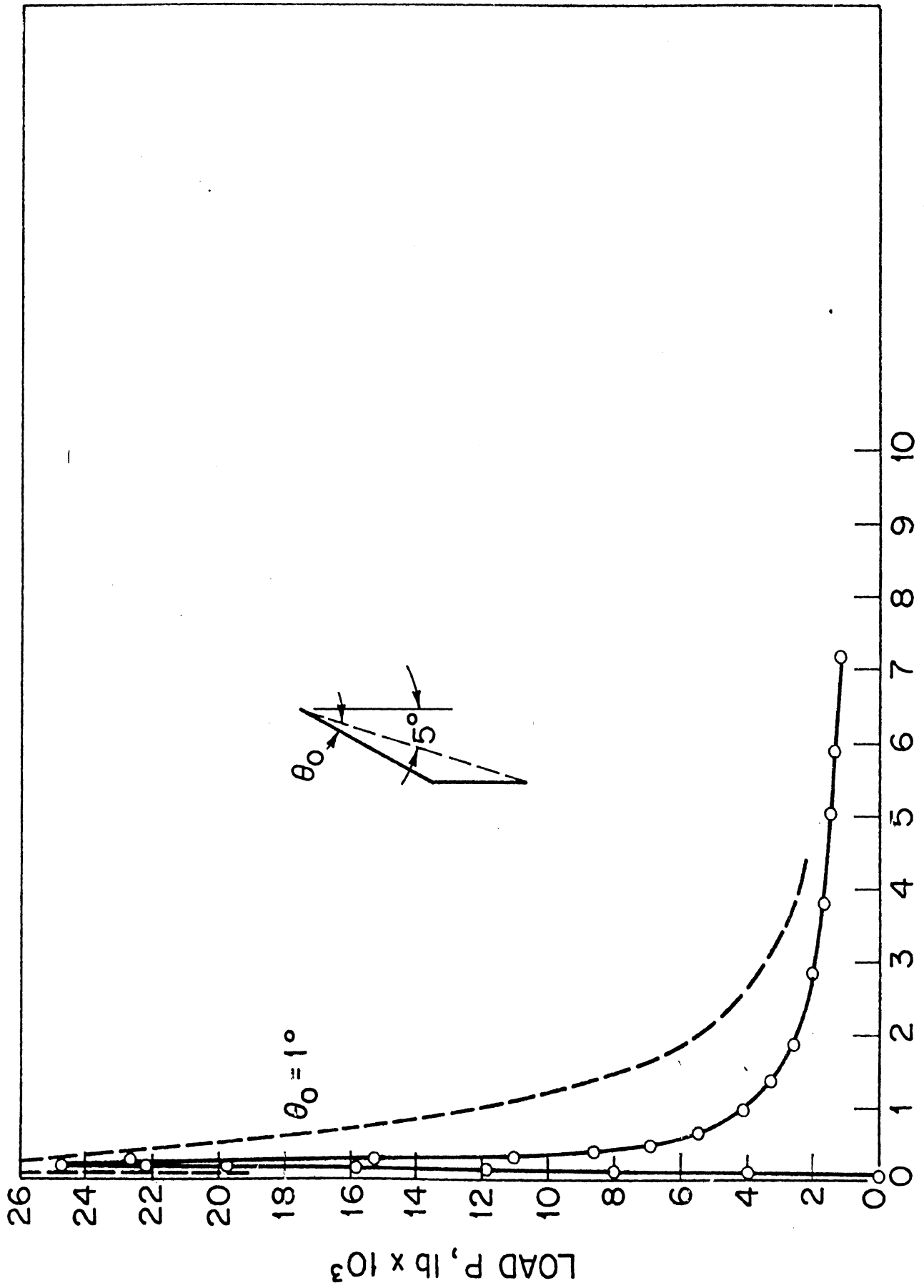


Fig. 25. Channel cross-section column in buckling. CB40I5TM

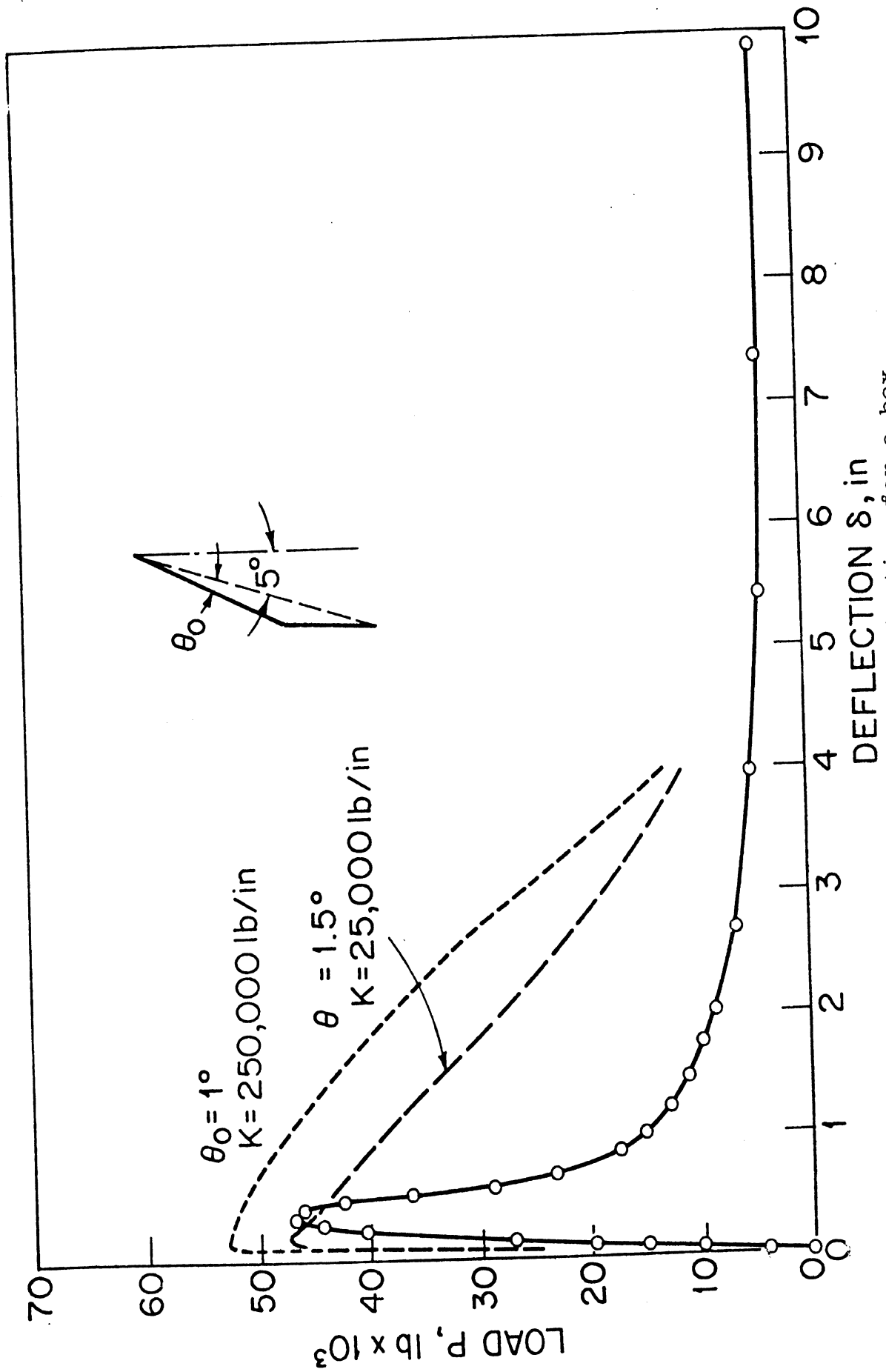


Fig. 26. Load-deflection for a box cross-section column in buckling.
BR3020UM

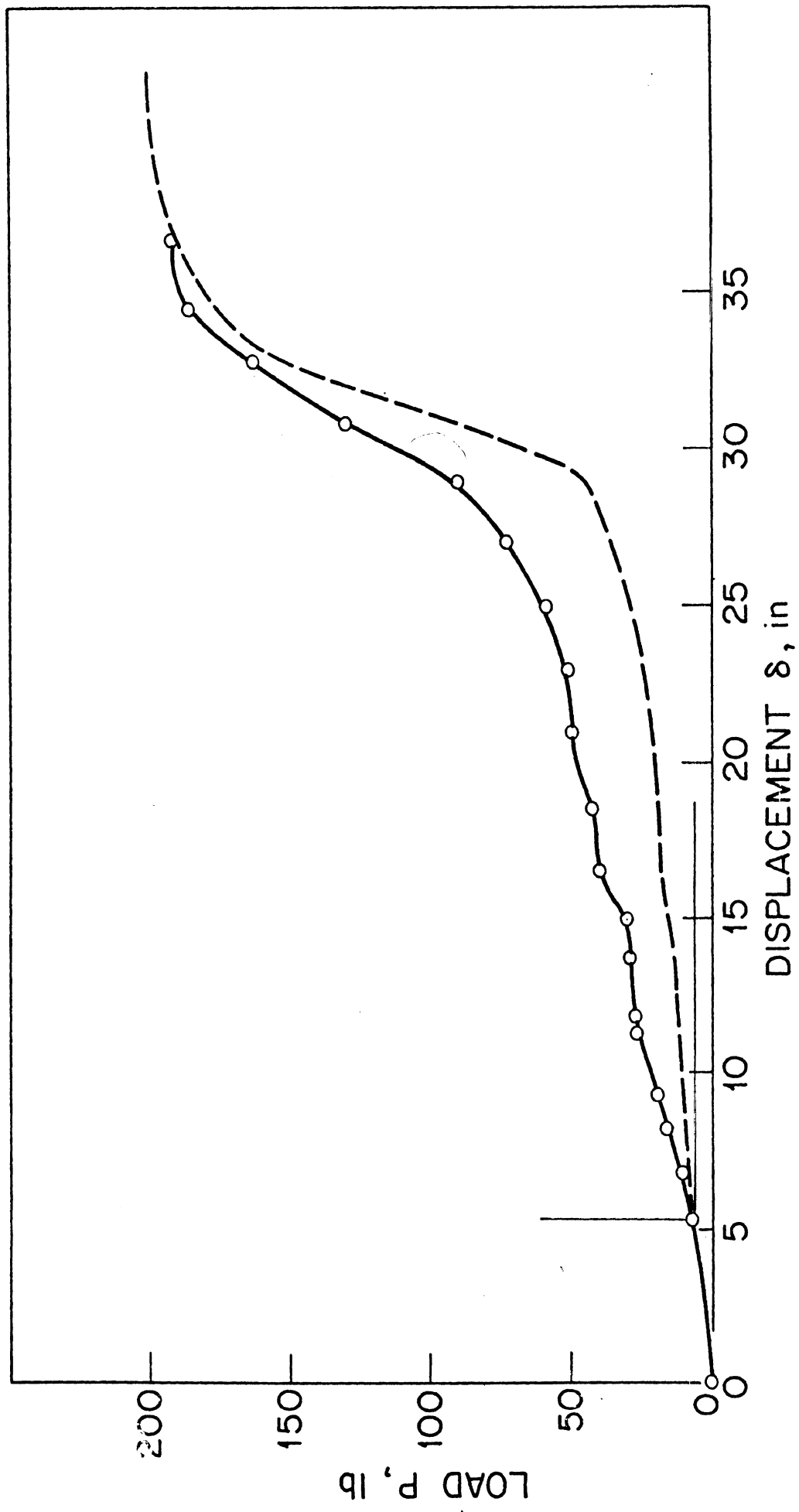


Fig. 27. Combined loading test.
CC3015RM

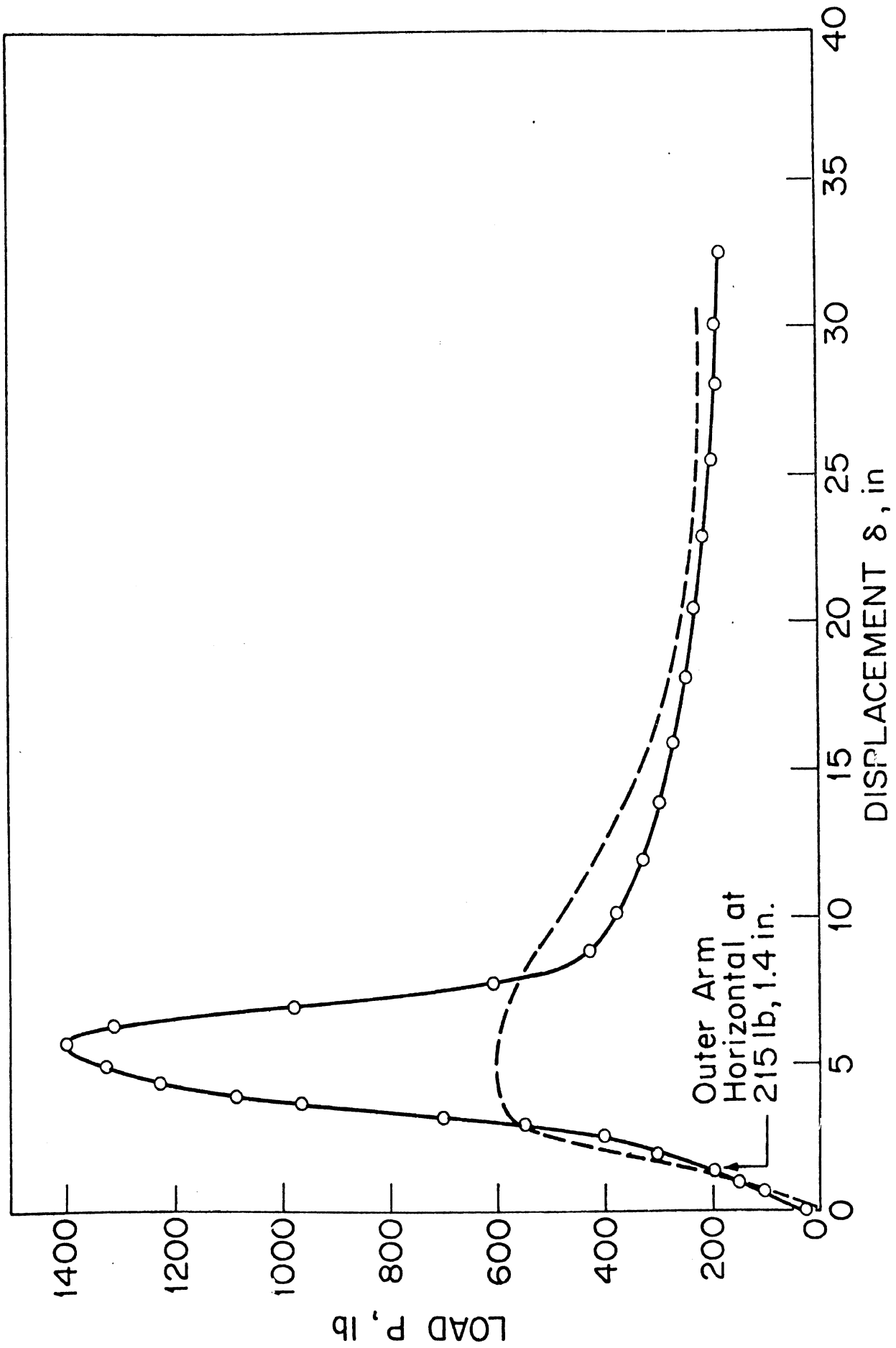


Fig. 28. Combined Loading Test.
BC3020RM

4. DETERMINATION OF HINGE PARAMETERS AND SCALING LAWS

4.1 INTRODUCTION

In addition to developing an experimental data book for the behavior of plastic hinges at large deformations, the test program was designed to provide data for the empirical determination of the scaling laws governing the hinge parameters associated with the theory discussed in Vol. 1. In the theory proposed, plastic hinge behavior is characterized in extension, biaxial bending and torsion by functions of the form.

$$\alpha = \alpha_o \left\{ a_i + b_i \left(1 + k_i(\theta - \theta_m) \right) \exp \left(-k_i(\theta - \theta_m) \right) \right\} \quad (1)$$

where θ is the accumulated plastic rotation (extension) and θ_m is the value of θ corresponding to the maximum value of α . For $\theta < \theta_m$, $i = 1$ and

$$a_1 = (1 - fy)/(1-y)$$

$$b_1 = (f - 1)/(1-y)$$

in which

$$y = (1 - k_1 \theta_m) \exp k_1 \theta_m$$

For $\theta > \theta_m$, $i = 2$ and

$$a_2 = \beta, \quad b_2 = f - \beta$$

Equation (1) is a function of six parameters. They are

α_o = Maximum elastic moment (force)

f = ratio of maximum value of α to α_o

β = ratio of the asymptotic values of α for large θ to m

θ_m = value of θ at maximum value of α

k_1 = hardening parameter in the range $\theta < \theta_m$

k_2 = softening parameter in the range $\theta > \theta_m$.

It should be noted that (1) reduces to an elastic-perfectly plastic relationship when

$$\theta_m = 0, \quad f = \beta = 1 \quad (2)$$

In this case α_0 is the constant yield moment.

4.2 DETERMINATION OF HINGE PARAMETERS

These six parameters were determined for each test. The procedure for bending about the major and minor principle axes and torsion is as follows:

1. α_0 was defined as the test load at 0.5° plastic rotation. This offset value was arbitrarily chosen since the actual onset of plasticity is not clearly defined in the experimental data, i.e. there is not a discontinuity in the curve but a gradual transition from purely elastic to plastic.
2. The maximum test load α_f and θ_m were obtained by inspection. The parameter $f = \alpha_f/\alpha_0$.
3. In general the experimental data is not a smooth curve to very large plastic rotations. The reason is at some point in the collapse of the cross section there is self-interference of the walls of the cross section. At this point there is generally an abrupt change in the slope of the curve and sometimes an increase in

load carrying capacity. The asymptotic value α_u was obtained by extrapolating the experimental data with a smooth curve through this region. The parameter $\beta = \alpha_u/\alpha_o$.

4. The hardening parameter k_1 and the softening parameter k_2 were determined by a least-square fit. With the four parameters determined above, k_1 is the only unknown in (1) for points $\theta < \theta_m$. Likewise k_2 is the only unknown for points $\theta > \theta_m$. In each region we form the error measure

$$E = \sum_{j=1}^N (E_j - \alpha_j)^2 \quad (3)$$

where j is summed over the number of experimental points θ_j , E_j is the experimental load, and α_j is the value obtained from (1). We now minimize the error with respect to k , i.e.

$$\frac{dE}{dk} = 0 \quad (4)$$

Thus

$$\sum_{j=1}^N (E_j - \alpha_j) \frac{d\alpha_j}{dk} = 0 \quad (5)$$

Equation 4 is a transcendental equation for k . It was solved by a half-interval method.

The six parameters for each test are summarized in Table 2. It should be noted that the theoretical range of k_1 is $-\infty < k_1 < \infty$ and for k_2 $0 \leq k_2 < \infty$. Also for some tests, primarily channel

strong axis bending, no value is given for k_1 . This occurs when the cross section collapses for very small values of θ_m , and there are not enough data points in the hardening region to employ (4). As discussed below, however, this case can be validly approximated by eliminating the hardening region.

The experimental data for the axial tests is qualitatively different. Although the initial yield stress and the ultimate stress are different, there is no significant cross section collapse. Thus the ultimate stress occurs at very large axial strains that normally will not occur in combined loading situations. Moreover the difference between the initial yield and the ultimate stress never exceeds 10%. Thus it is reasonable to model the material as an elastic-perfectly plastic material. The experimental stress-strain curves were fit over the plastic strain region of interest by this idealization. The values of the yield stress and slope of the linear portion are summarized for each specimen in Table 2.

All the steel cross sections were nominally the same material. It is interesting to note that the experimental yield stress varies from 49,500 to 62,000 psi. The actual experimental values were used in the determination of the scaling laws below. The large variability in the properties of nominally the same material illustrates, however, the difficulty of application to real vehicle structures since similar variations can be expected from vehicle to vehicle or even component to component.

4.3 SCALING LAWS

The test program included cross section sizes that span the range of interest in vehicle structures. To interpolate the results to intermediate sizes, a set of scaling laws were derived on the basis of dimensional analysis and least square fitting techniques. For bending about each of the principal axes and torsion we consider the six quantities α_o , α_f , α_u , θ_m , k_1 and k_2 . Letting P denote any one of the first three quantities (moments having dimensions of force x length), we assume that P depends upon the yield stress σ_y and the dimensions of the cross section h , b , t where h is the height, b the width, and t the thickness. It then follows from dimensional analysis that

$$P/\sigma = F(\lambda, \epsilon) \quad (6)$$

where σ is the yield stress times a combination of h , b , t which has dimensions of length cubed and λ, ϵ are dimensionless combinations of h , b , t . Here σ was chosen in the form of the initial yield moment obtained from elementary beam theory. The choice of λ and ϵ was based on preliminary correlation studies of various combinations of h , b , t with the experimental data.

A similar procedure is followed when P denotes any of the last three dimensionless quantities except that it is now assumed that these quantities may depend upon the elastic stiffness E . It now follows that

$$P = F(E/\sigma_y, \lambda, \epsilon) \quad (7)$$

It was found that the hardening parameters did not exhibit any strong correlation with E/σ_y and thus it was suppressed. For

θ_m we assume that the dependence on the elastic modulus is linear giving the form

$$\theta_m = (E/\sigma_y) F(\lambda, \epsilon) \quad (8)$$

From (6) (7) (8) it follows that all six parameters have the functional form

$$P = A F(\lambda, \epsilon) \quad (9)$$

The actual definition of the scale factor A in each case is given in Table 1. The definitions of λ and ϵ are given in Table 4.

With (9) the problem reduces to determining the function F through a least square fit to the test values of the parameters. Here the data has been fit with a cubic polynomial, i.e. we assume

$$F = \sum_{j=0}^3 \sum_{i=0}^j a_{ij} \lambda^{j-i} \epsilon^i$$

As in (3) we form the error measure

$$E = \sum_{n=1}^N \left[(E_n/A) - F_n \right]^2 \quad (10)$$

where E_n are the experimental data points. Minimizing the error with respect to the coefficients leads to

$$\sum_{n=1}^N \left[(E_n/A) - F_n \right] \frac{\partial F_n}{\partial a_{ij}} = 0 \quad (11)$$

Equation (11) is a set of ten linear equations in the ten unknown coefficients.

The set of coefficients was determined for each case indicated in Table 3. These values together with the definitions of A , λ , ϵ are programmed in the simulation UMVCS-1 (see Vol. 3). The elastic-perfectly plastic approximation for the axial behavior is also included. Thus for box and channel sections the simulation computes all necessary hinge properties internally when the user specifies σ_y , E , h , b , t . The user also has the option of specifying the hinge parameters as input data.

As mentioned above, for channel strong axis bending there were not enough data points to obtain k_1 . In general the collapse of the cross section occurred at very small values of plastic rotation with only small differences (1-2%) between α_o and α_f . Thus in the simulation the hardening region for channel strong axis bending is neglected, i.e. f is set to unity and θ_m to zero.

Finally it should be noted that the statistical validity of the above scaling laws is marginal. Each data point was determined from a single test. Variability in both material properties and dimensional tolerances of nominally the same specimen is at least 10%. There will be additional scatter in the experiments themselves. Thus we are fitting data for which each point is subject to scatter. Consequently the resulting scaling laws should be viewed as interpolation formulas which are reliable (with the same scatter) for intermediate points. Extrapolation outside the range of the test program, however, should be done with considerable caution.

5. CONCLUSIONS

Several major goals have been reached. Many careful, uniform experiments were done with steel and aluminum specimens. A large bank of hinge data has been created. Material properties are obtainable from the small strain region of the axial hinge tests. The data bank can be used as source material for any future simulation theories and computer codes.

The experiments did not clear up all questions about hinge behavior, of course. If one wished to derive more accurate theories, it might be important to do more tests for channels in bending about the weak axis, to determine to what extent the flanges act differently in compression than in tension. It would also be of interest to obtain more combined load data to more clearly define the failure surface. The present tests certainly show an interaction between bending and torsional hinging. Perhaps extensional hinging might also have a strong interaction effect on the other types. These points must be left to future study.

6. APPENDIX A: TABLES

TABLE 1
CODE FOR APPROXIMATE WALL THICKNESS

<u>LETTER</u>	<u>APPROXIMATE THICKNESS</u>
P	0.074"
Q	0.080
R	0.084
S	0.093
T	0.113
U	0.117
V	0.128

TABLE 2. RUN LOG AND HINGE PARAMETERS

STEEL TESTS

			$M_o = A$	$f = U$	$\beta = B$	$\Theta_m = X_o$	k_1	k_2	
of M RUN#	CODE	THICKNESS IN	$\sigma_y \times 10^{-3}$	$E \times 10^{-6}$					PAGE
101	BA 30 20 RM	0.084	51.3	20.8					55,56, 57
102	BA 30 20 UM	.117	50.6	20.0					58,59, 60
110	BA 30 30 PM	.074	55.8	23.7					61,62, 63
107	BA 30 30 TM	.113	52.0	21.4					64,65, 66
103	BA 40 20 SM	.093	50.0	20.4					67,68, 69
113	BA 40 30 TM	.113	52.4	20.8					70,71 72
120	BA 40 40 QM	.080	59.0	17.9					73,74 75
114	BA 40 40 TM	.113	54.5	22.2					76,77 78
9	BX 30 20 RM	.084	35,470	1.2232	0.5021	4.173	1.760	32.789	79
43	BX 30 20 UM	.118	49,350	1.2265	0.3540	4.533	5.979	8.989	80
3	BX 30 30 PM	.074	48,470	1.0370	0.2909	0.689	--	72.530	81
8	BX 30 30 TM	.113	63,750	1.1796	0.3465	2.987	-11.725	21.542	82
41	BX 40 20 SM	.093	64,810	1.1356	0.4629	4.156	-5.186	41.166	83
17	BX 40 30 TM	.113	96,790	1.1647	0.4133	3.379	-3.229	53.626	84
13	BX 40 40 QM	.080	Poor	test.	Weld split.				
14	BX 40 40 TM	.113	130,910	1.0141	0.3056	0.990	--	52.184	85
1	BY 20 30 RM	.084	27,270	1.1404	0.3084	1.199	--	28.284	86
2	BY 20 30 UM	.117	34,380	1.2437	0.3461	4.454	-2.2080	14.058	87
4	BY 20 40 SM	.093	37,330	1.0799	0.2679	0.909	--	33.688	88
16	BY 30 40 TM	.113	83,610	1.0883	0.2972	1.329	--	40.172	89
5	BZ 30 20 RM	.084	12,215	1.1825	0.243	6.52	5.275	10.746	90
6	BZ 30 20 UM	.117	29,700	1.2158	0.3082	10.32	3.926	7.940	91
7	BZ 30 30 PM	.074	34,010	1.0909	0.1877	3.73	-12.621	19.947	92

TABLE 2. (Continued)

STEEL TESTS

U of M RUN#	CODE	THICKNESS IN	$M_o = A$ $\sigma_y \times 10^{-3}$	$f = U$ $E \times 10^{-6}$	$\beta = B$	$\theta_m = X_o$	k_1	k_2	PAGE
40	BZ 30 30 TM	.113	44,990	1.2247	0.1814	11.27	6.444	14.737	93
20	BZ 40 20 SM	.093	31,580	1.0861	0.2583	1.74	--	11.875	94
42	BZ 40 30 TM	.113	58,030	1.1821	0.2642	4.26			95
31	BZ 40 40 QM	.082	Bad test. Weld split immediately.						
29	BZ 40 40 TM	.113	69,200	1.4747	0.2370	7.09	22.243	13.879	96
108	CA 30 10 QM	.080	51.4	18.6					97,98, 99
109	CA 30 10 UM	.117	62.0	19.7					100,101 102
106	CA 30 15 RM	.084	51.3	20.8					103,104 105
104	CA 30 15 UM	.117	50.6	20.0					106,107 108
105	CA 40 15 SM	.093	50.0	20.4					109,110 111
111	CA 40 15 TM	.113	49.5	21.6					112,113 114
115	CA 40 20 QM	.080	59.0	17.9					115,116 117
112	CA 40 20 TM	.113	52.4	20.8					118,119 120
	CA 60 20 VM	.128	51.0	20.4	Estimated values.	Specimen not tested;	too large for fixture.		
	CA 60 30 VM	.128	51.0	20.4	Estimated values.	Specimen not tested;	too large for fixture.		
27	CX 30 10 QM	.080	18,290	1.0480	0.2165	0.961	--	27.637	121
39	CX 30 10 UM	.121	27,130	1.1223	--	1.653	--	--	122
45	CX 30 15 RM	.084	20,400	1.0544	0.5534	0.952	--	52.509	123
47	CX 30 15 UM	.118	31,950	1.0592	0.4695	0.822	--	20.029	124
61	CX 40 15 SM	.093	35,560	1.0348	0.4640	0.912	--	65.950	125
35	CX 40 15 TM	.113	45,740	1.0146	0.3811	0.758	--	33.853	126
71	CX 40 20 QM	.082	34,110	1.0149	0.3398	0.640	--	70.785	127

TABLE 2. (Continued)

STEEL TESTS

of M RUN#	CODE	THICKNESS IN	$M_o = A$ $\sigma_y \times 10^{-3}$	$F = U$ $E \times 10^{-6}$	$\beta = B$	$\theta_m = \kappa_o$	k_1	k_2	PAGE
73	CX 40 20 TM	.113	51,340	1.0592	0.4905	1.276	--	44.819	128
77	CX 60 20 VM	.128	120,790	1.0000	0.2880	0.349	--	56.605	129
79	CX 60 30 VM	.128	129,050	1.0000	0.3100	0.597	--	54.311	130
11	CY 10 30 QM	.080	3,220	1.2422	0.3385	5.919	17.540	3.629	131
10	CY 10 30 UM	.117	4,850	1.3460	0.4598	7.357	19.417	2.467	132
23	CY 15 30 RM	.084	7,640	1.1936	0.2814	4.137	-6.297	4.089	133
24	CY 15 30 UM	.117	11,480	1.1551	0.3833	3.464	-6.602	6.914	134
37	CY 15 40 SM	.093	7,300	1.2075	0.1578	4.981	3.792	4.659	135
26	CY 15 40 TM	.113	9,770	1.2009	0.1955	4.940	-5.880	3.385	136
21	CY 20 40 QM	.080	12,580	1.1223	0.1248	4.662	-5.538	7.431	137
22	CY 20 40 TM	.113	17,470	1.1752	0.1723	4.559	-3.042	4.399	138
75	CY 20 60 VM	.129	23,130	1.1708	0.2408	5.557	-0.048	6.160	139
30	CY 30 60 VM	.128	55,670	1.0963	0.2037	4.603	22.262	6.400	140
18B	CZ 30 10 QM	.080	1,290	2.0388	1.1760	12.42	-7.734	6.536	141
12C	CZ 30 10 UM	.117	2,340	2.1325	1.5152	18.34	-5.213	6.791	142
19	CZ 30 15 RM	.084	2,770	1.7112	0.5693	14.83	-1.717	7.988	143
25	CZ 30 15 UM	.117	4,390	1.8314	0.7463	23.03	1.198	8.551	144
36	CZ 40 15 SM	.093	3,040	1.9452	0.6645	16.53	-1.795	7.736	145
44	CZ 40 15 TM	.113	3,840	1.9805	1.0417	15.19	-4.065	6.270	146
28	CZ 40 20 QM	.0825	3,710	1.6981	0.5660	10.15	-7.450	5.368	147
33	CZ 40 20 TM	.1125	6,450	1.7504	0.4898	18.90	1.060	7.178	148
50	CZ 60 20 VM	.128	Bad test; split weld.						
38	CZ 60 30 VM	.128	16,630	1.6747	0.8371	28.01	2.413	14.717	149

TABLE 2. (Continued)

ALUMINUM TESTS

JOE M RUN#	CODE	THICKNESS IN	$M_o = A$	$f = U$	$\beta = B$	$\Theta_m = X_o$	k_1	k_2	PAGE	
			$\sigma_y \times 10^{-3}$	$E \times 10^{-6}$						
122	BA 30 30 RA	.083	25.2	8.80					150,151 152	
116	BA 30 30 VA	.125	25.2	8.80					153,154 155	
59	BX 30 30 RA	.085	23,880	1.0000	0.2513	0.220	--	31.483	156	
57	BX 30 30 VA	.118	34,470	1.0868	0.2901	2.196	62.24	20.951	157	
46	BZ 30 30 RA	.083	14,360	1.0864	0.1922	2.070	--	15.816	158	
54	BZ 30 30 VA	.125	24,170	1.1378	0.2640	6.470	--	13.584	159	
121	CA 30 10 RA	.083	25.2	8.80					160,161 162	
117	CA 30 10 VA	.125	25.2	8.80					163,164 165	
119	CA 40 15 RA	.083	22.2	7.80					166,167 168	
118	CA 40 15 VA	.125	22.2	7.80					169,170 171	
53	CX 30 10 RA	.088	9,560	1.0076	0.2929	0.844	--	40.716	172	
51	CX 30 10 VA	.128	13,490	1.0964	0.2128	2.124	--	17.445	173	
65	CX 40 15 RA	.084	13,140	1.0000	0.3044	0.289	--		174	
63	CX 40 15 VA	.121	22,390	1.0044	0.3828	0.520	--	27.804	175	
55	CY 10 30 RA	.092	1,490	1.2295	0.8047	7.765	13.218	7.290	176	
49	CY 10 30 VA	.130	2,350	1.2315	0.4255	13.631	6.090	4.427	177	
69	CY 15 40 RA	.082	3,490	1.1476	0.2149	4.238	-2.897	5.529	178	
67	CY 15 40 VA	.121	4,980	1.2054	0.3841	5.168	-3.741	4.493	179	
52	CZ 30 10 RA	.083	790	Test aborted - premature failure.						
48	CZ 30 10 VA	.128	1,054	2.0702	1.6433	14.49	-2.944	8.315	180	
58	CZ 40 15 RA	.083	1,180	Test aborted - premature failure.						
56	CZ 40 15 VA	.125	1,980	1.9798	1.0101	10.85	-1.711	6.658	181	

HINGE PARAMETER		SCALE FACTOR	
		A	
k_1, k_2		1.0	
θ_m		E/σ_y	
α_o α_f α_u	BOX	BENDING	$\sigma_y t h^2$
		TORSION	$\sigma_y t^3$
$(f = \alpha_f / \alpha_o)$ $(\beta = \alpha_u / \alpha_o)$	CHANNEL	BENDING-STRONG AXIS	$\sigma_y t h^2$
		BENDING-WEAK AXIS	$\sigma_y t b^2$
		TORSION	$\sigma_y t^2 (h+2b)$

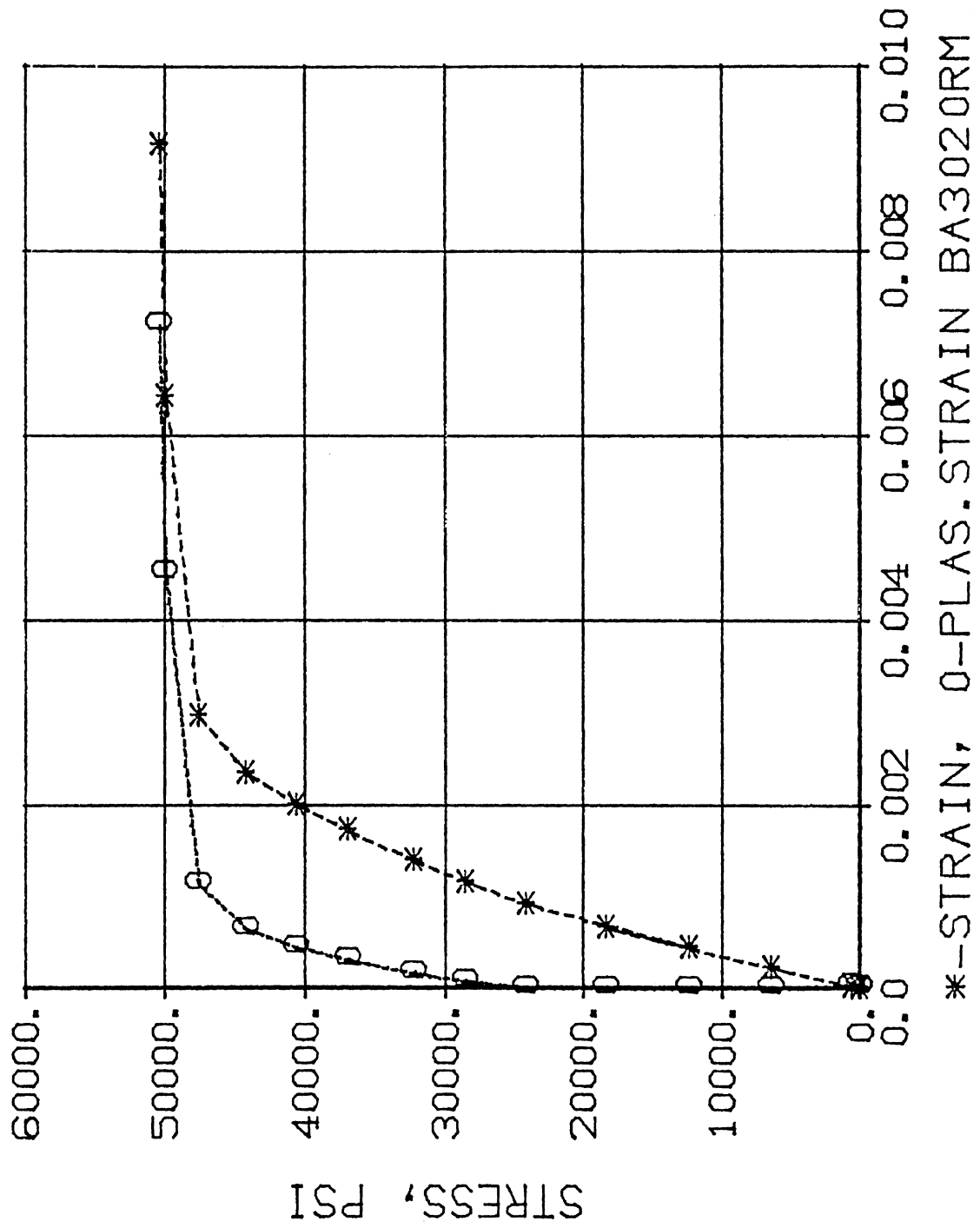
TABLE 3: SCALE FACTORS FOR SCALING LAWS

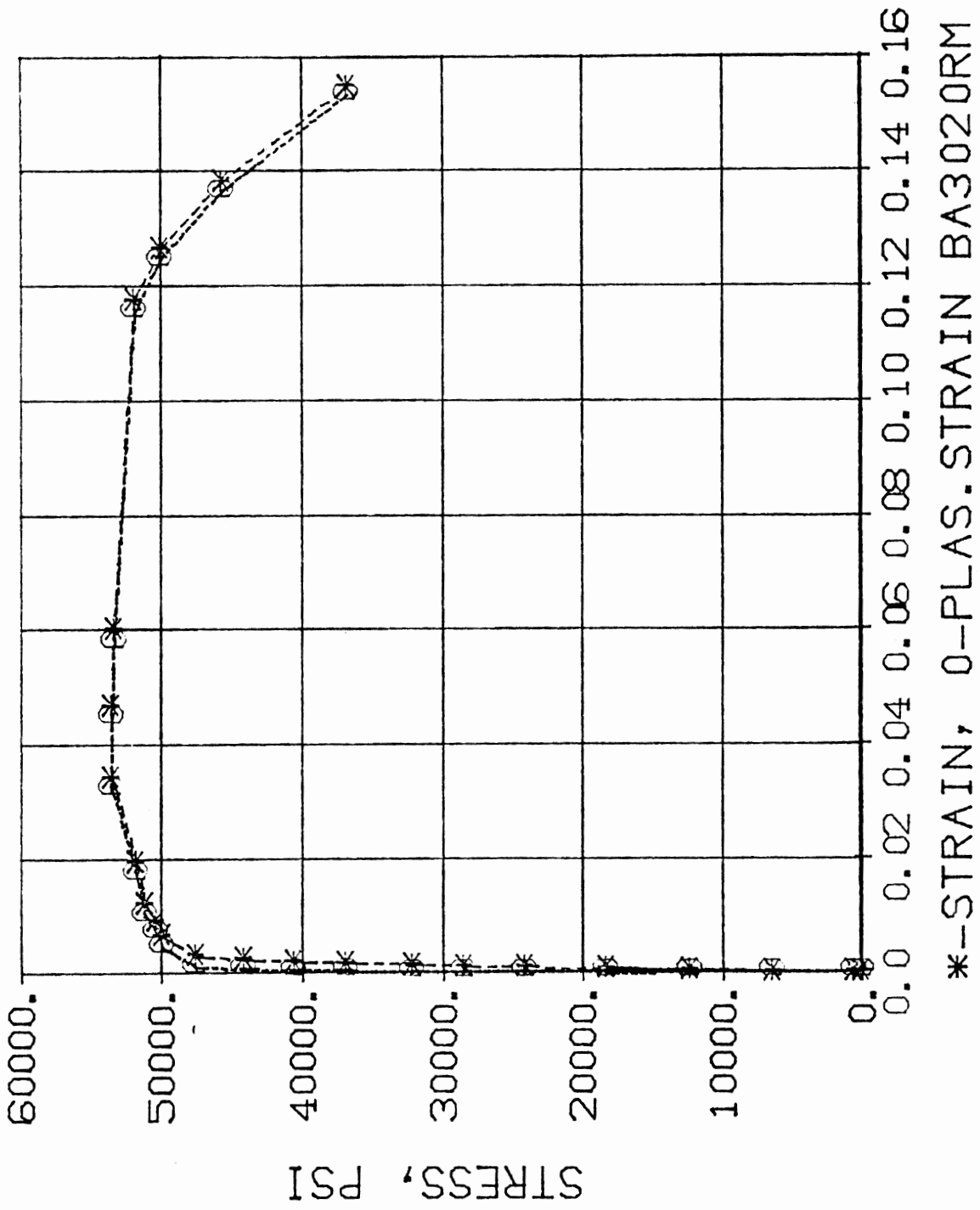
LOADING CASE	SECTION TYPE	GEOMETRIC PARAMETERS
TORSION	BOX	$\lambda = (h+b)/t \quad \epsilon = hb/t^2$
	CHANNEL	$\lambda = \frac{b}{h}, \quad \epsilon = \frac{b}{t}$
BENDING	BOX	$\lambda = \frac{b}{h}, \quad \epsilon = \frac{t}{h}$
	CHANNEL STRONG AXIS	$\lambda = \frac{b}{h} \quad \epsilon = \frac{t}{h}$
	CHANNEL WEAK AXIS	$\lambda = \frac{h}{b} \quad \epsilon = \frac{t}{b}$

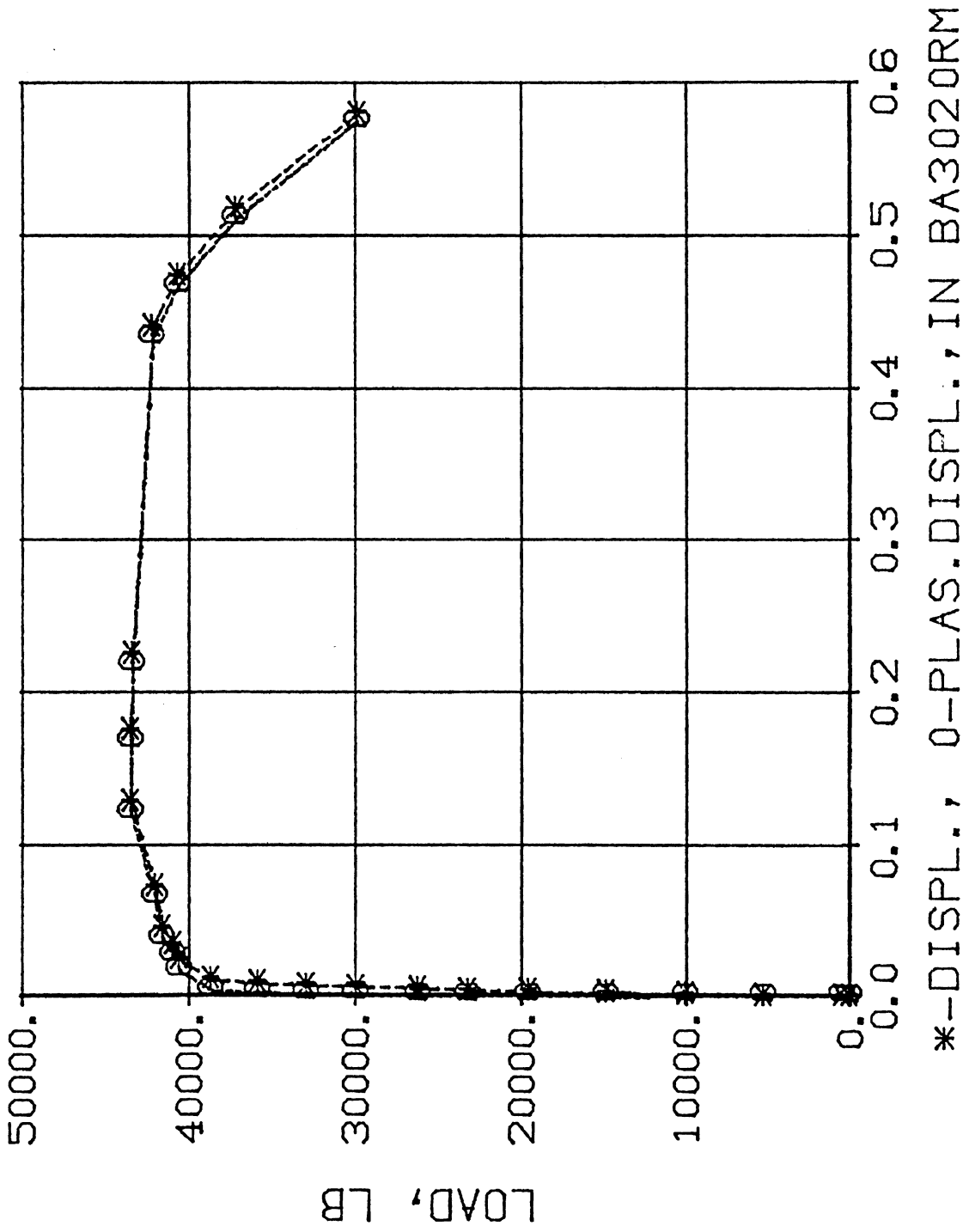
TABLE 4: GEOMETRIC PARAMETERS FOR SCALING LAWS

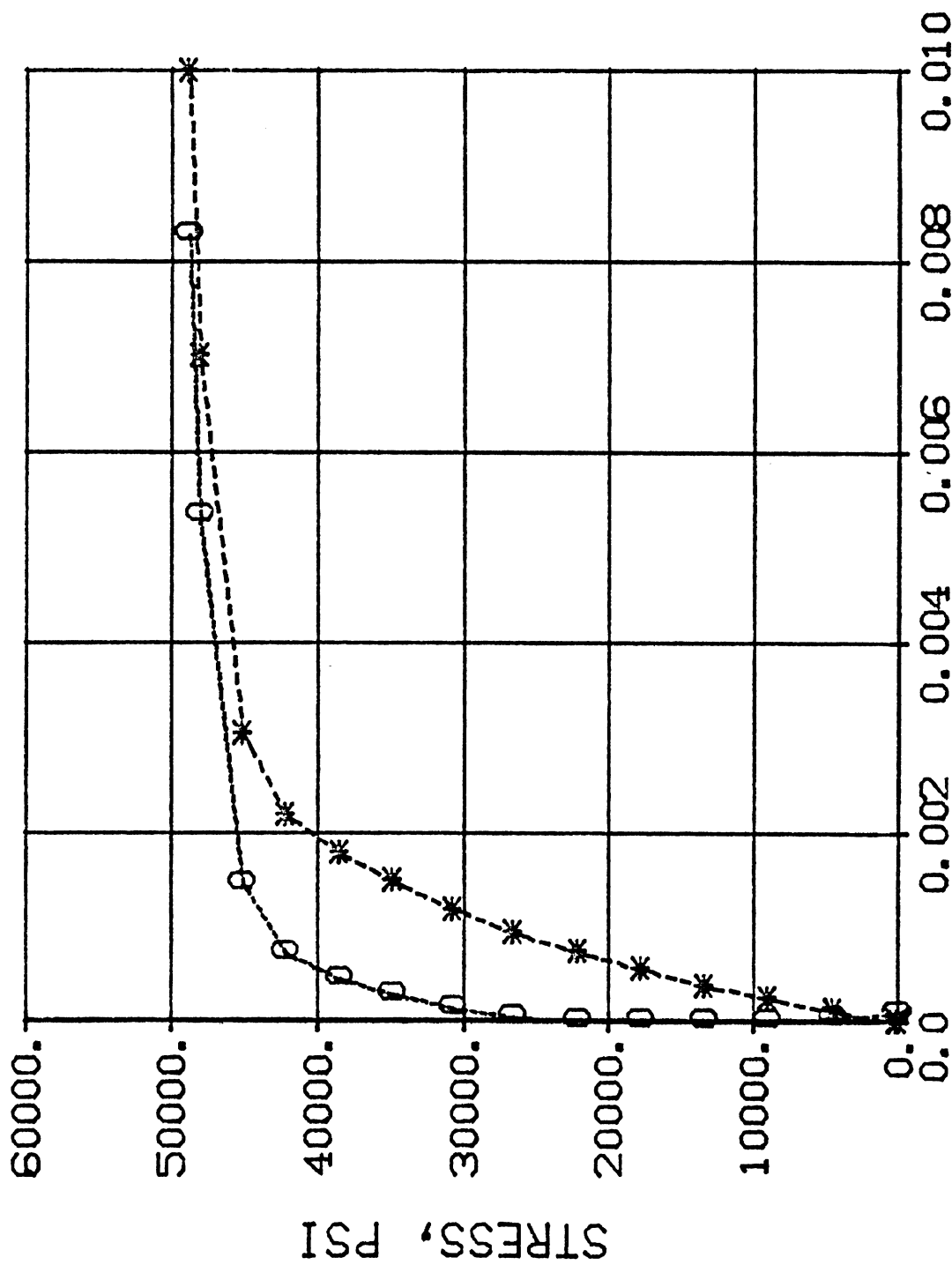
7. APPENDIX B: HINGE DATA BANK

NOTE: In the figures to follow, axial strain is given the conventional interpretation but displacement and rotation are given as half-displacement and half-rotation. This definition of hinge deformation is the required form for an interior hinge in The University of Michigan computer simulation.

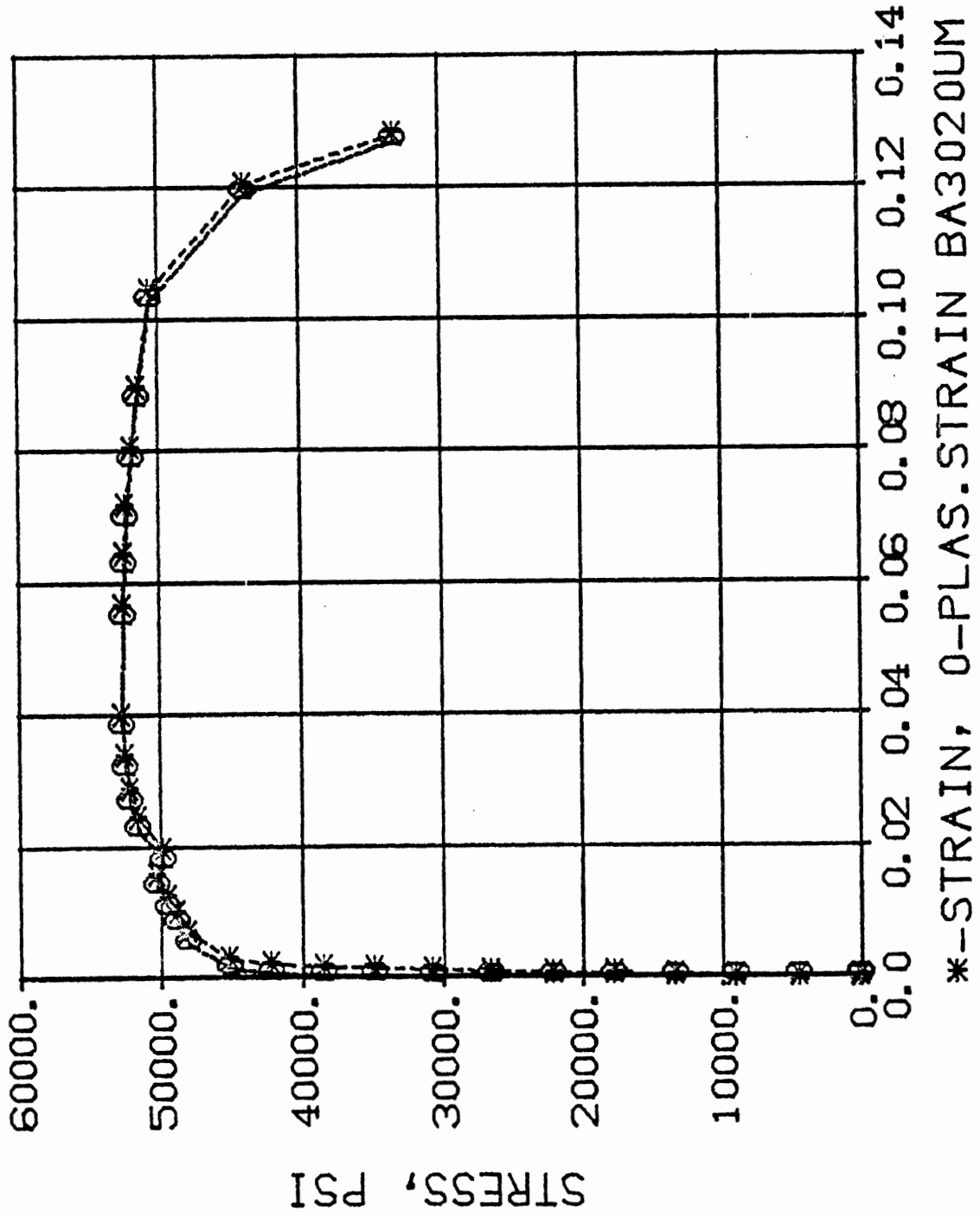


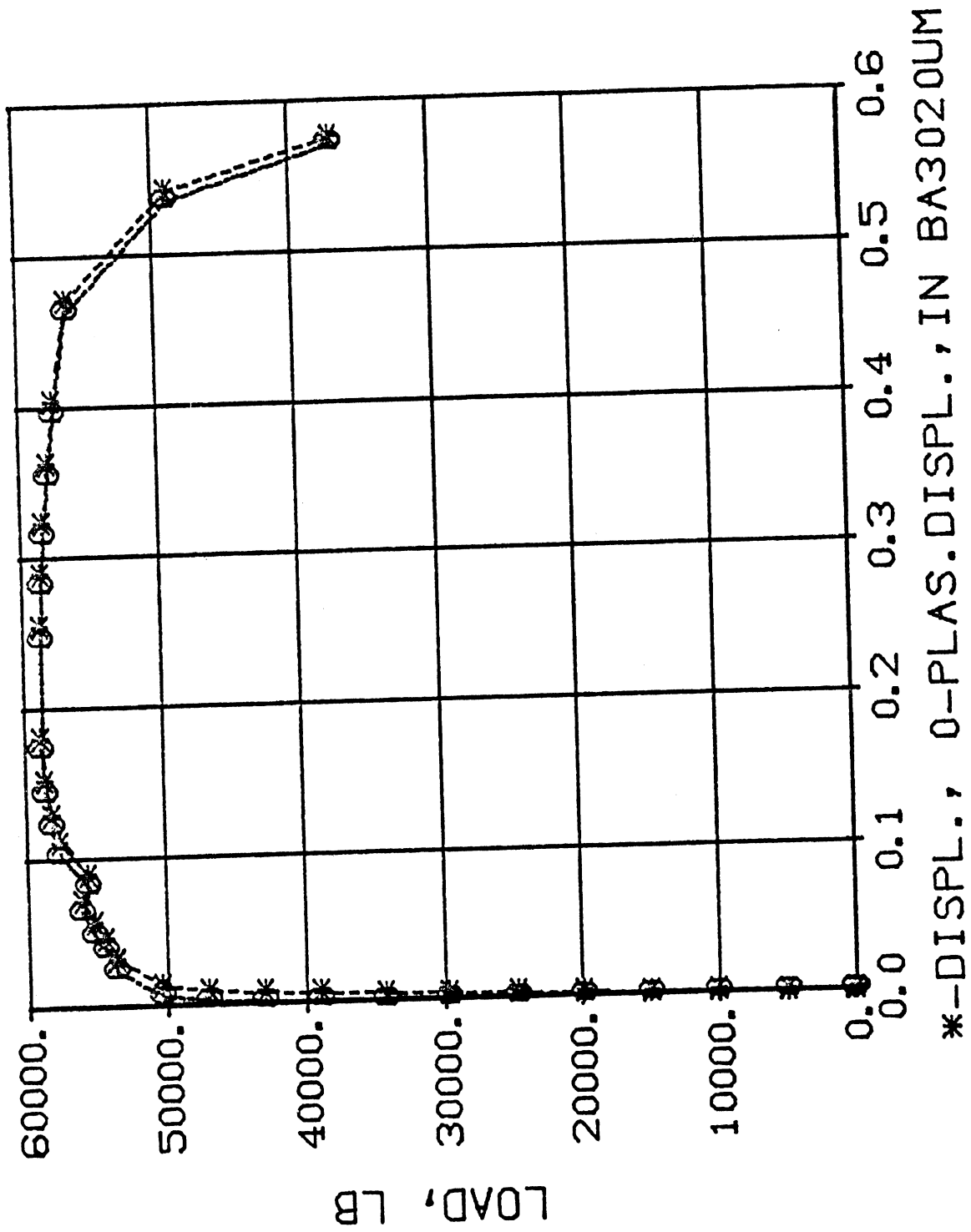


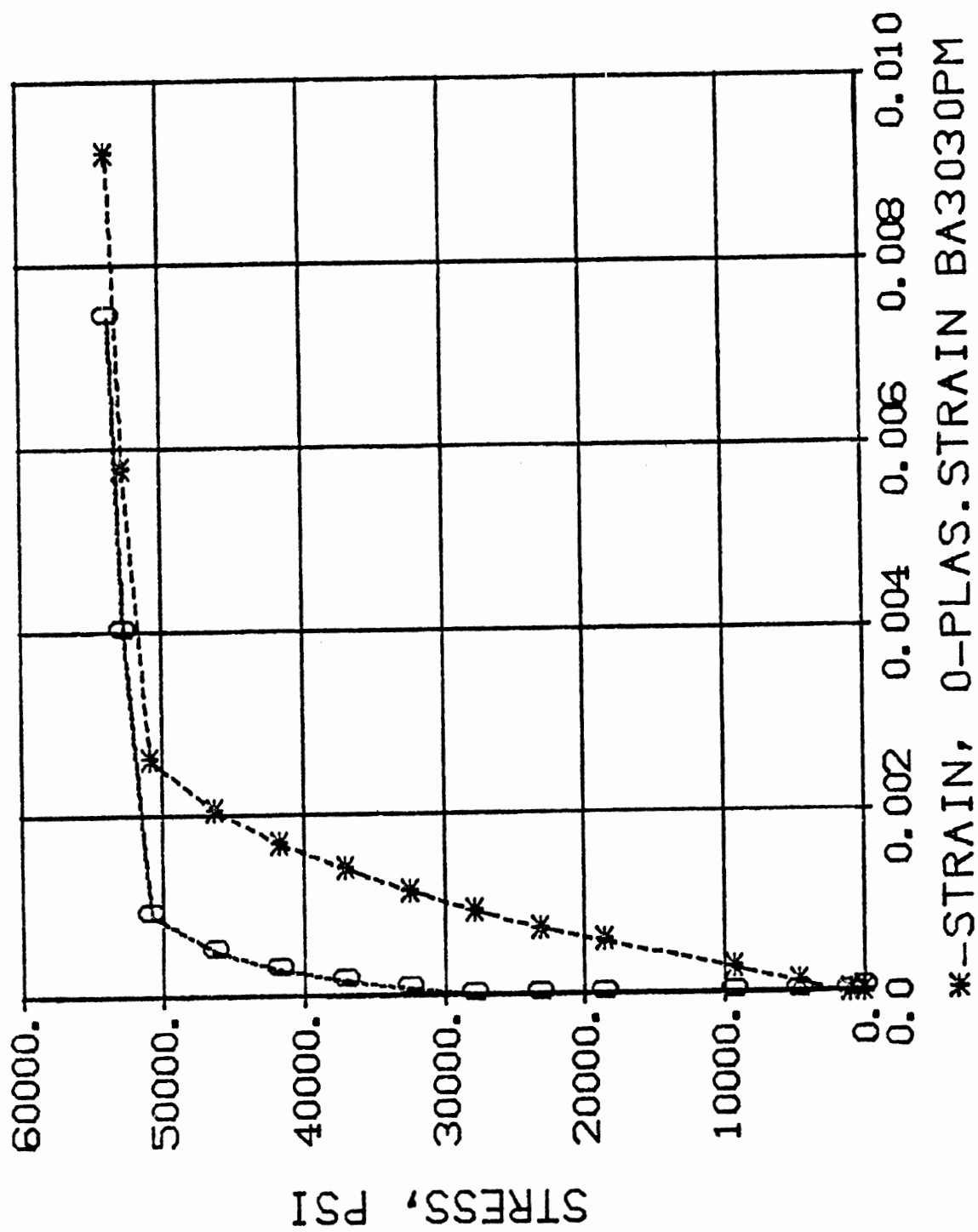


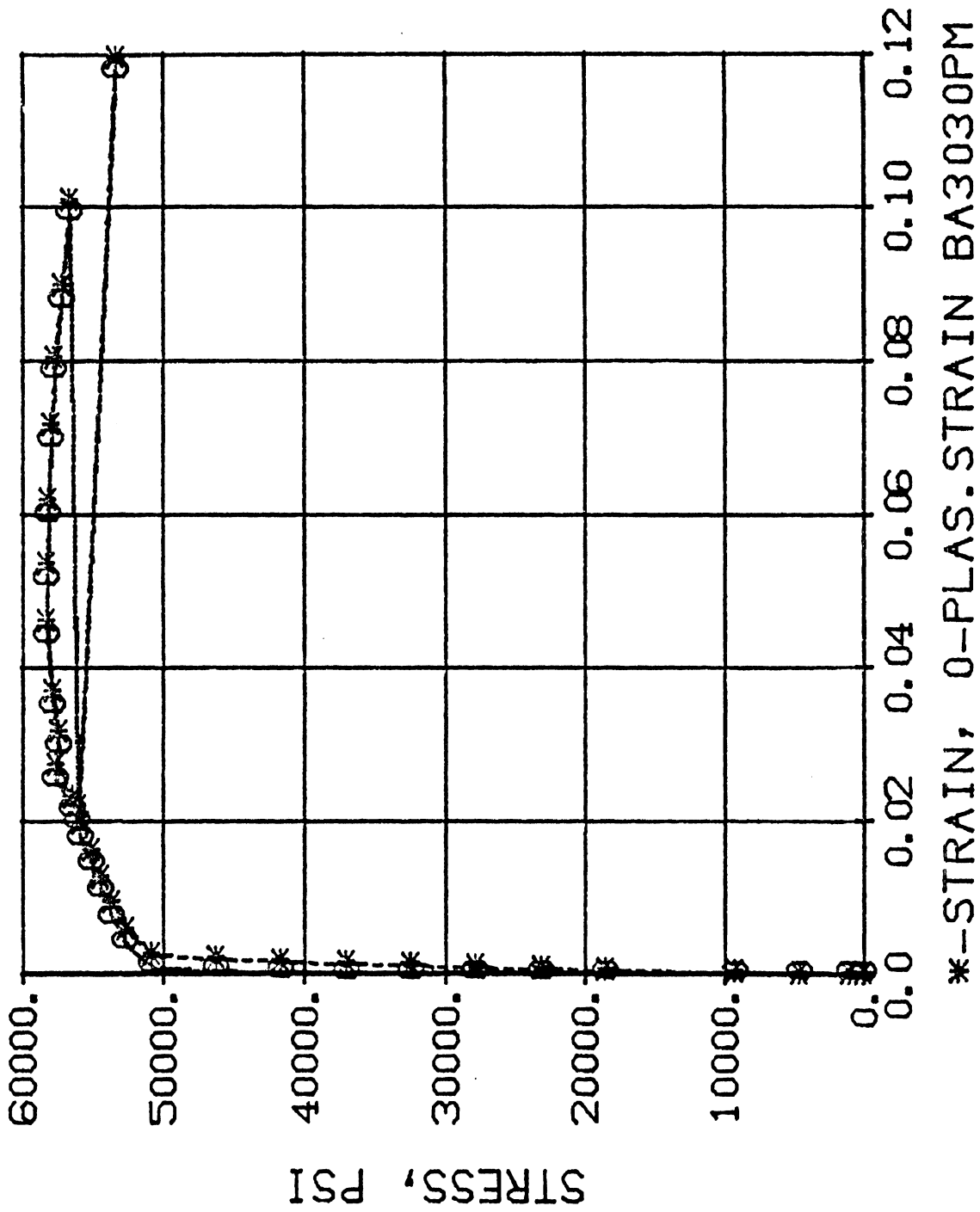


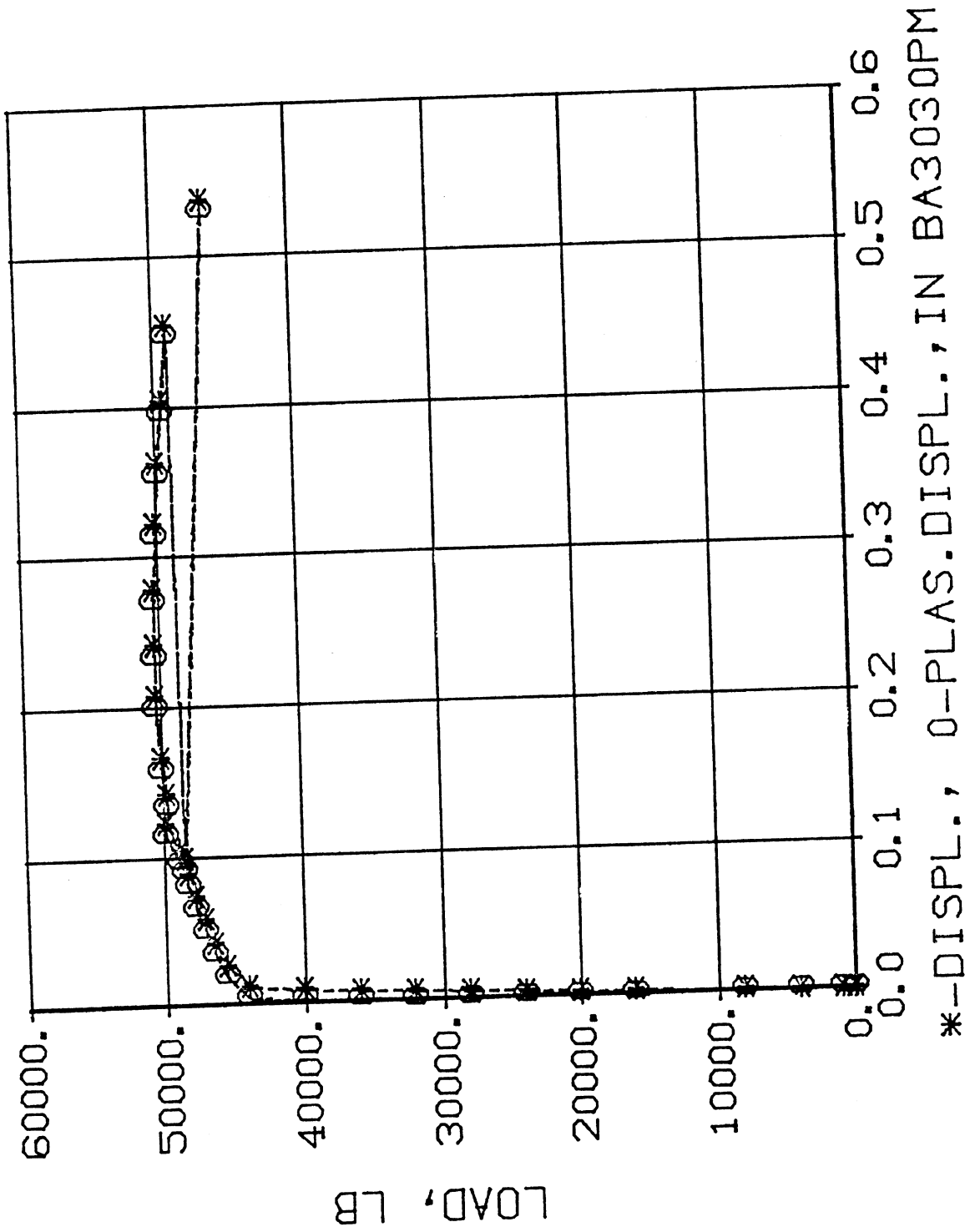
*--STRAIN, 0-PLAS. STRAIN BA3020UM

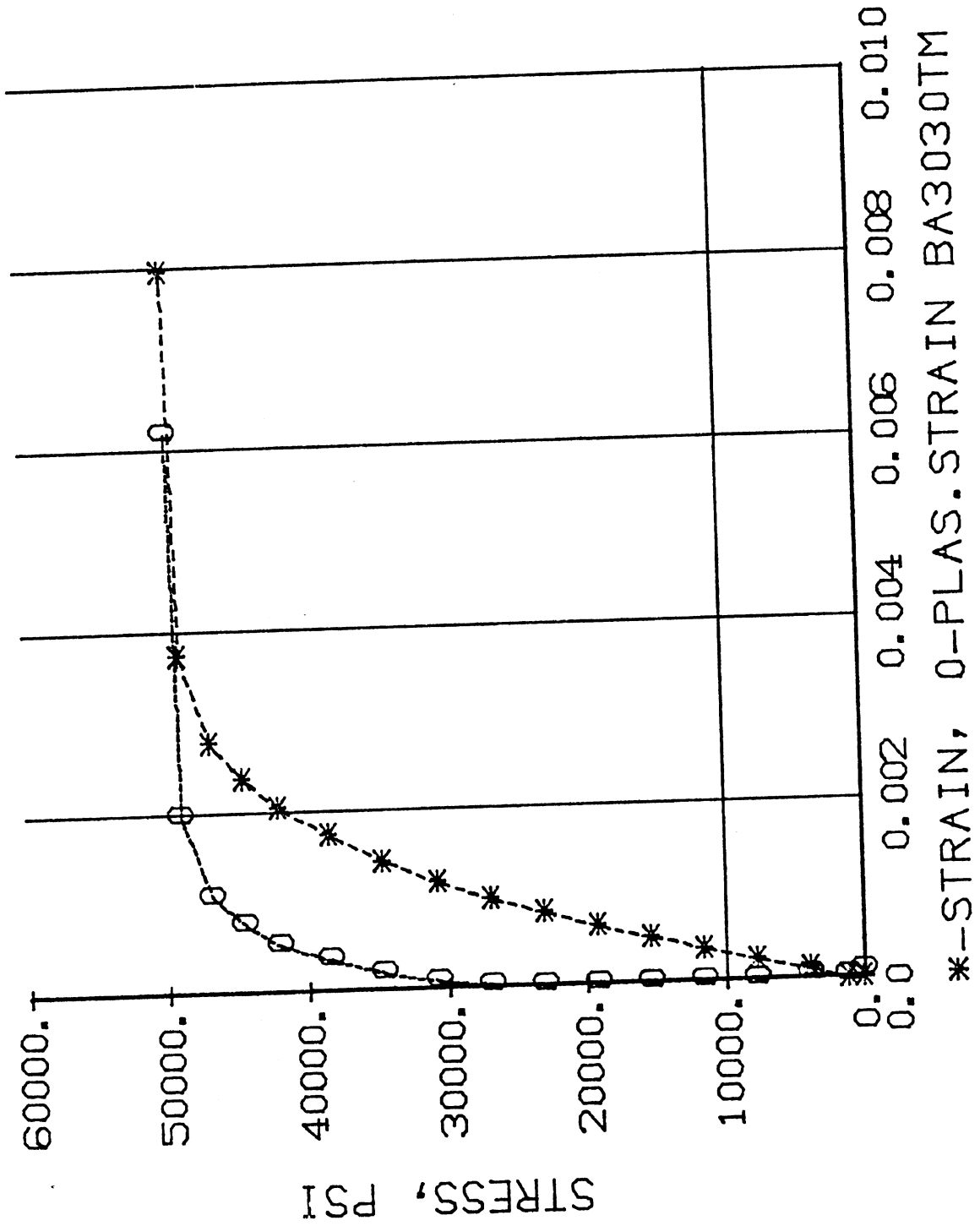


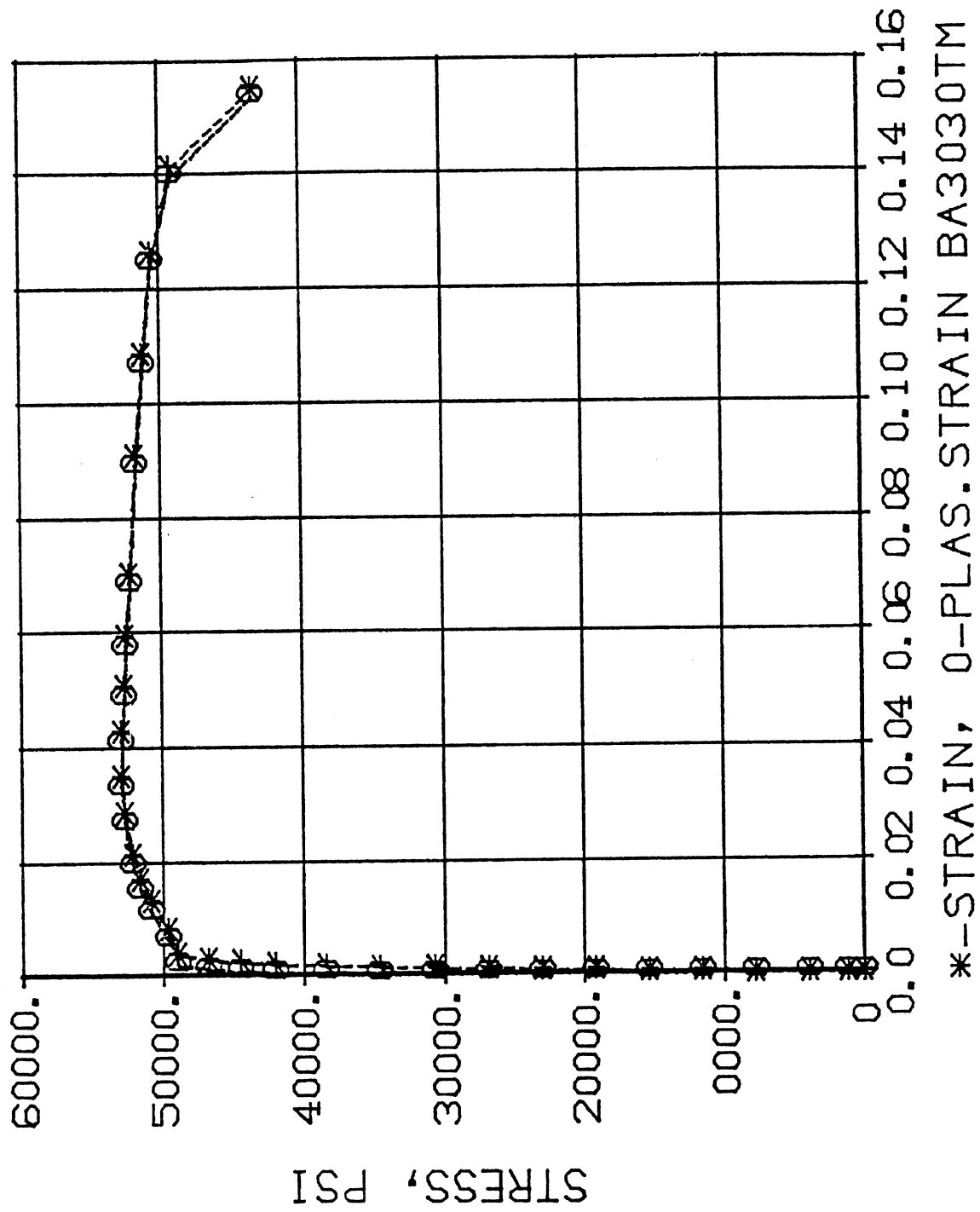


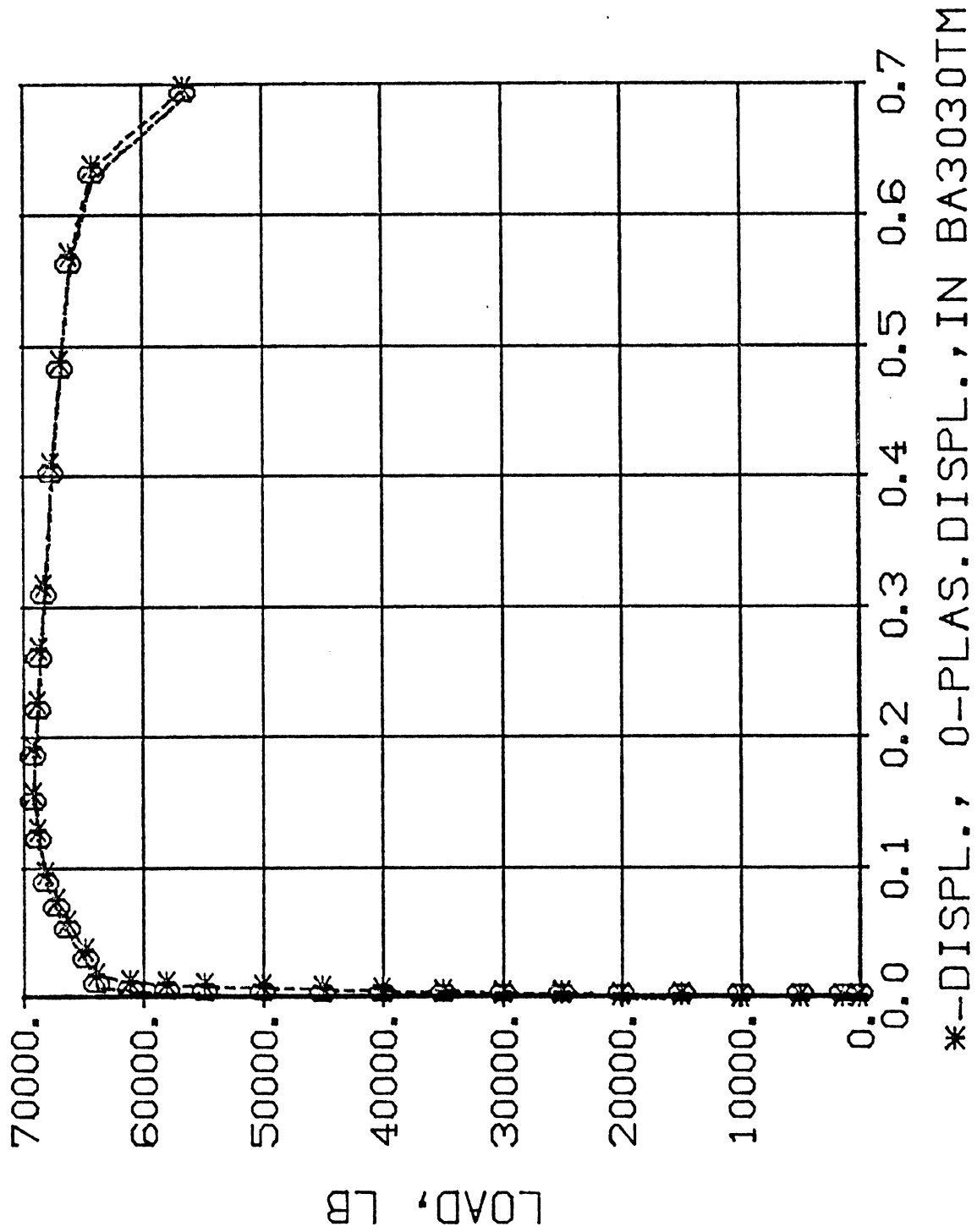


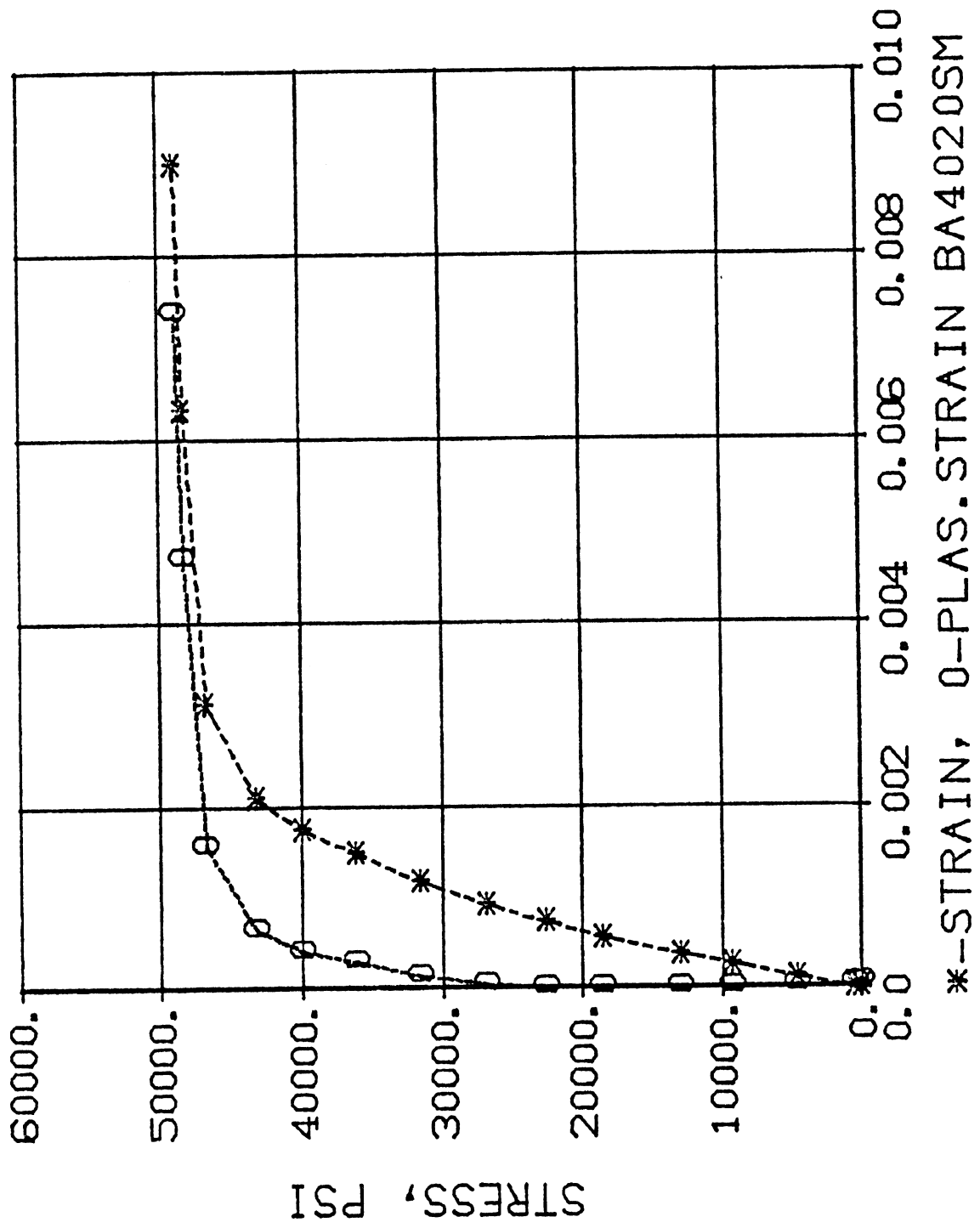


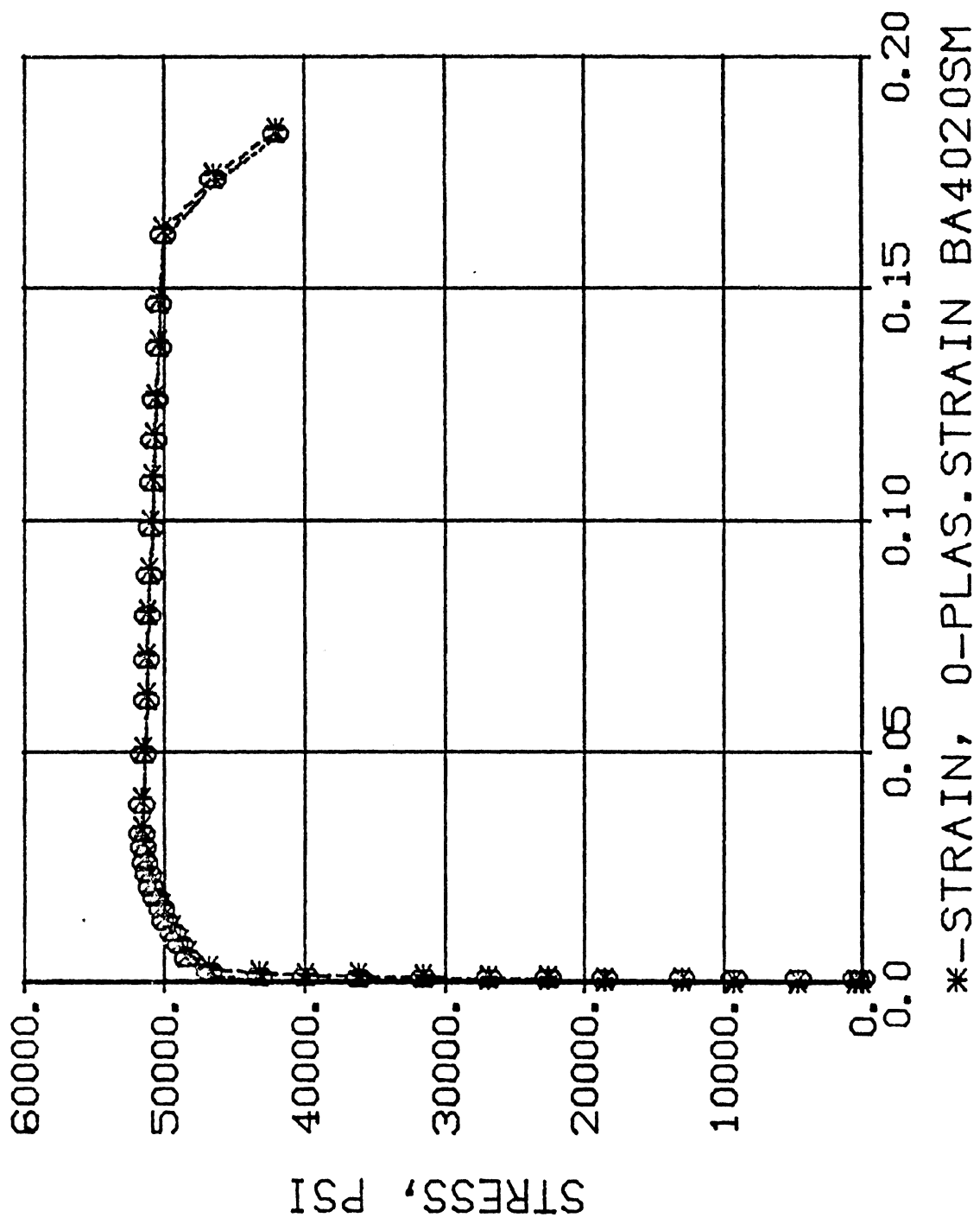


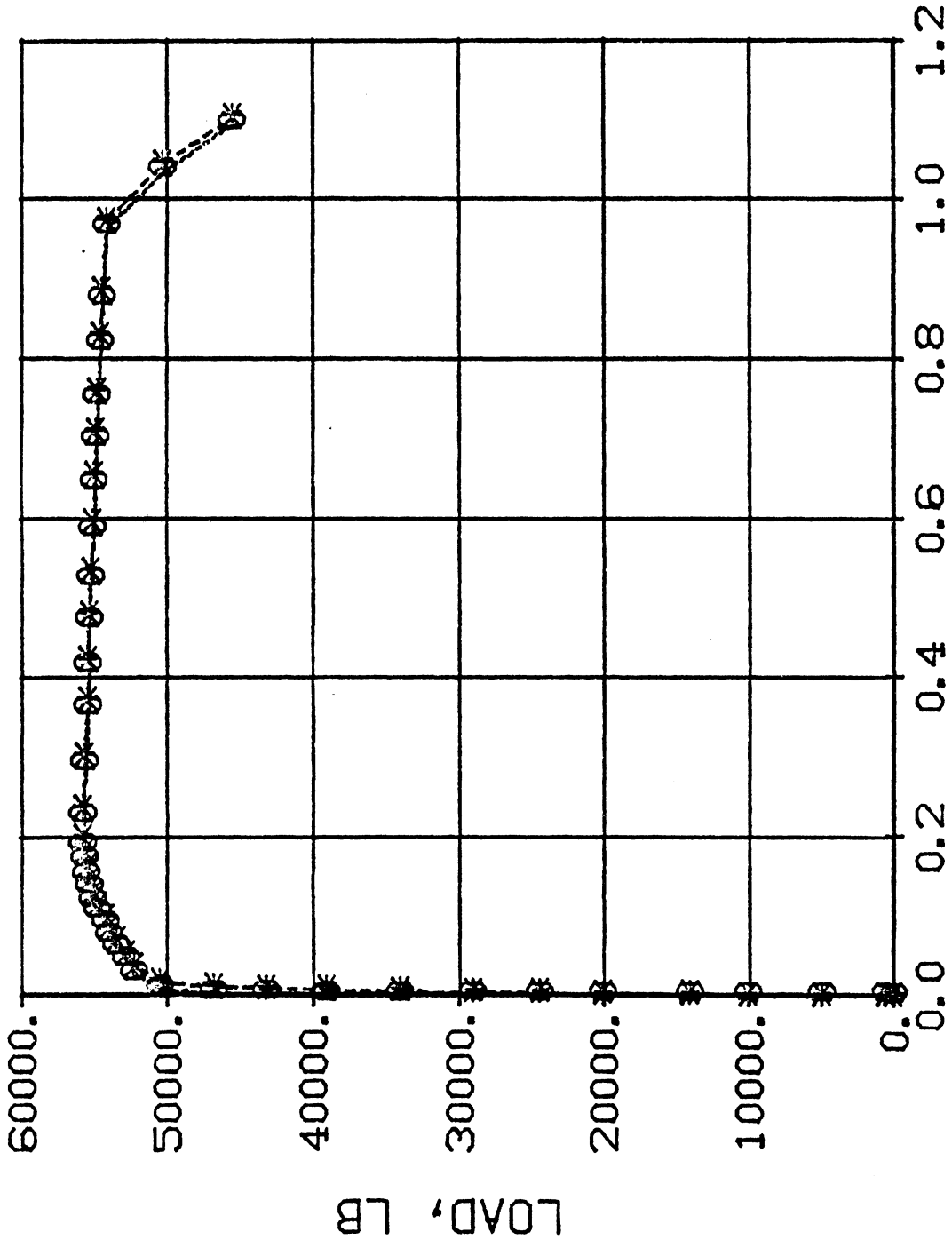




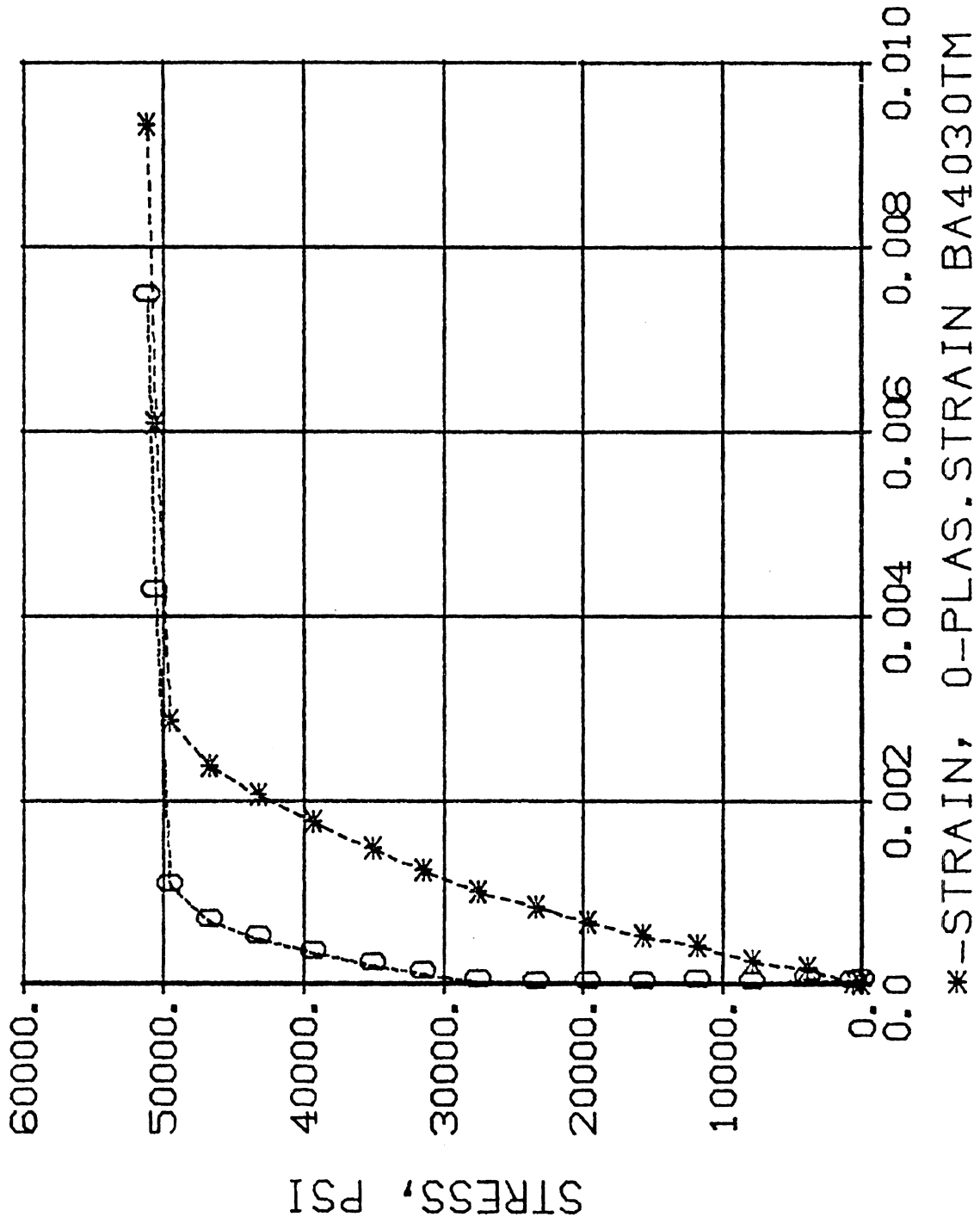


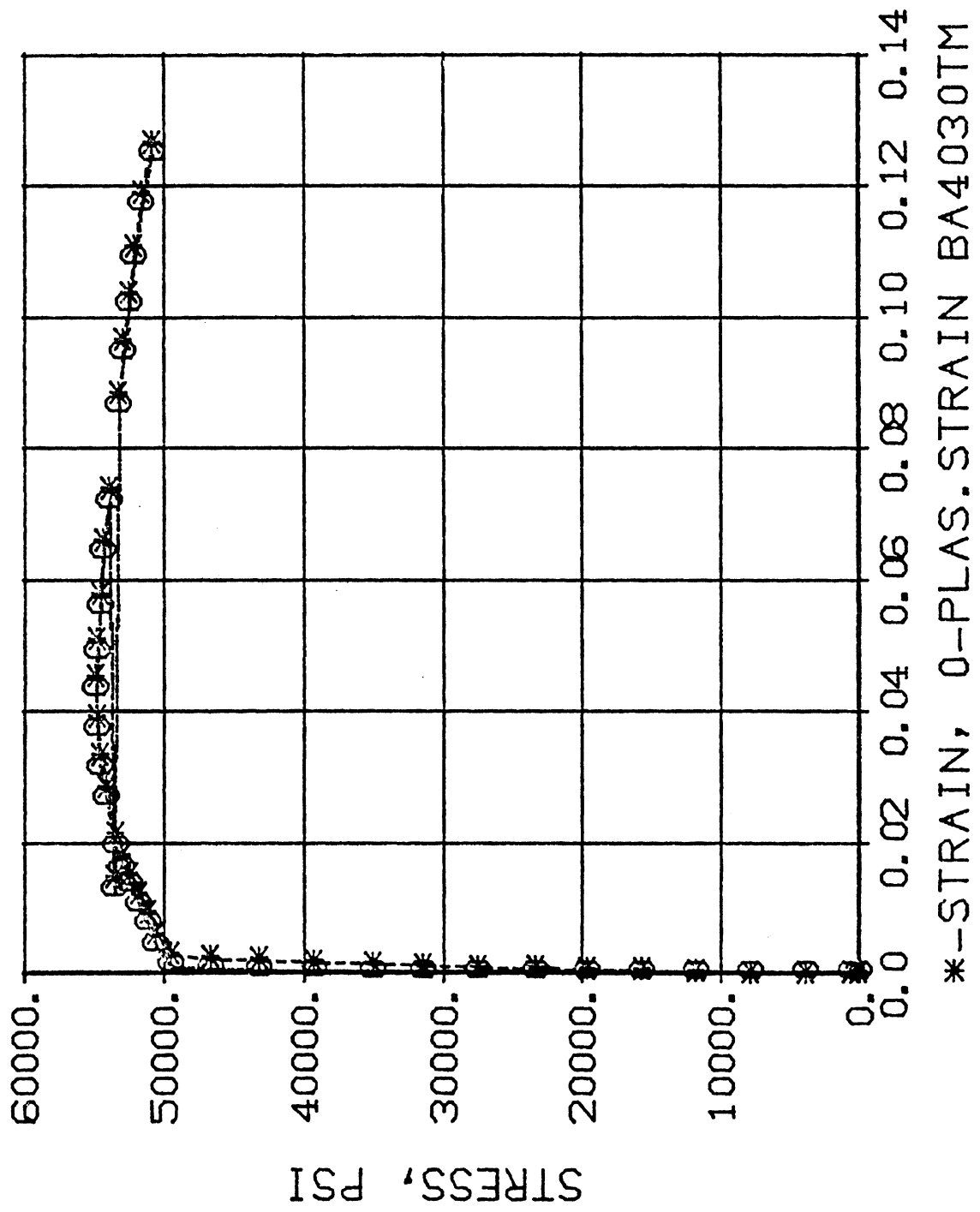


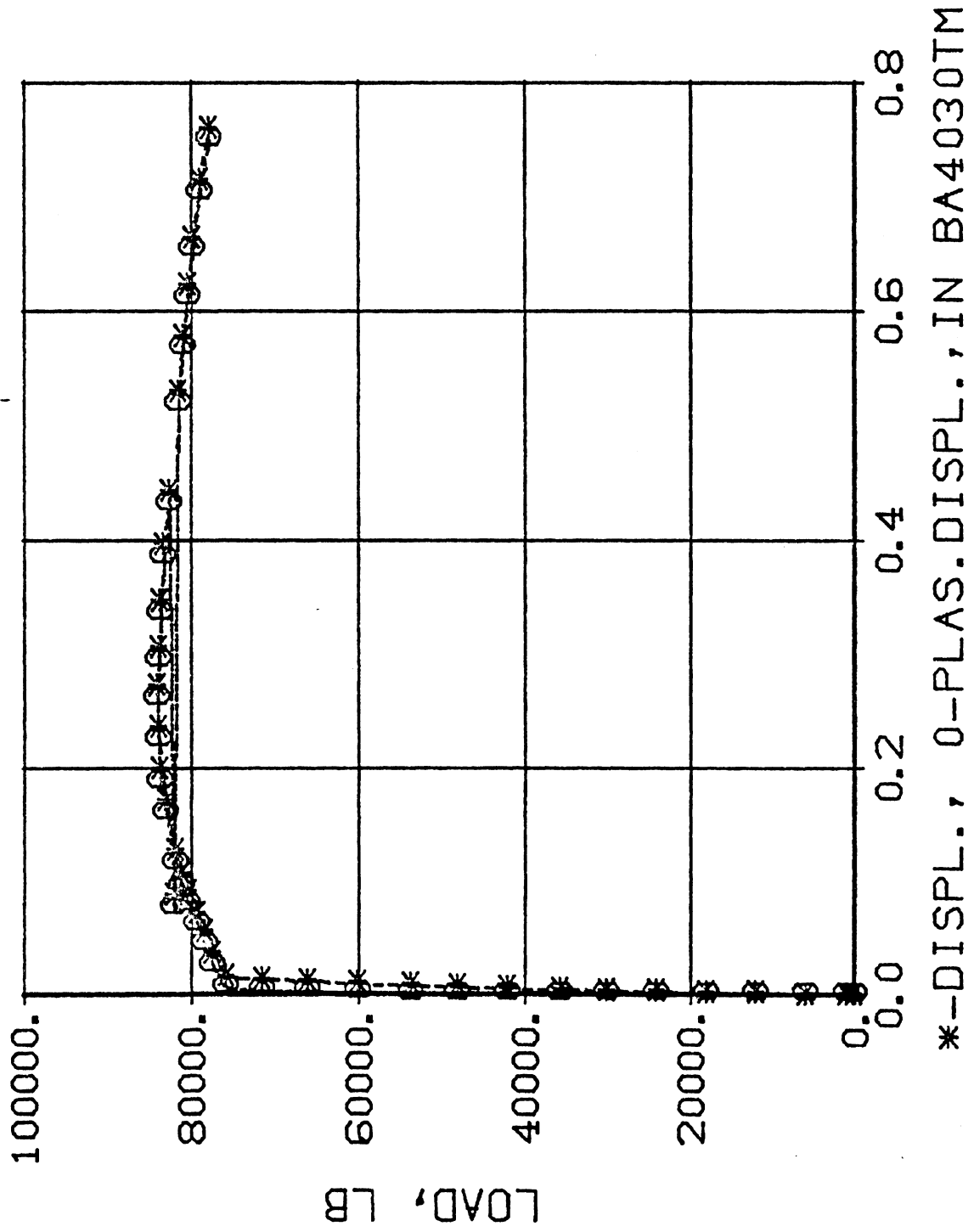


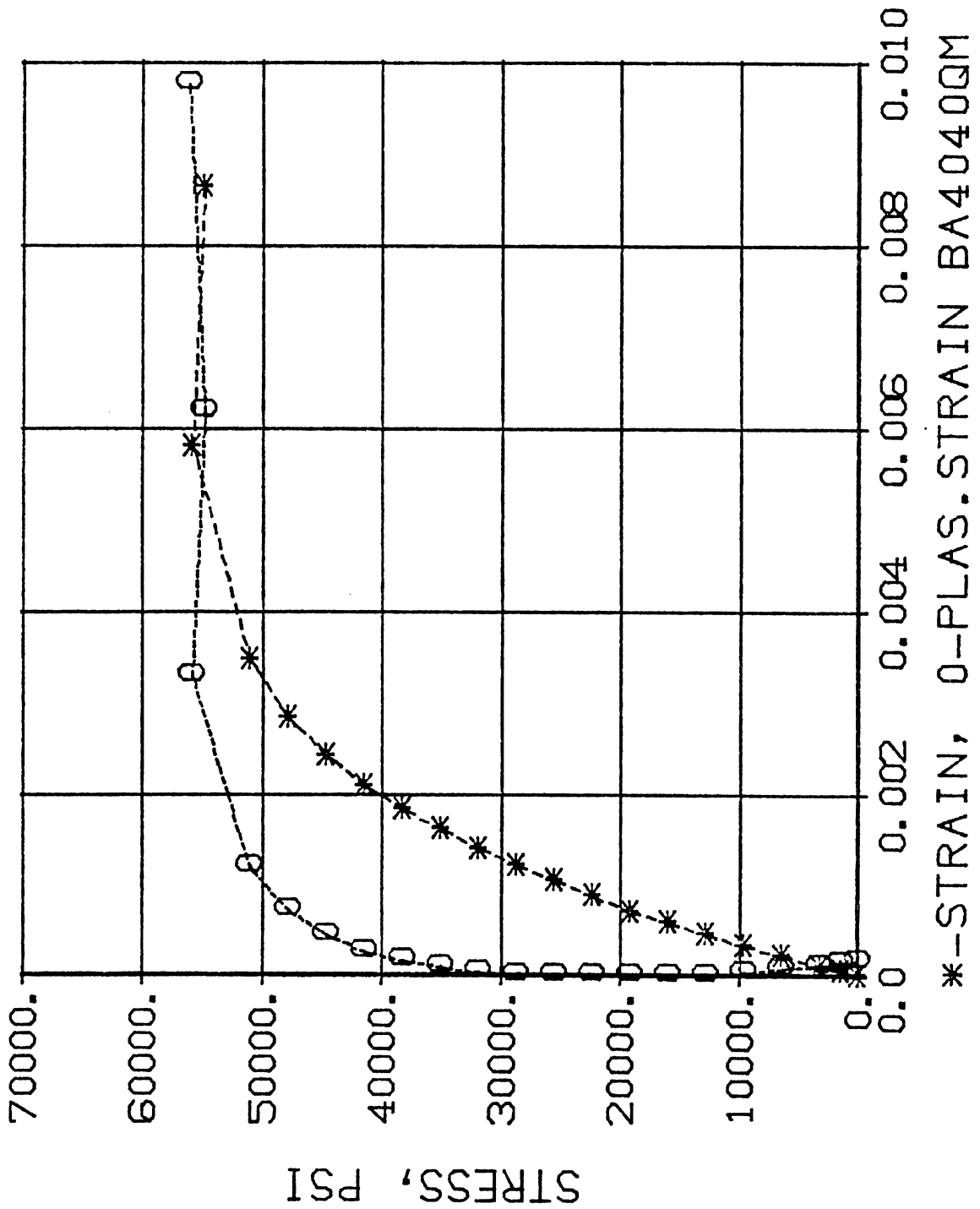


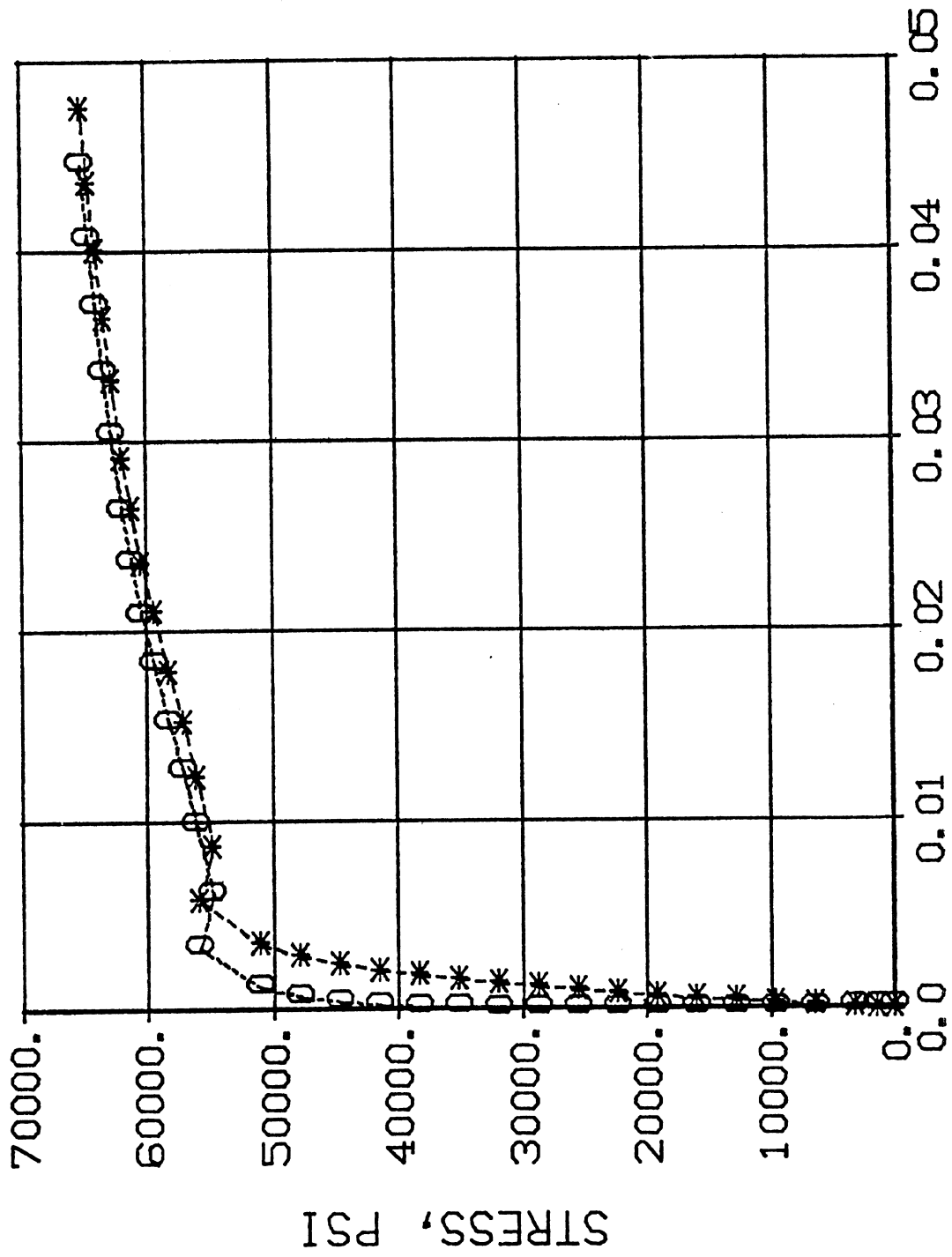
*-DISPL., 0-PLAS.DISPL., IN BA4020SM



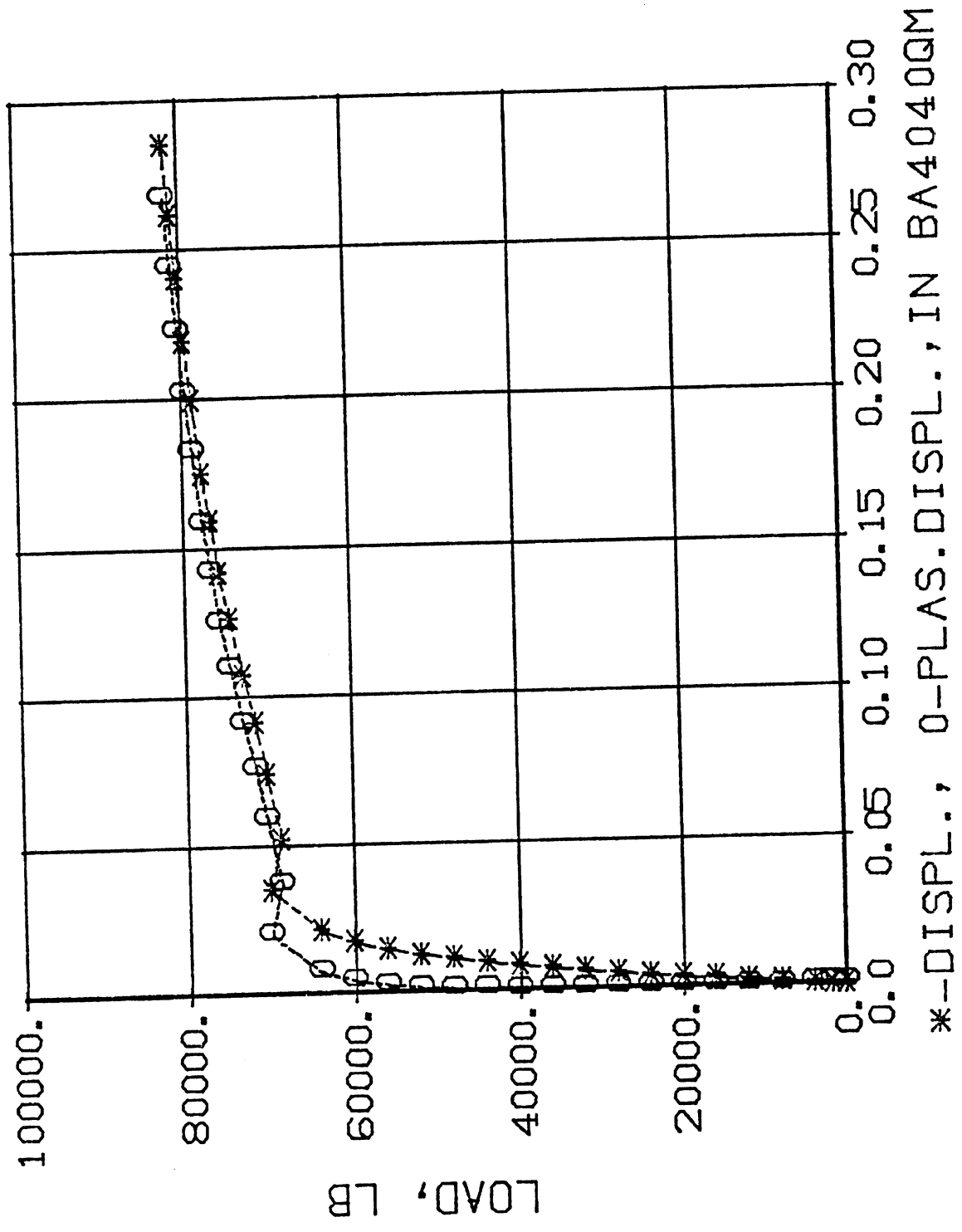


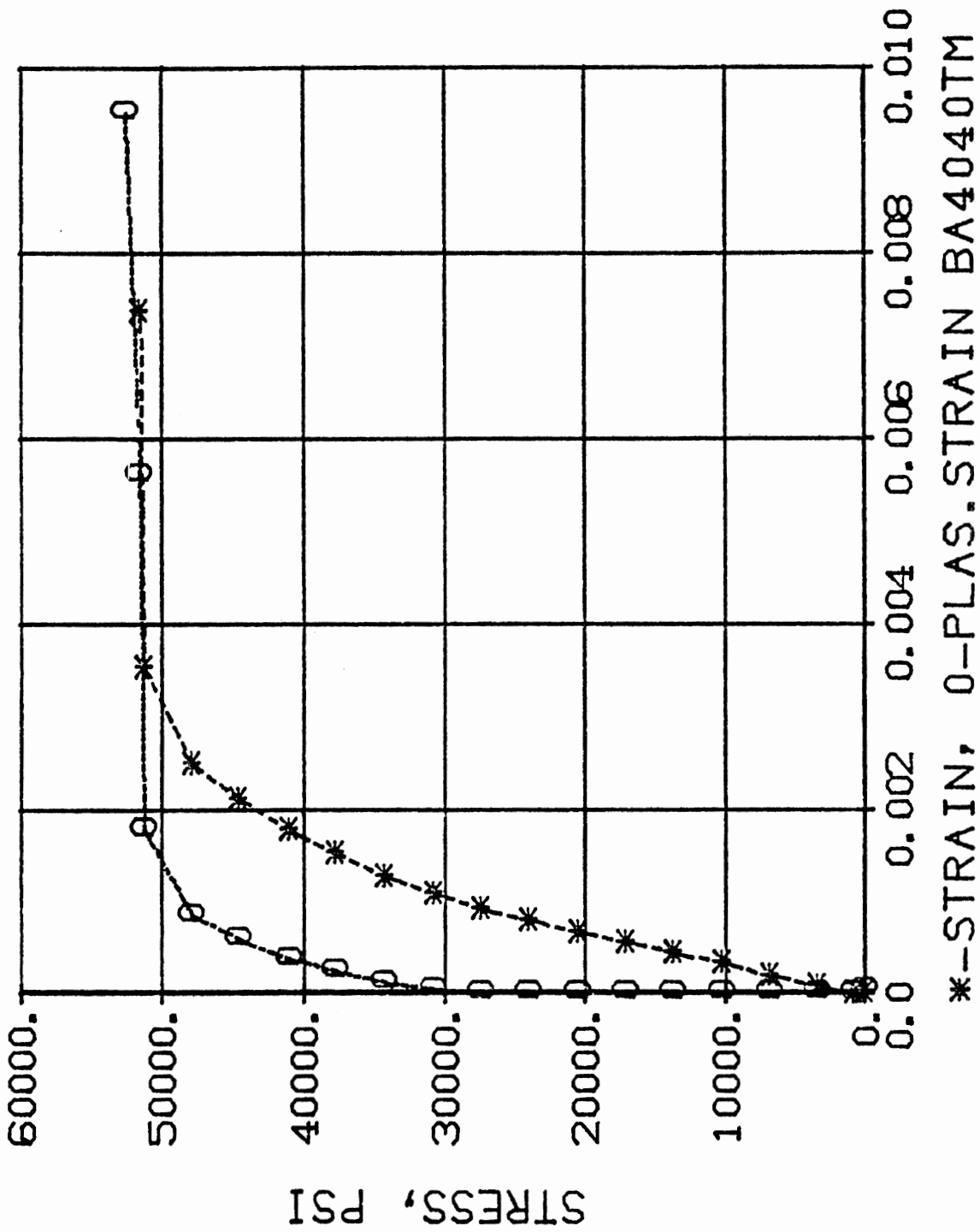


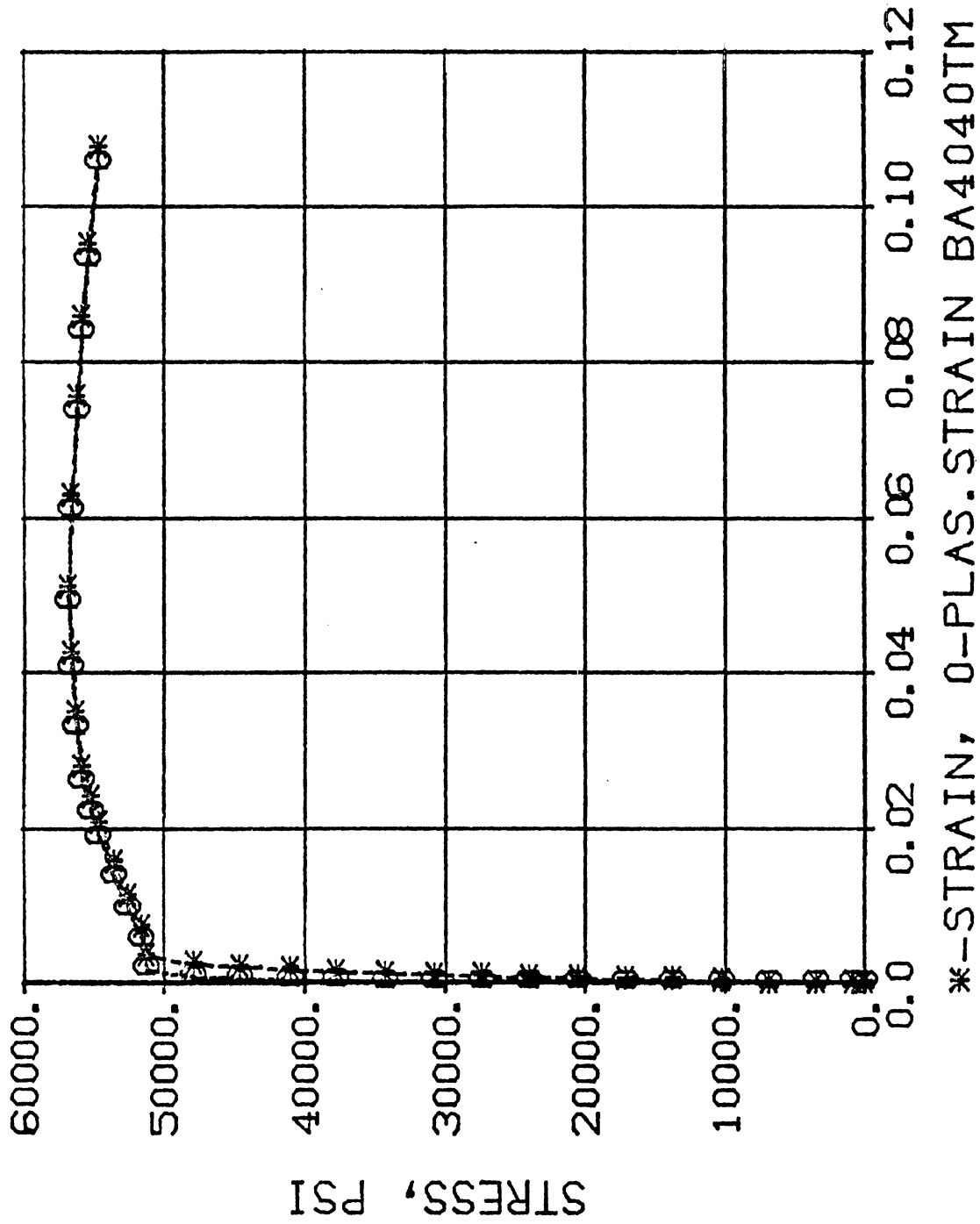


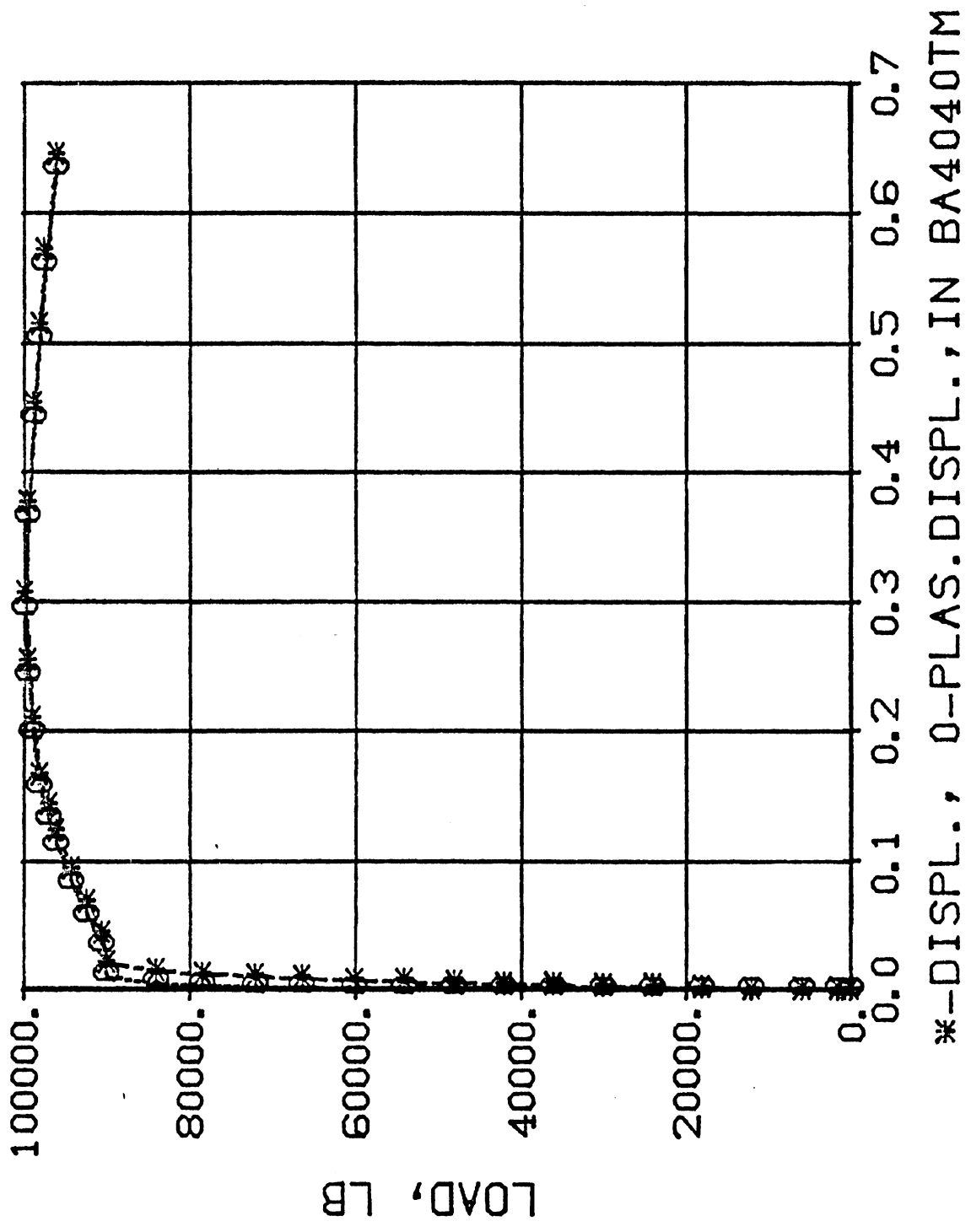


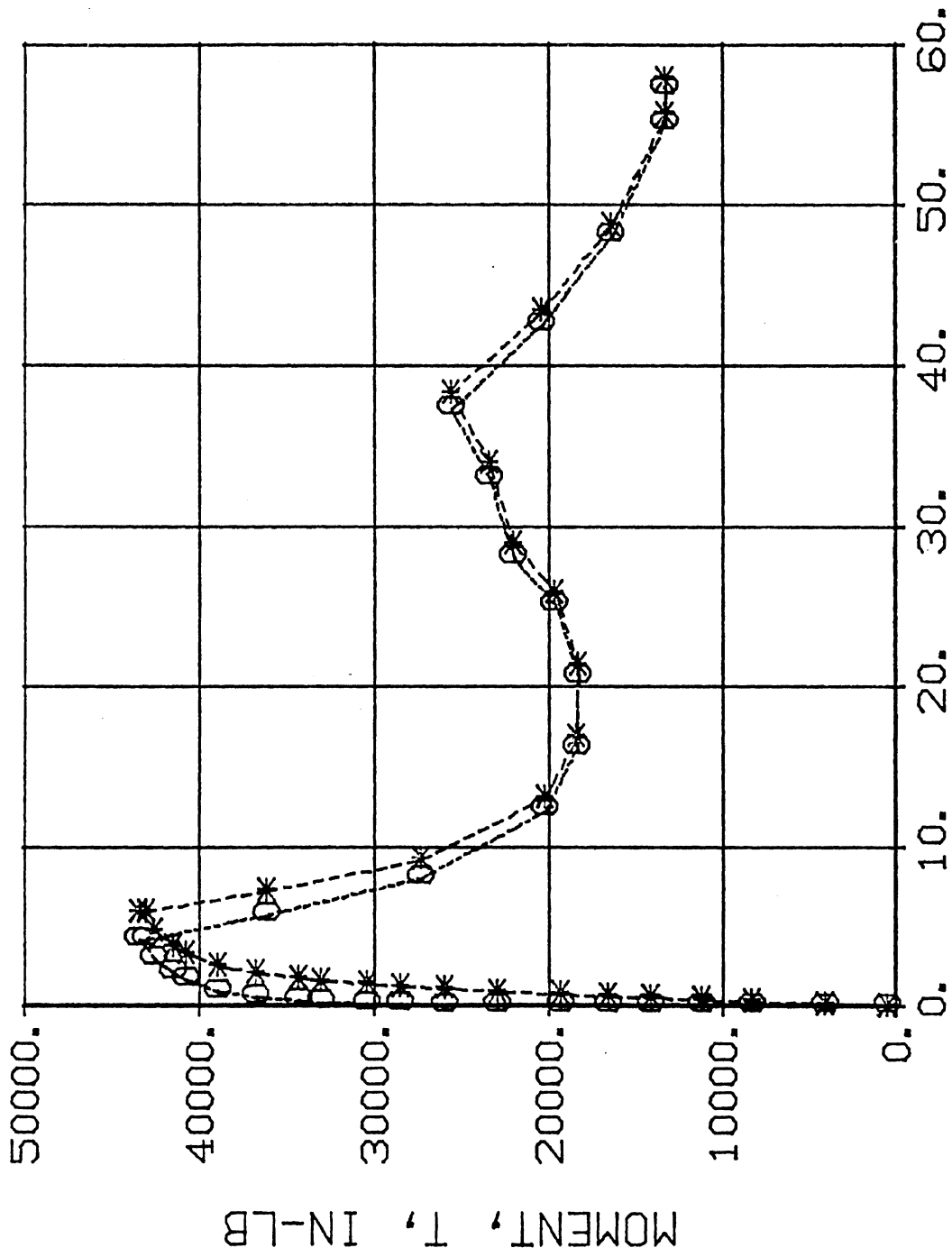
*-STRAIN, 0-PLAS. STRAIN BA4040QM



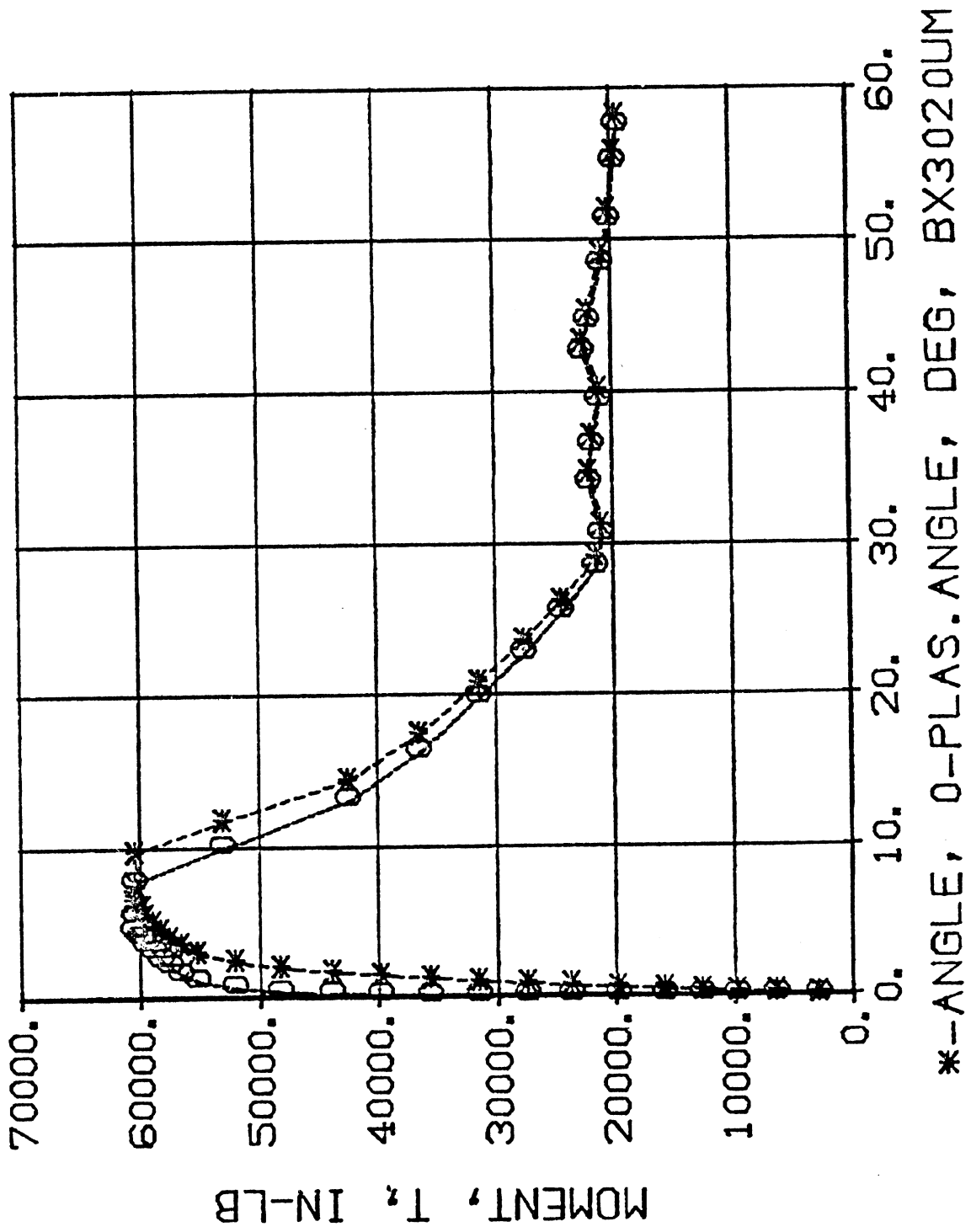


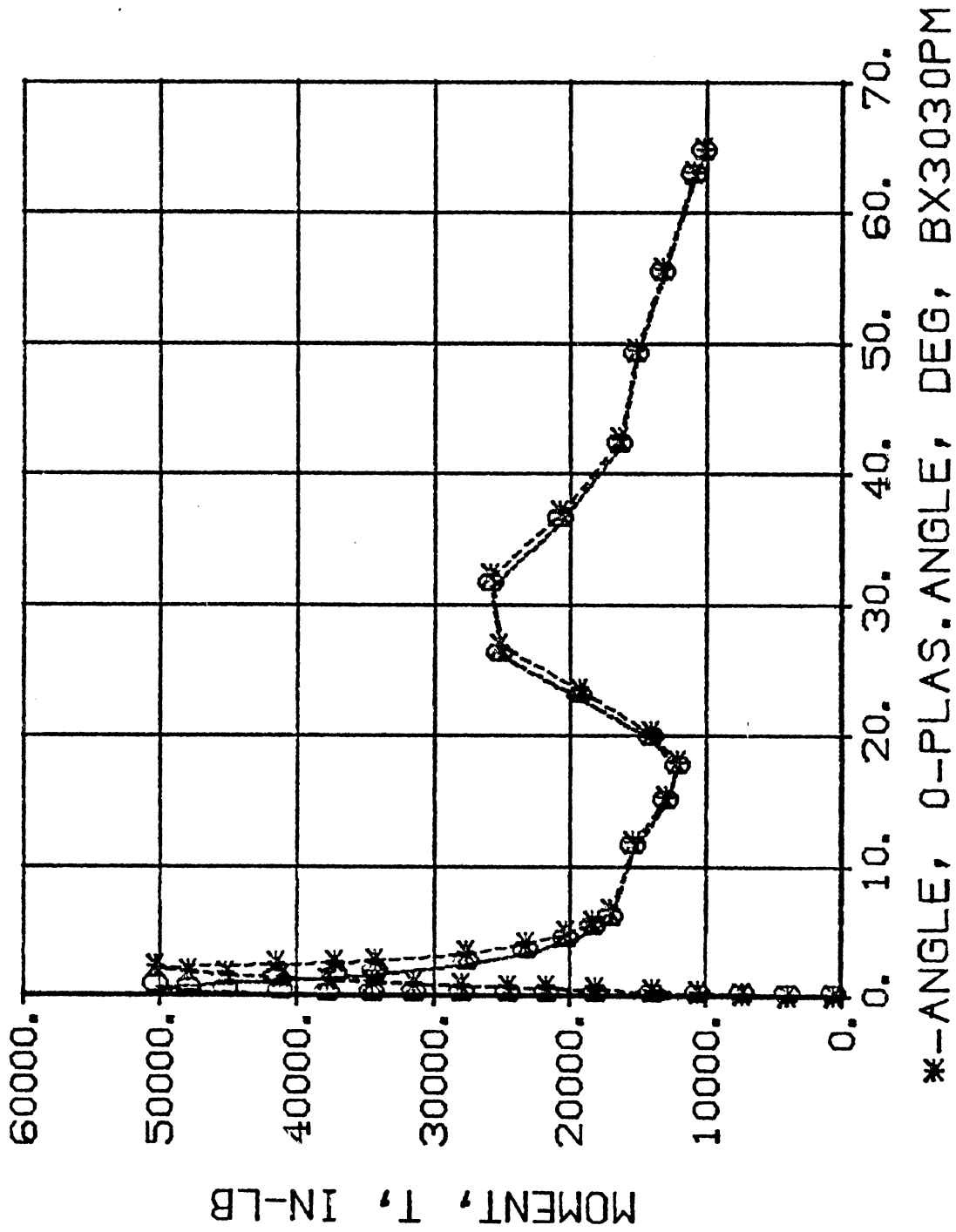


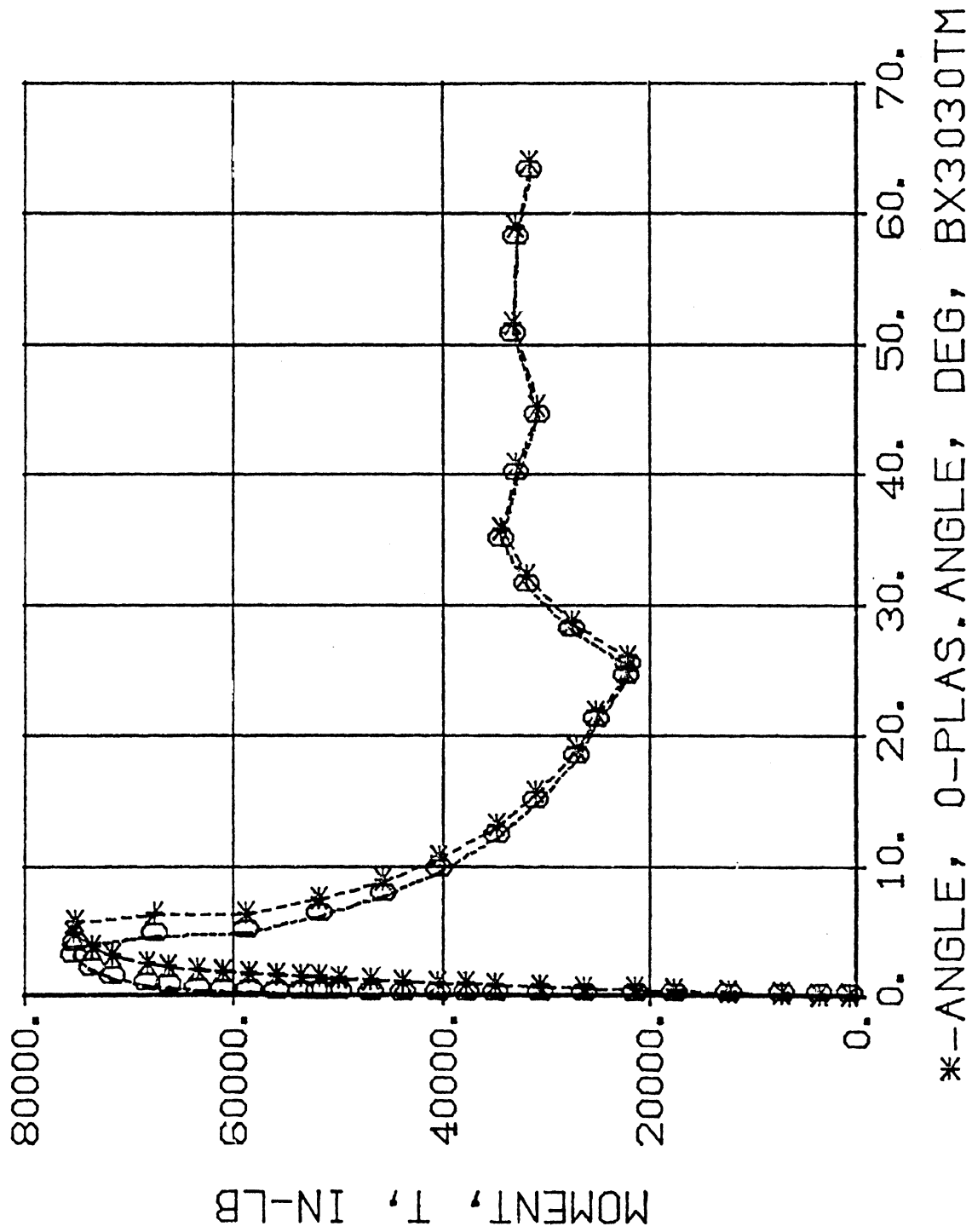


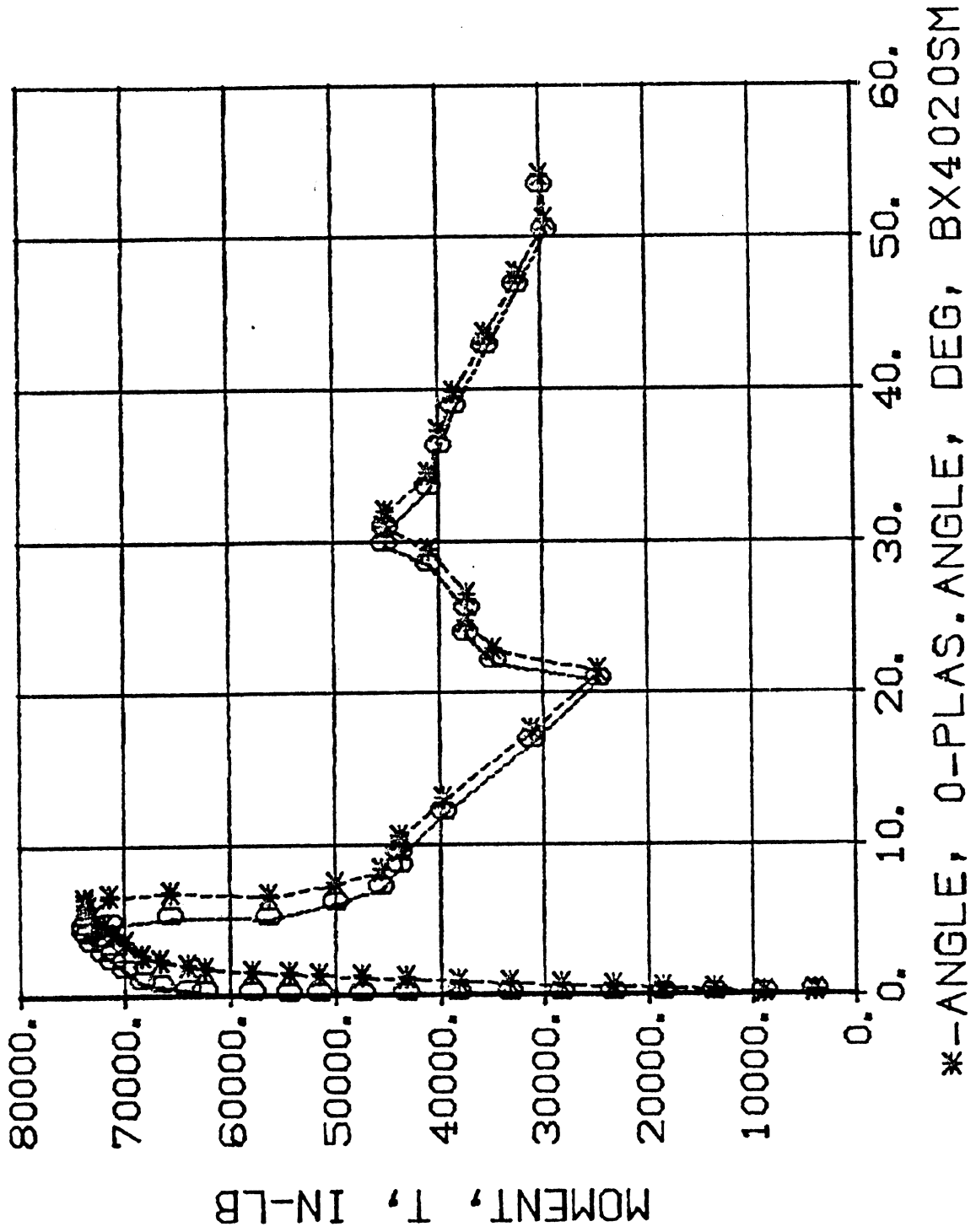


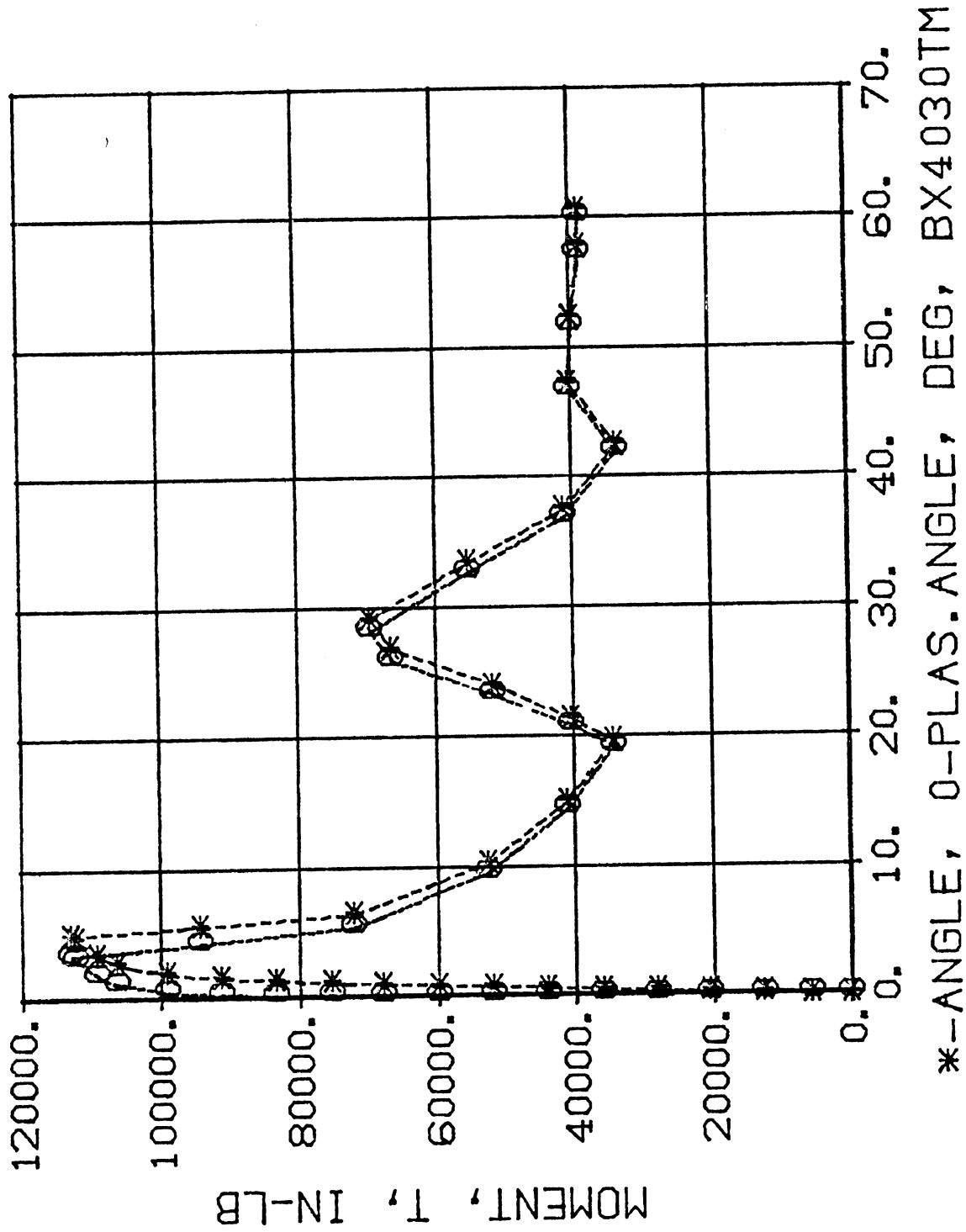
*-ANGLE, O-PLAS. ANGLE, DEG, BX3020RM

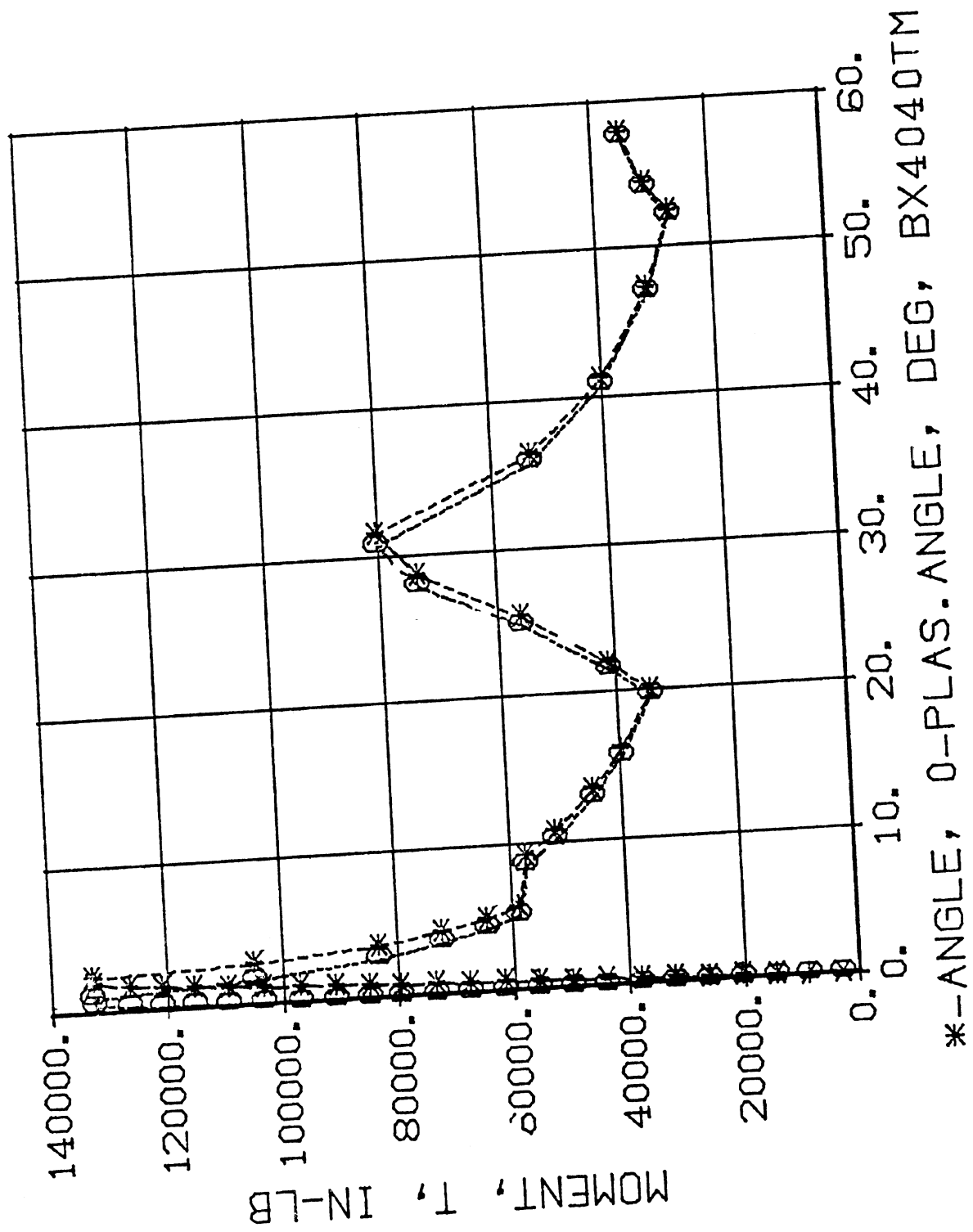


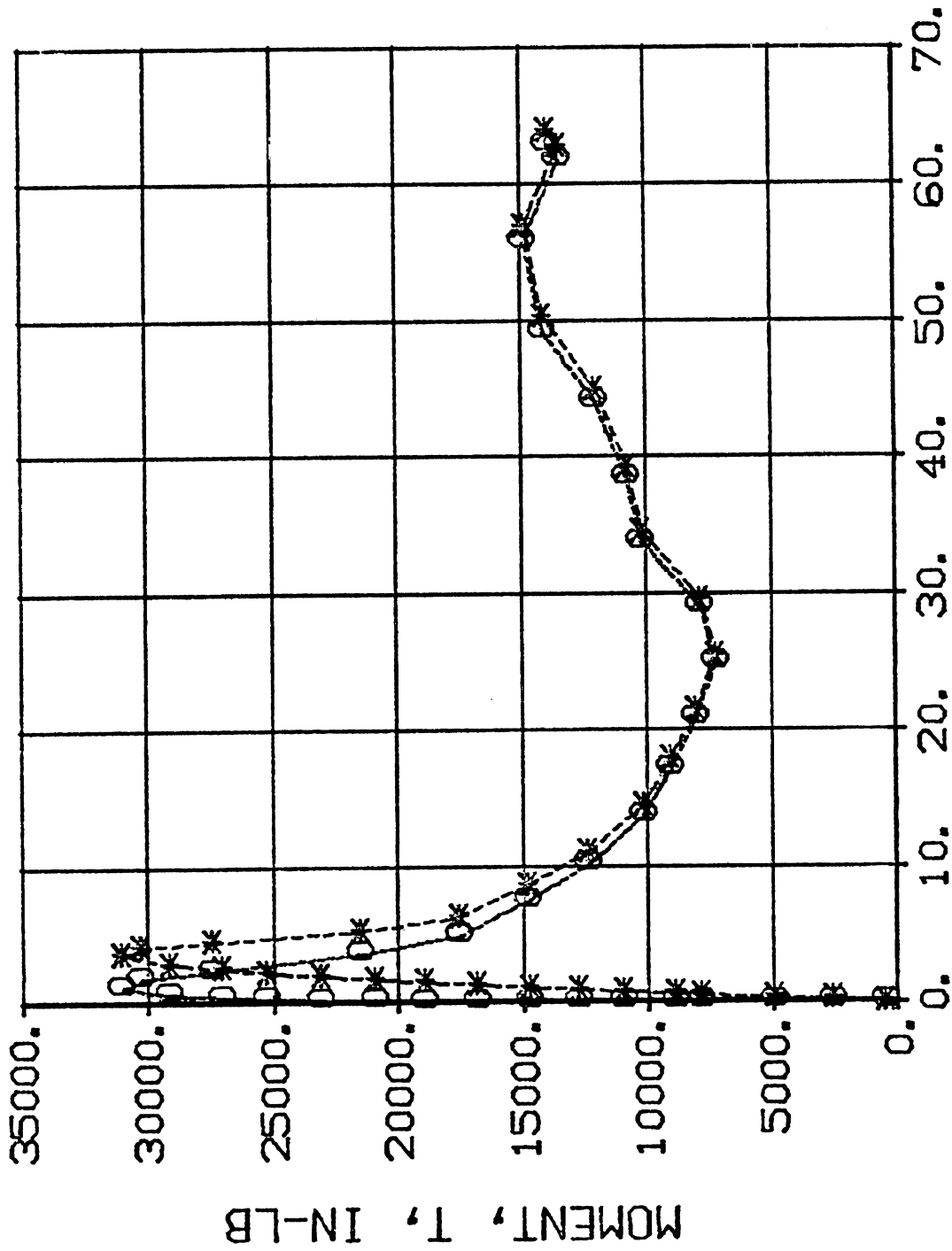




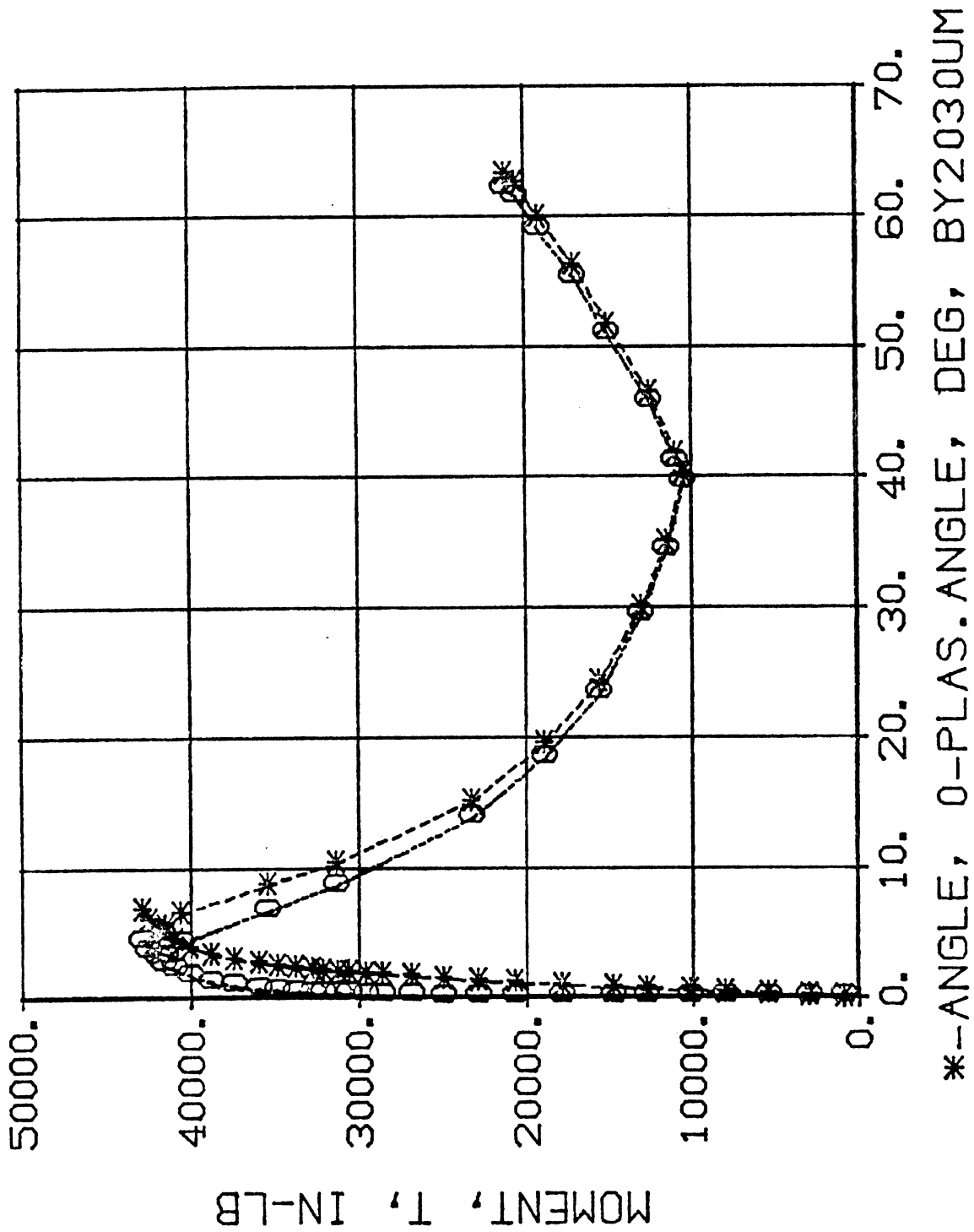


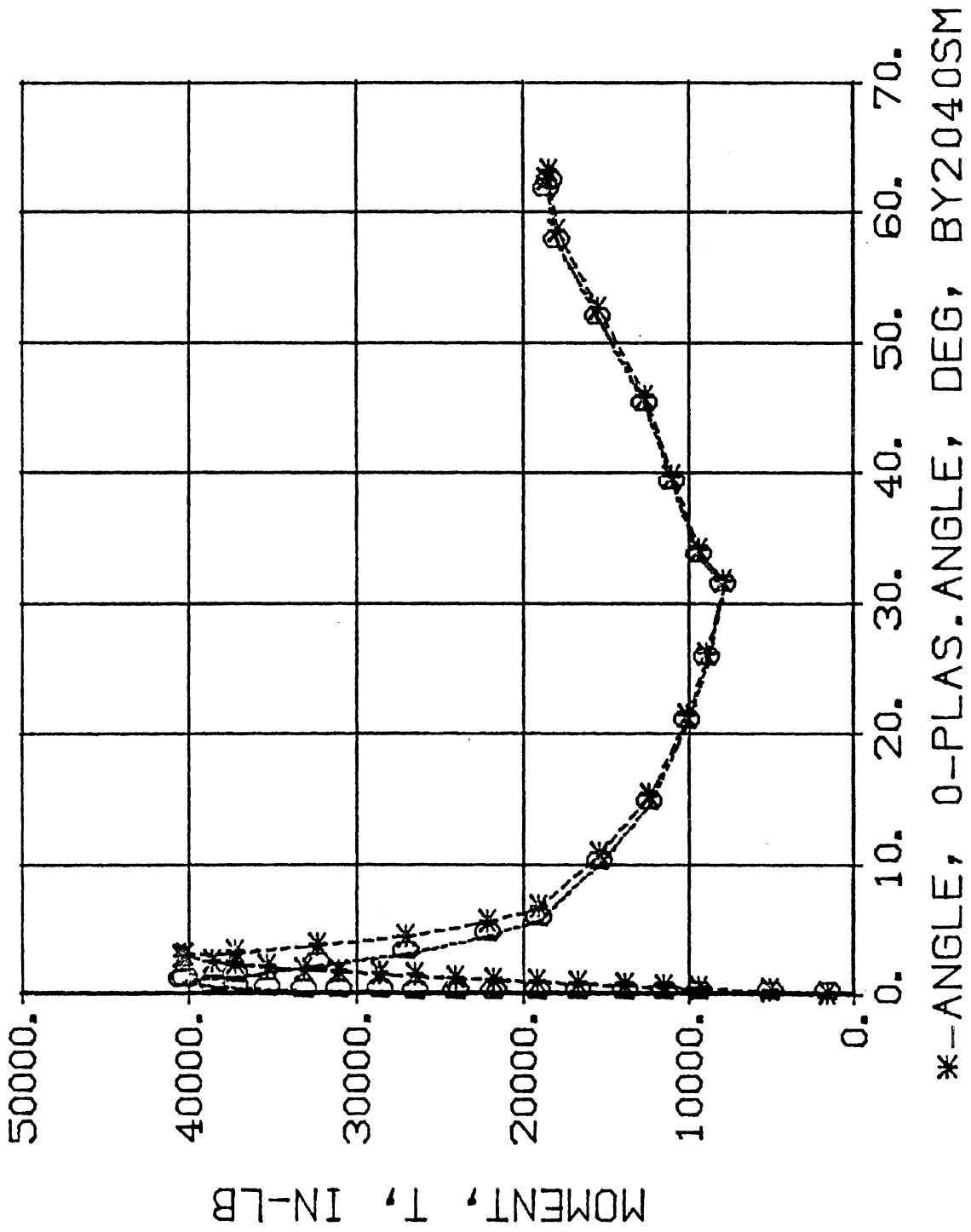


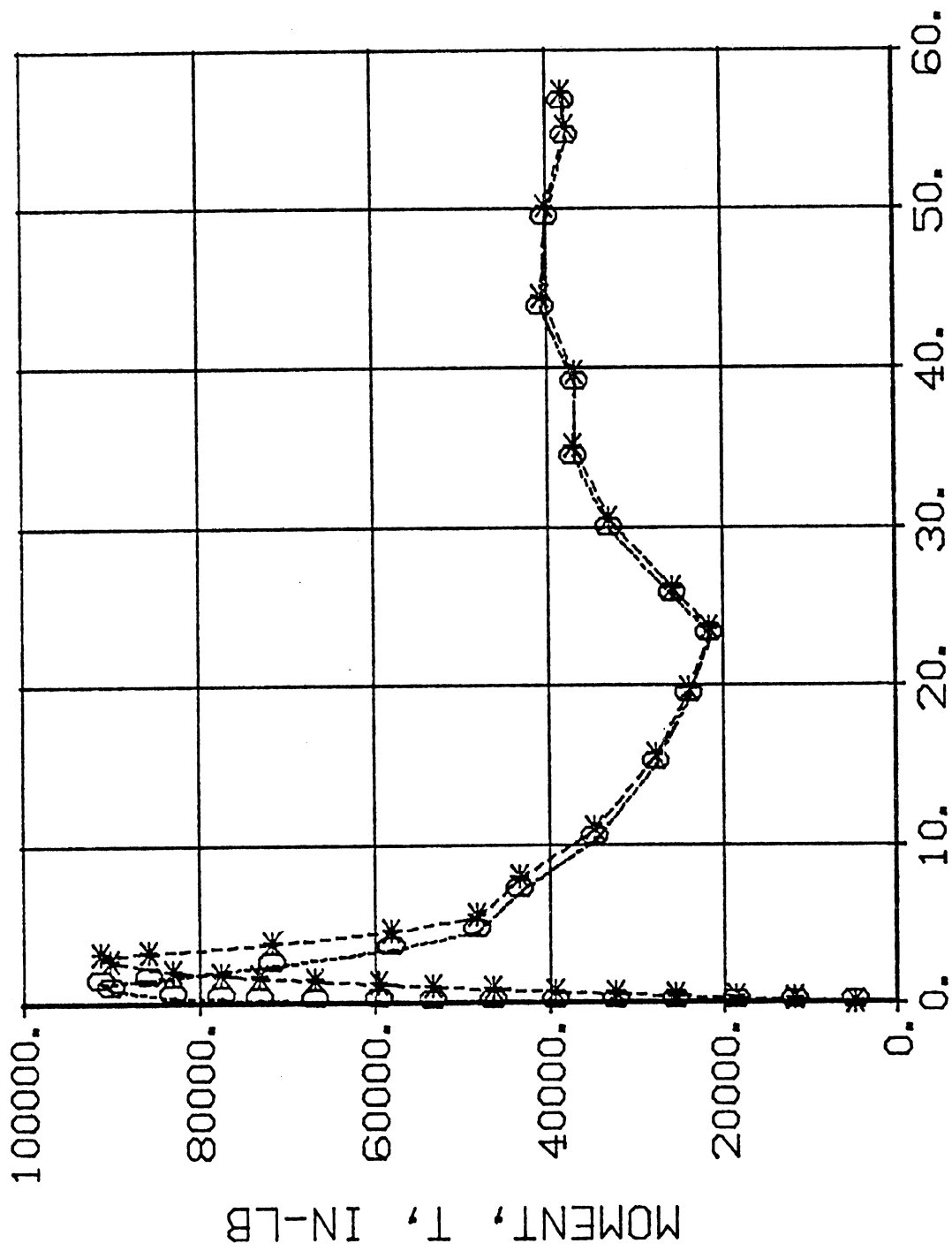




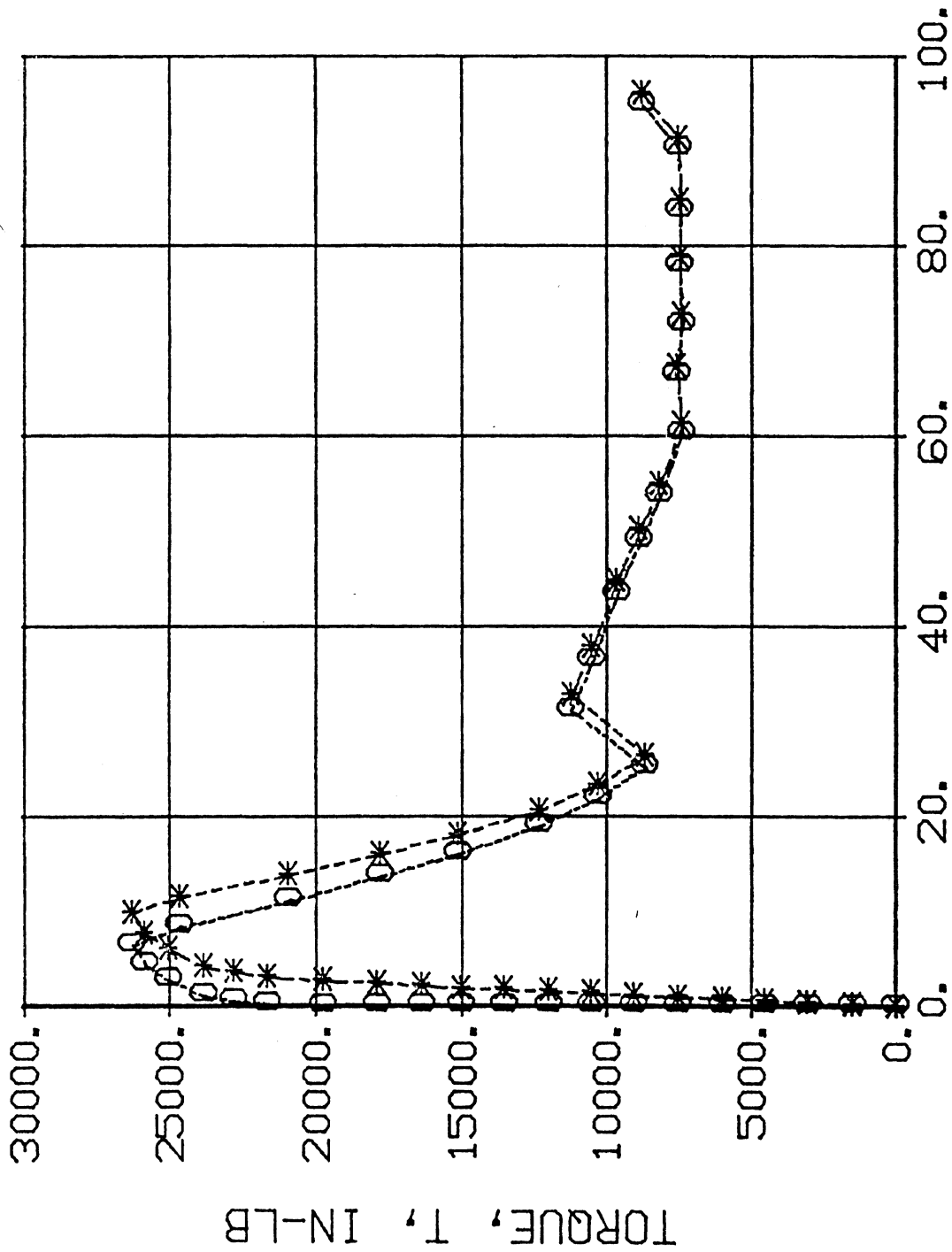
*--ANGLE, O-PLAS. ANGLE, DEG, BY2030RM



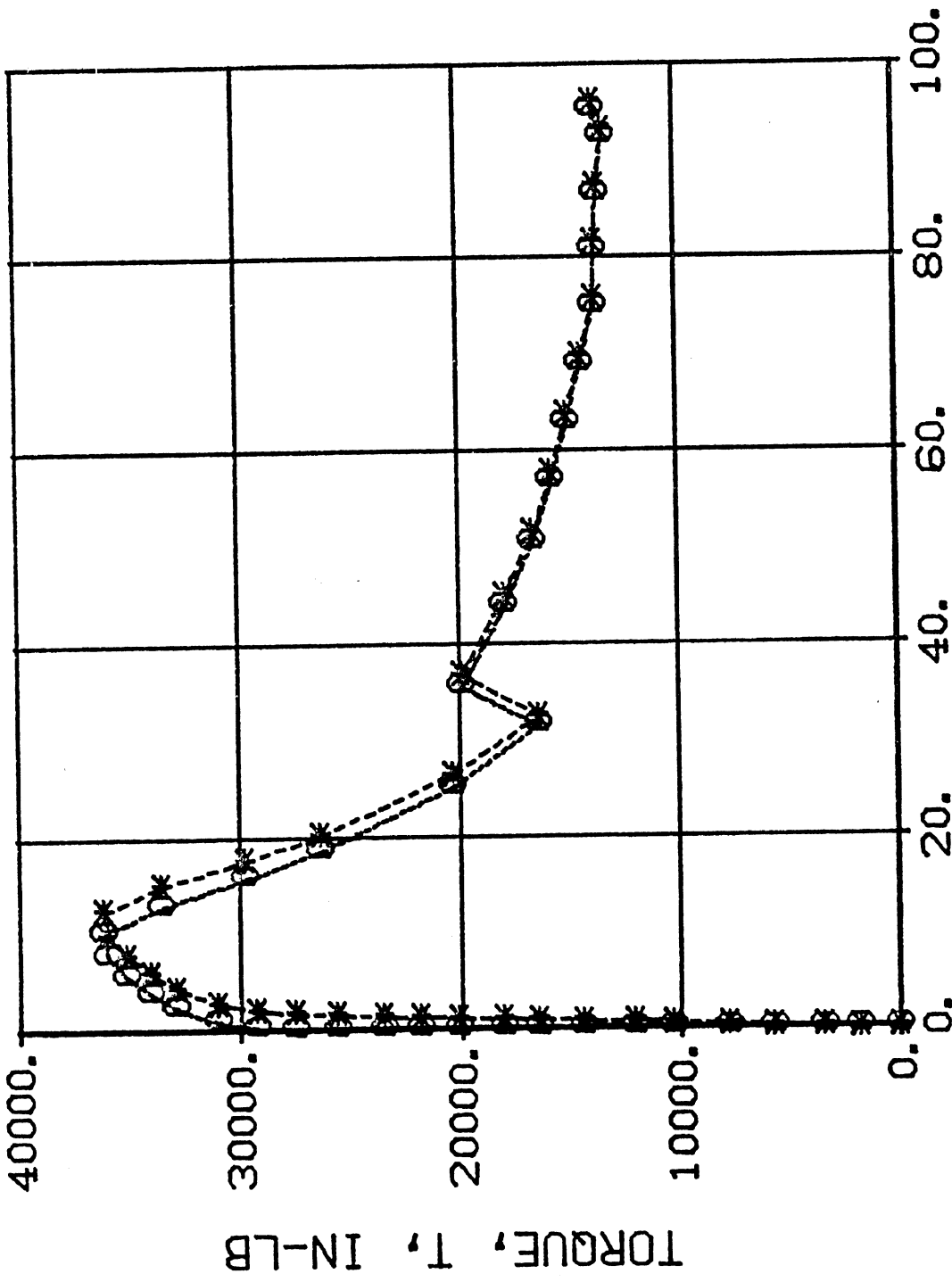




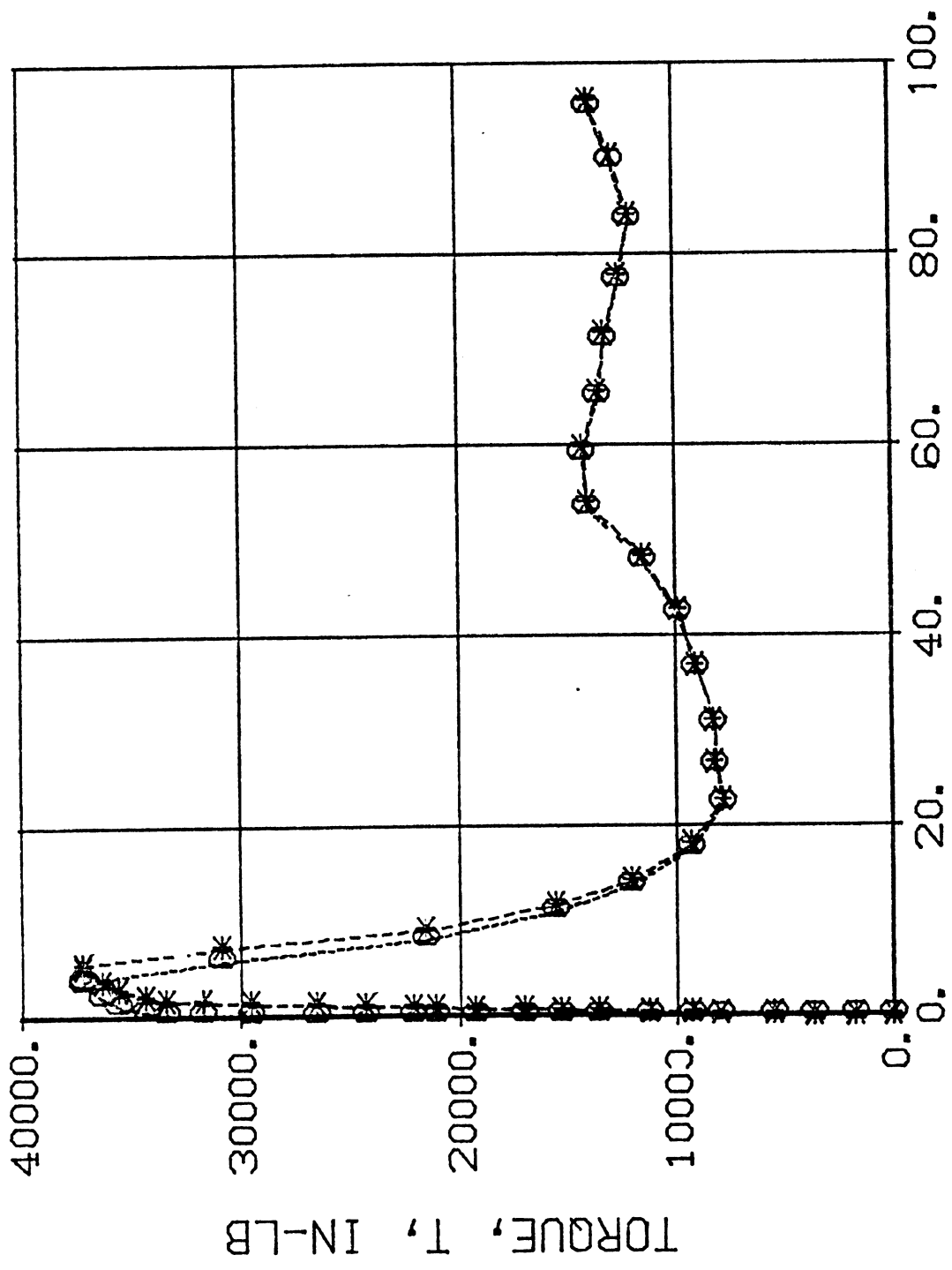
*--ANGLE, 0-PLAS.ANGLE, DEG, BY3040TM



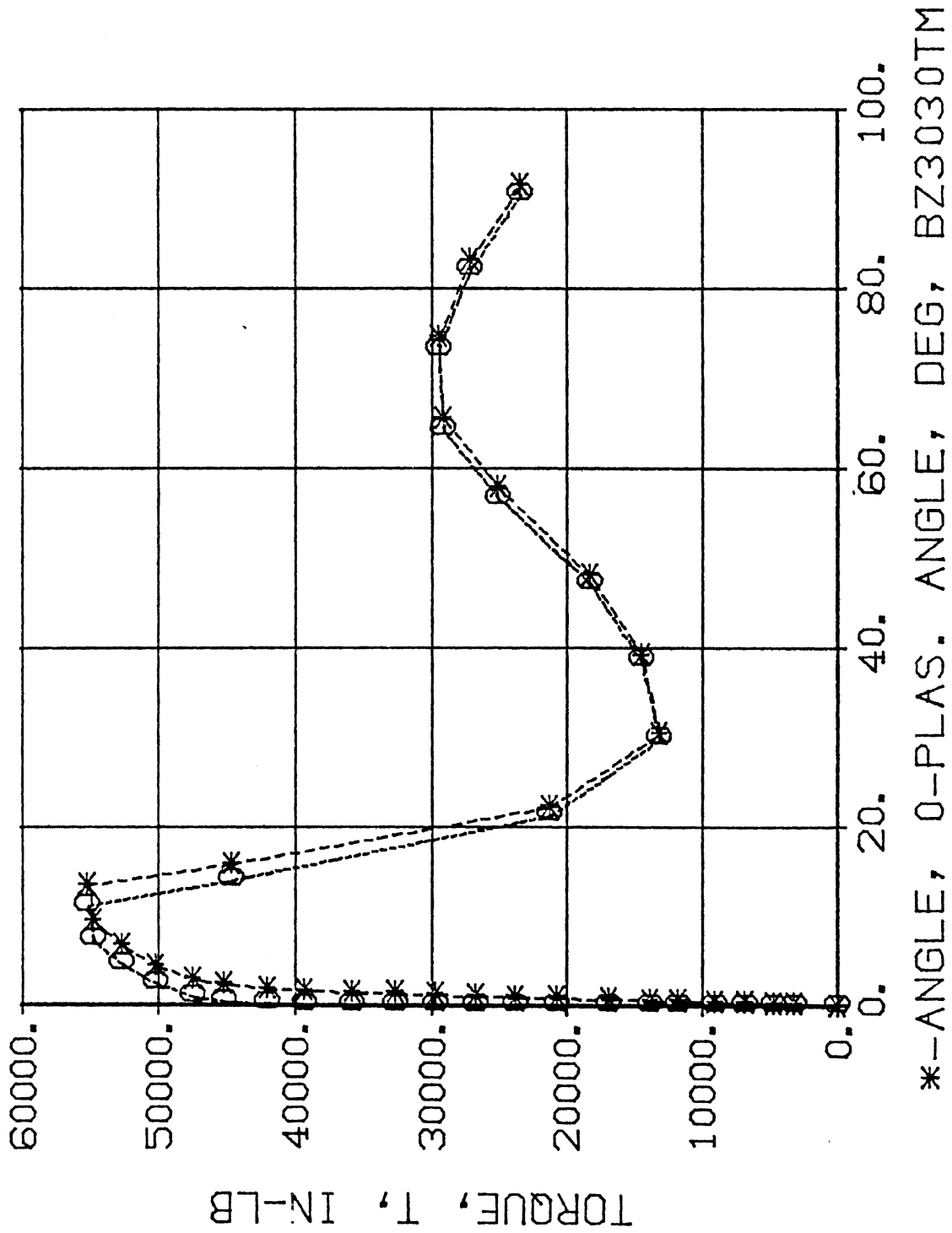
*--ANGLE, 0-PLAS. ANGLE, DEG, BZ3020RM

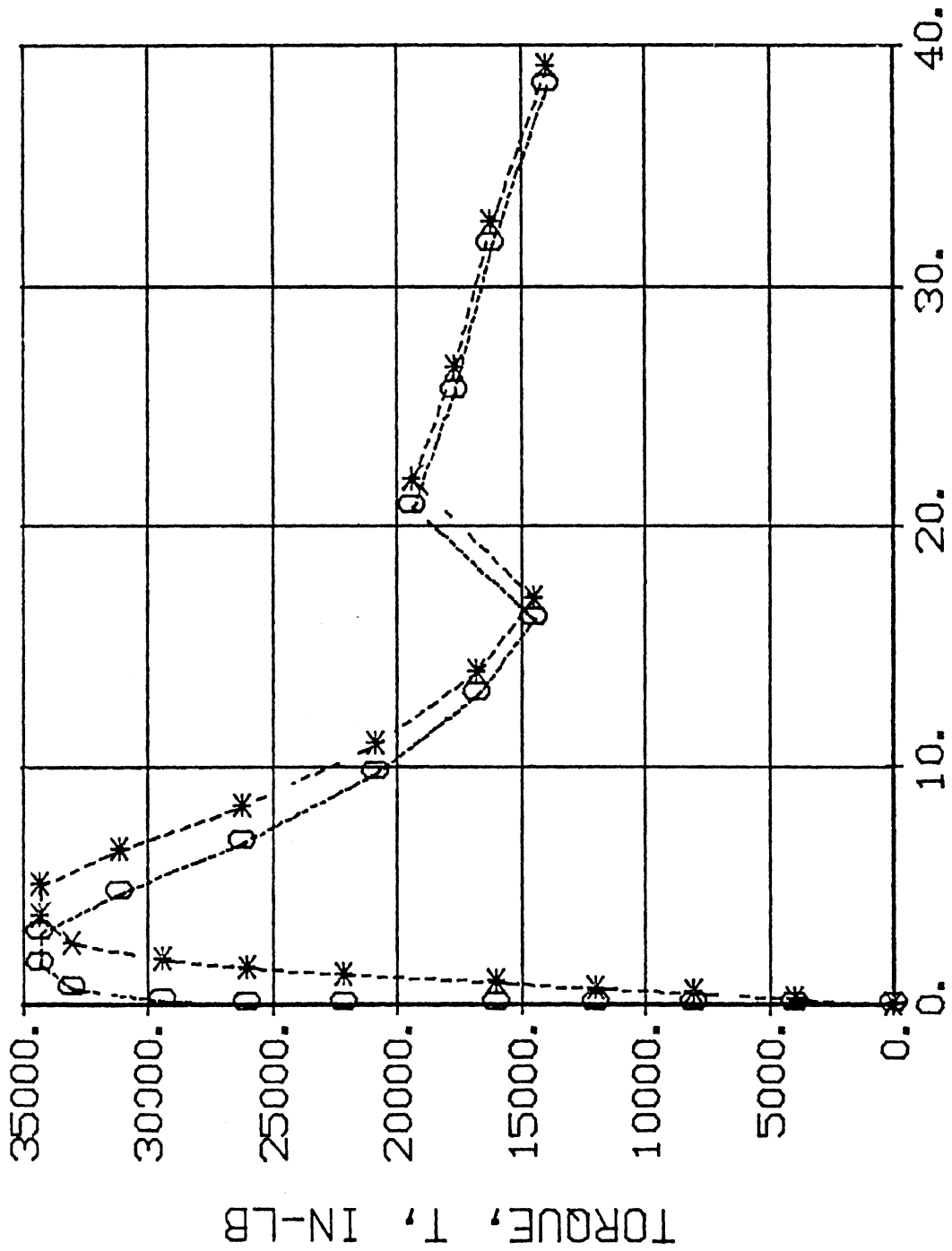


*-ANGLE, 0-PLAS. ANGLE, DEG, BZ3020UM

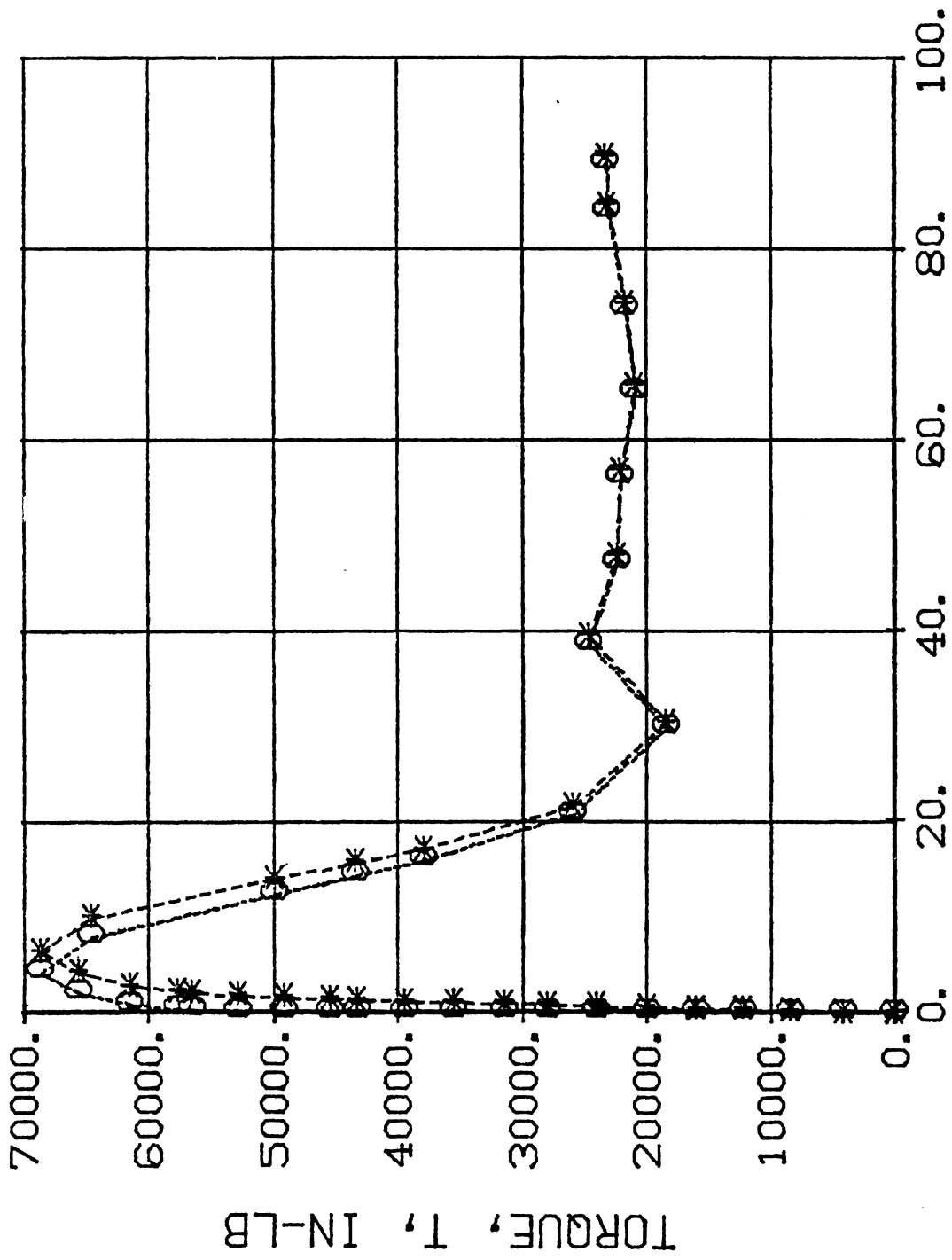


*-ANGLE, 0-PLAS. ANGLE, DEG, BZ3030PM

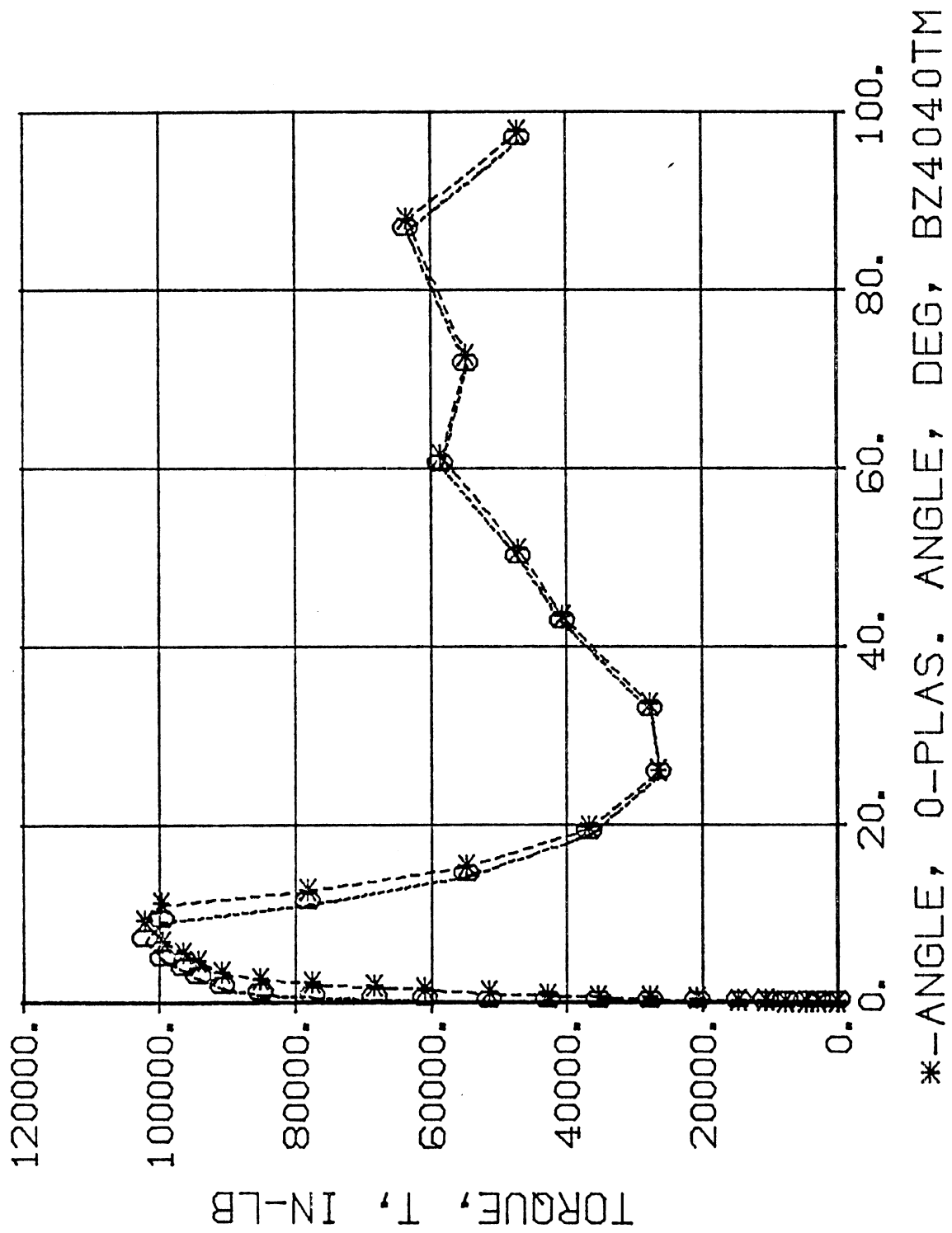


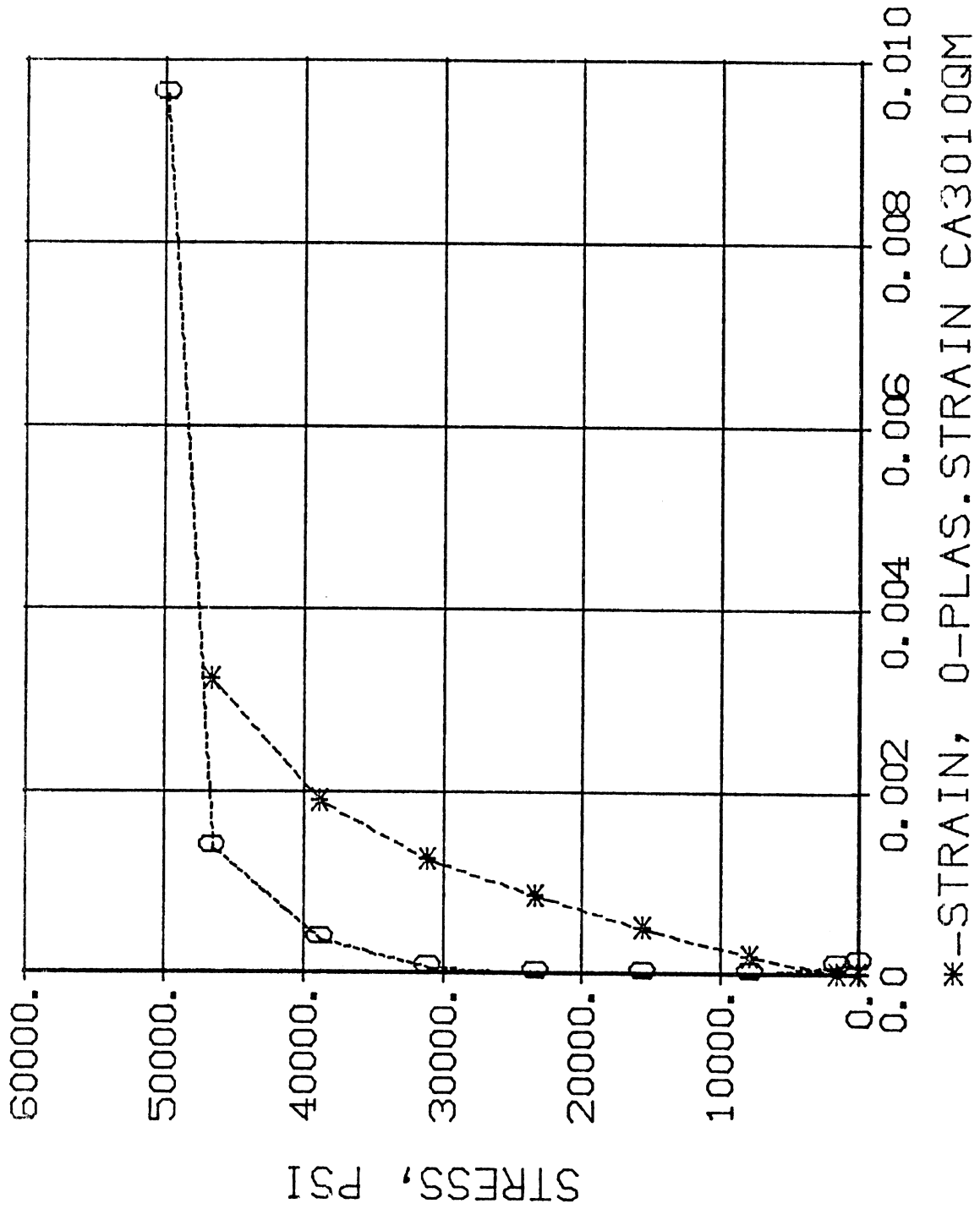


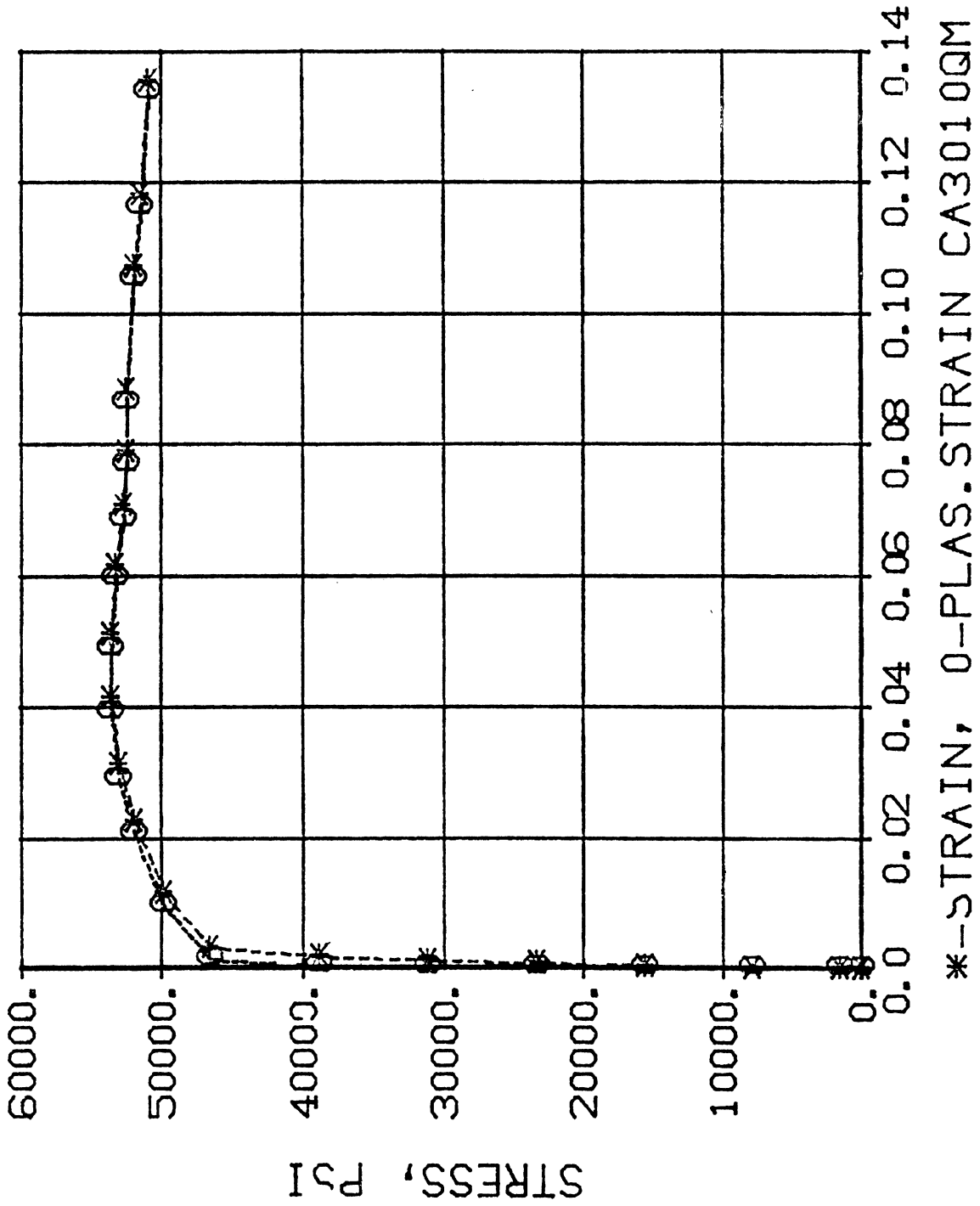
*--ANGLE, 0-PLAS. ANGLE, DEG, BZ4020SM

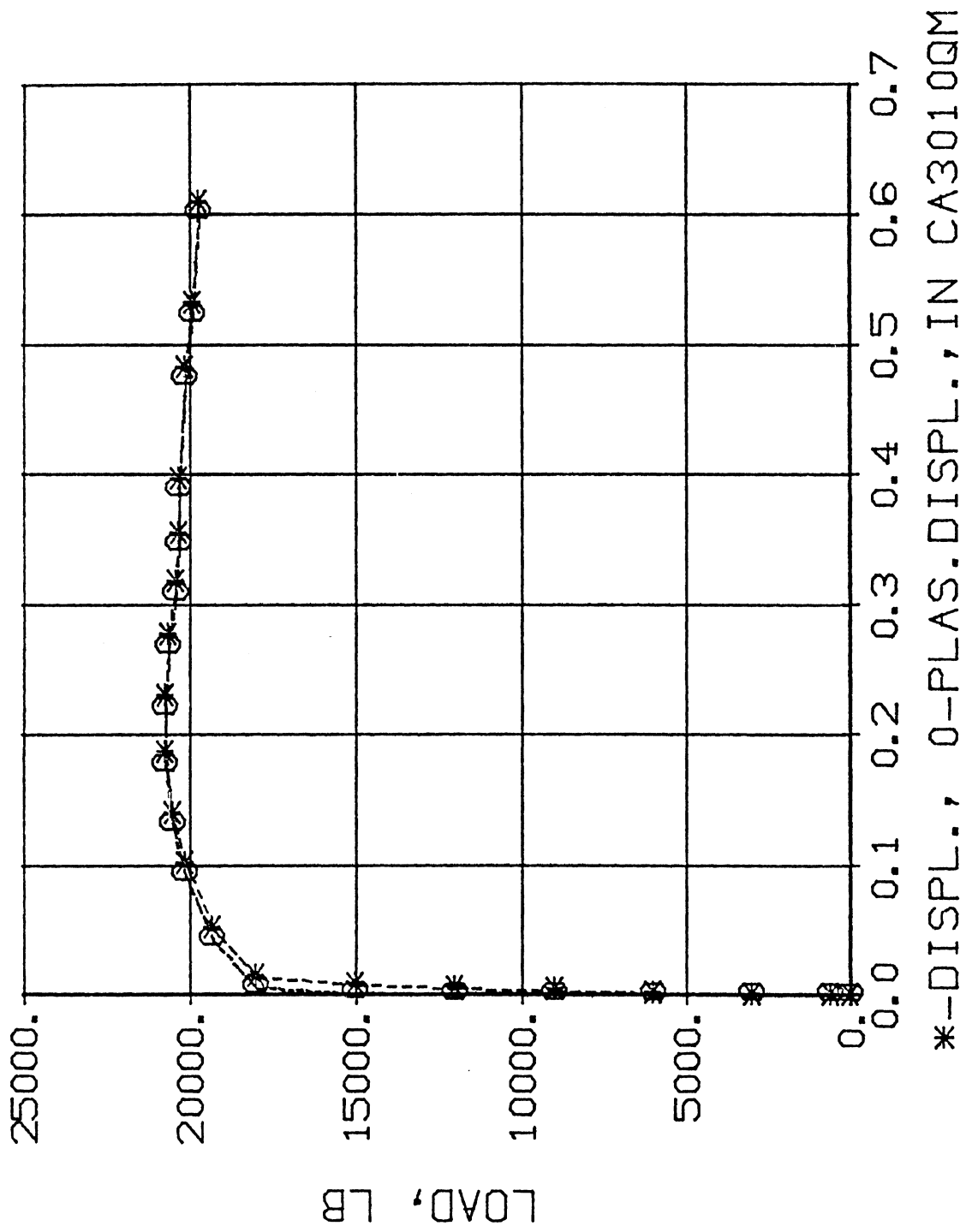


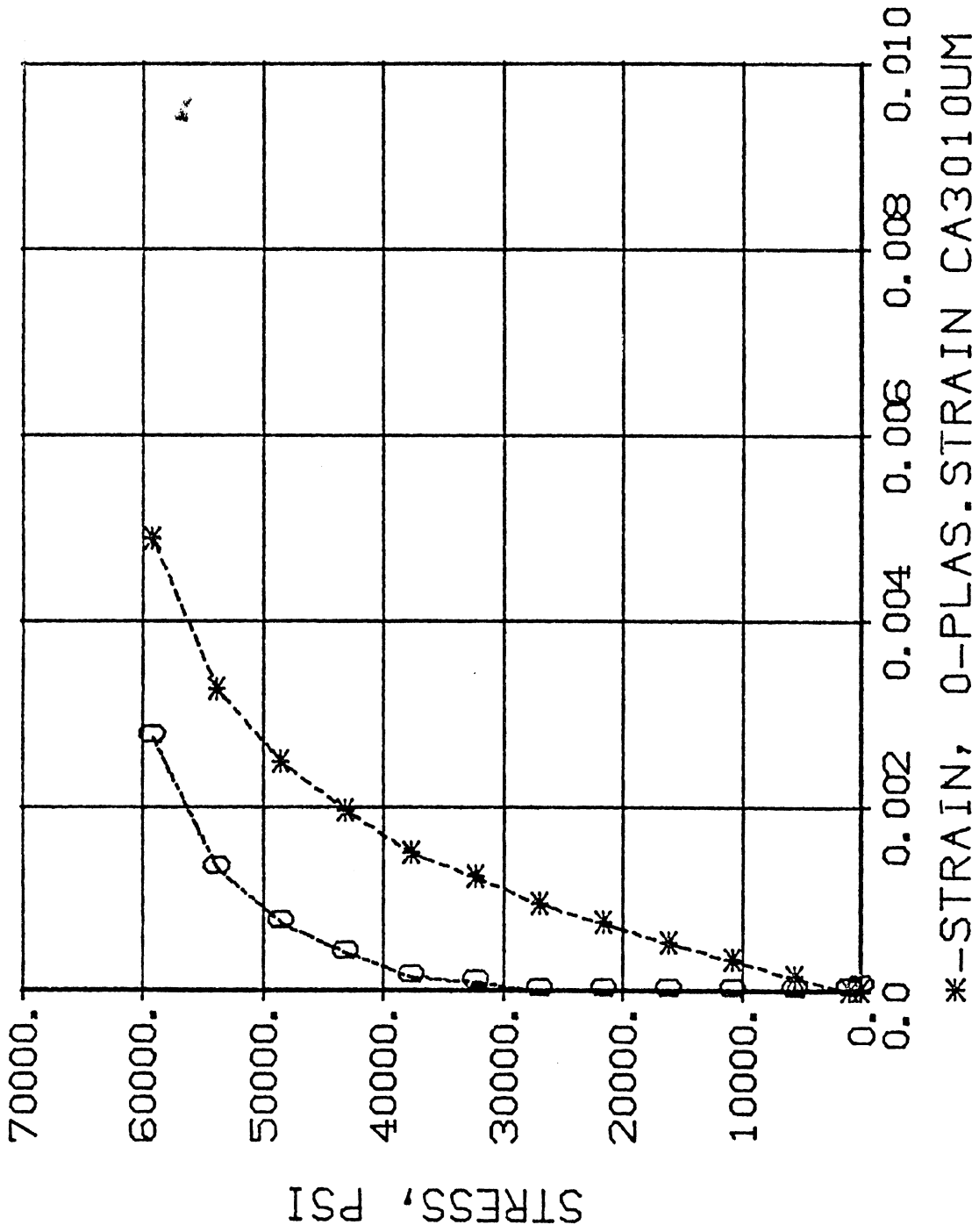
*--ANGLE, 0-PLAS. ANGLE, DEG, BZ4030TM

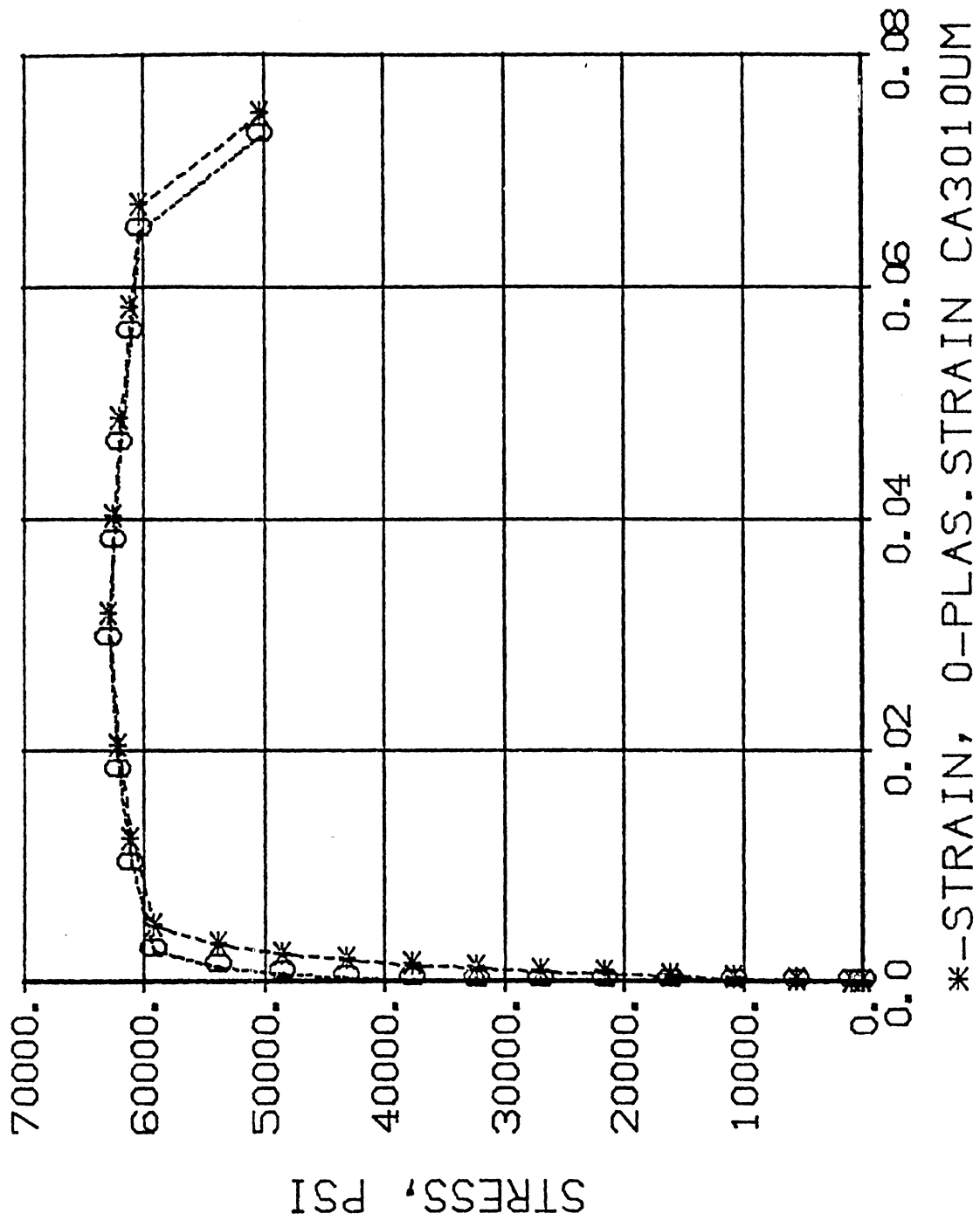






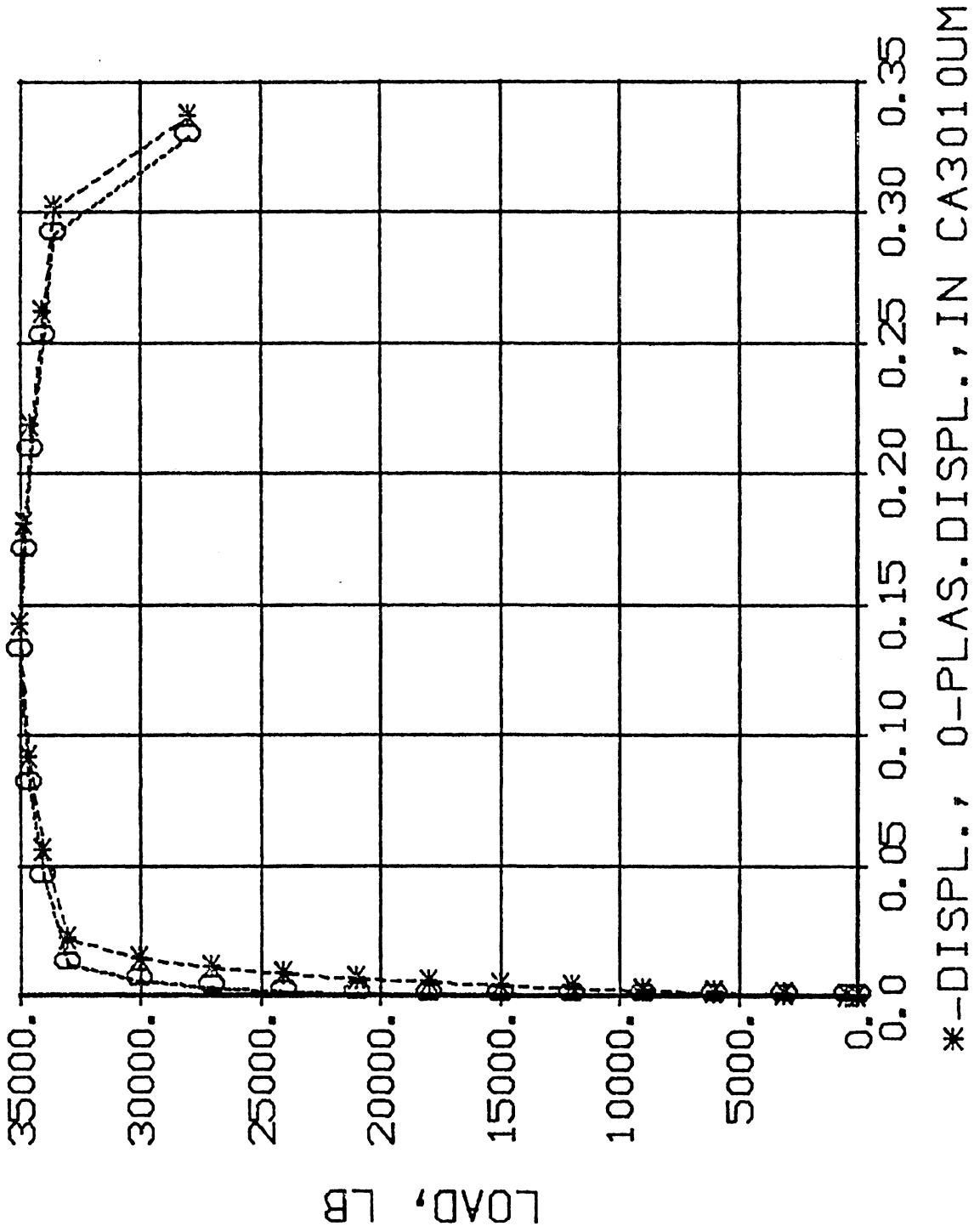


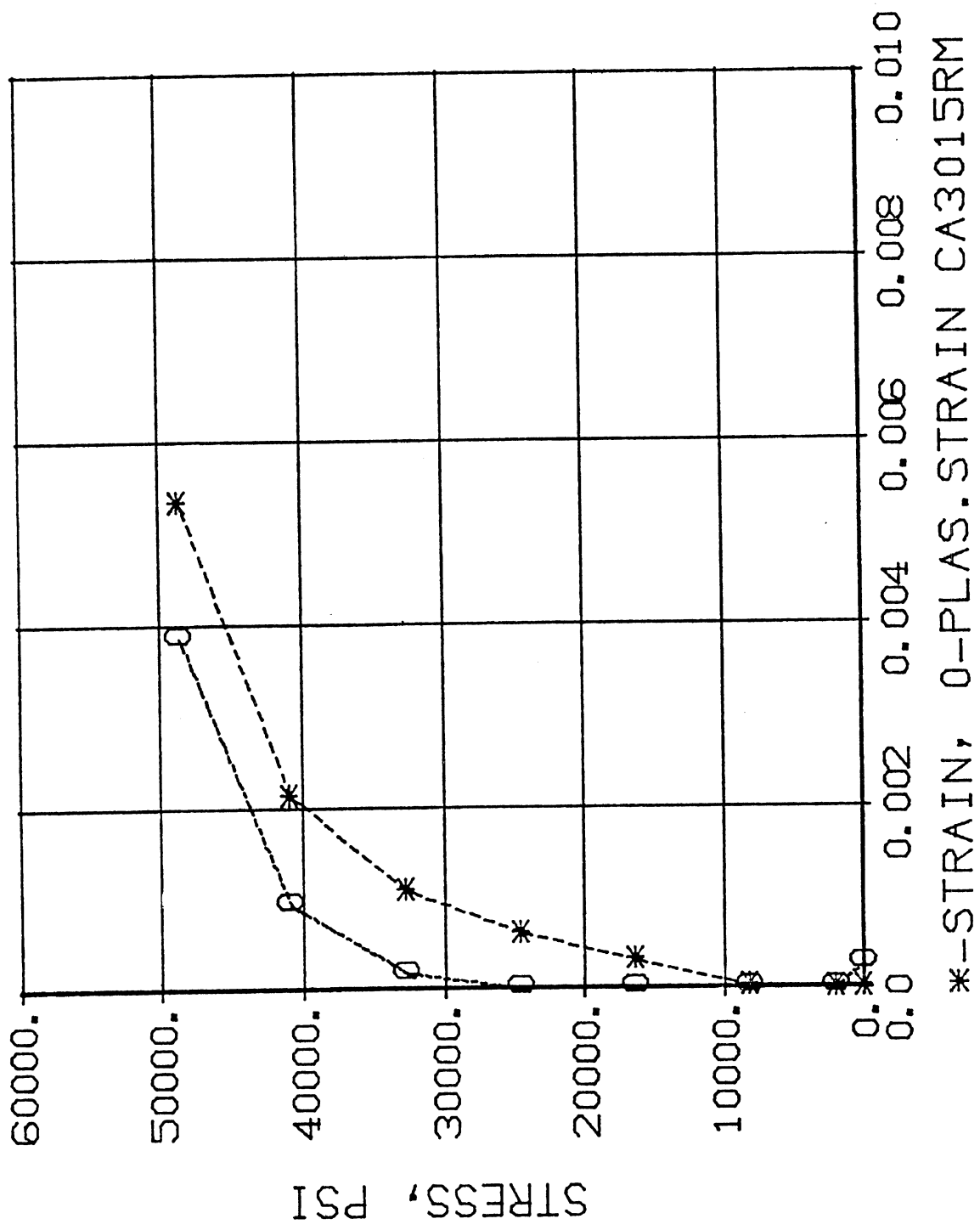


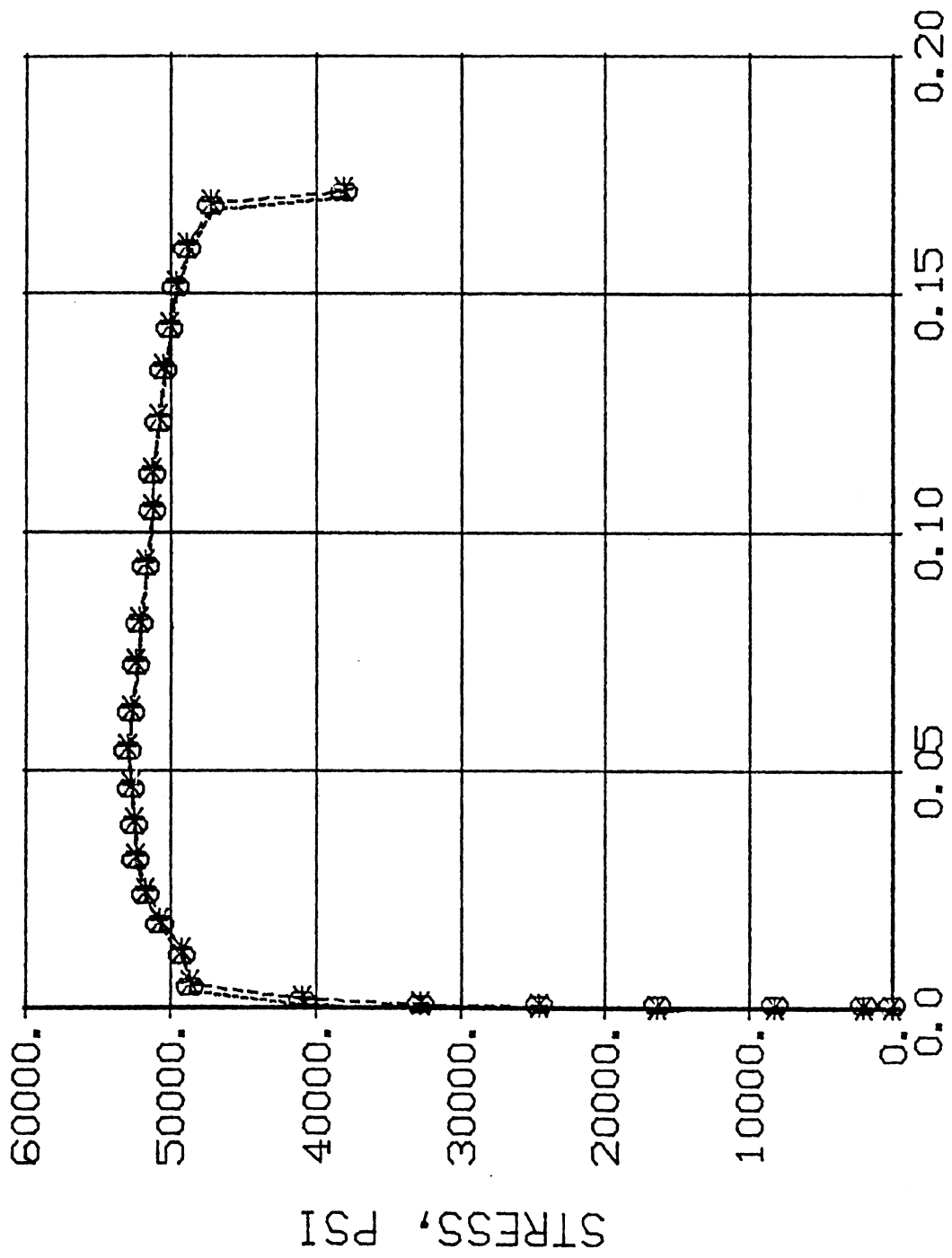


*-STRAIN, 0-PLAS. STRAIN CA3010UM

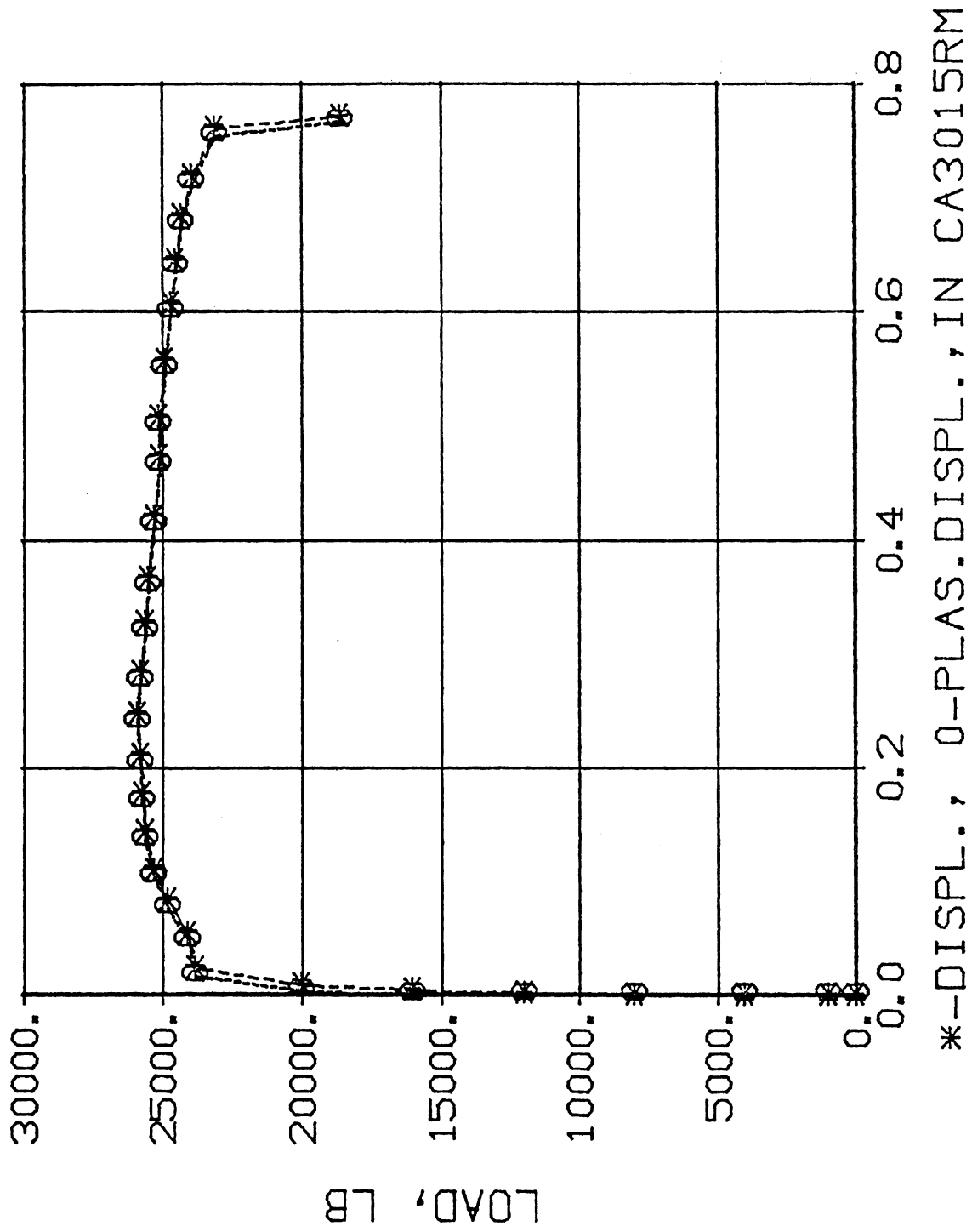
4

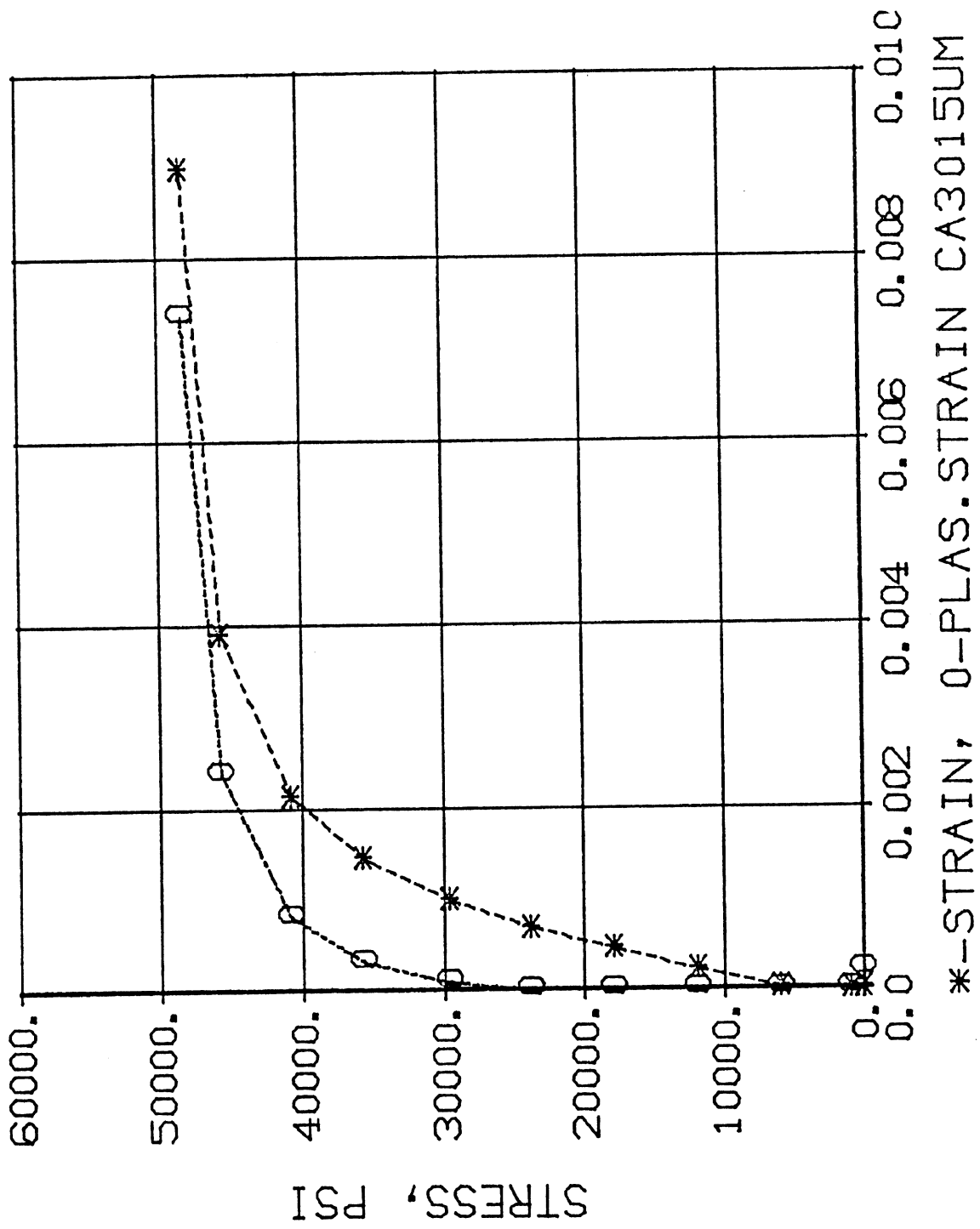


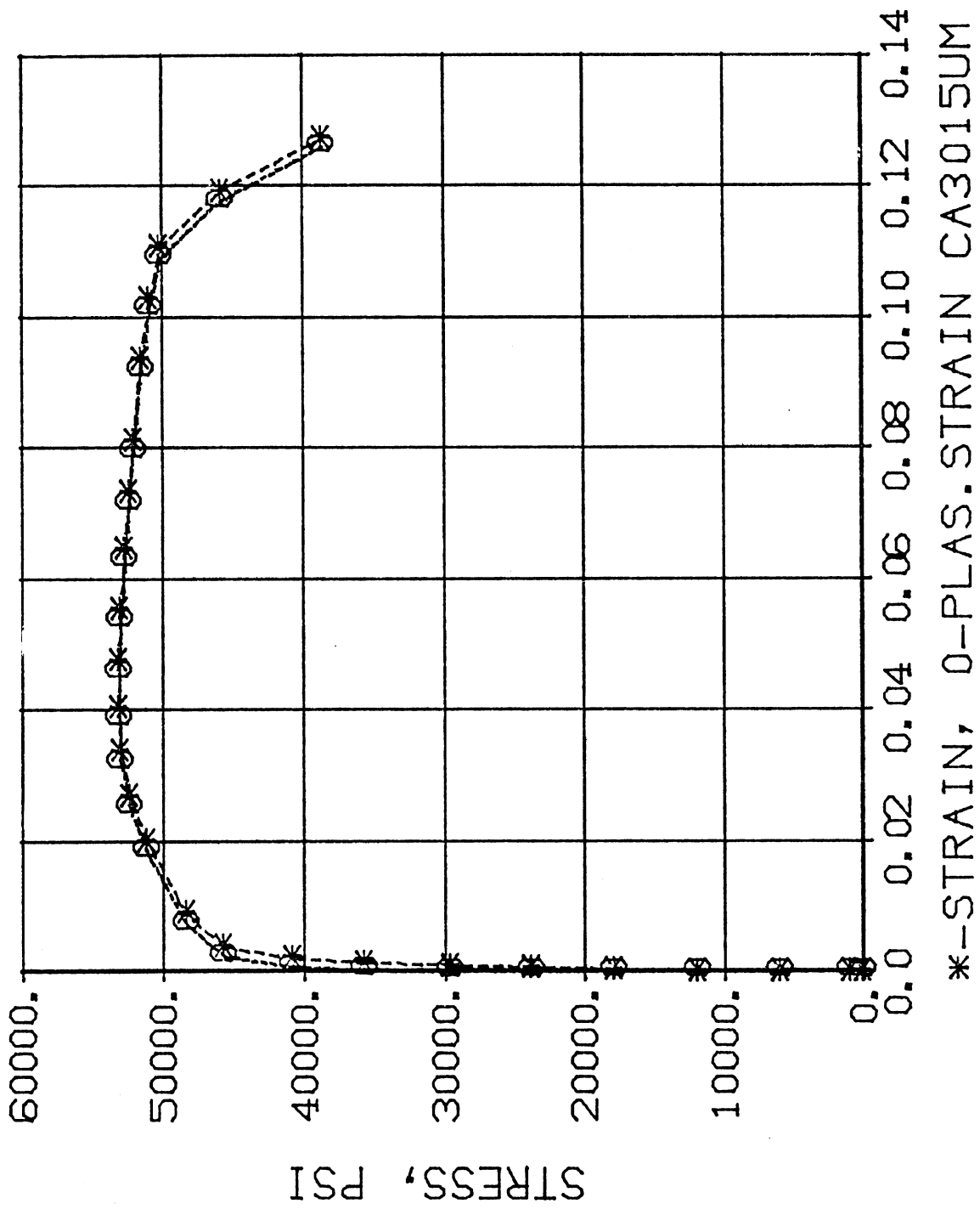


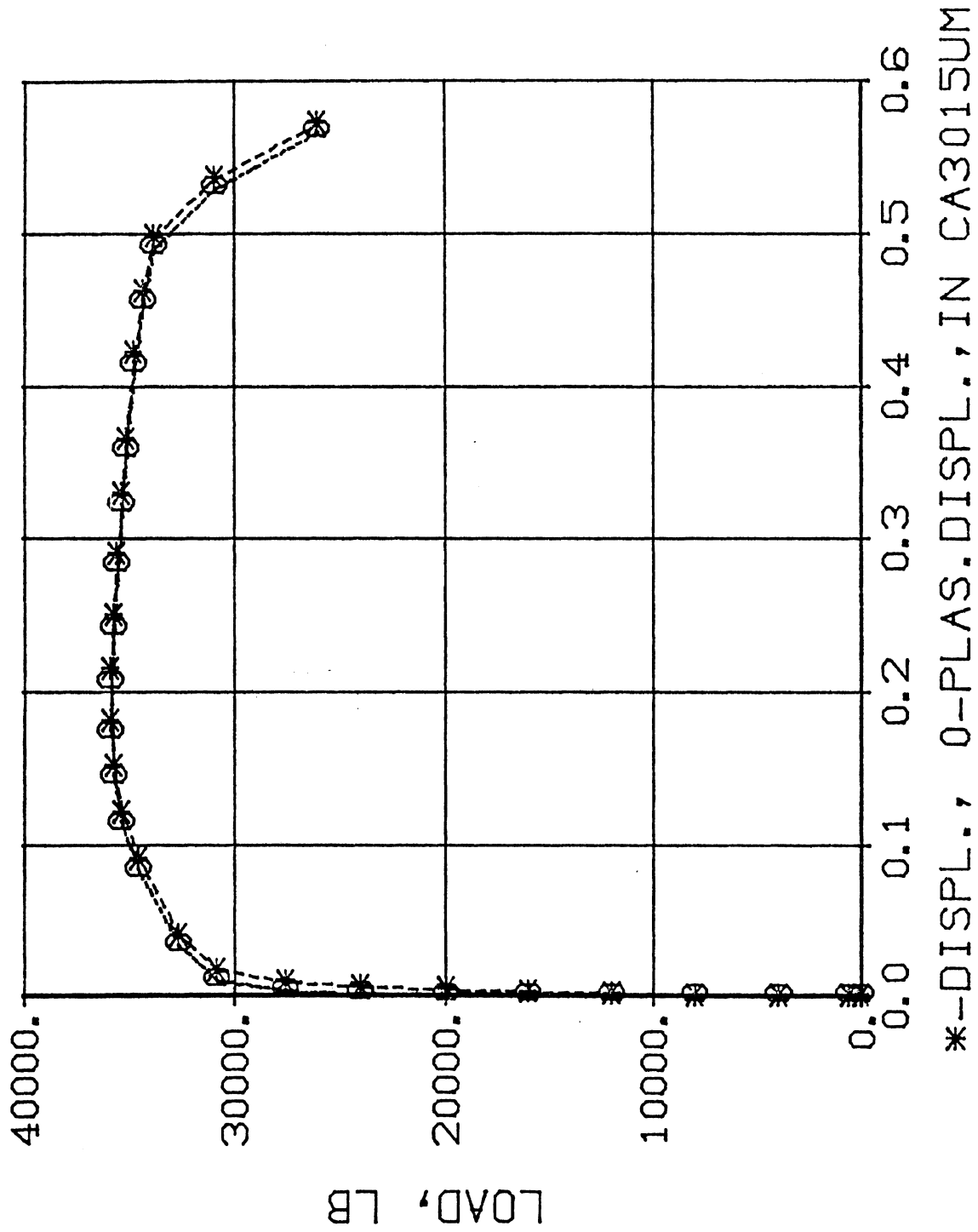


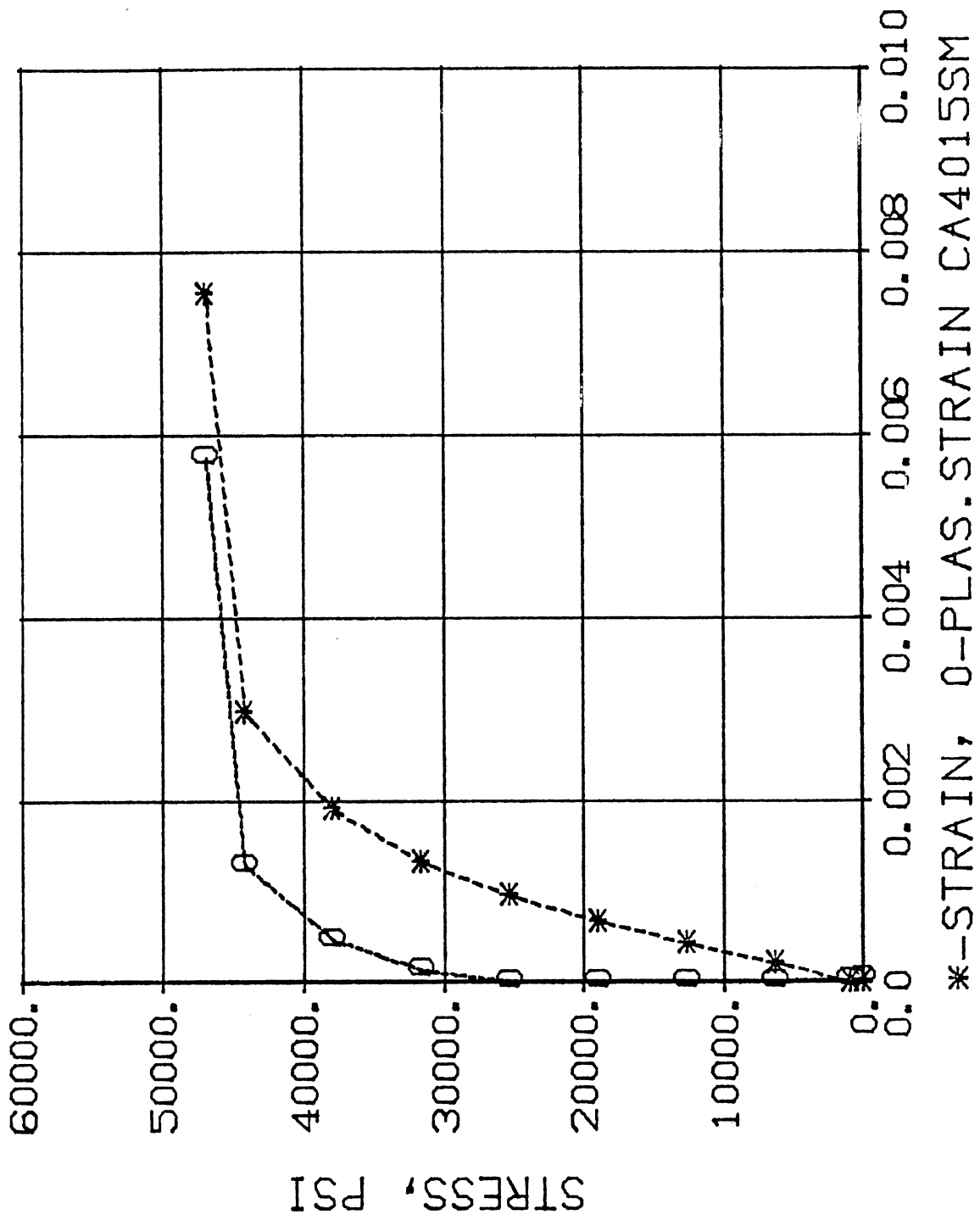
*--STRAIN, 0-PLAS. STRAIN CA3015RM

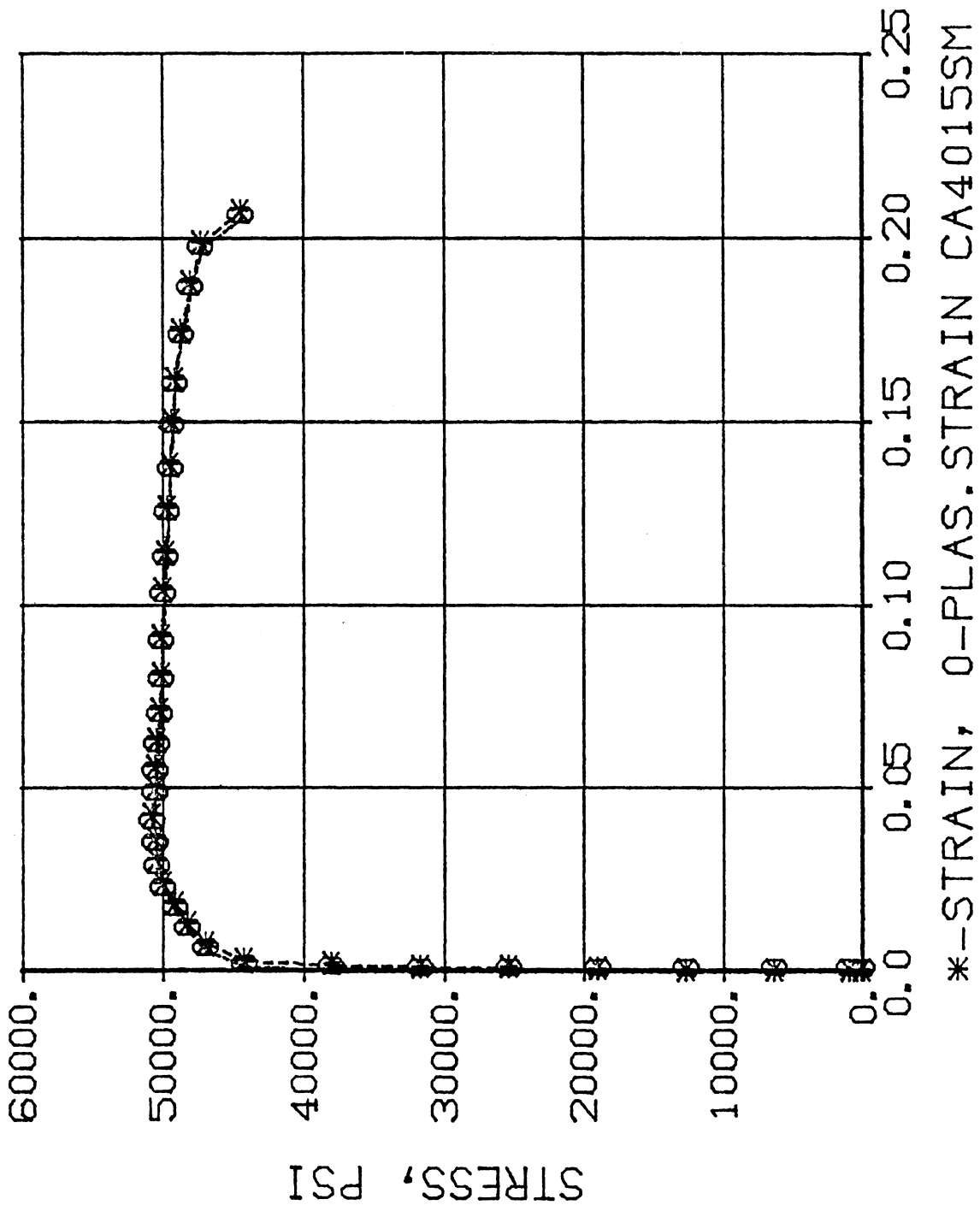


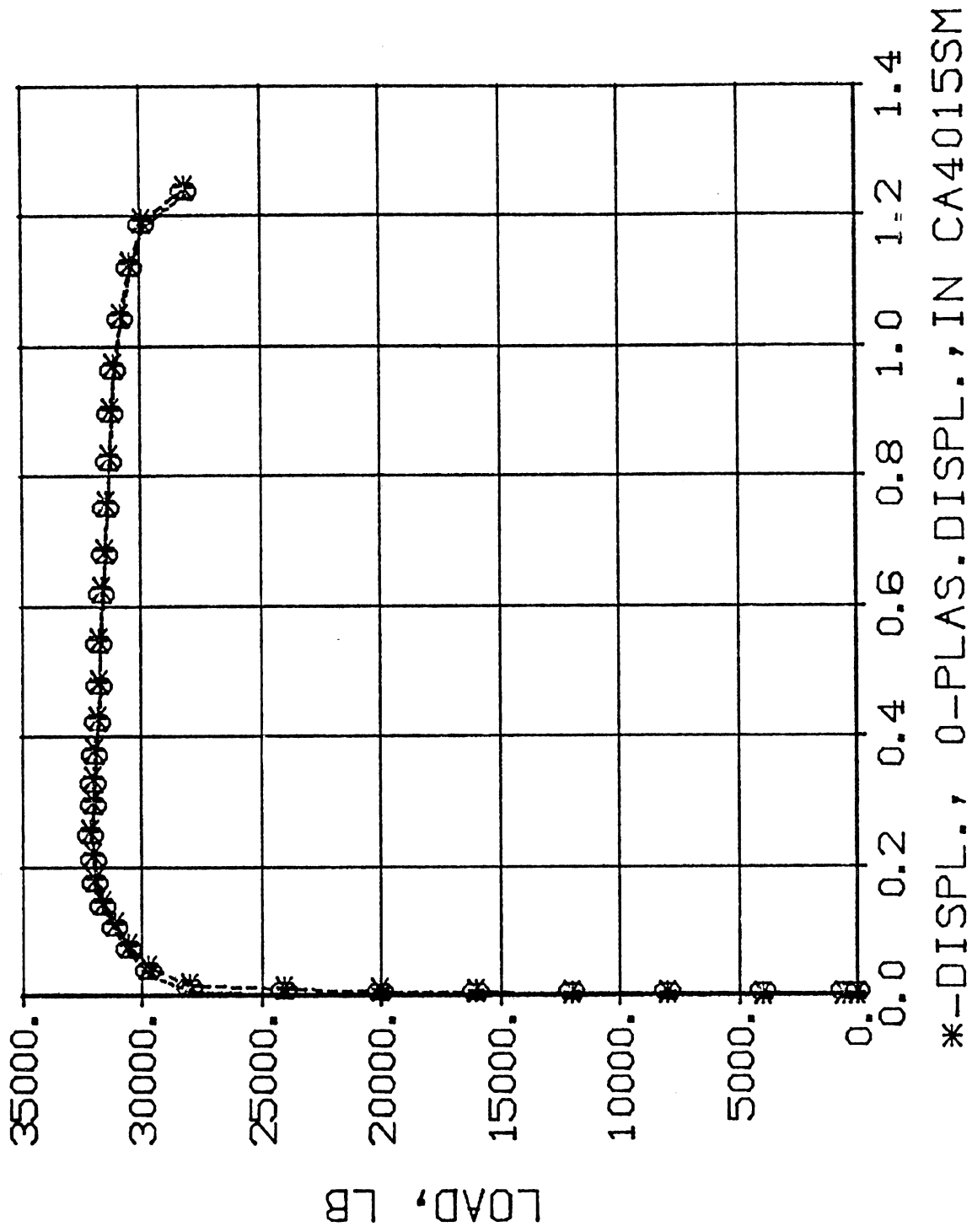


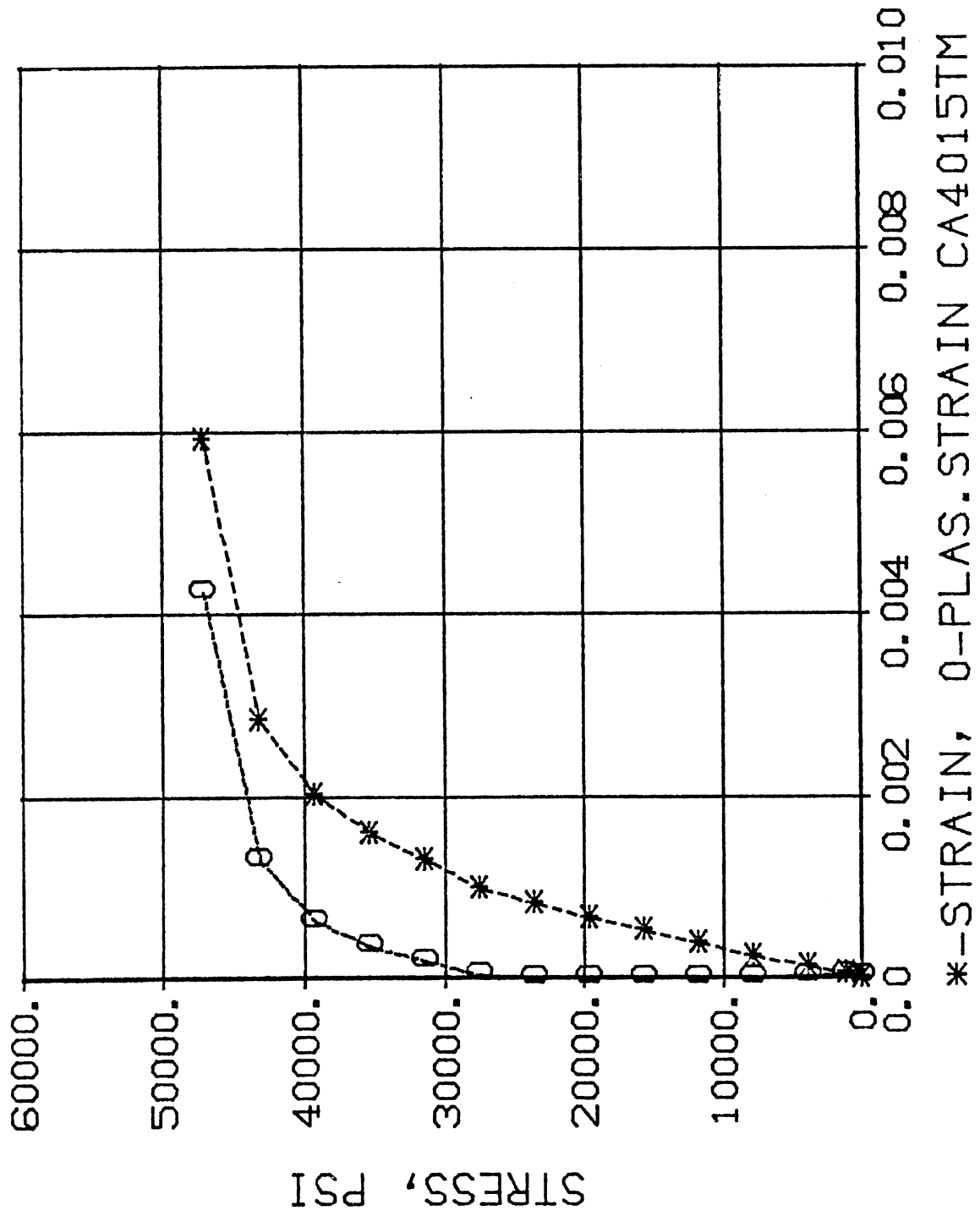


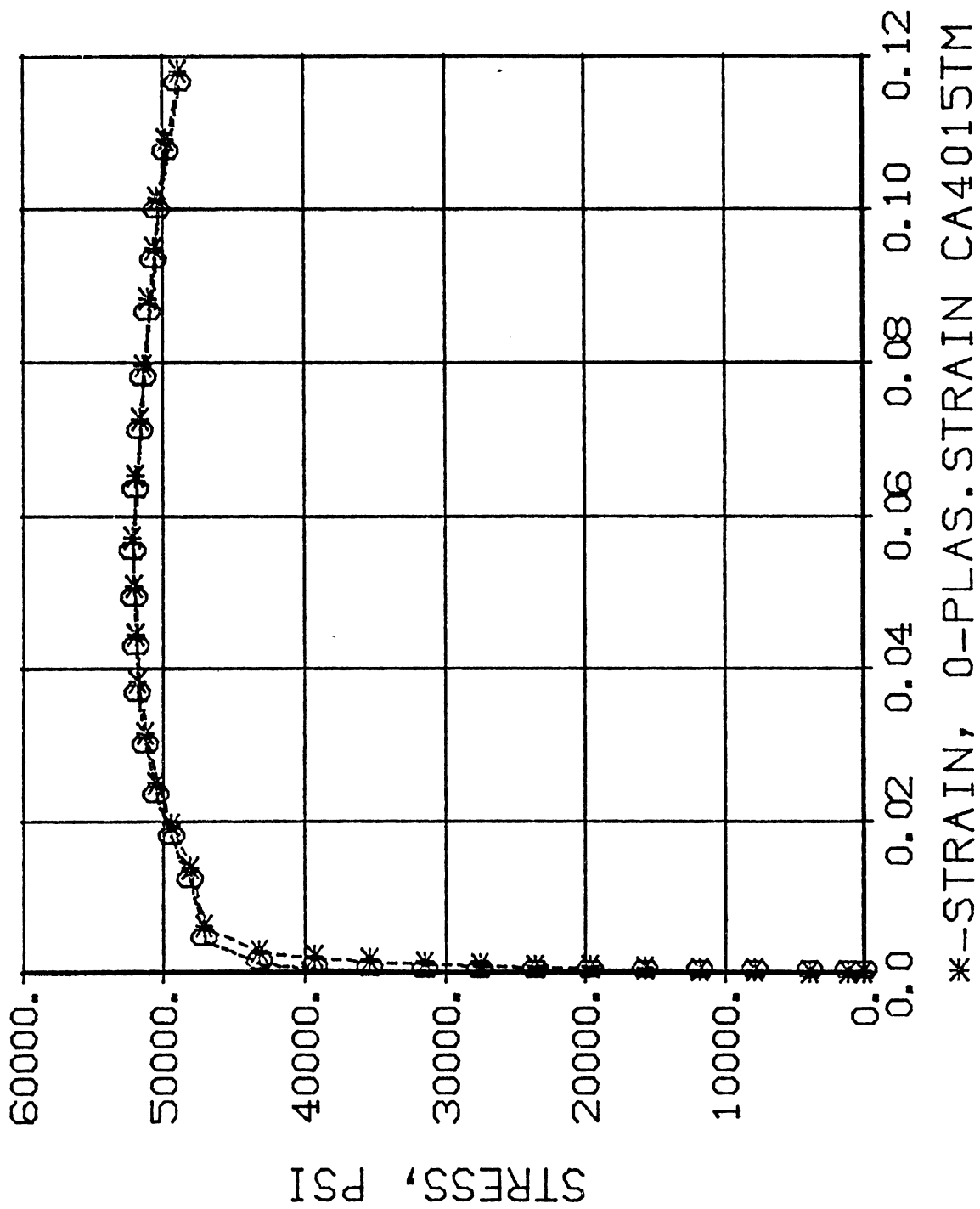


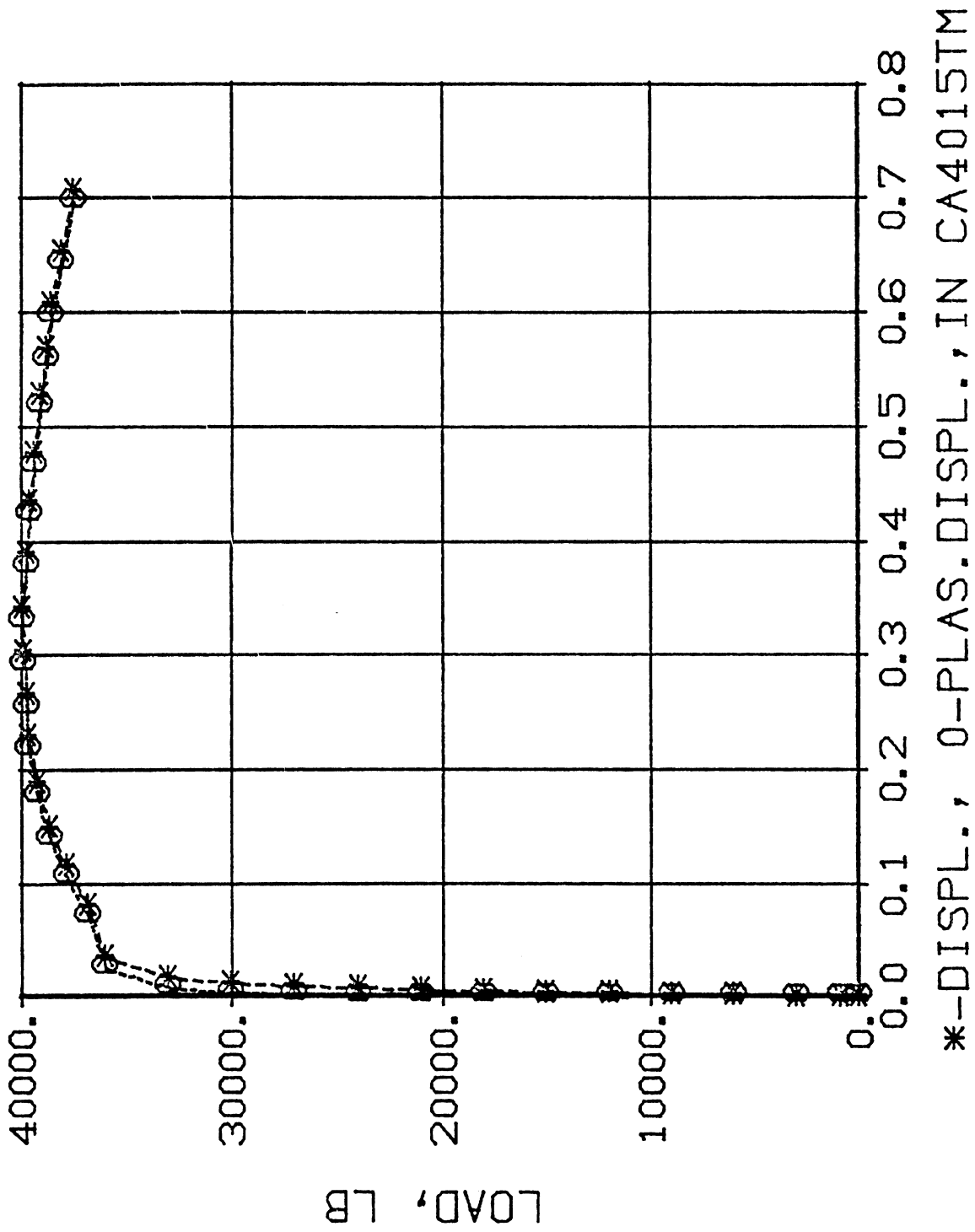


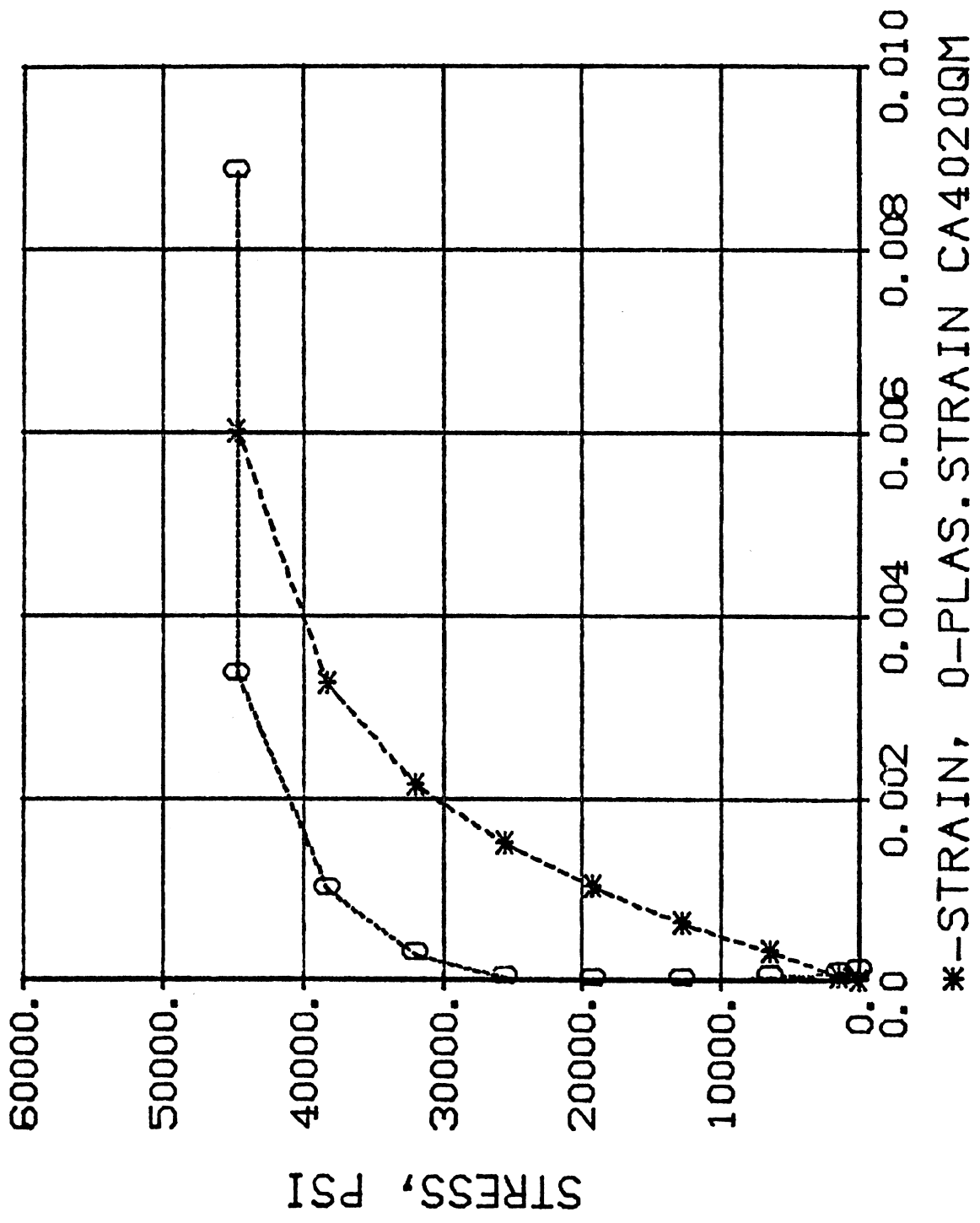


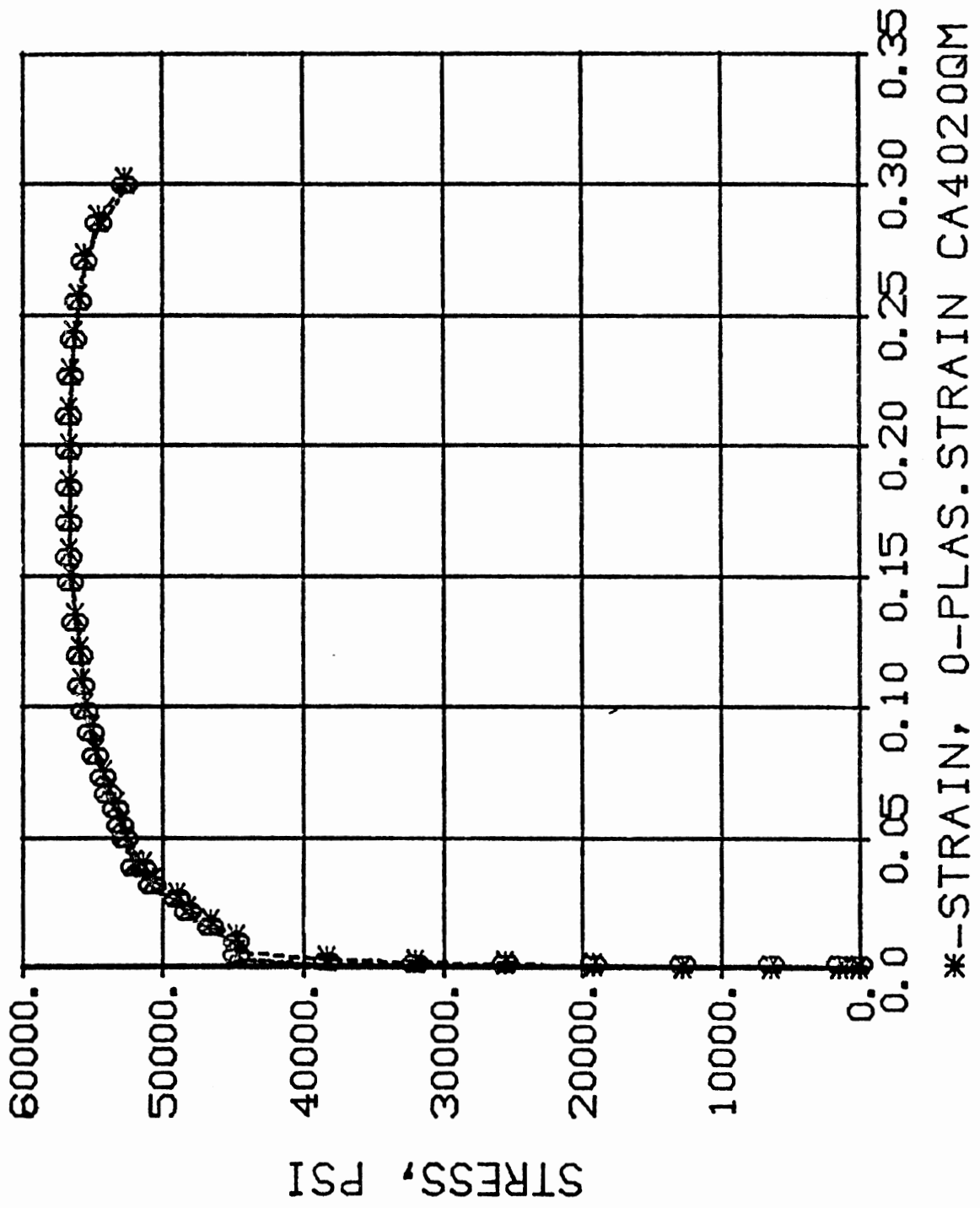


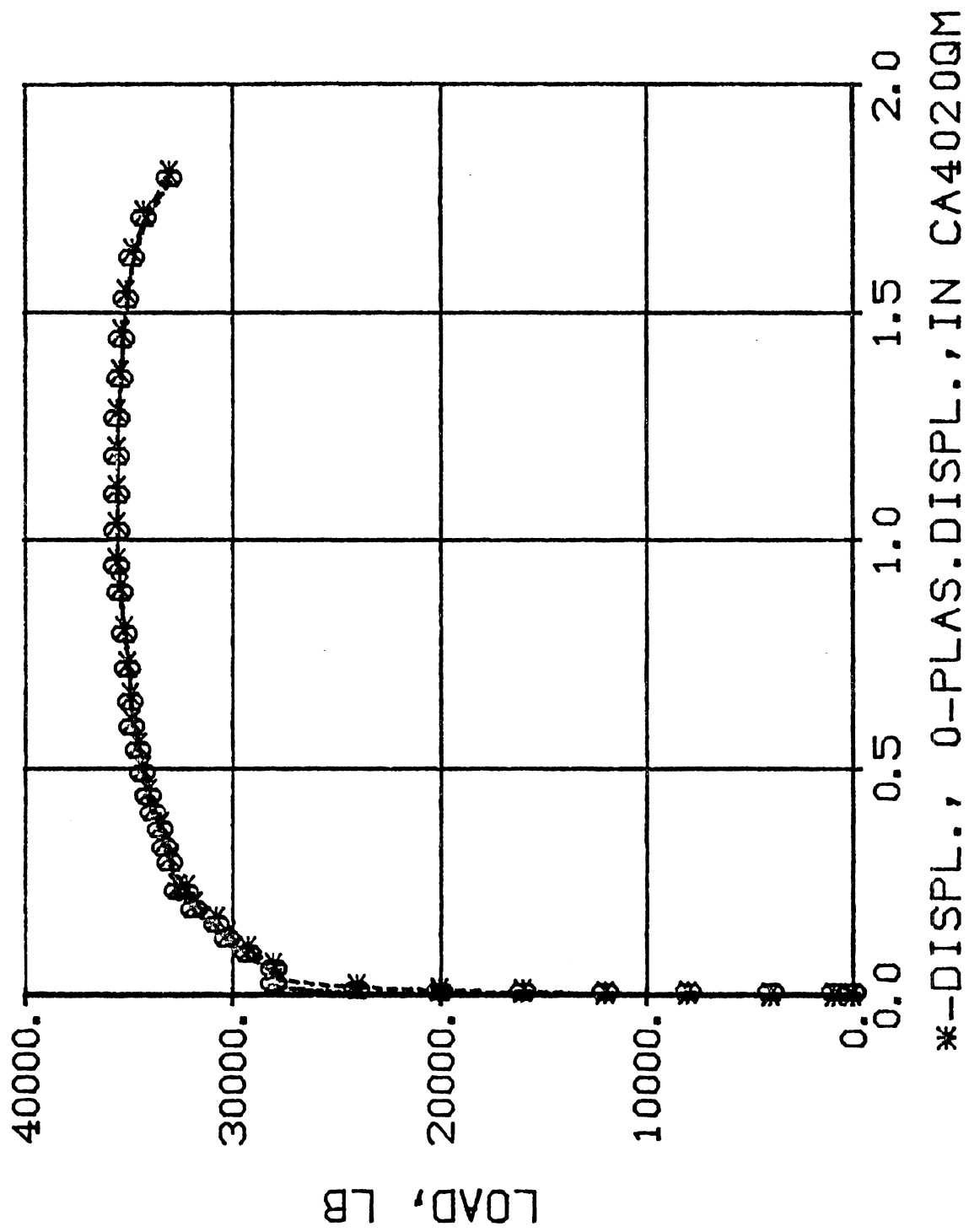


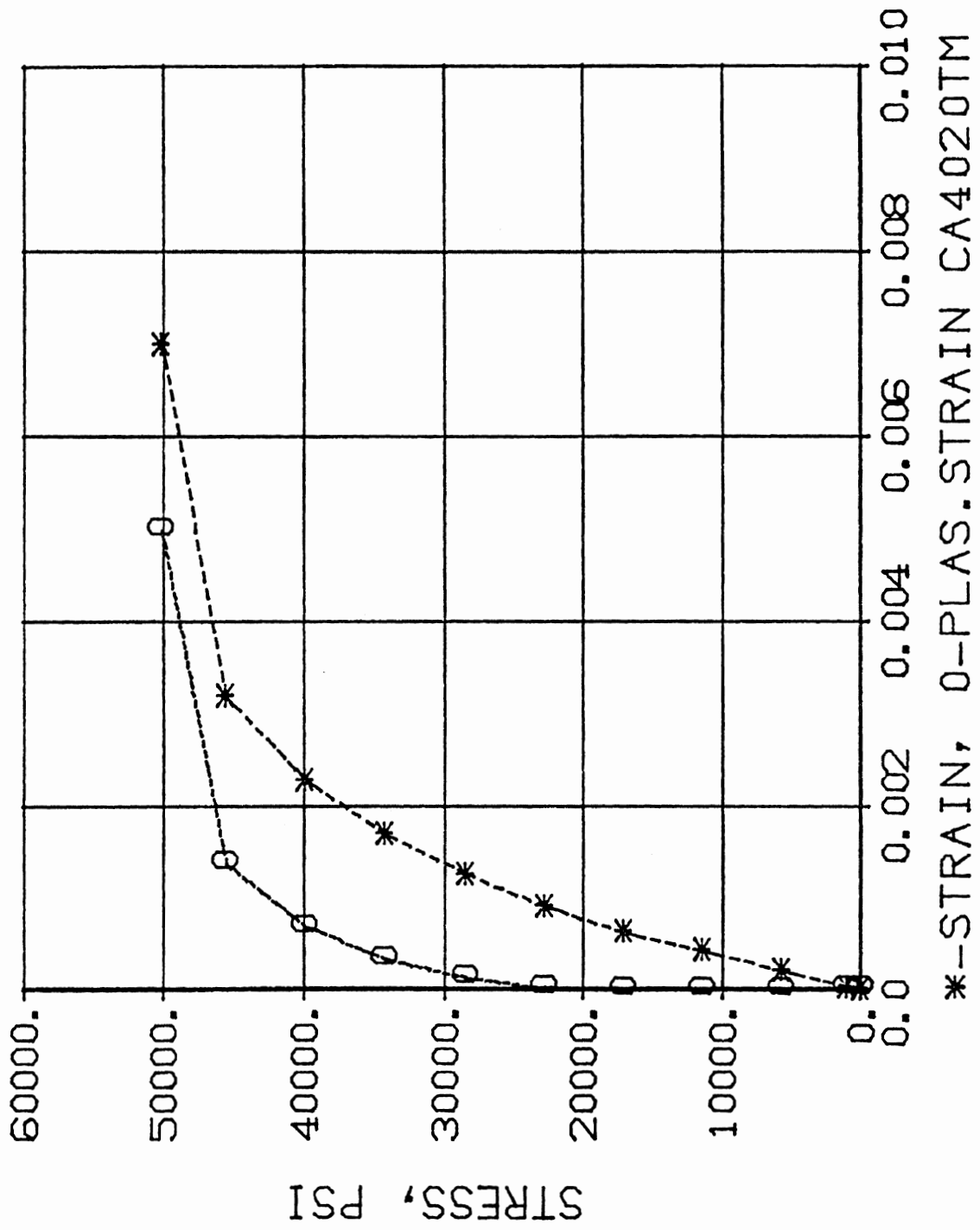


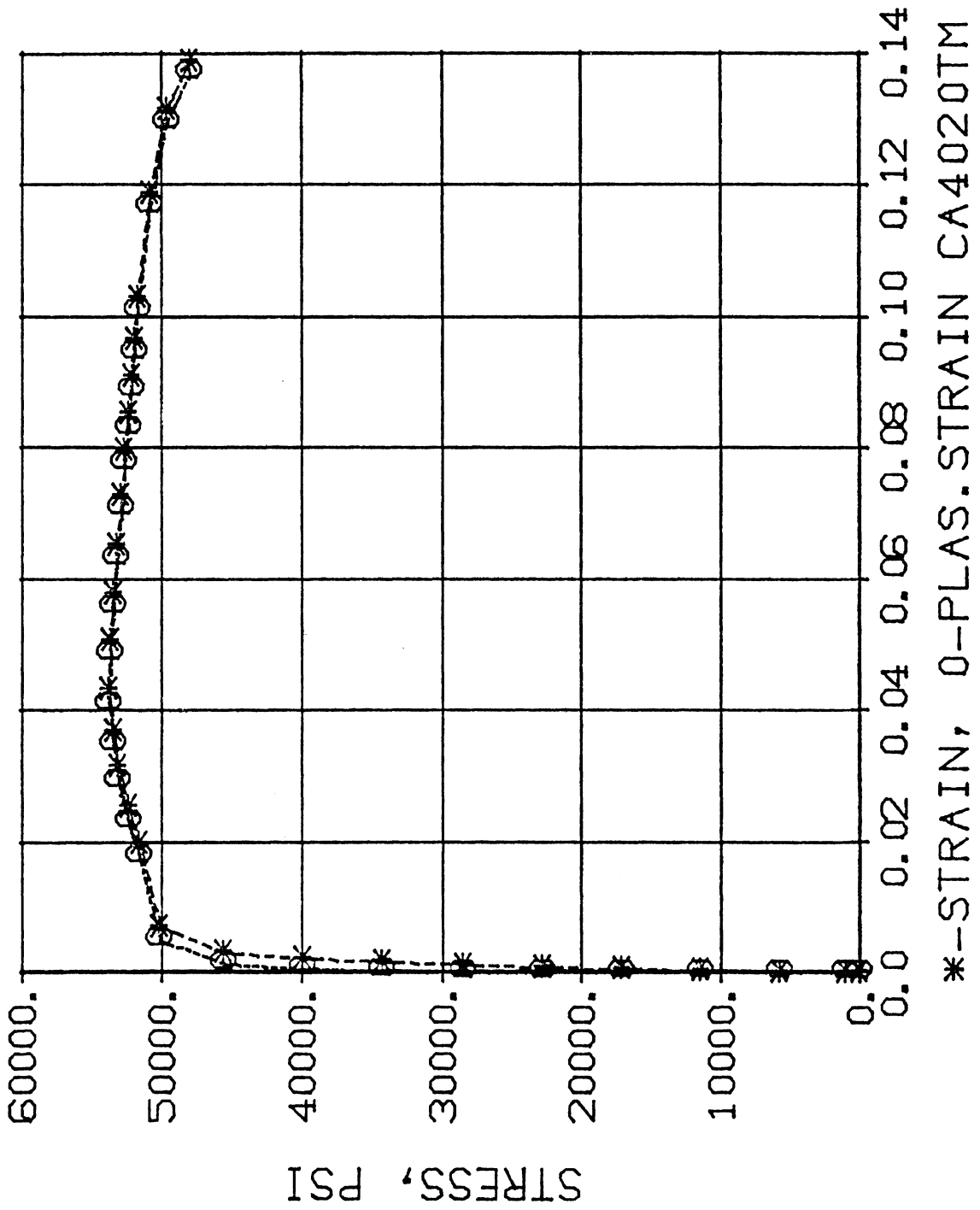


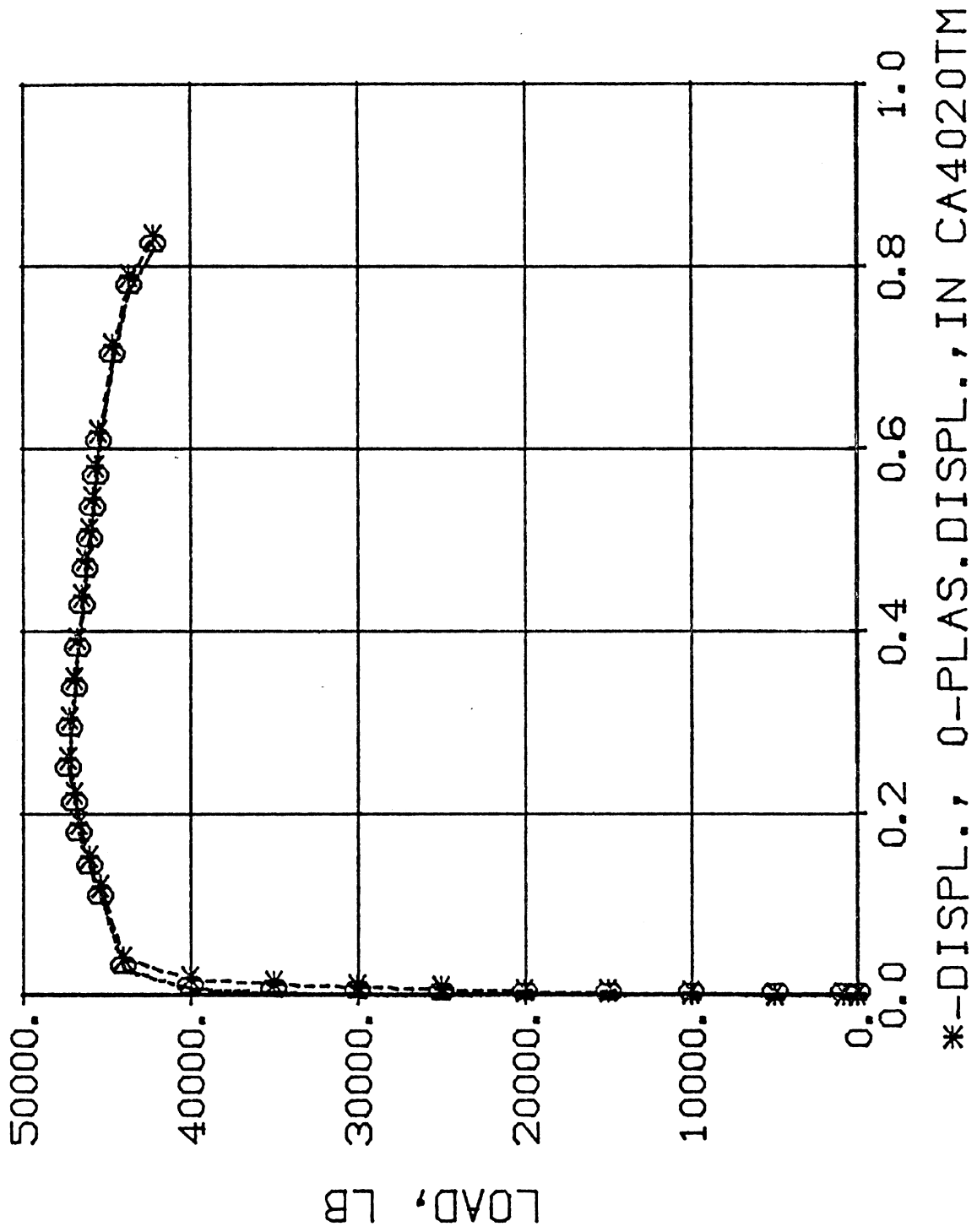


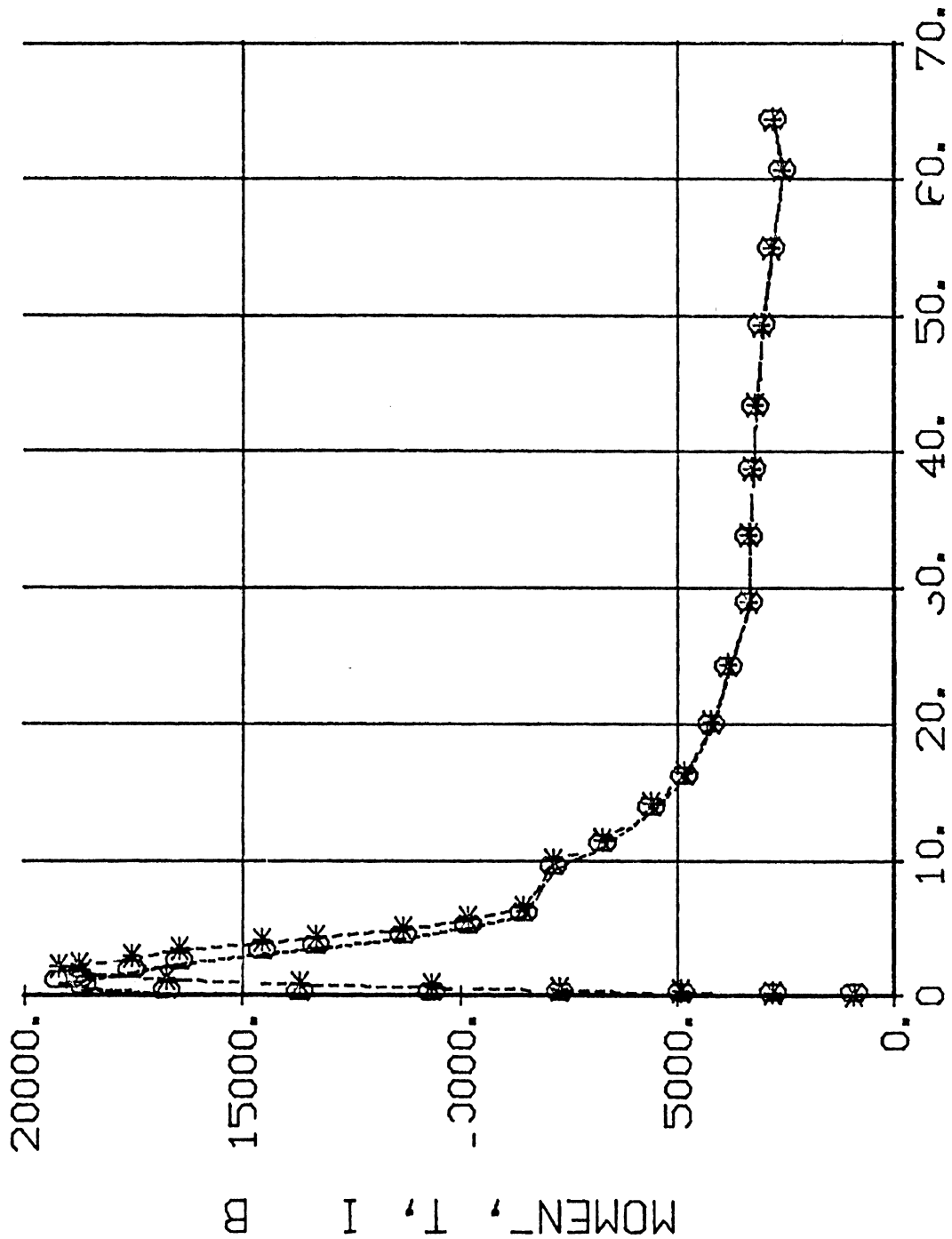




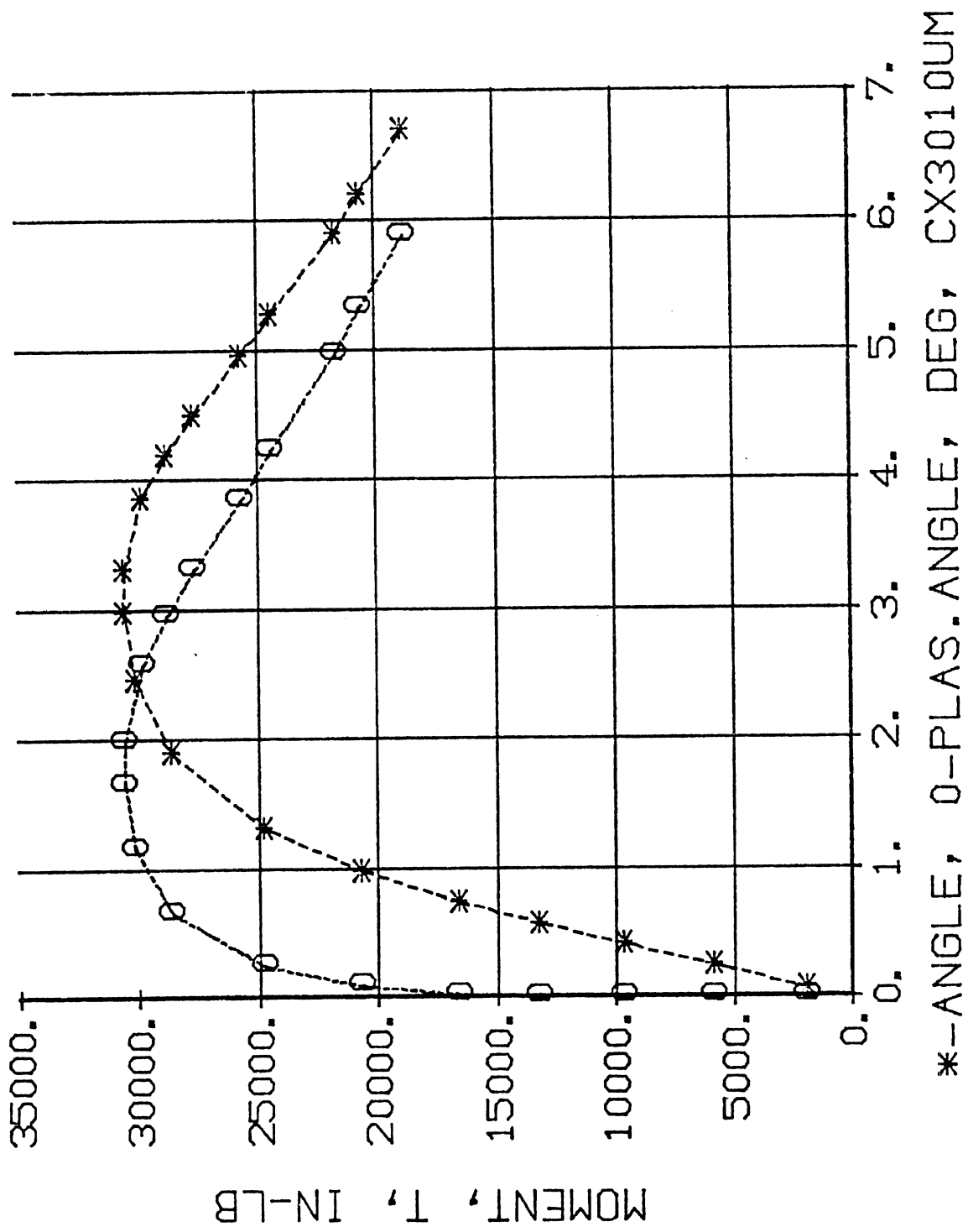


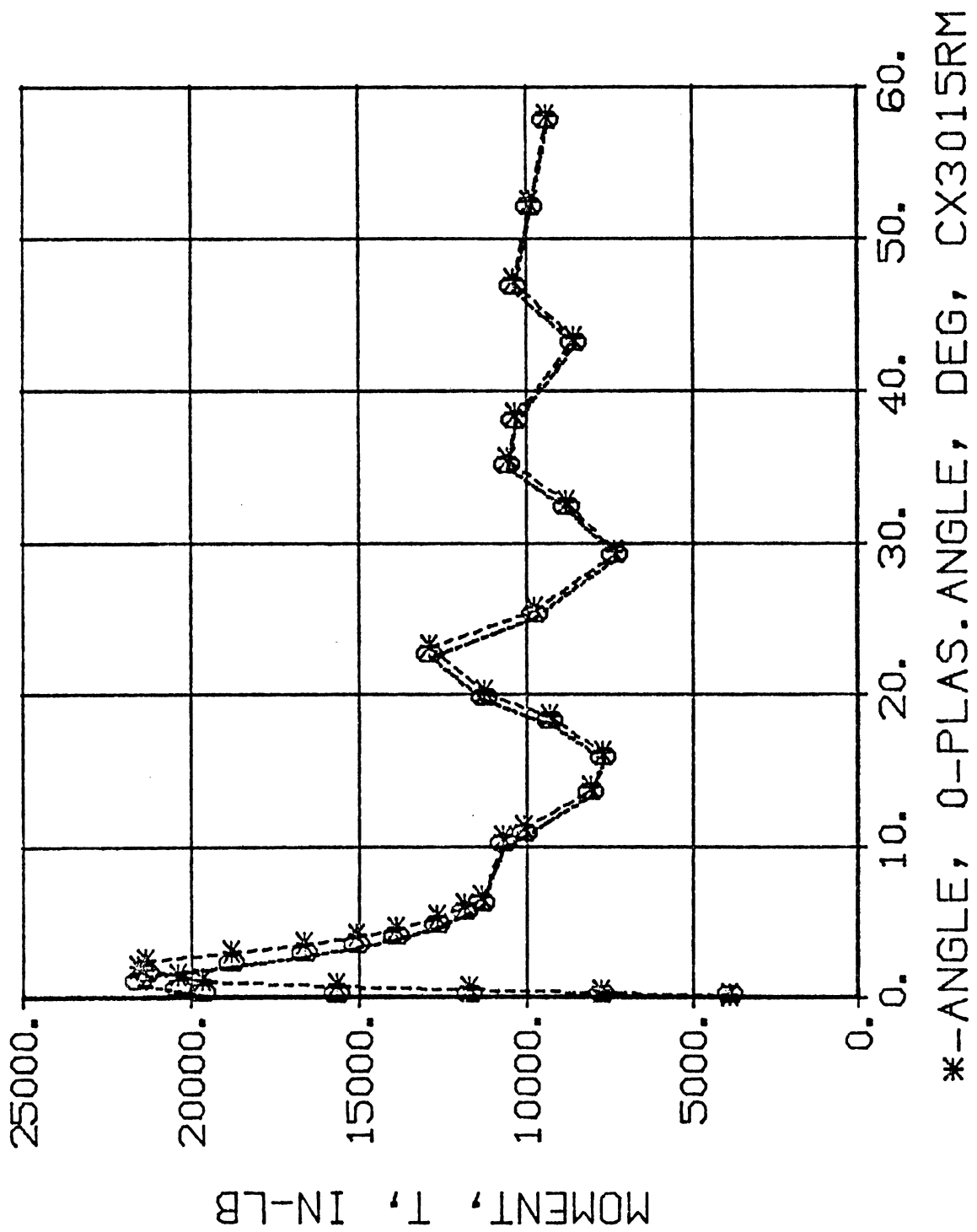


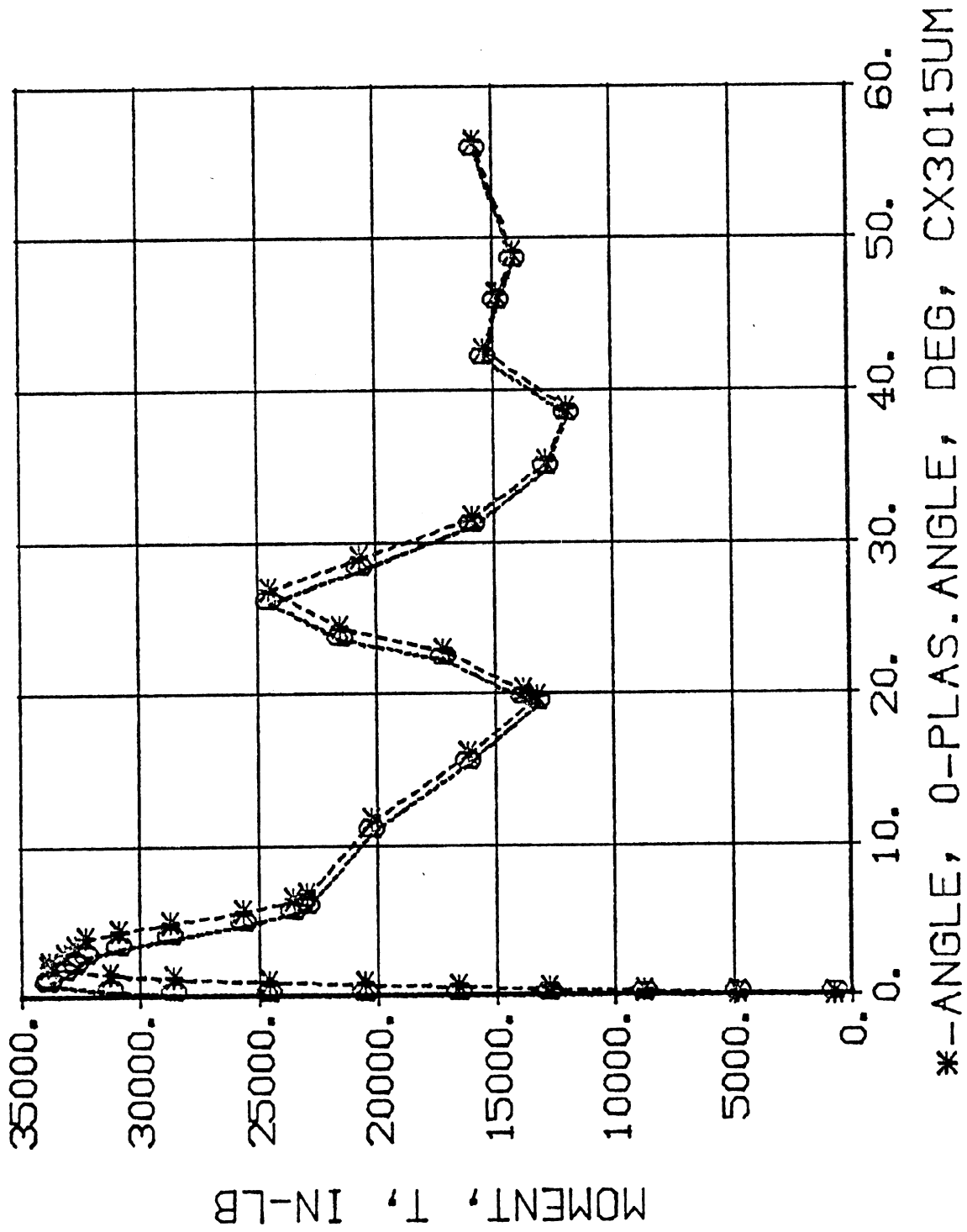




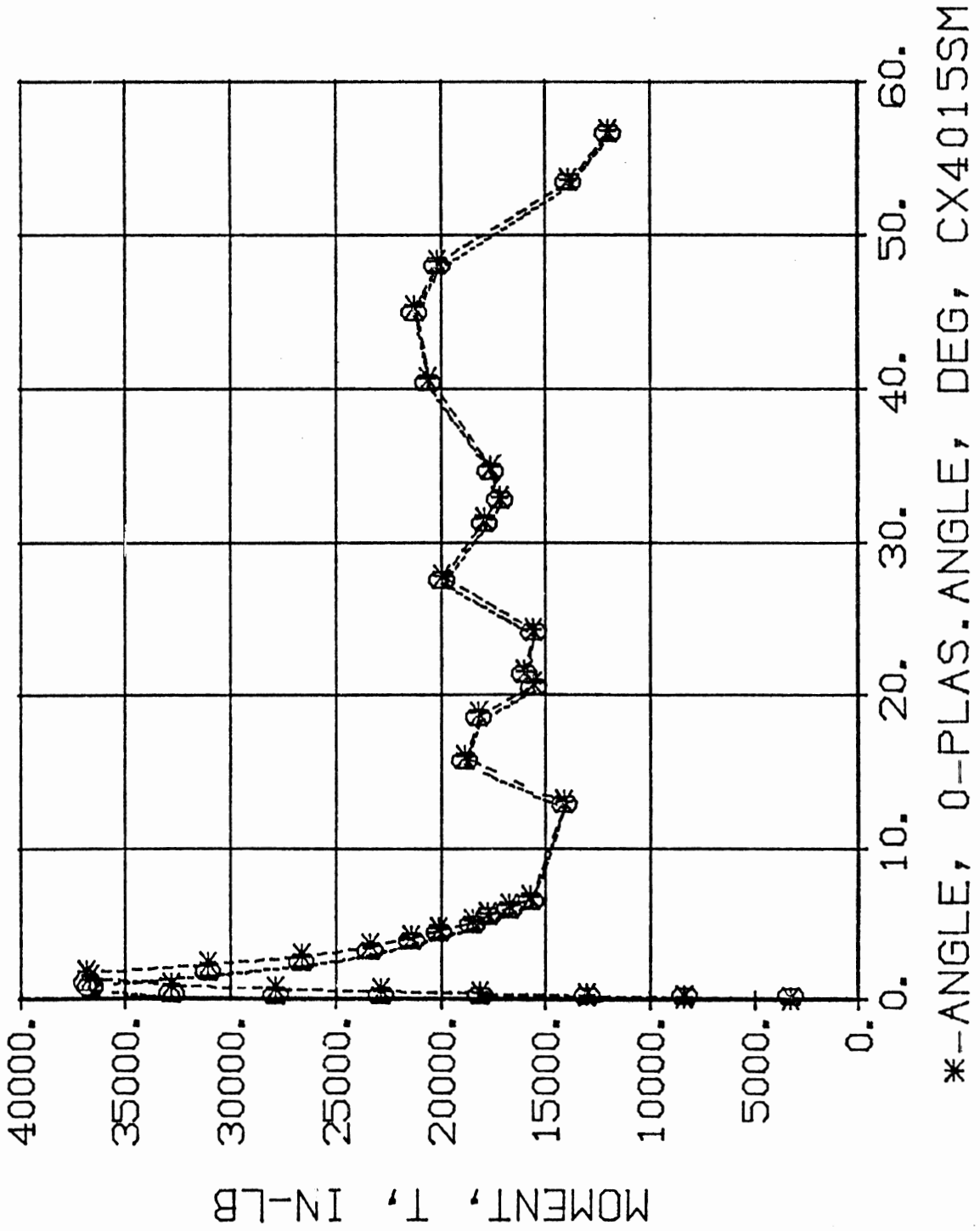
*-ANGLE, 0-PLAS.ANGL-, D=G, CXS010QM



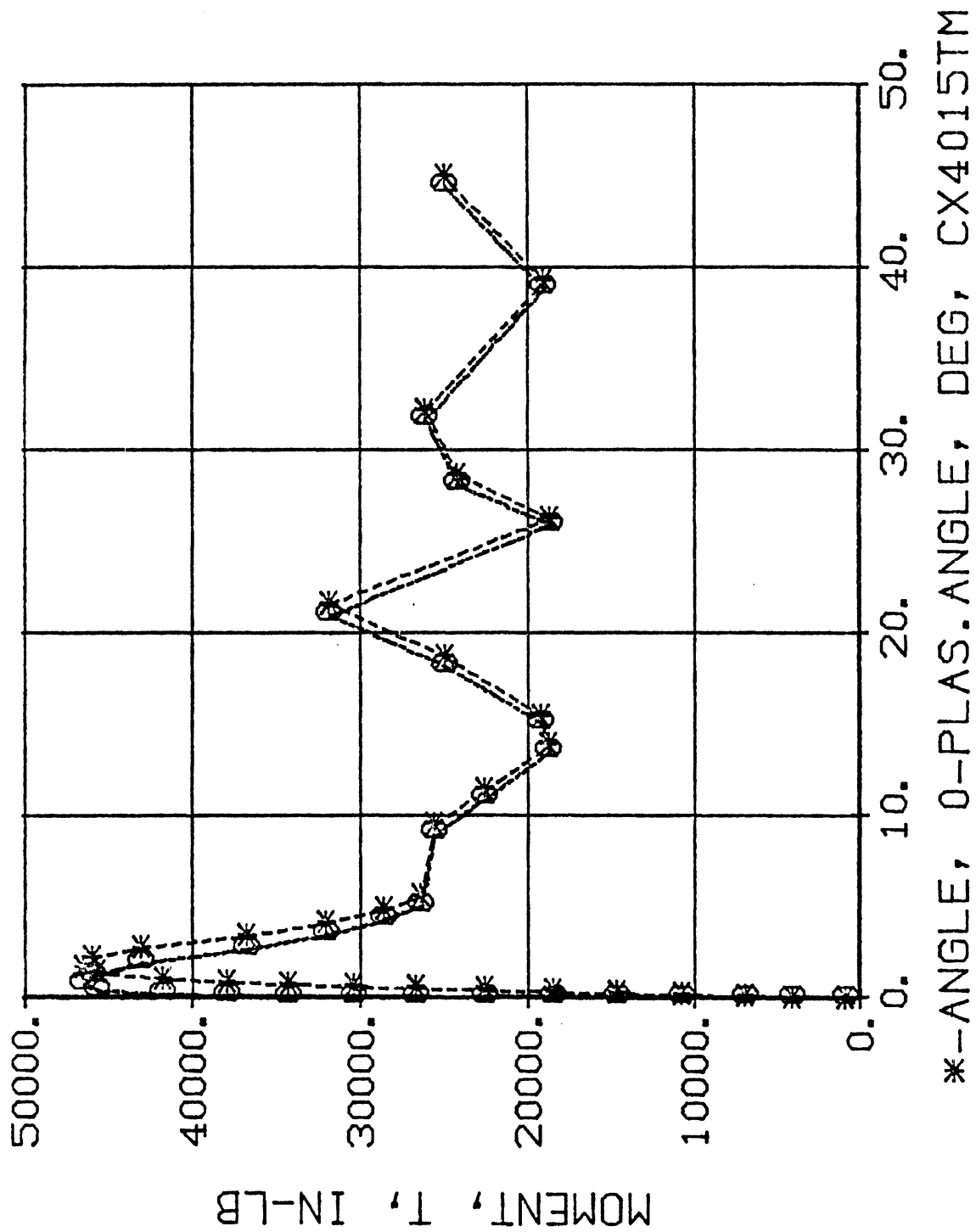


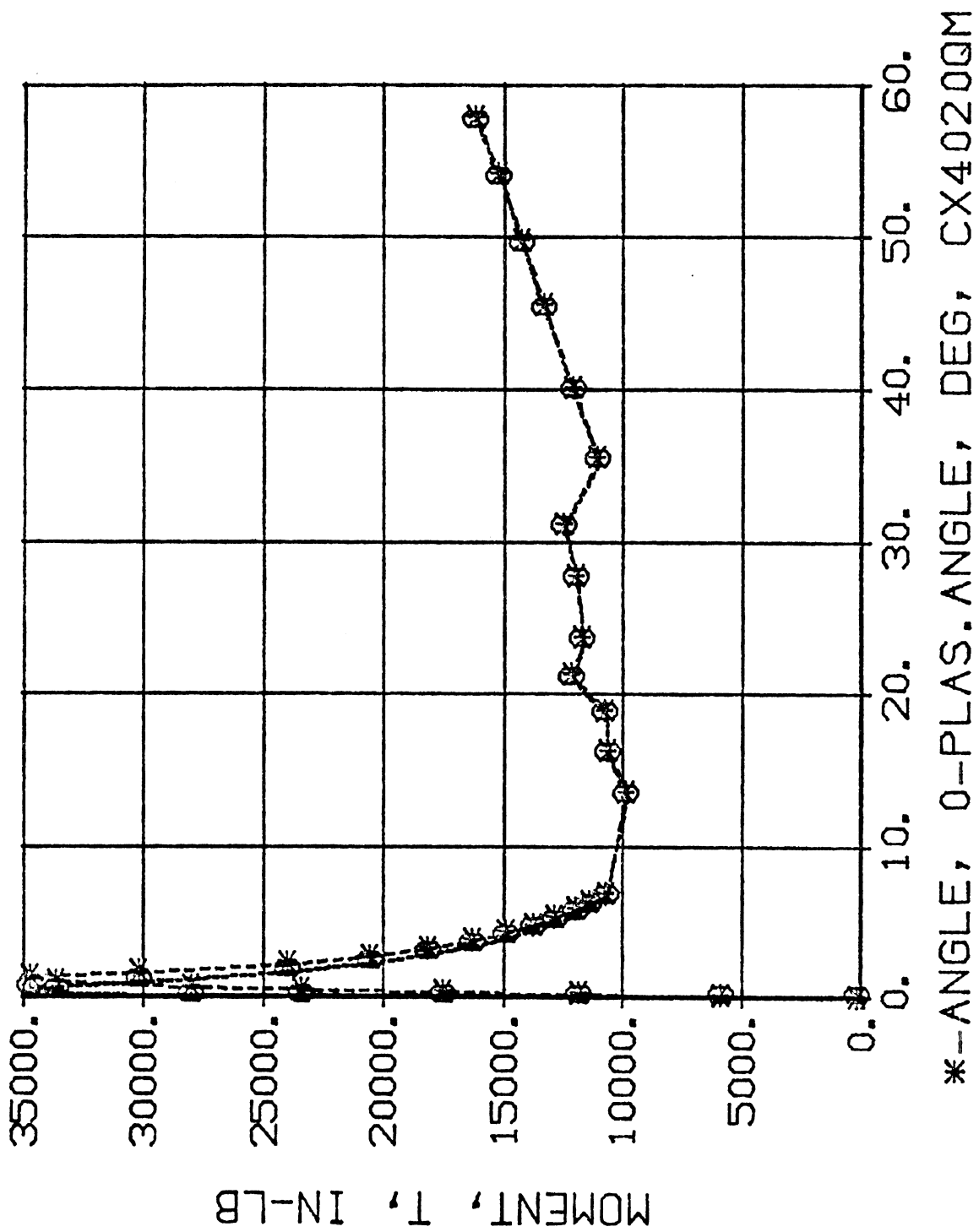


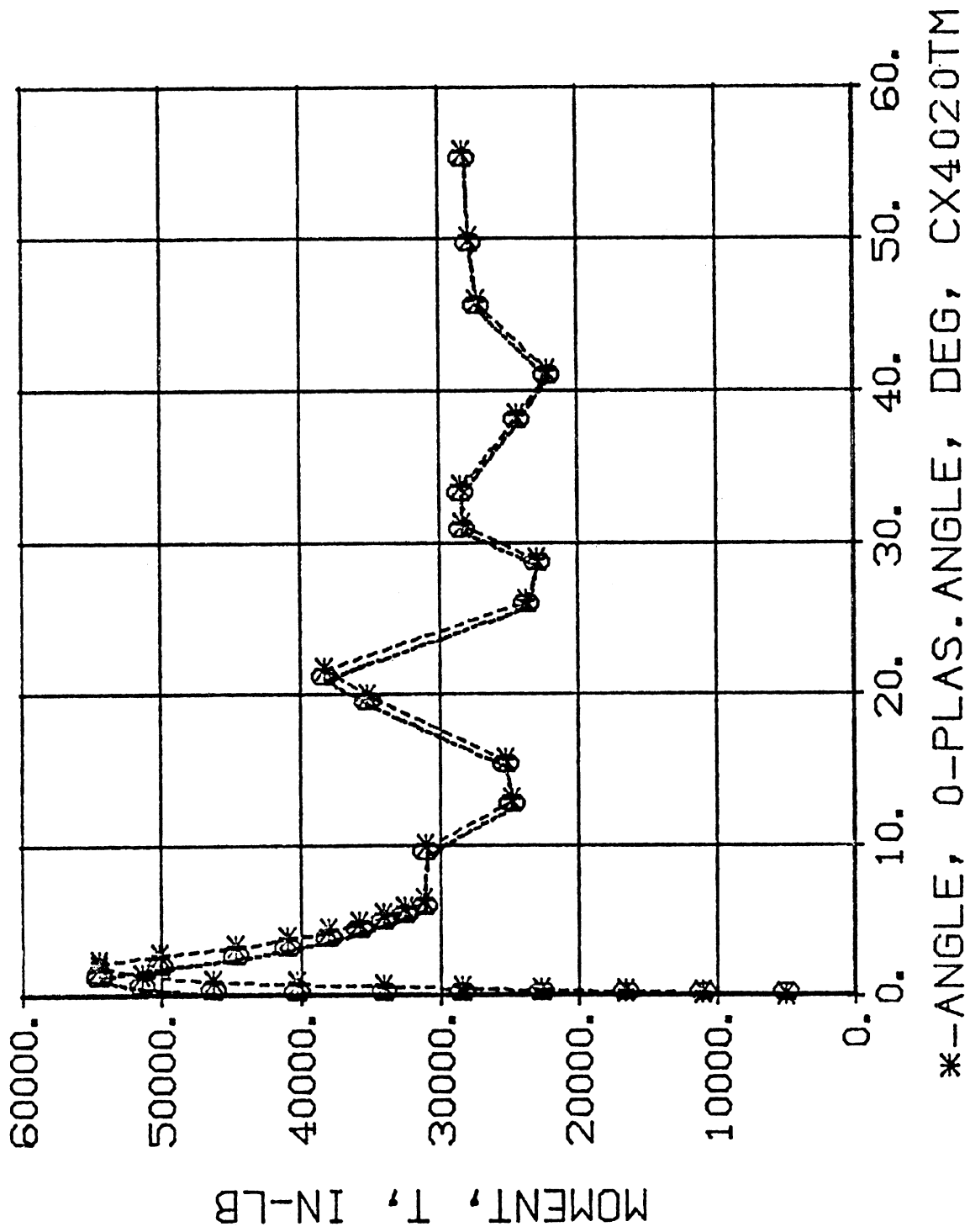
2 MIN 03 SEC.

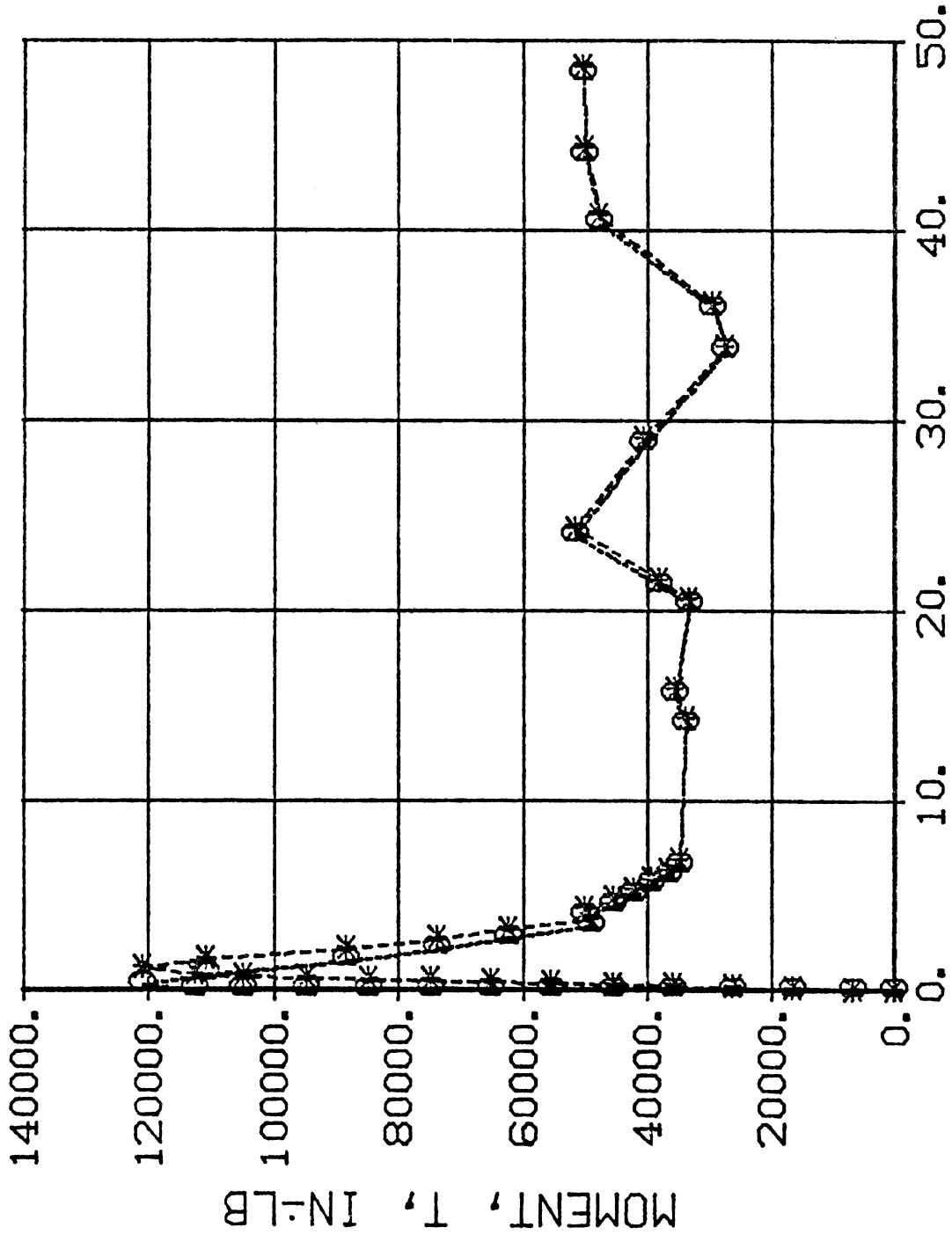


*--ANGLE, 0--PLAS.ANGLE, DEG, CX4015SM

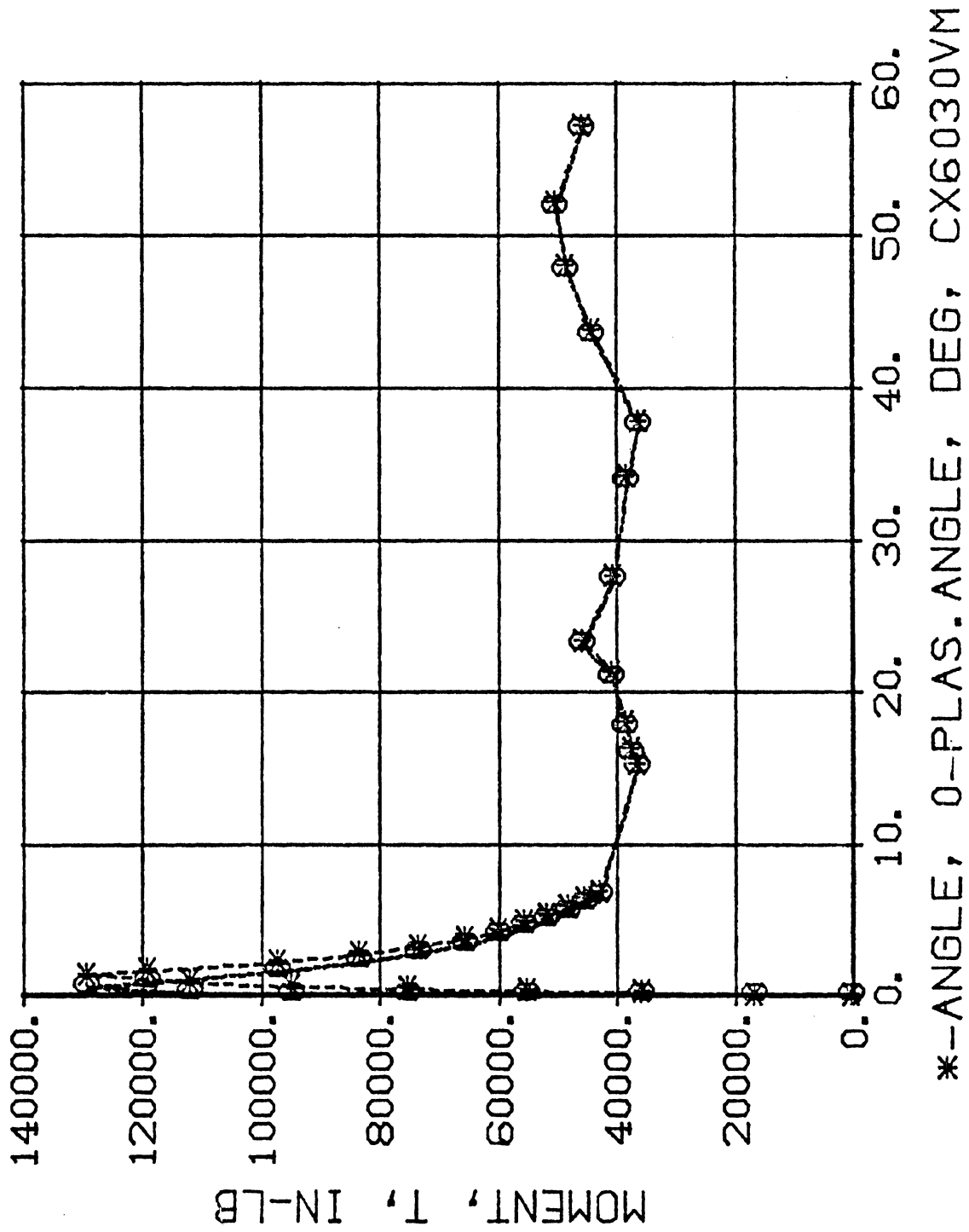


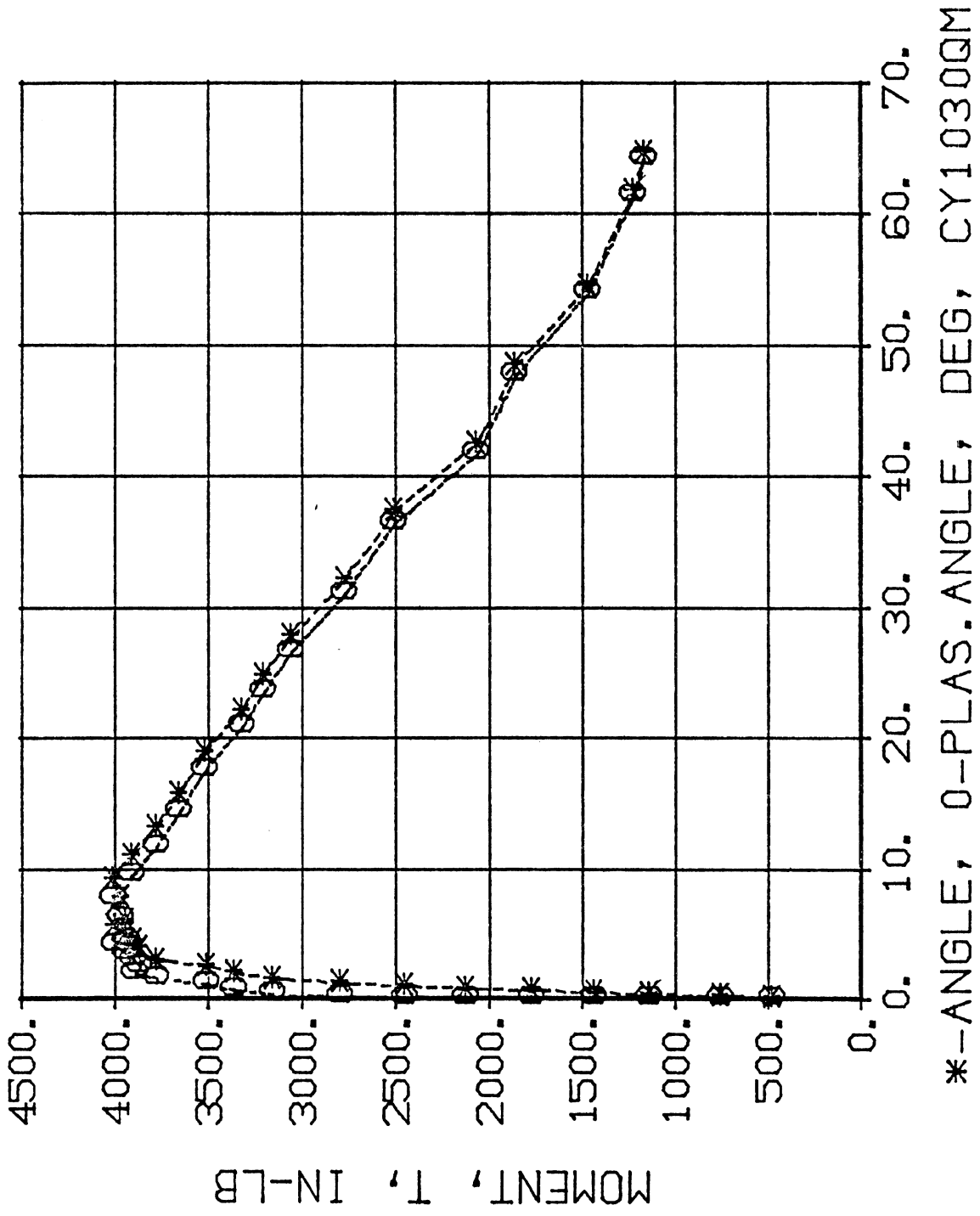


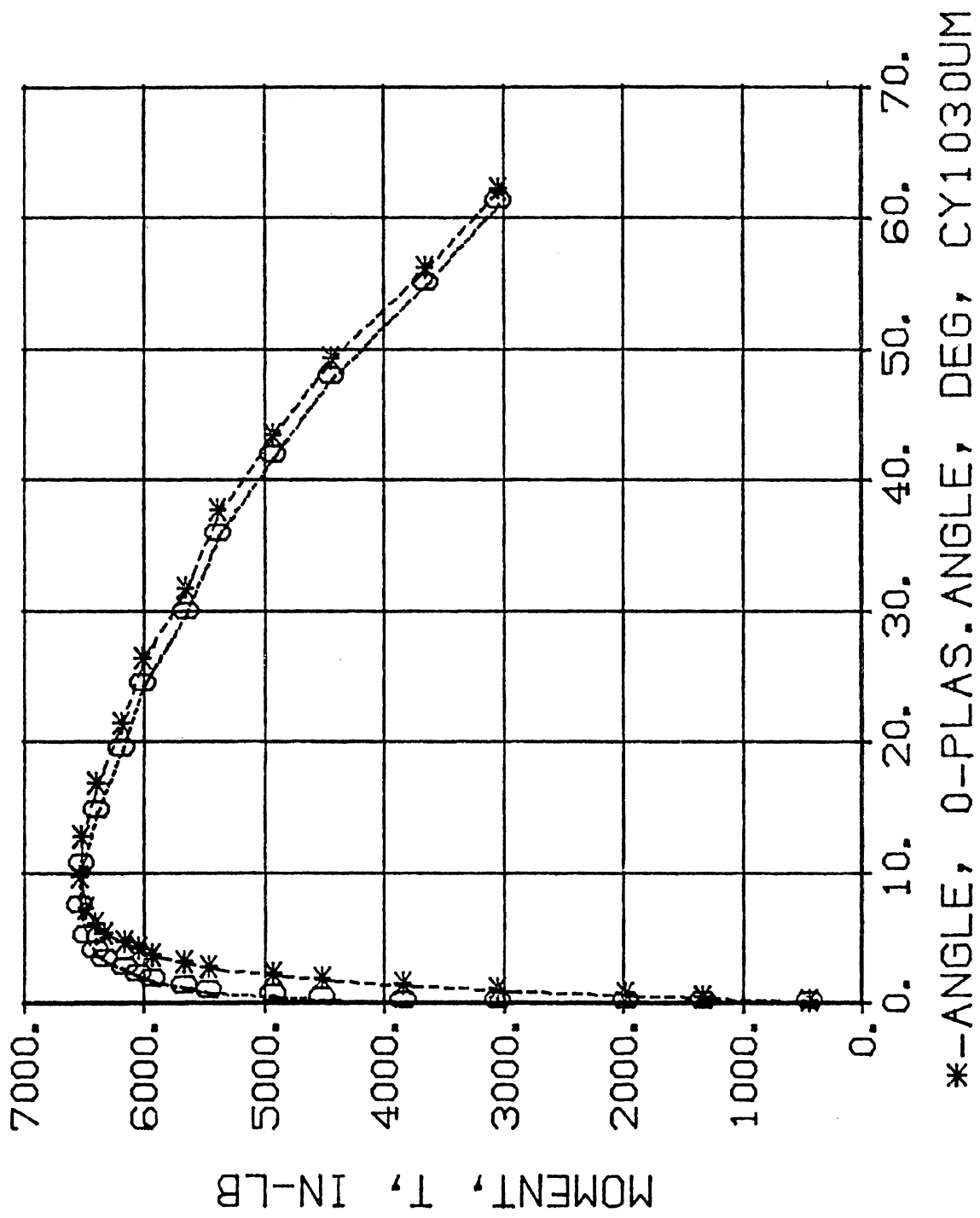


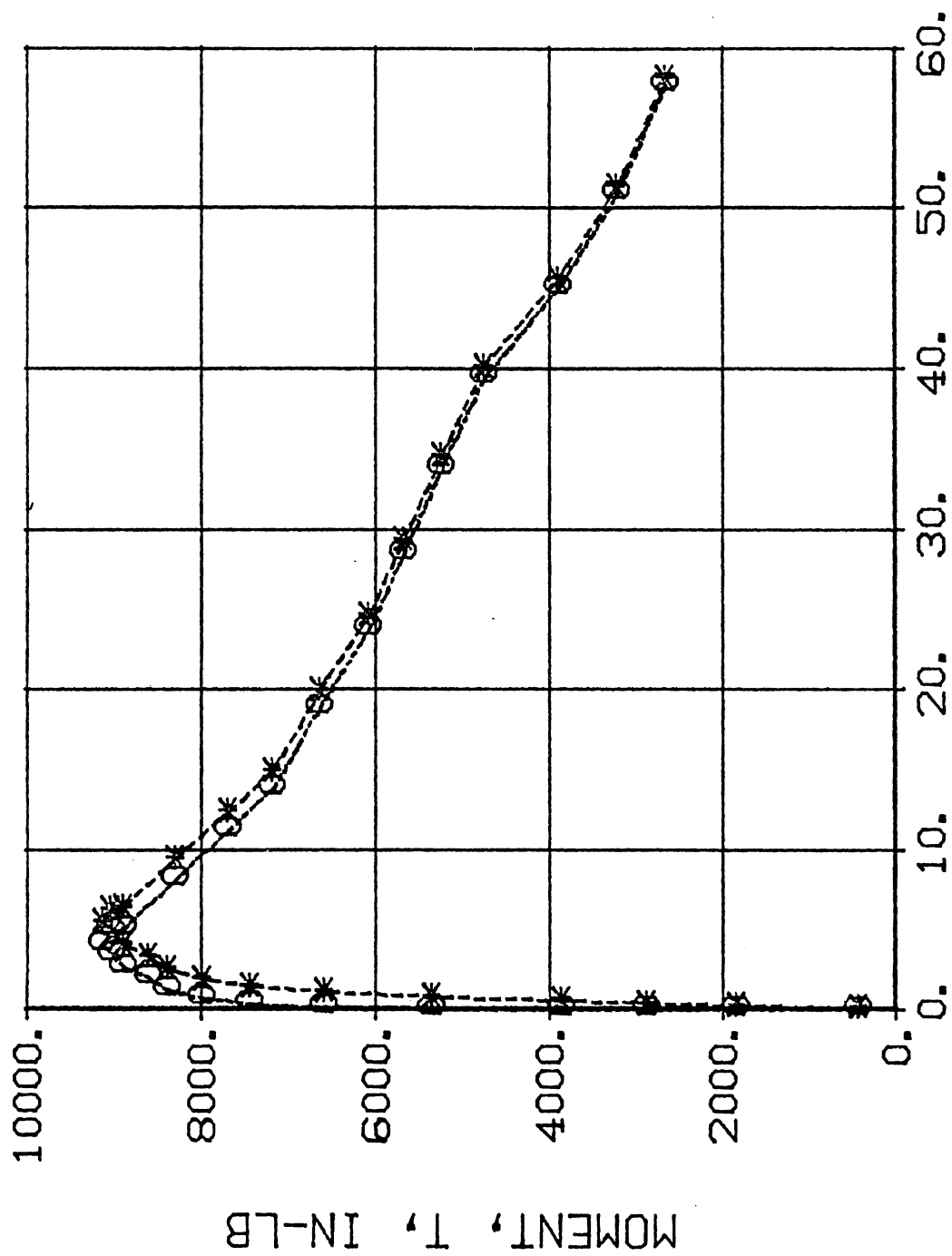


*--ANGLE, 0-PLAS. ANGLE, DEG, CX6020VM

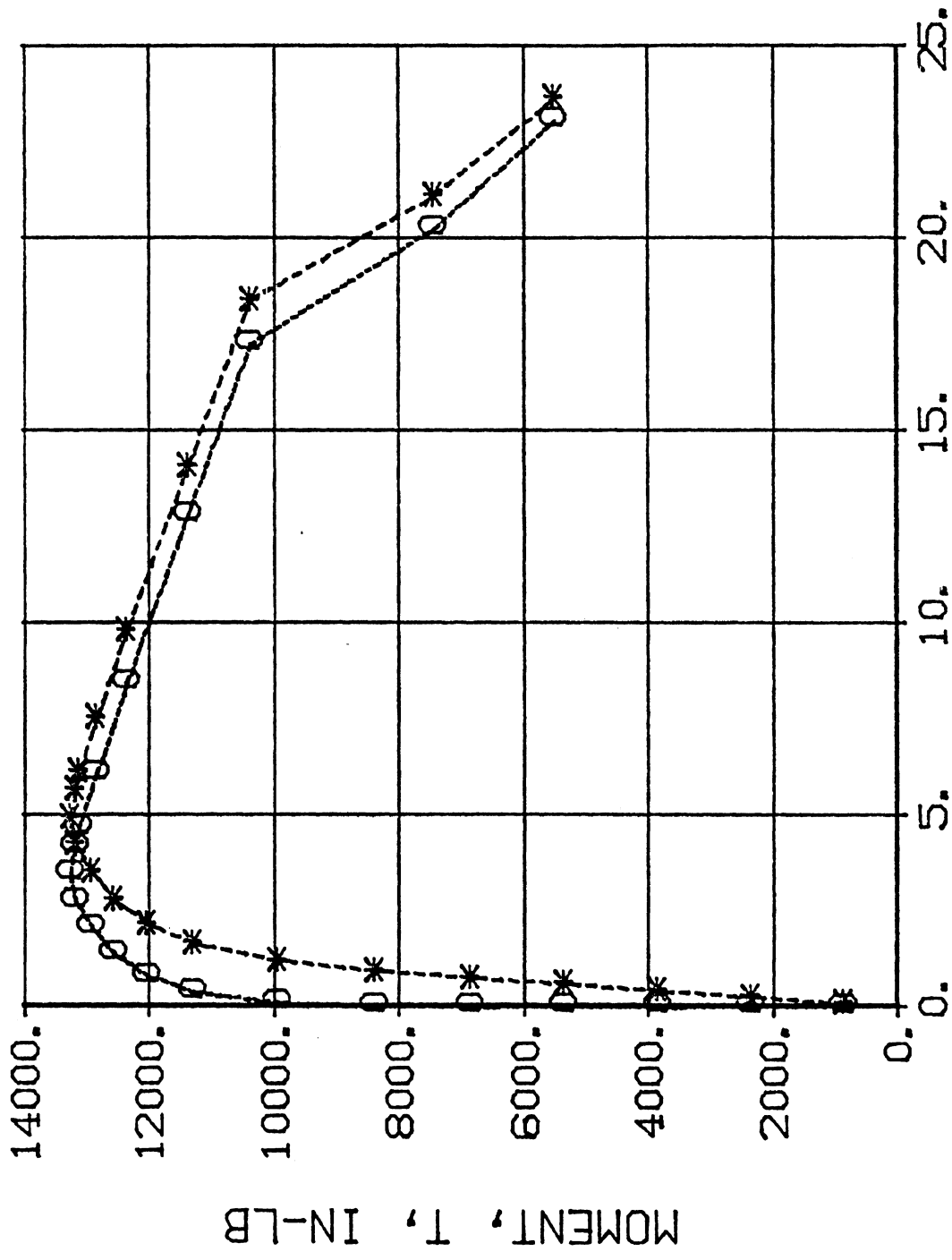






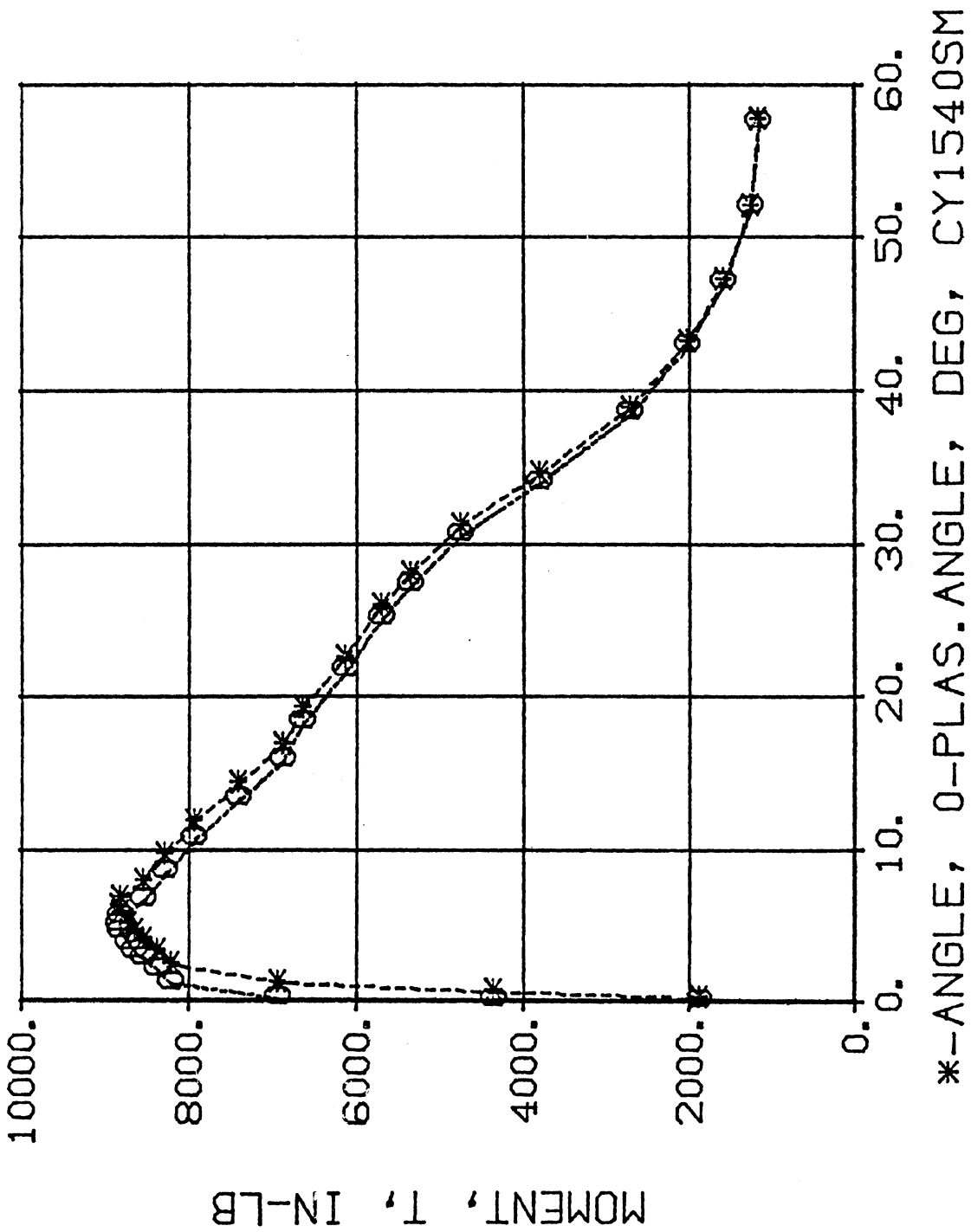


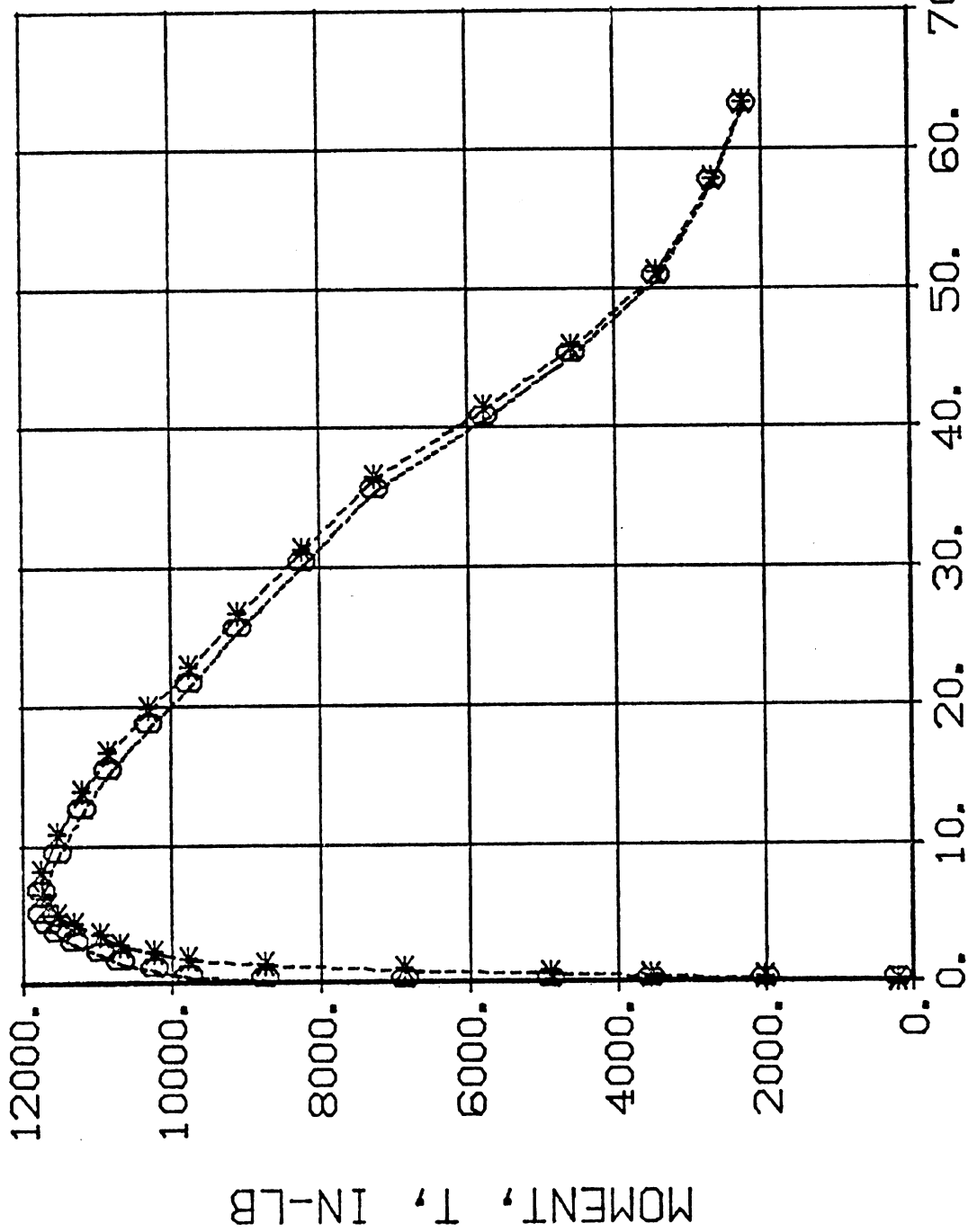
*-ANGLE, 0-PLAS. ANGLE, DEG, CY1530RM



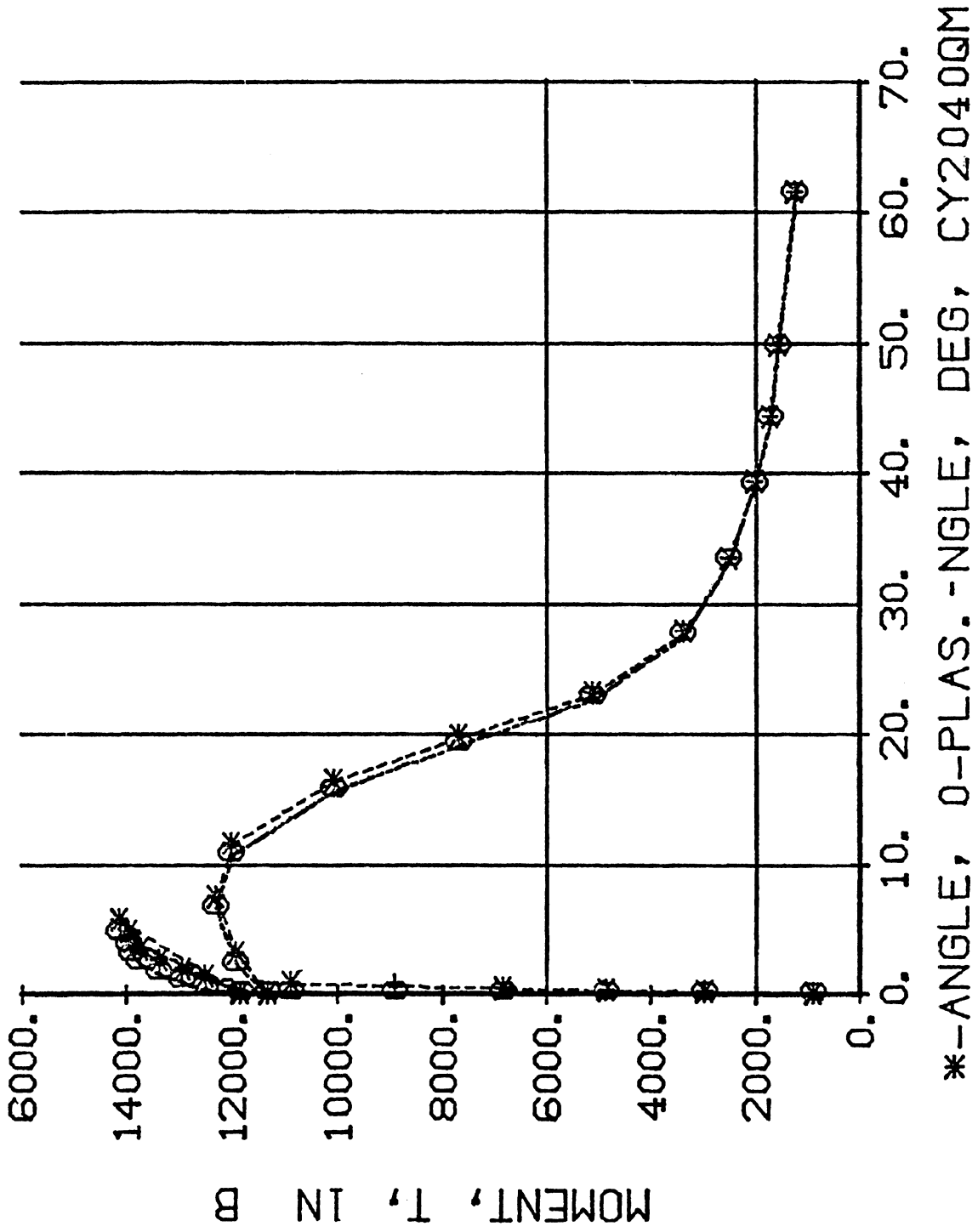
*--ANGLE, 0-PLAS. ANGLE, DEG, CY1530UM

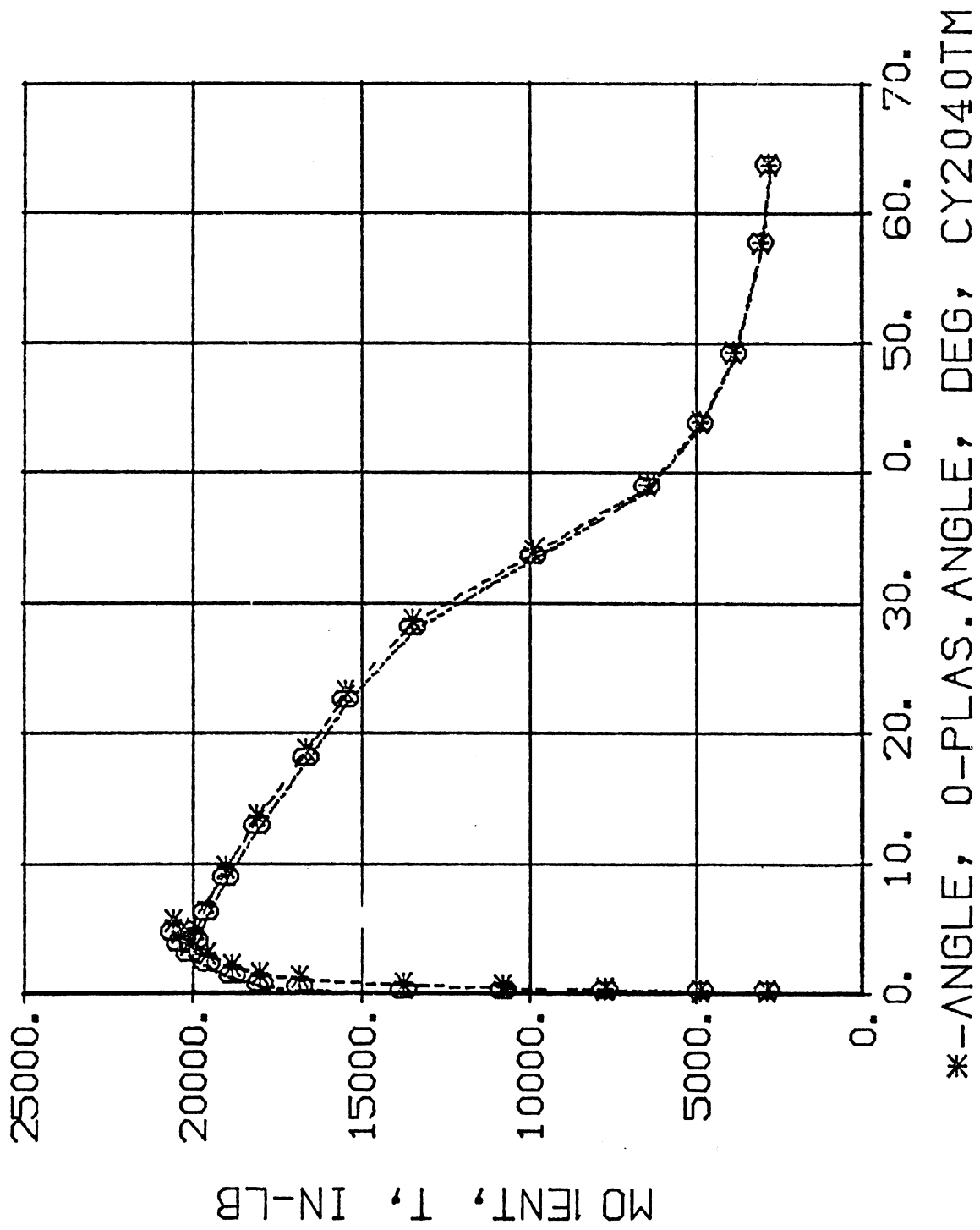
1 MIN 48 SEC.

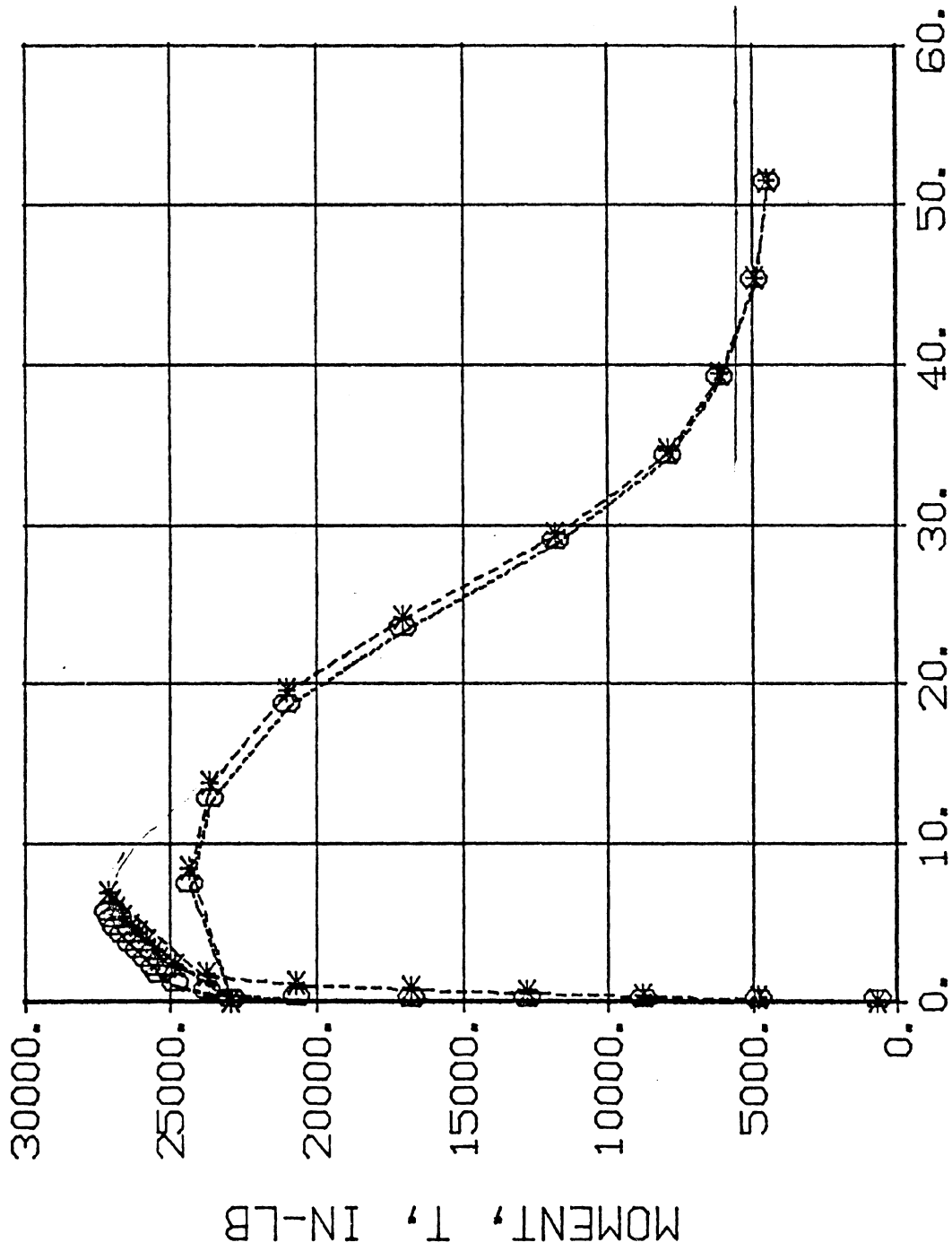




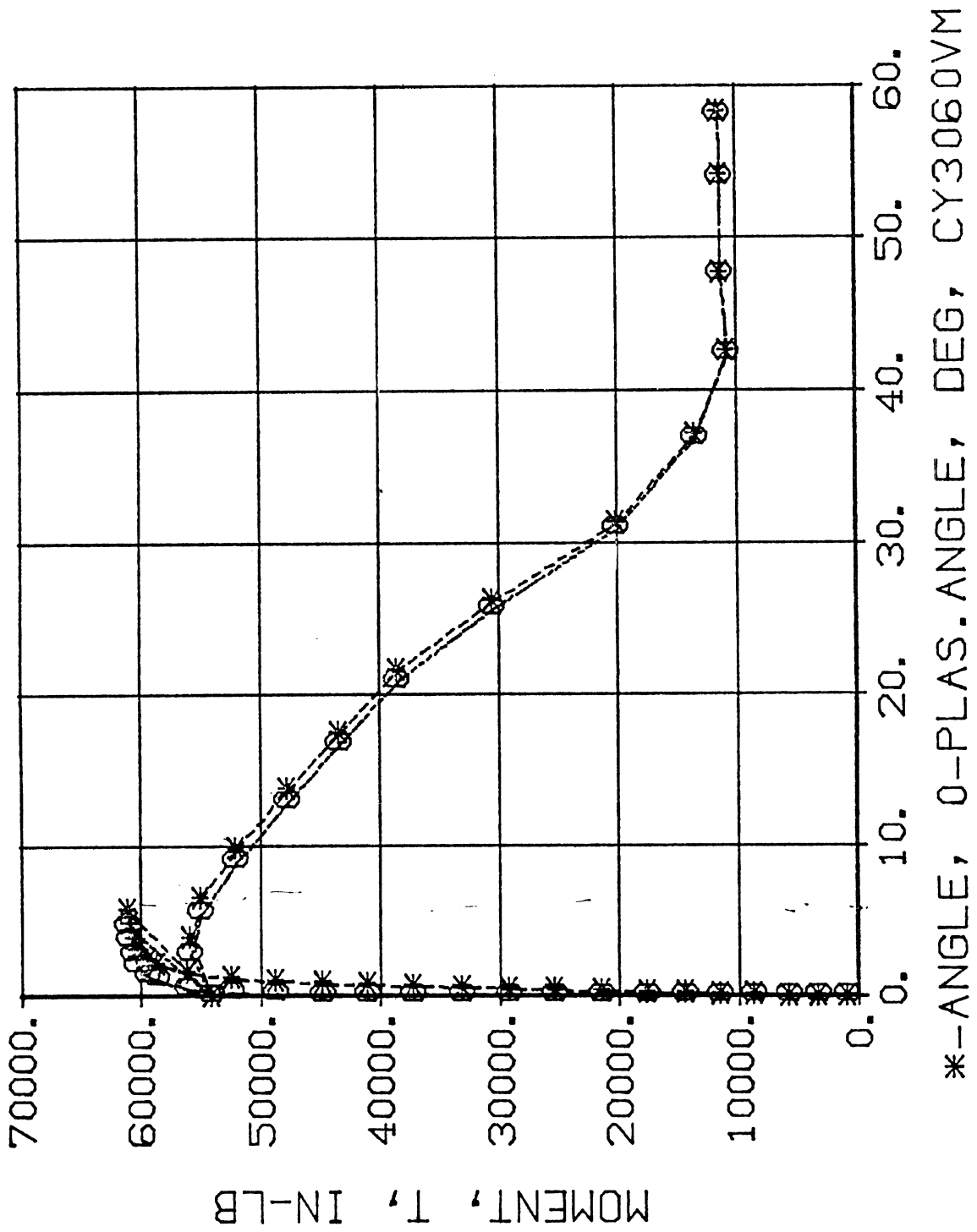
*--ANGLE, 0-PLAS. ANGLE, DEG, CY1540TM

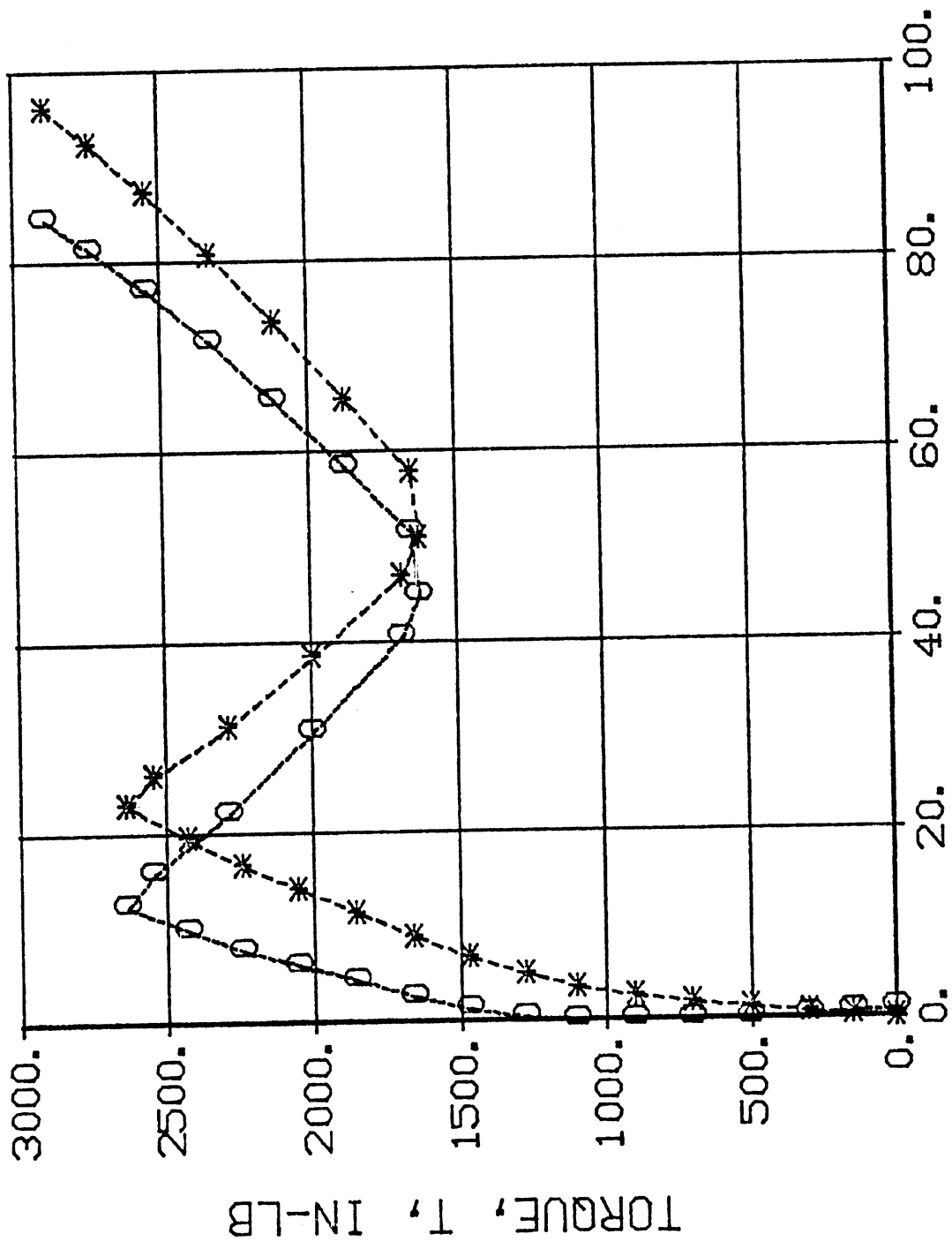




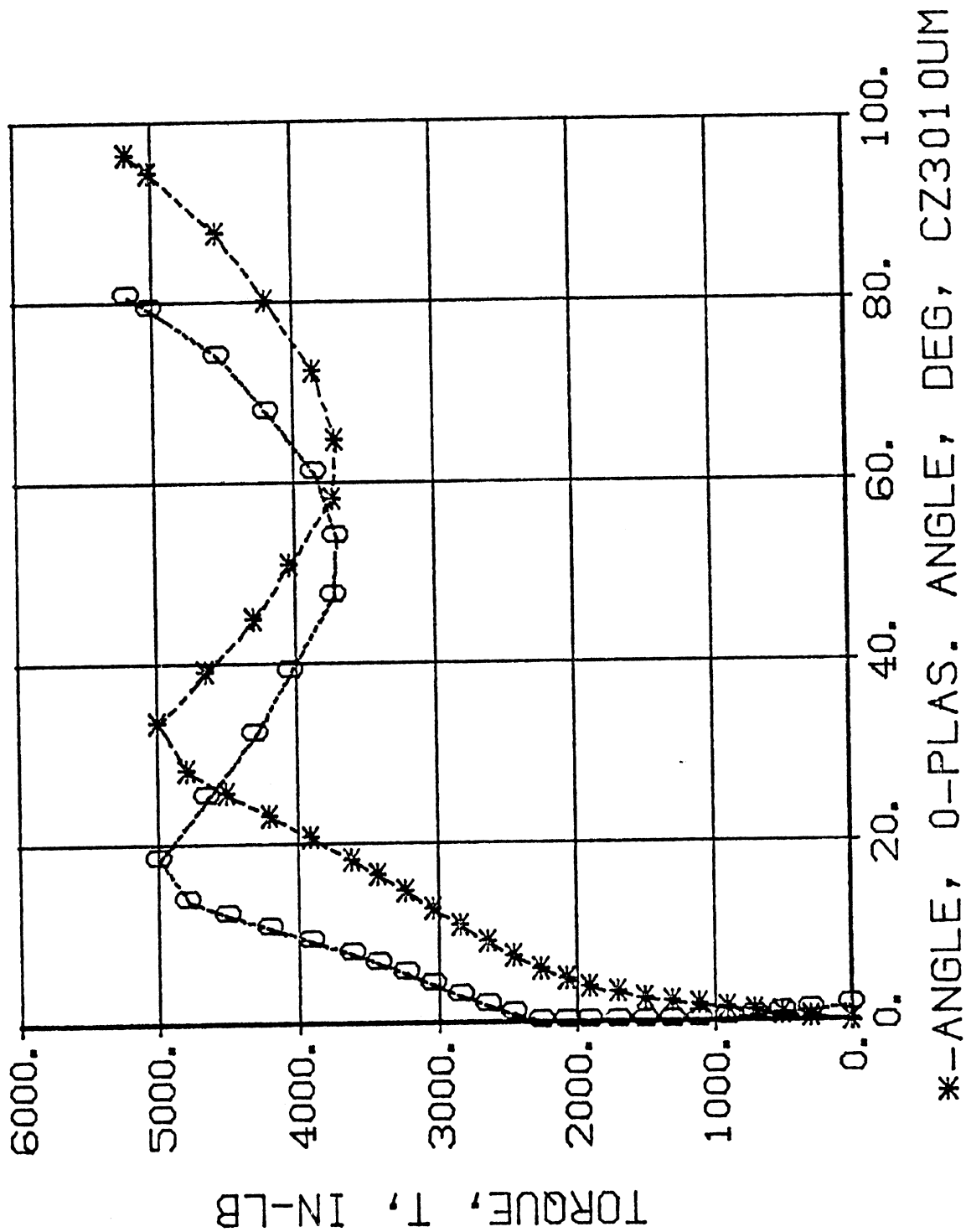


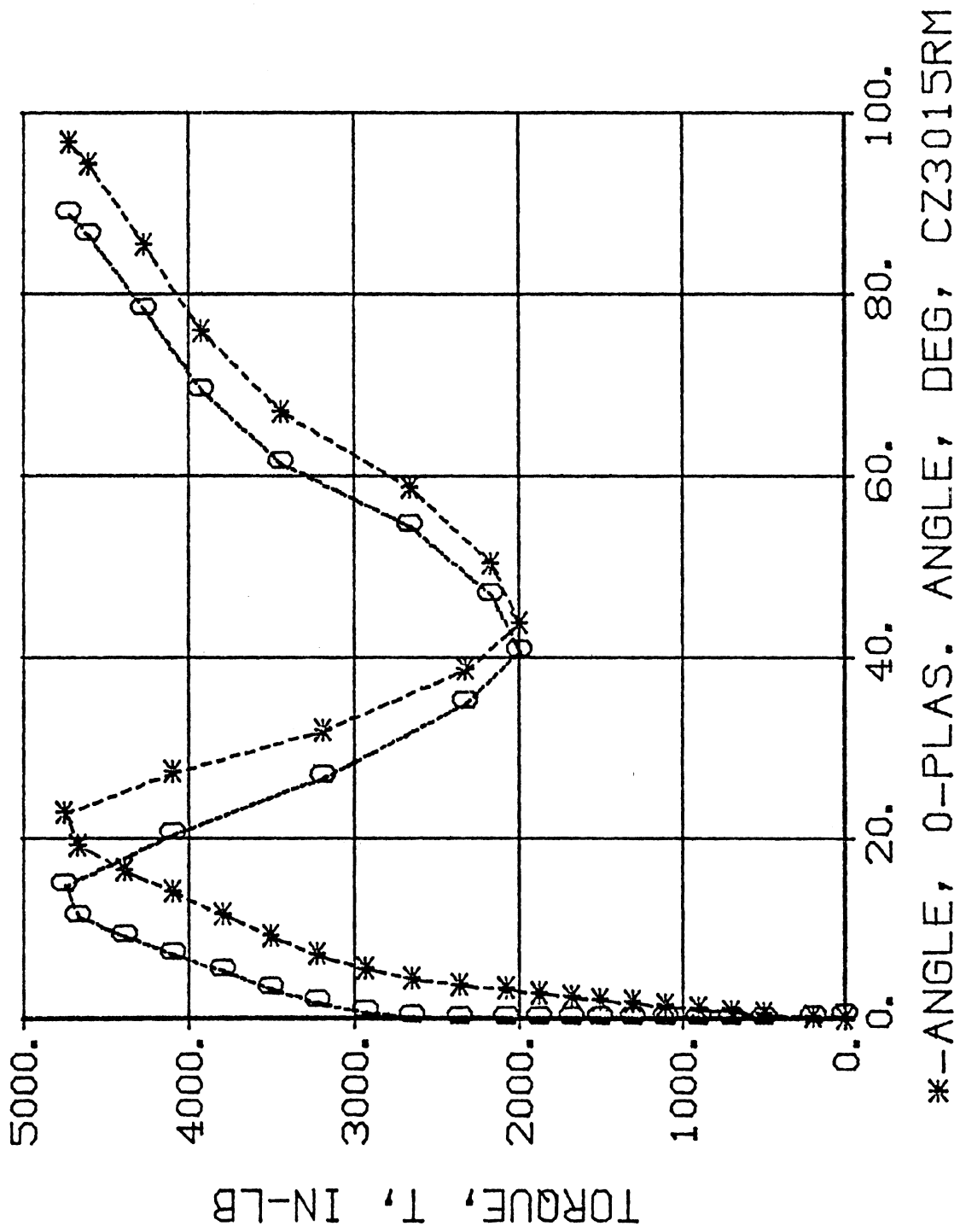
*-ANGLE, 0-PLAS. ANGLE, DEG, CY2060VM

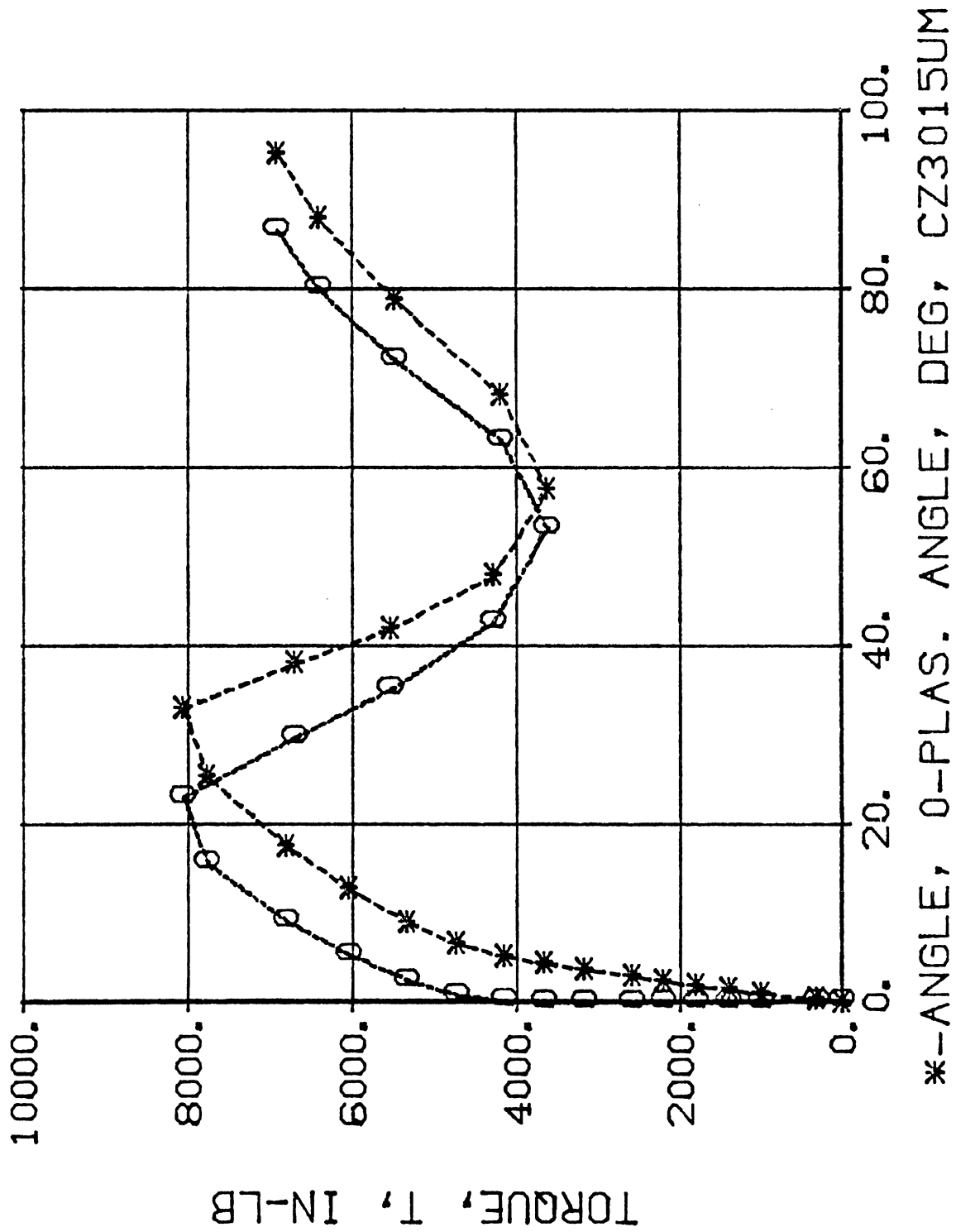


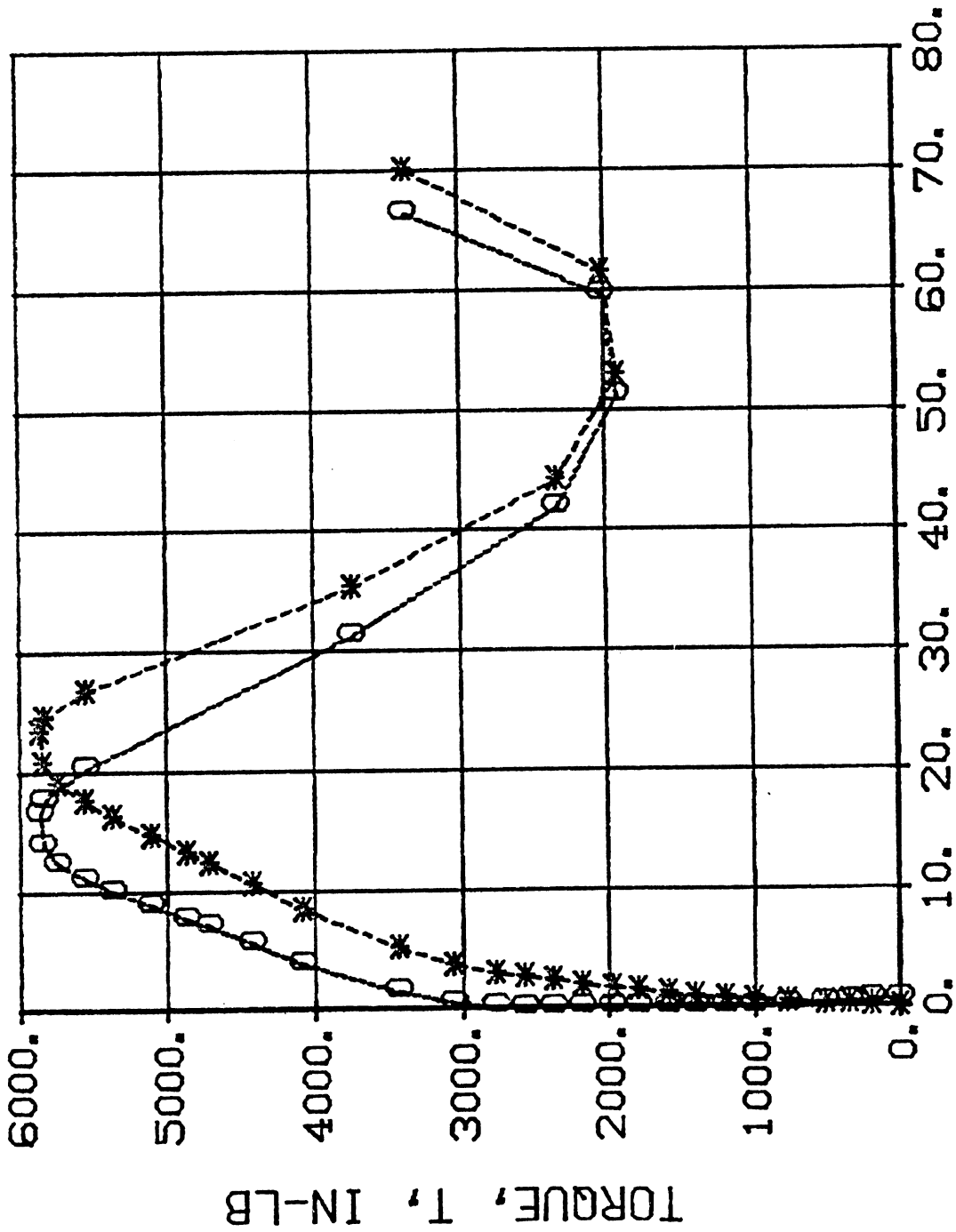


*--ANGLE, 0-PLAS. ANGLE, DEG, CZ3010QM

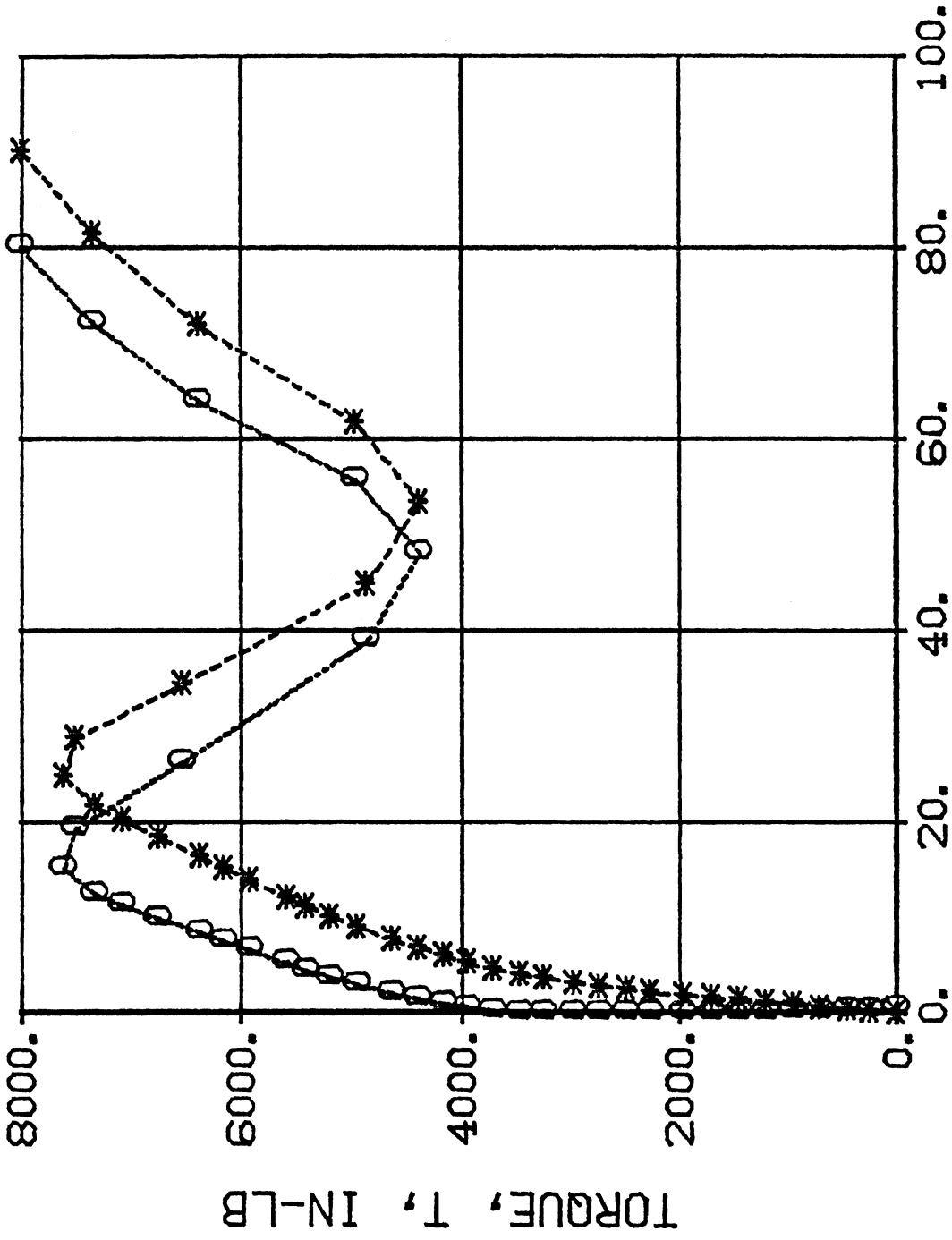




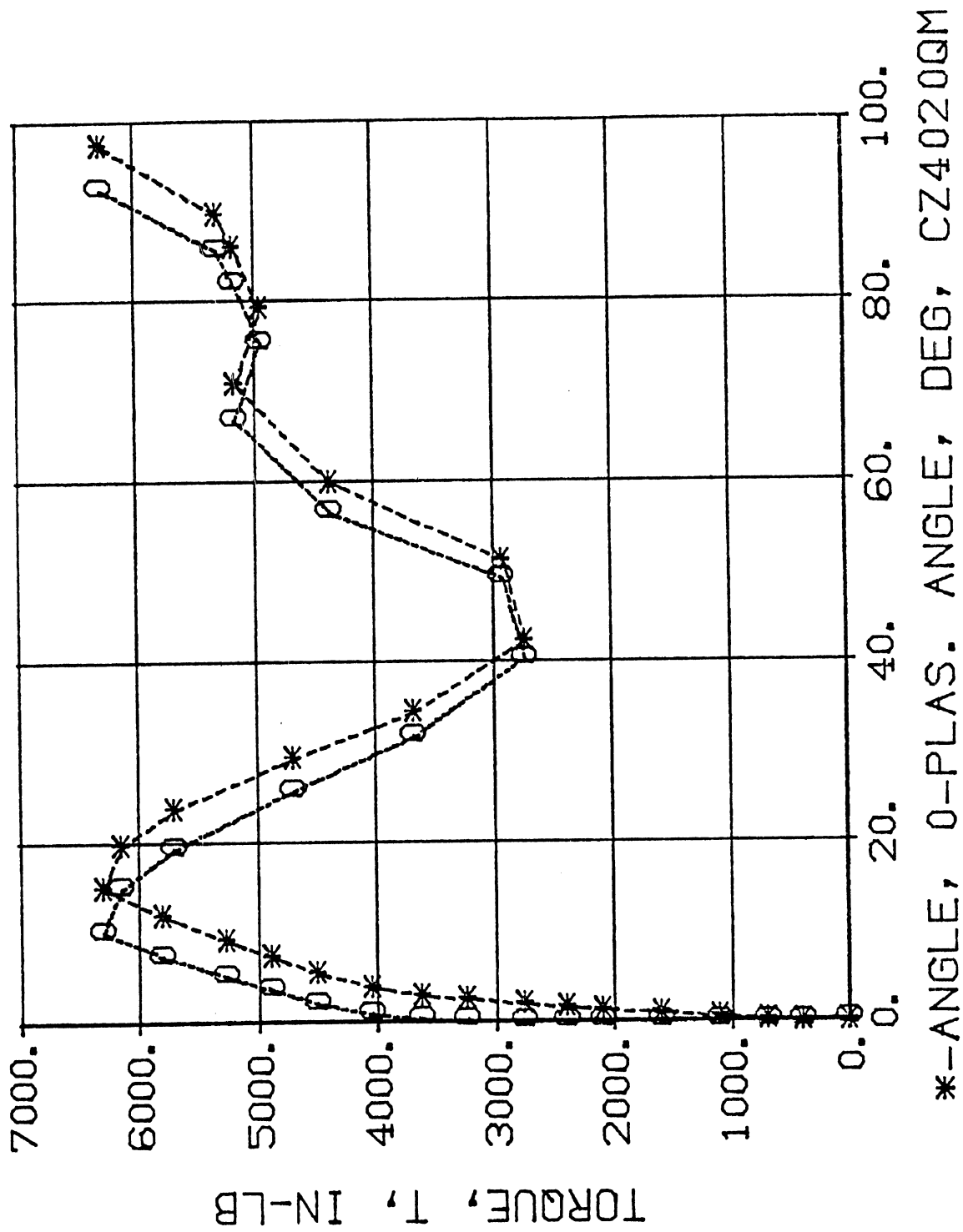


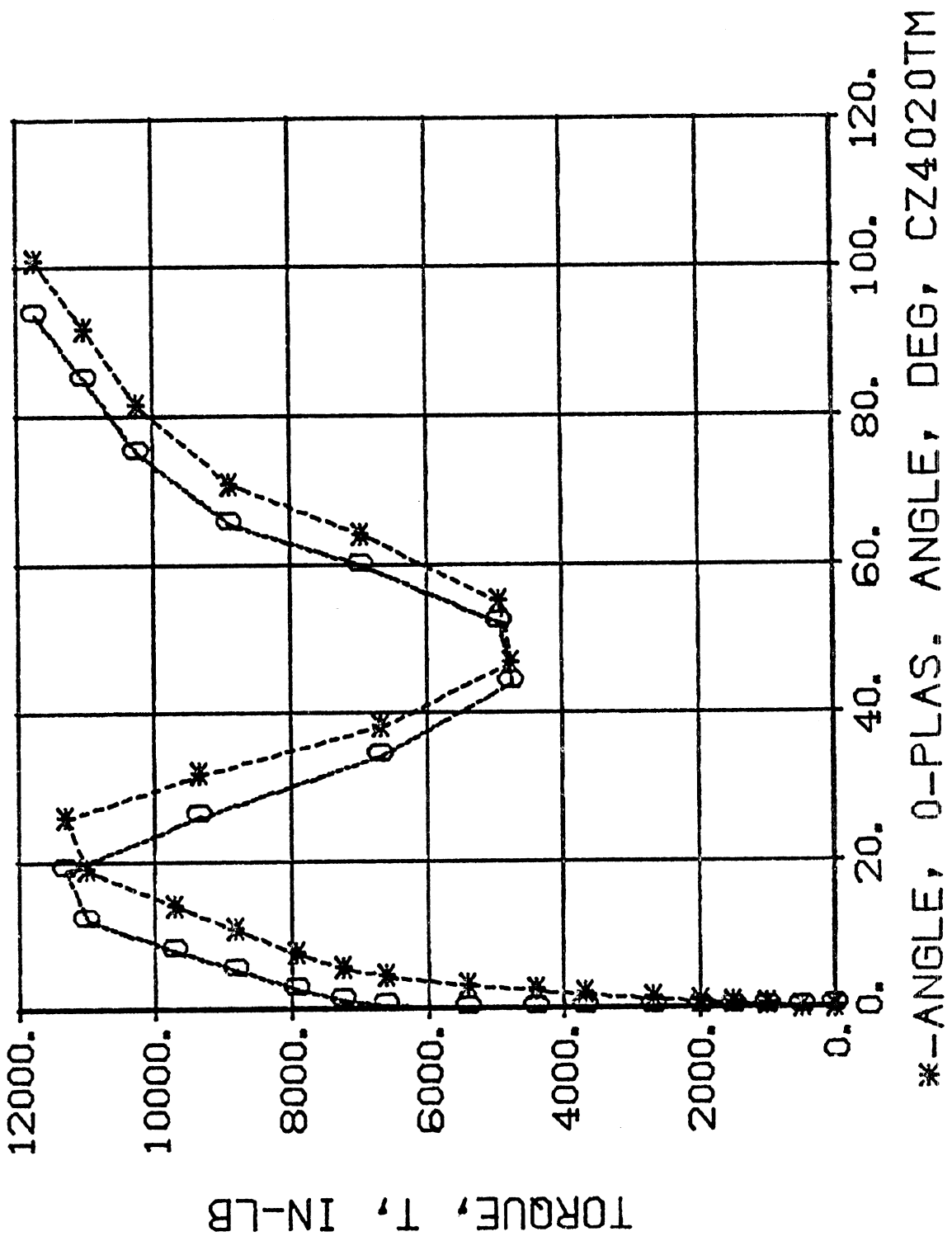


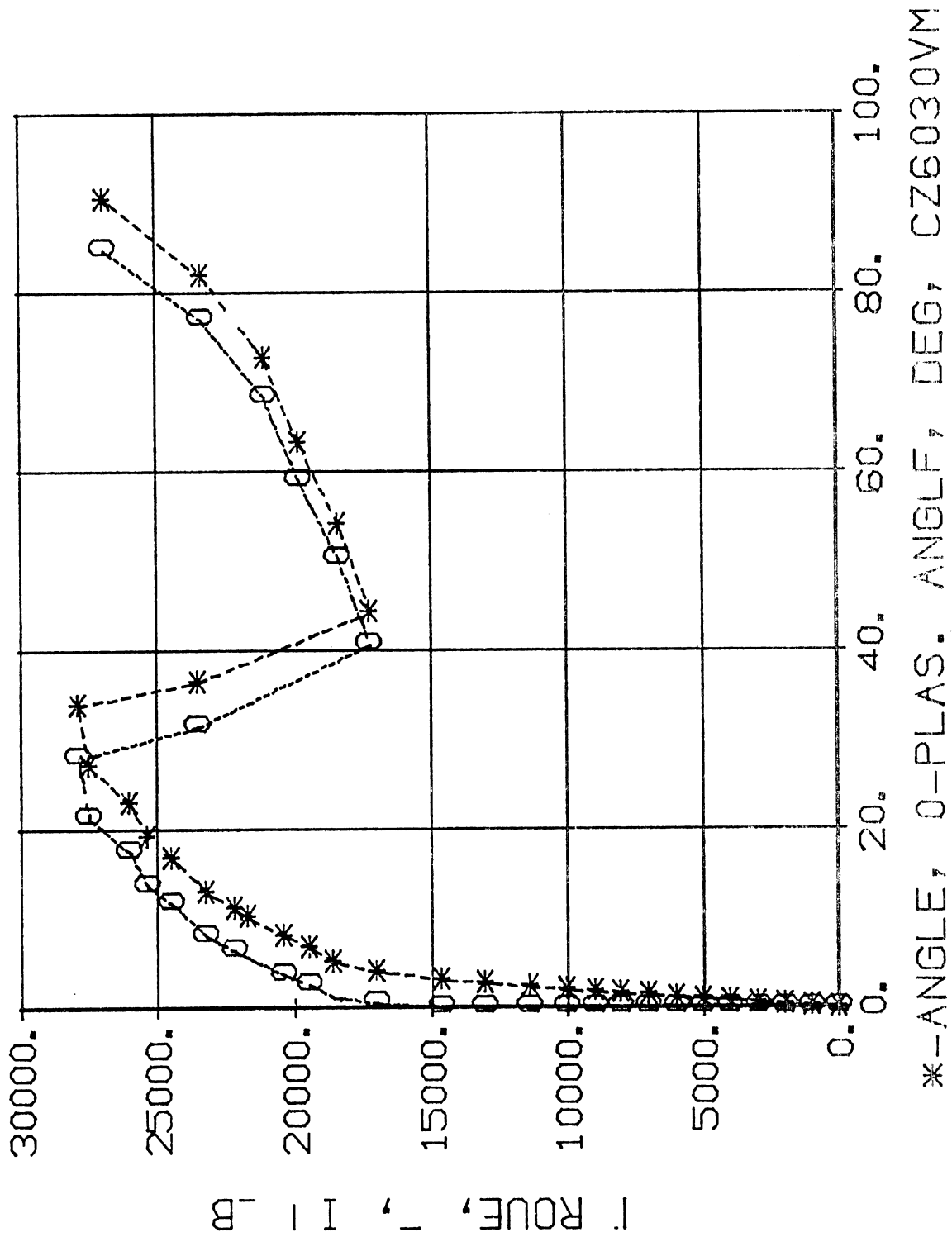
*--ANGLE, 0-PLAS. ANGLE, DEG, CZ4015SM



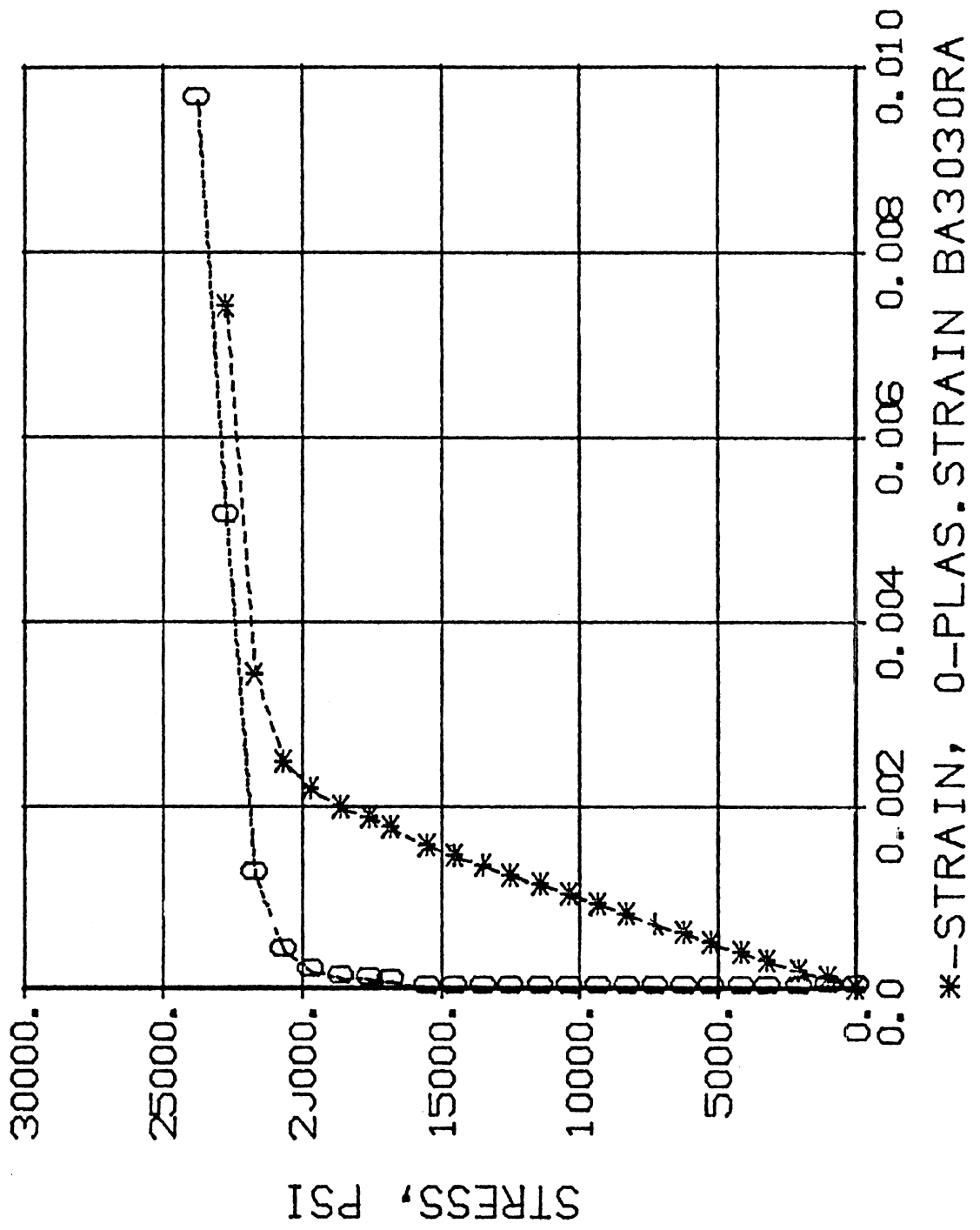
*-ANGLE, 0-PLAS. ANGLE, DEG, CZ4015TM

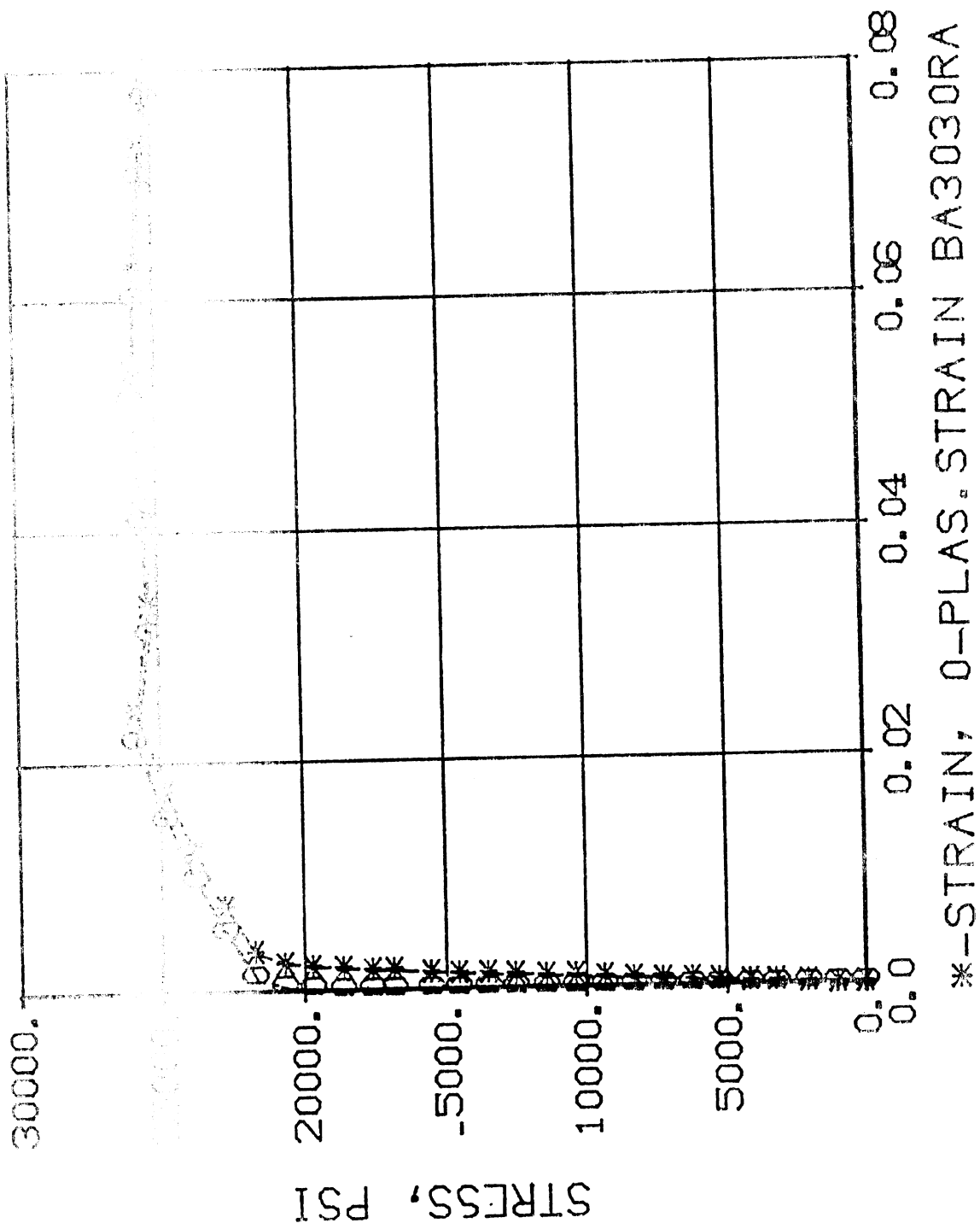


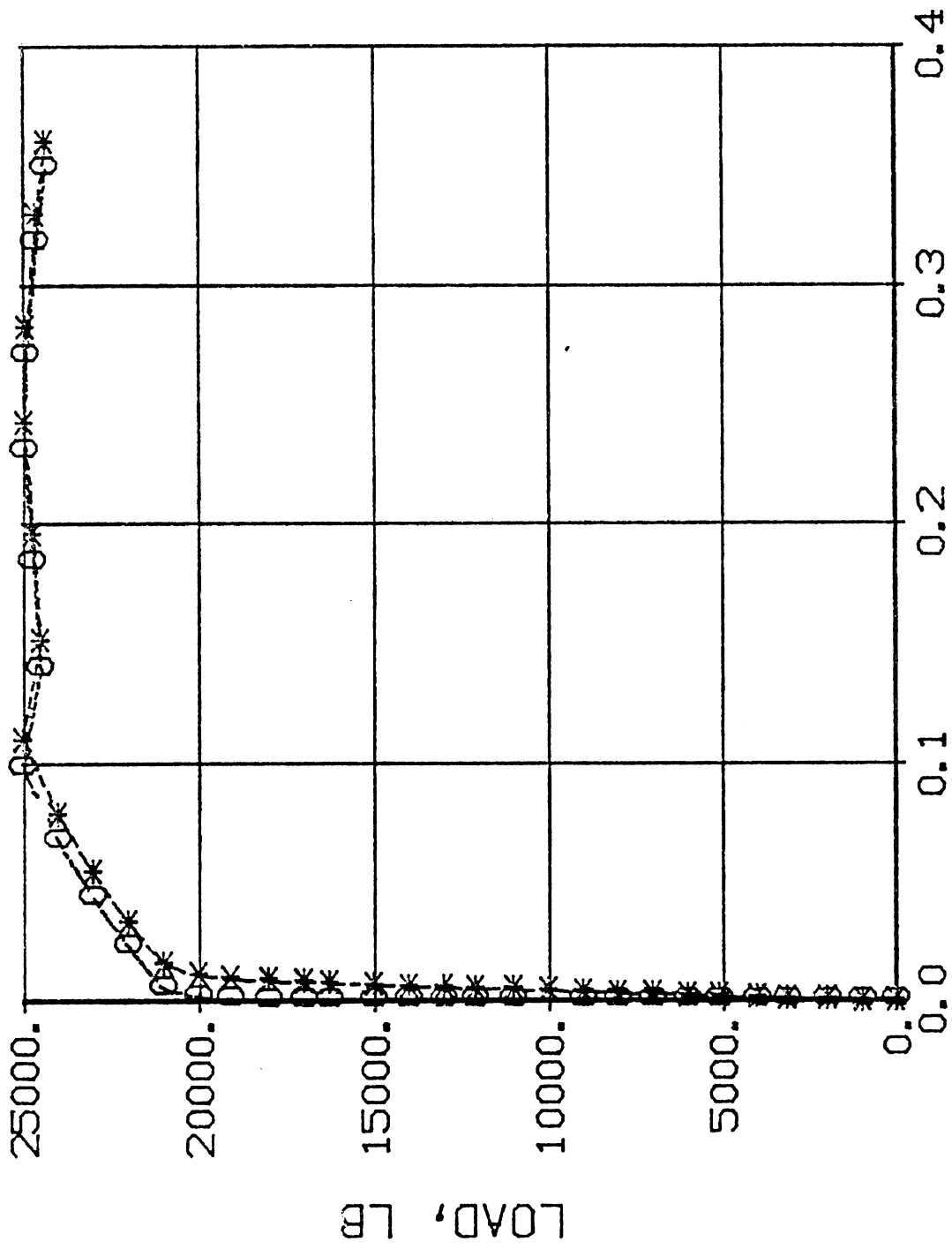




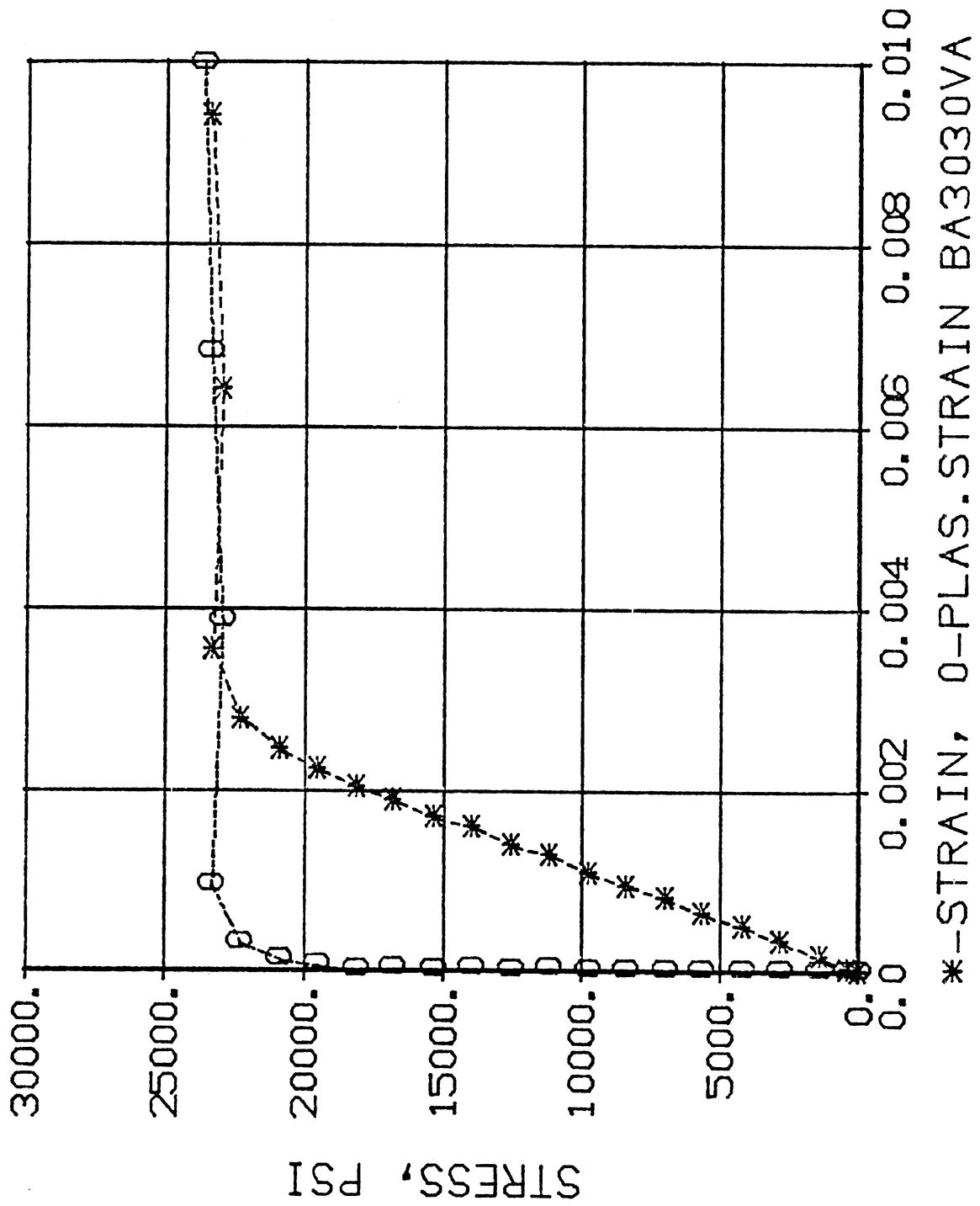
*-ANGLE, O-PLAS. ANGLE, DEG, CZ6030VM

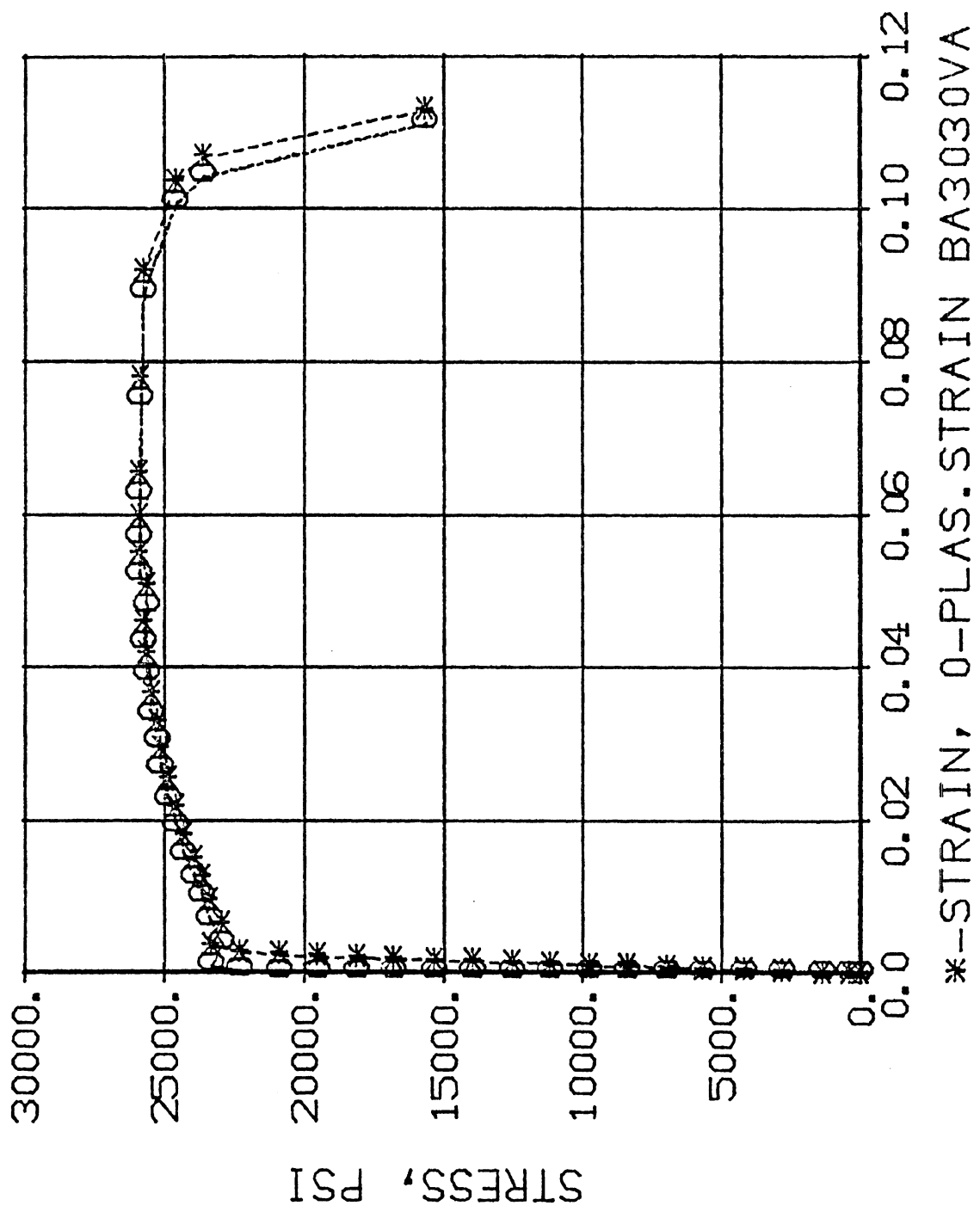


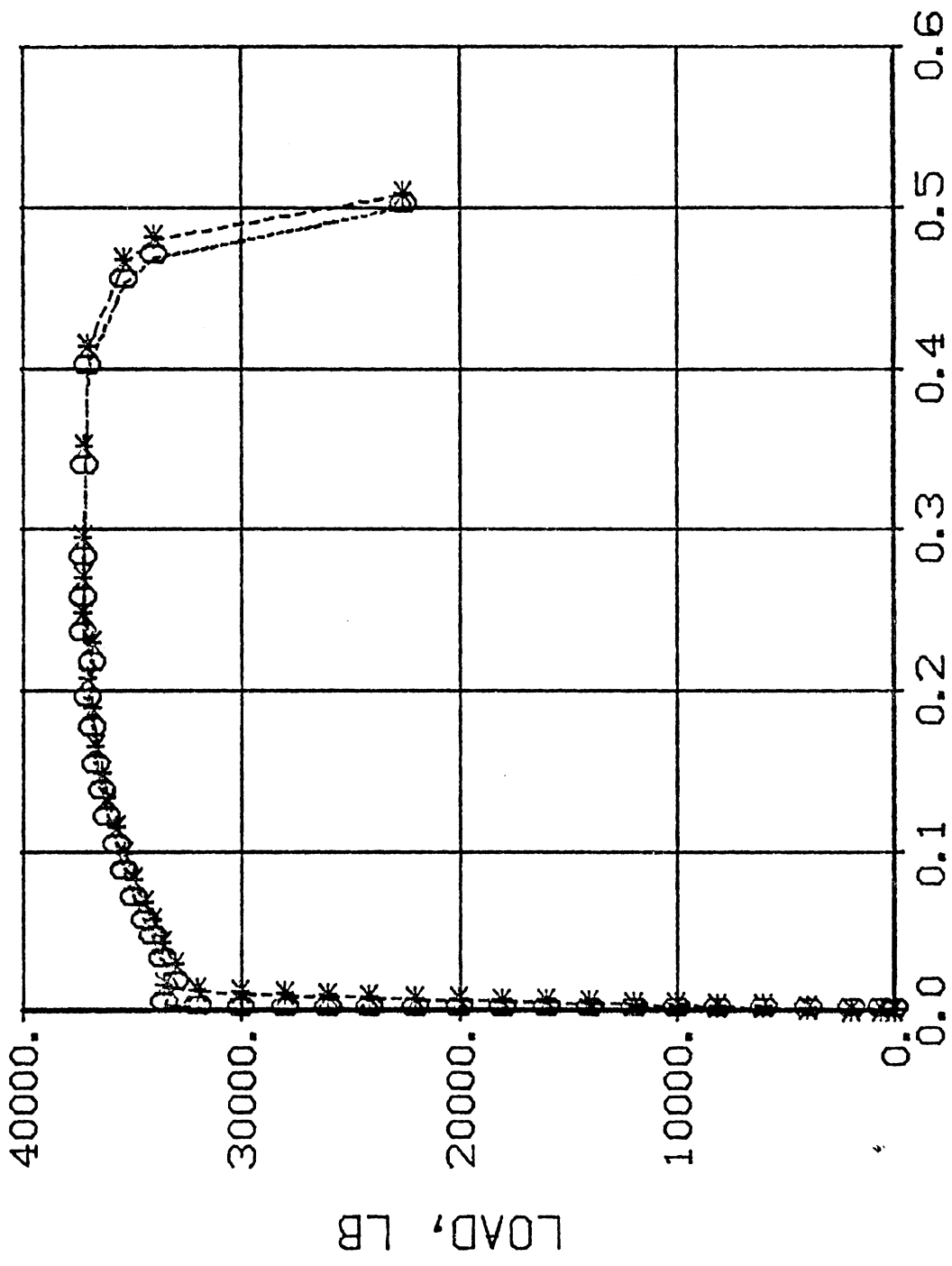




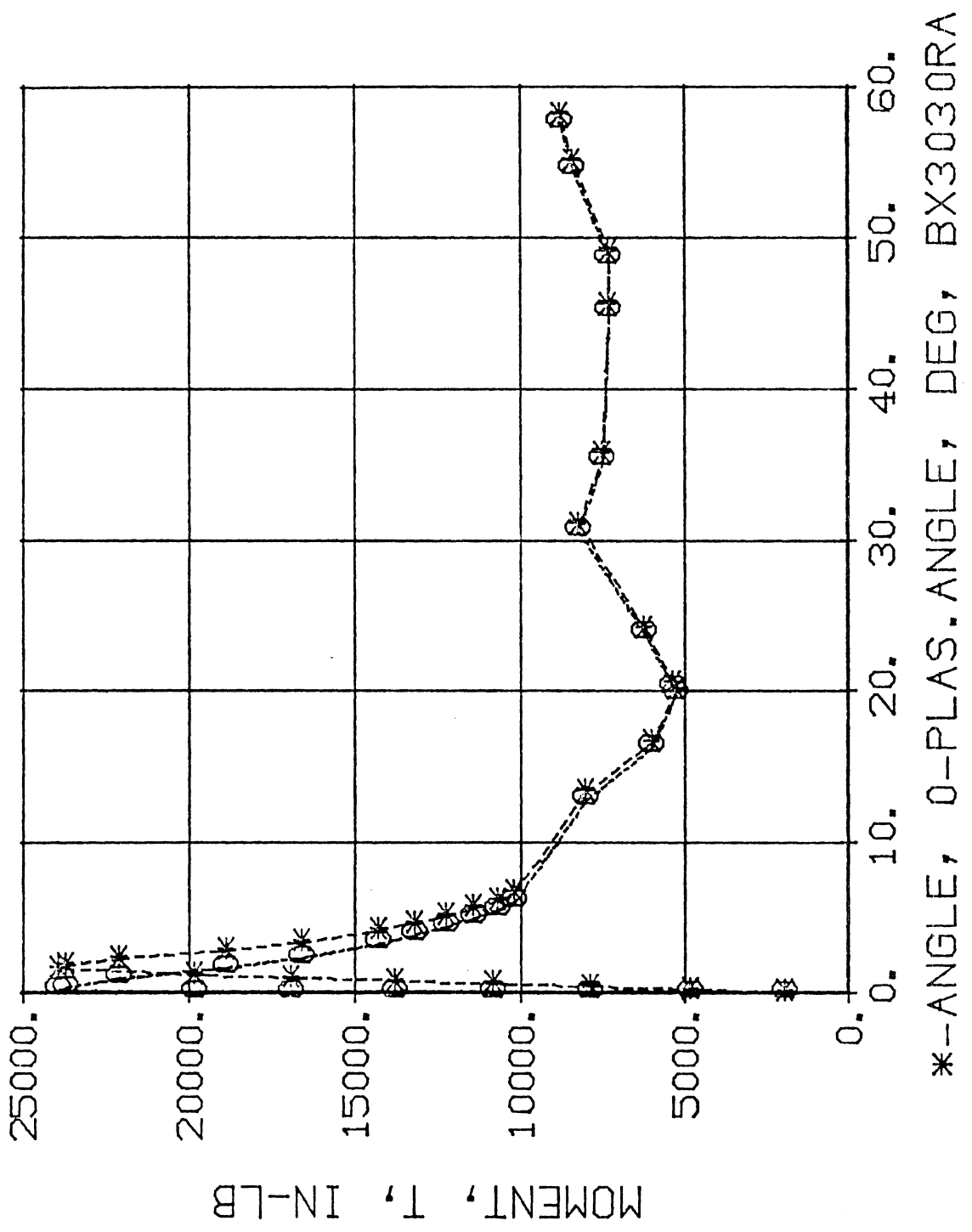
* DISPL., 0-PLAS.DISPL., IN BA3030RA

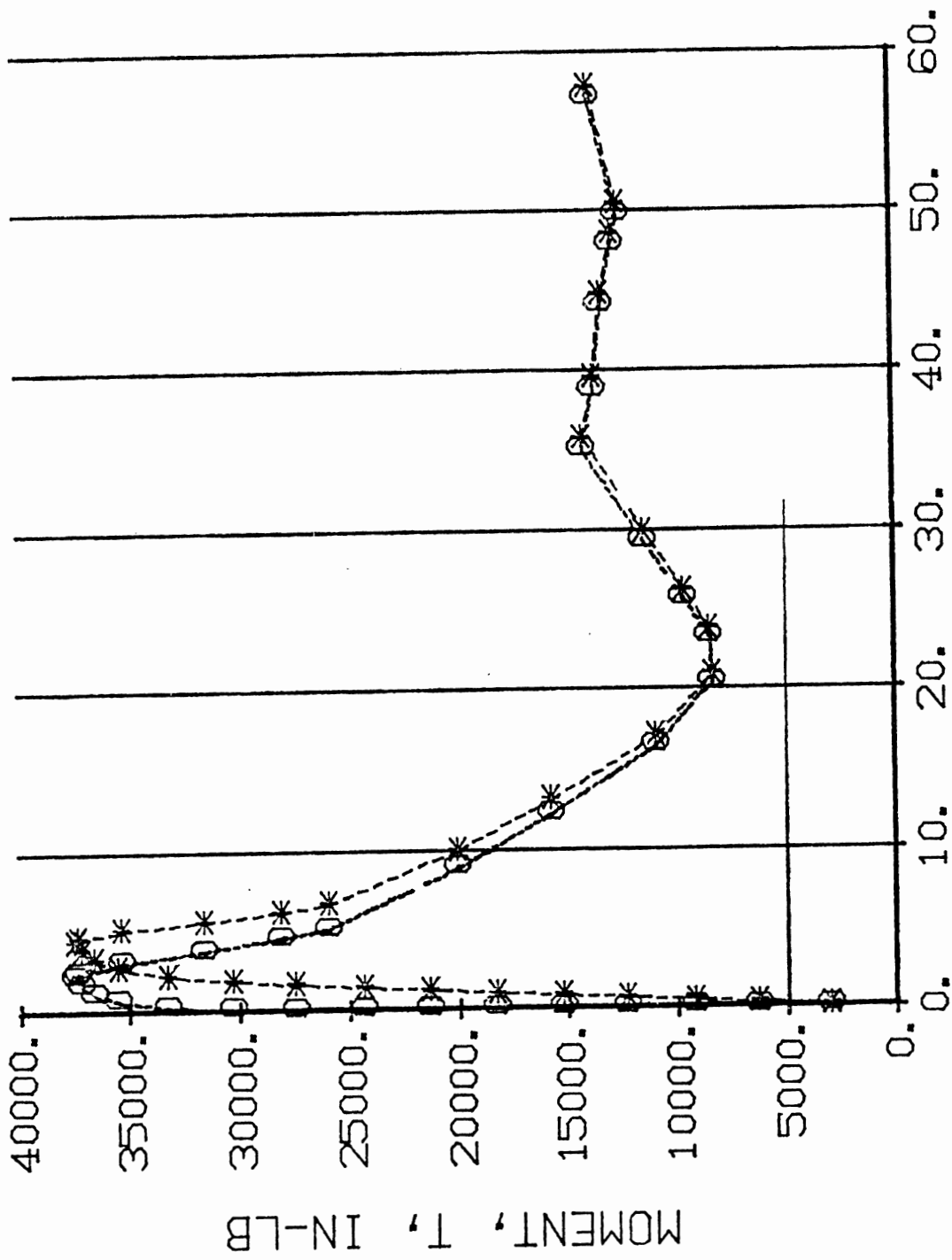




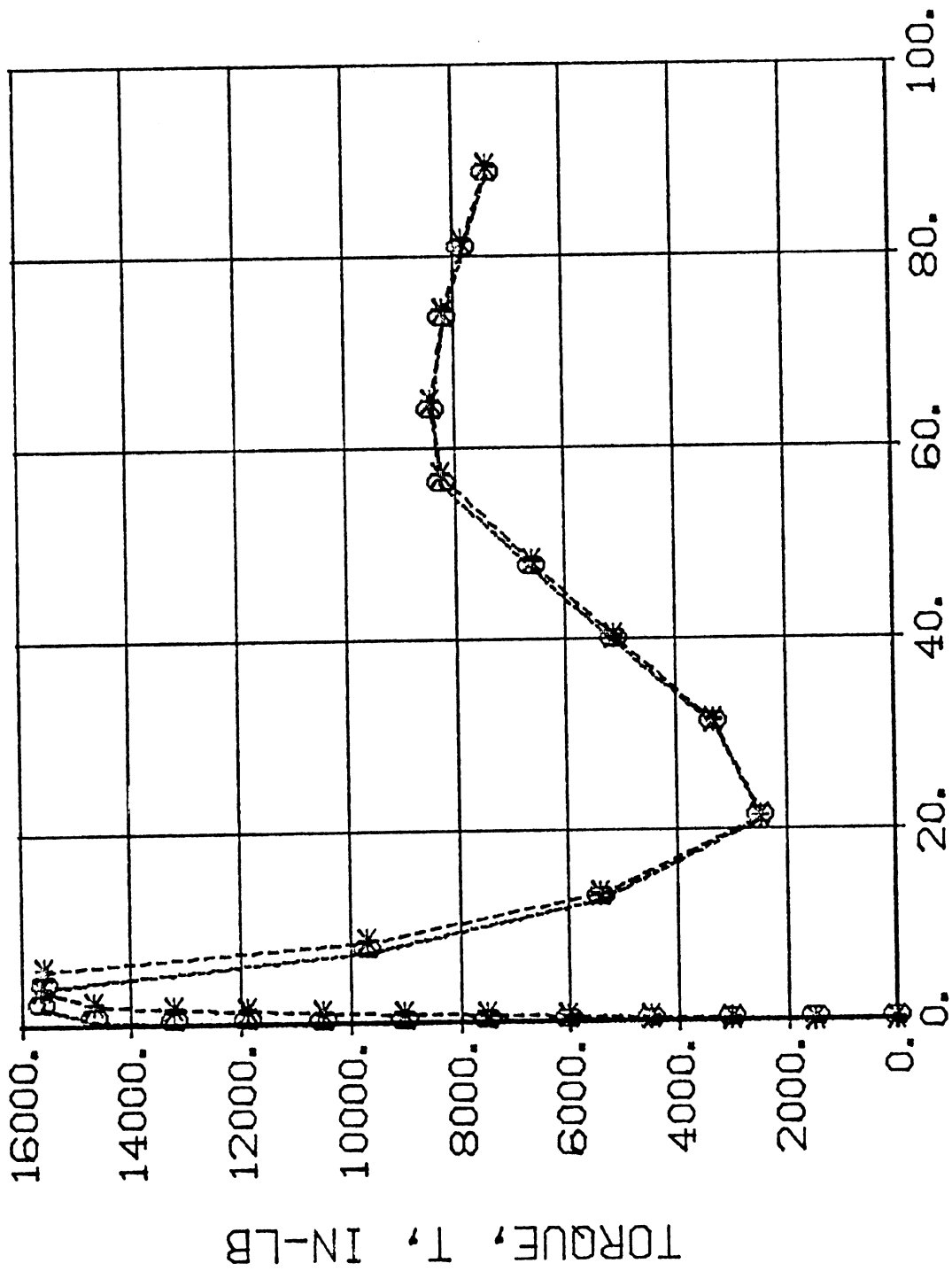


*-DISPL., 0-PLAS.DISPL., IN BA3030VA

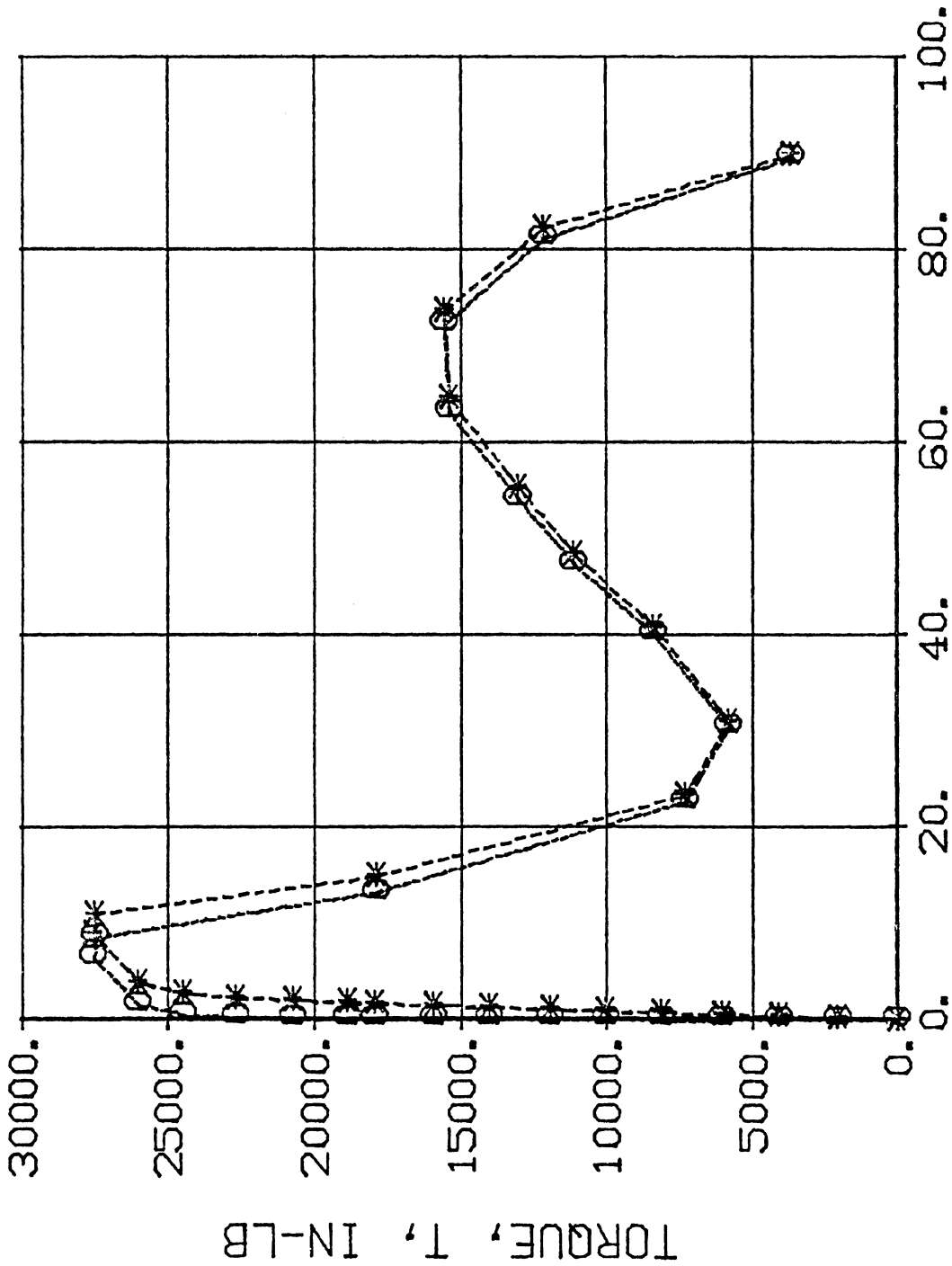




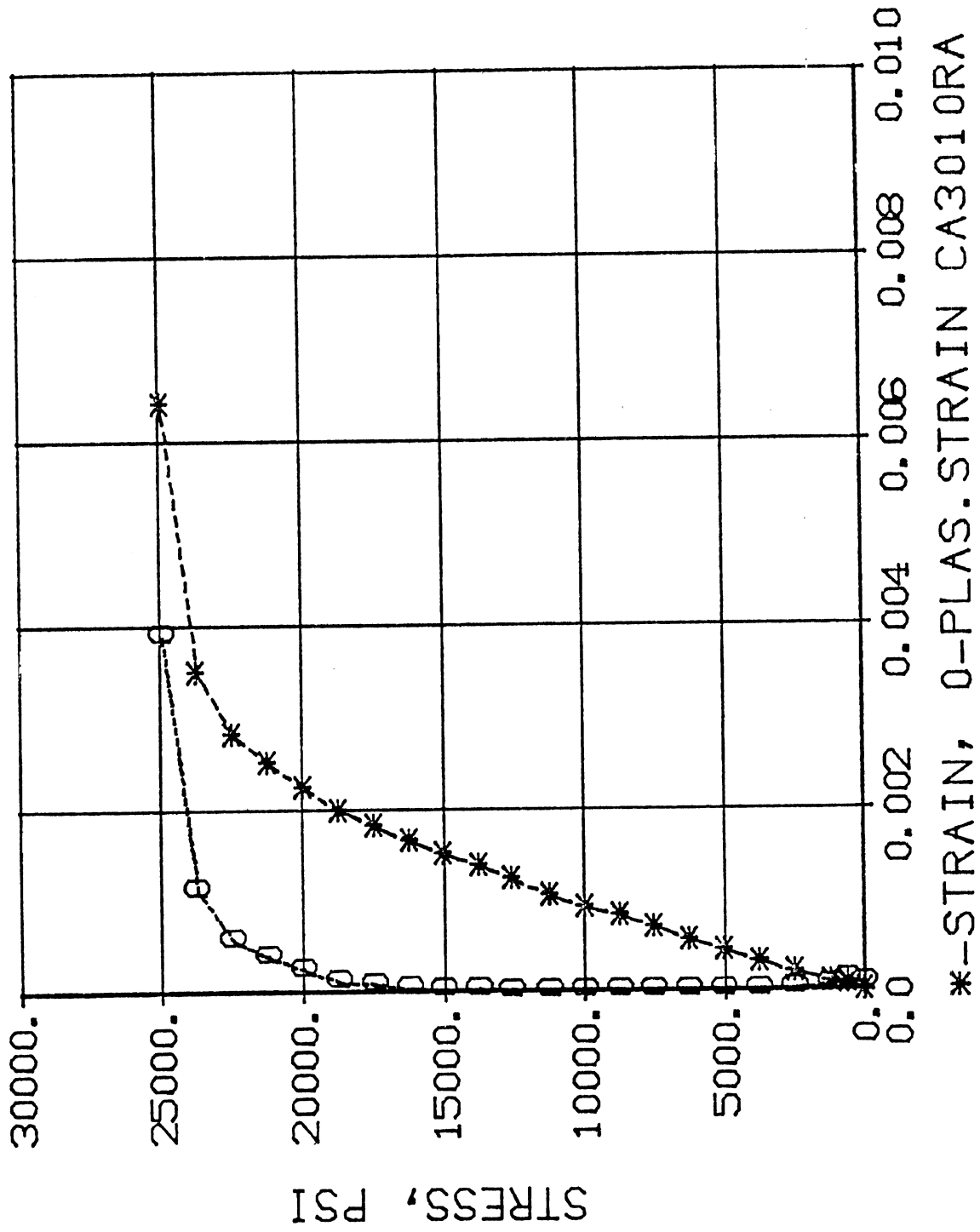
*--ANGLE, 0--PLAS. ANGLE, DEG, BX3030VA

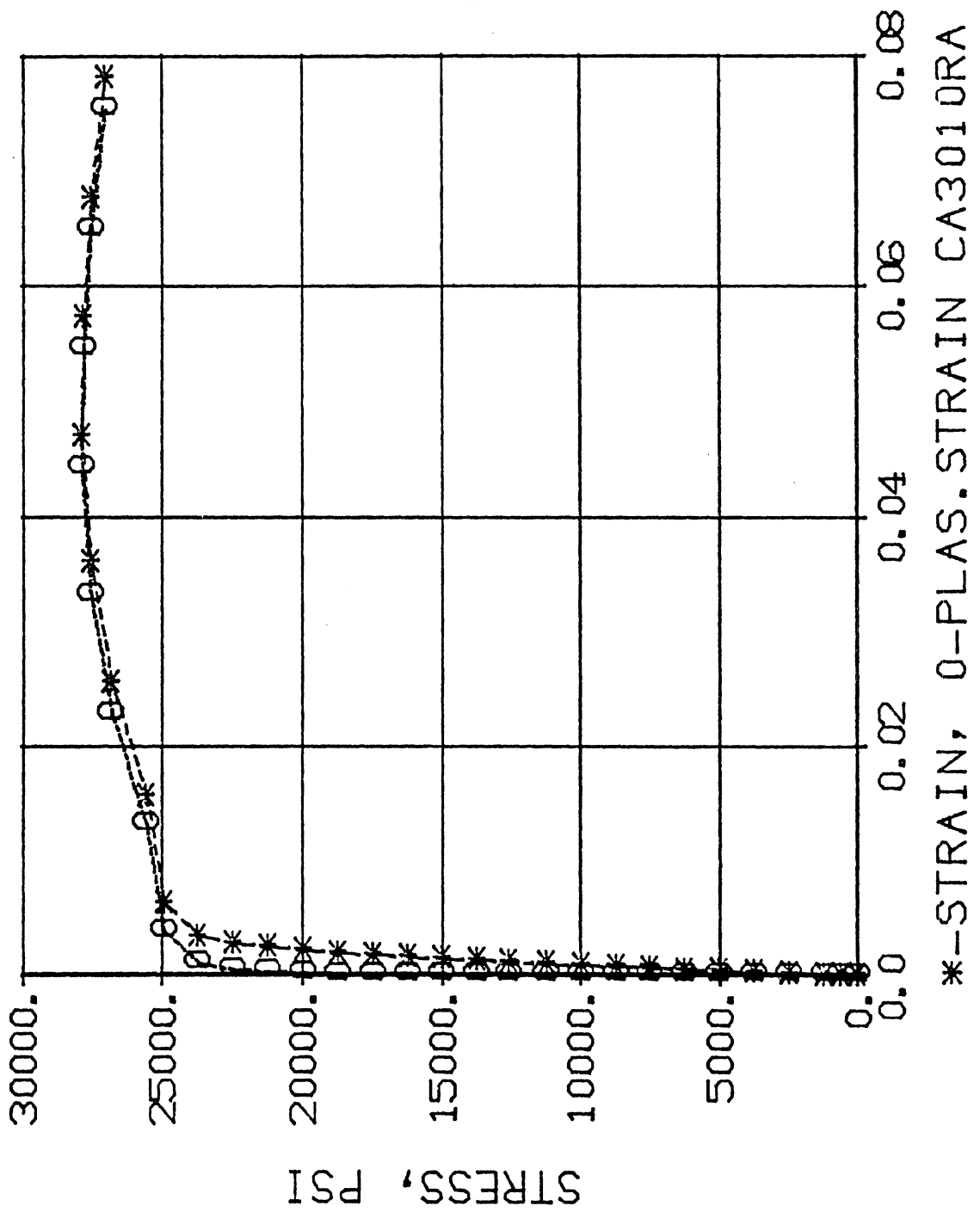


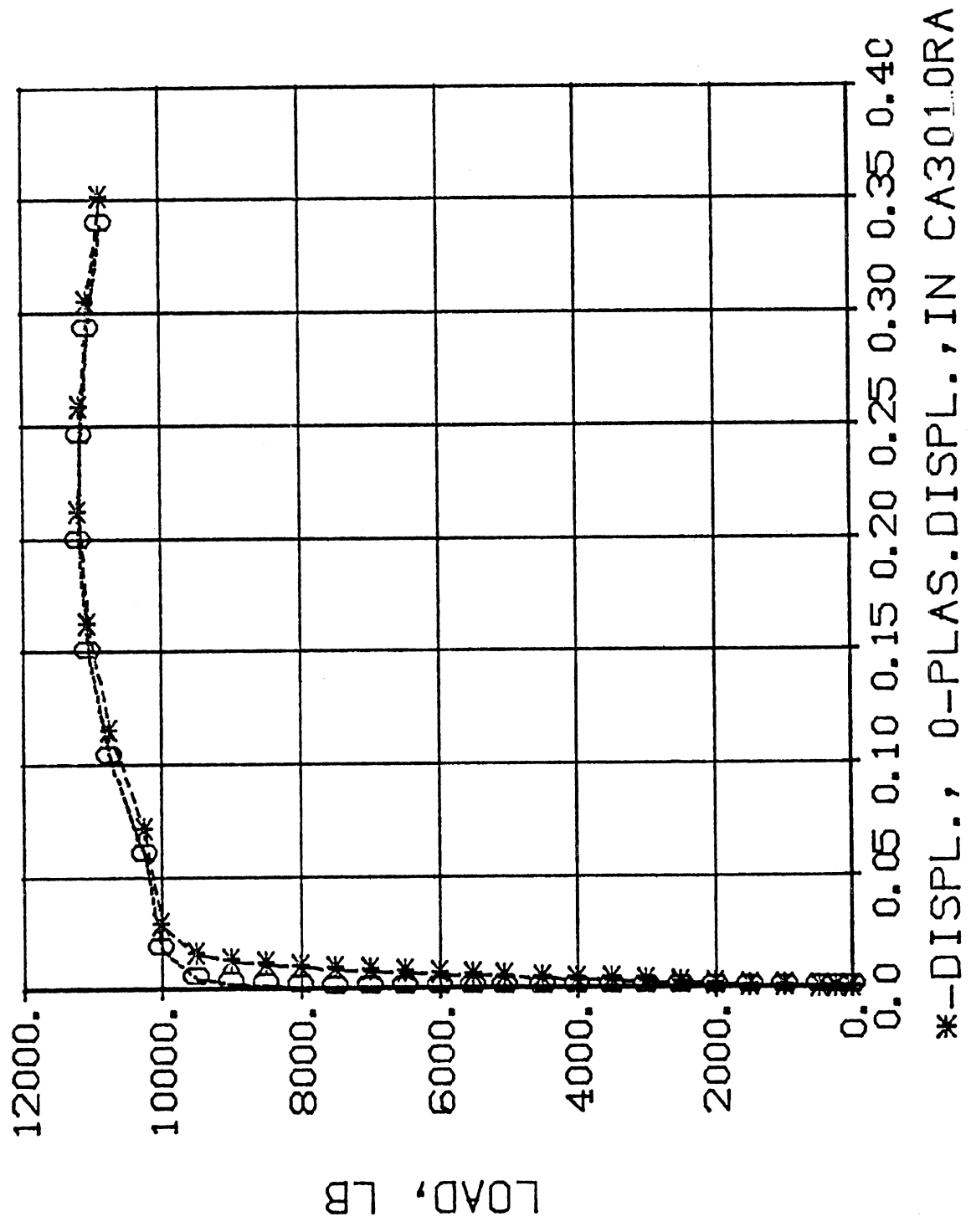
*--ANGLE, 0-PLAS. ANGLE, DEG, BZ3030RA

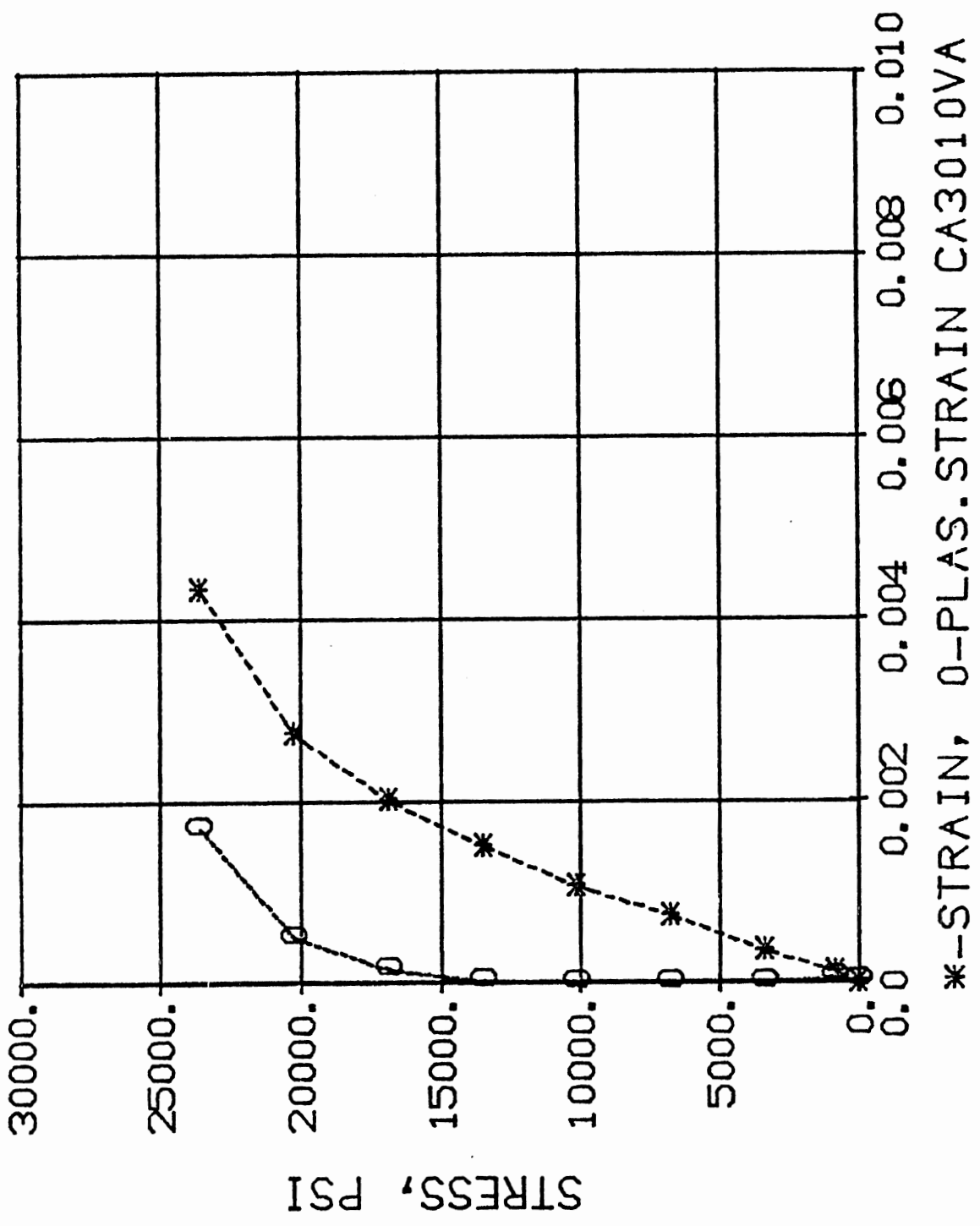


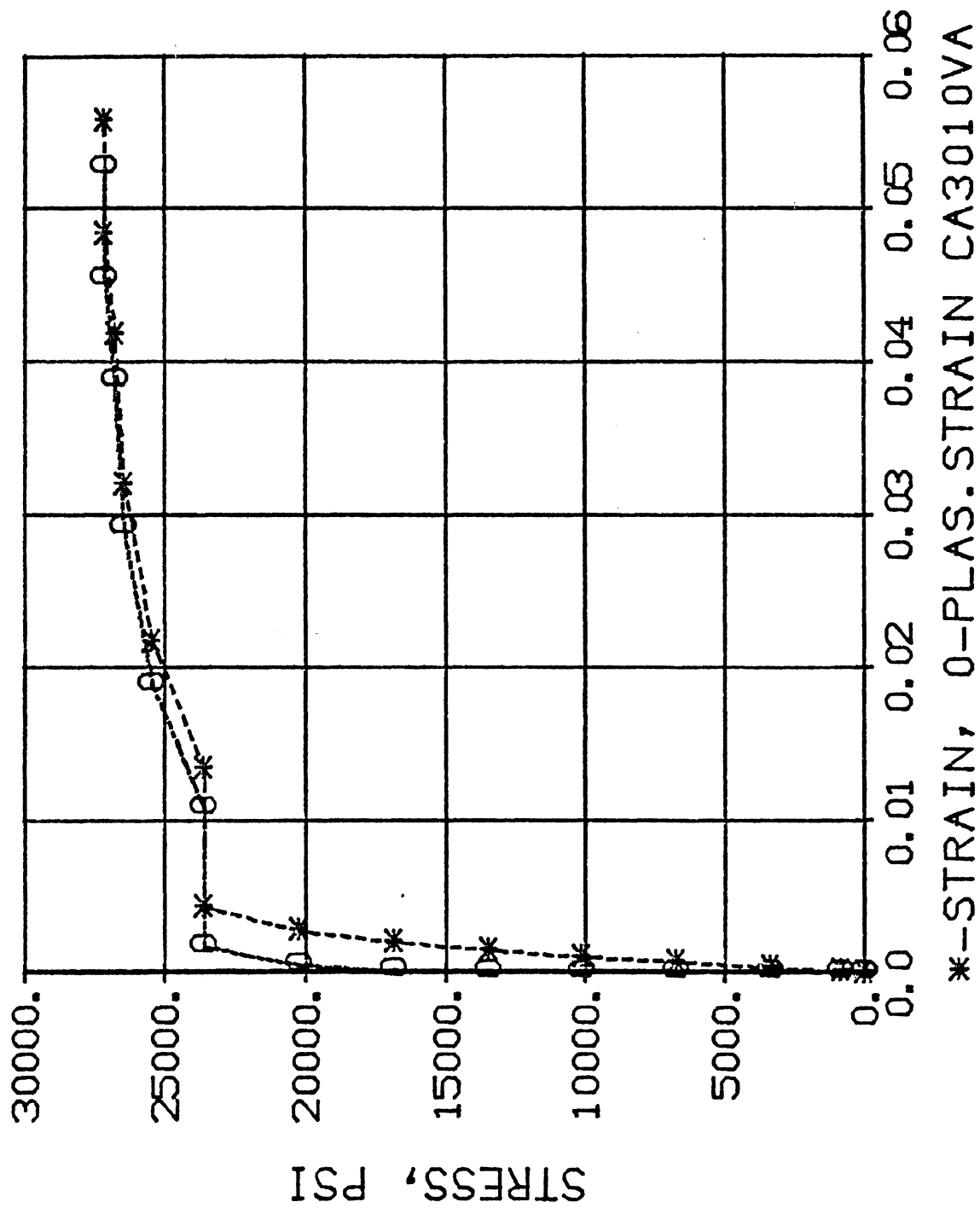
*--ANGLE, 0-PLAS. ANGLE, DEG, BZ3030VA

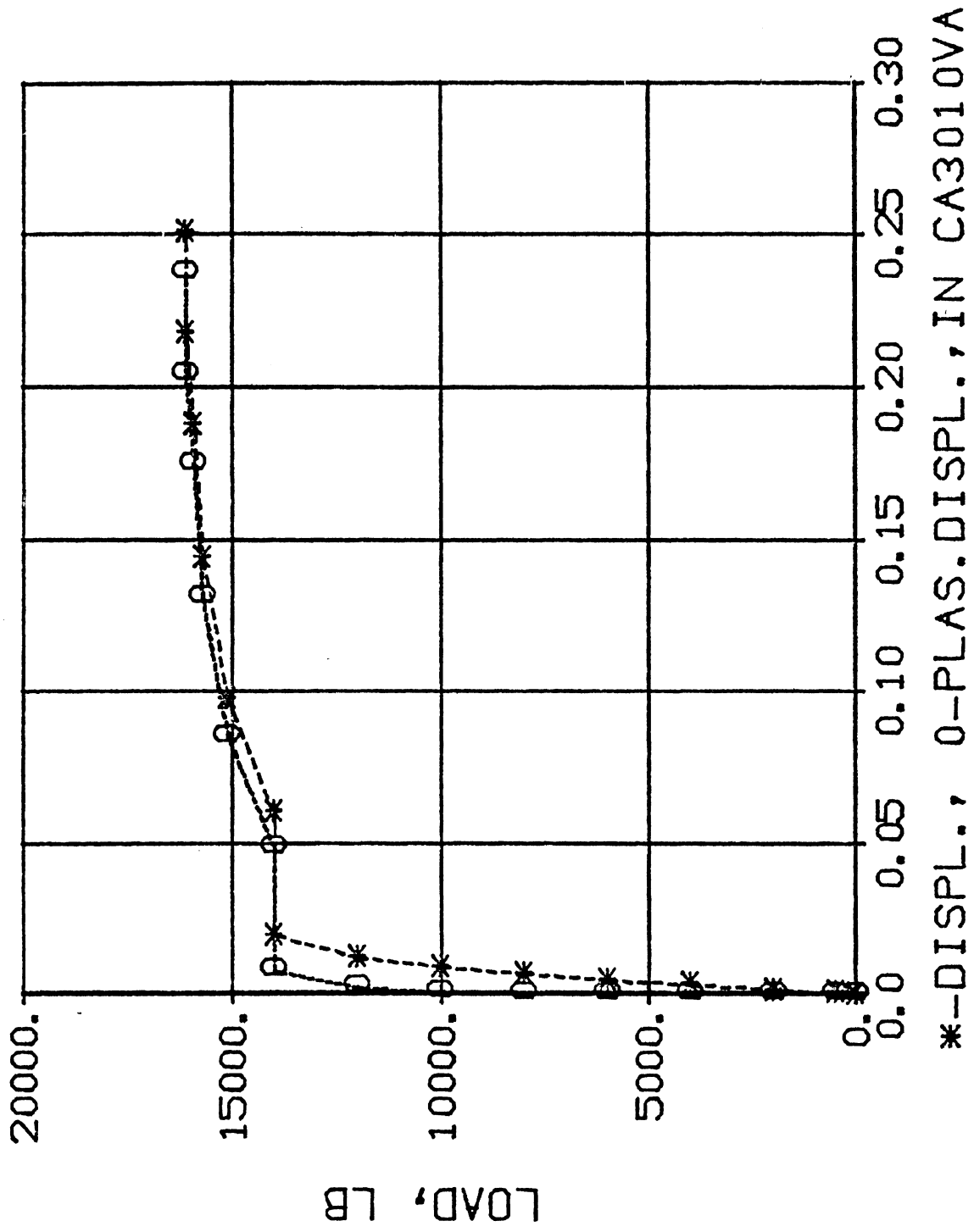


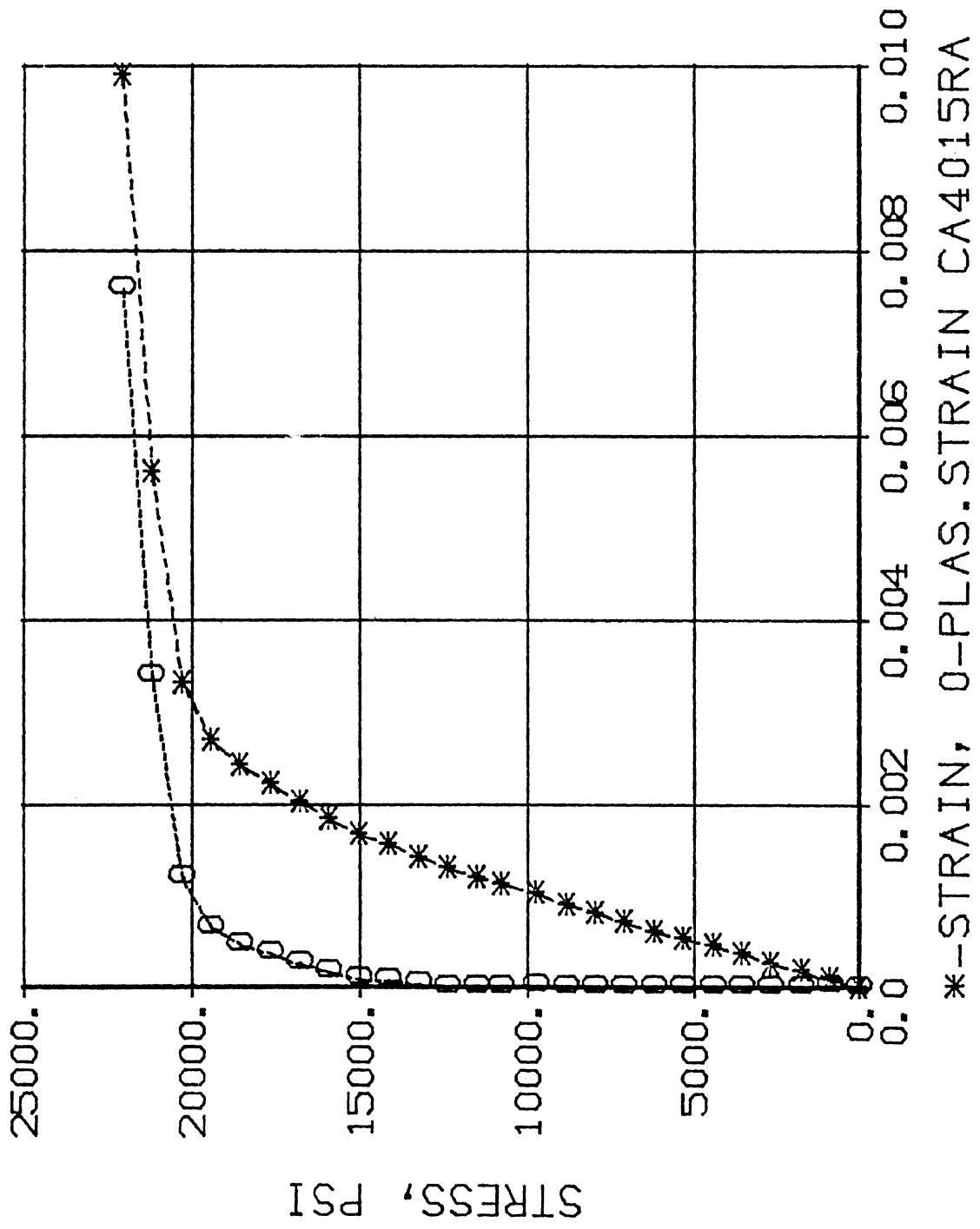


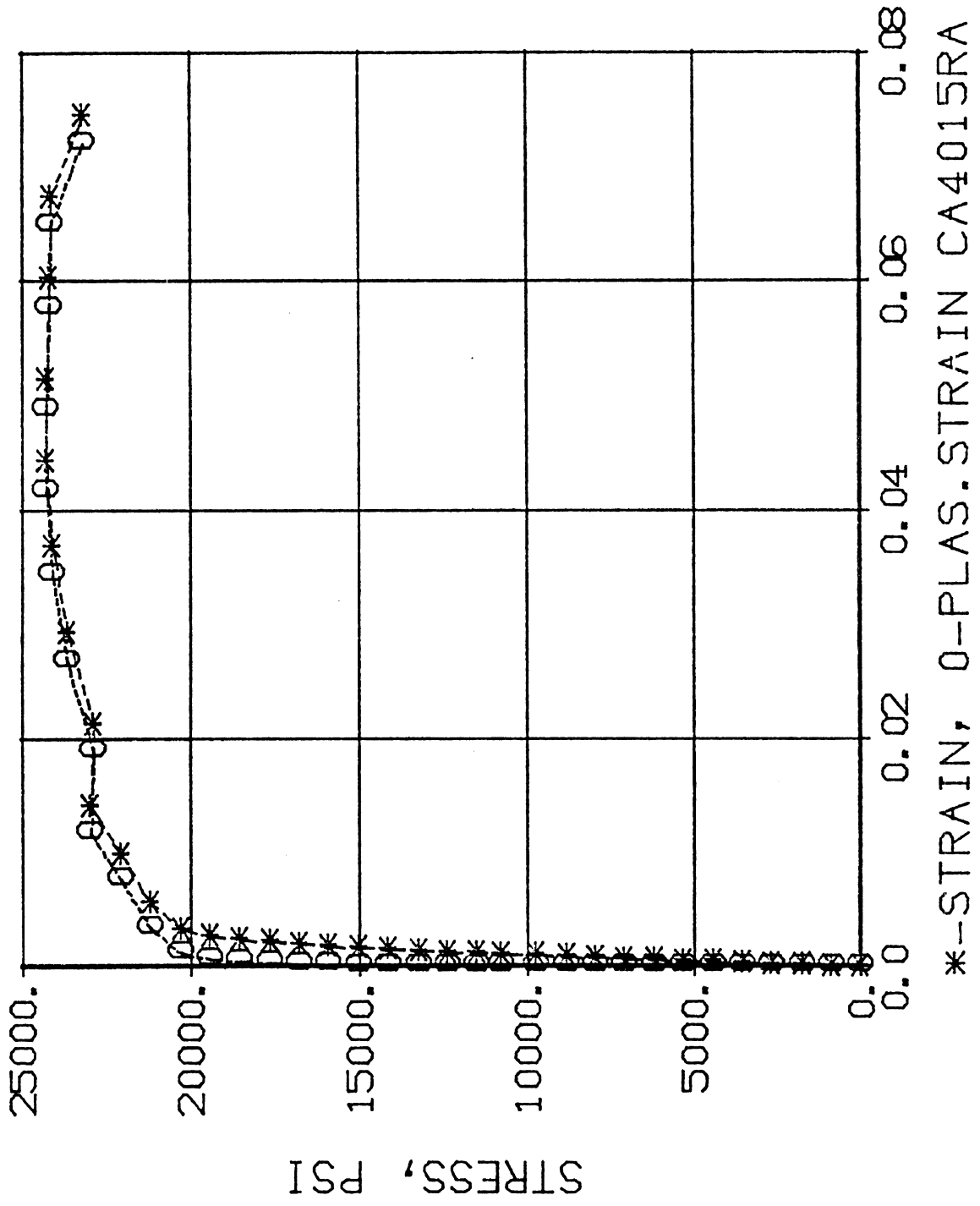


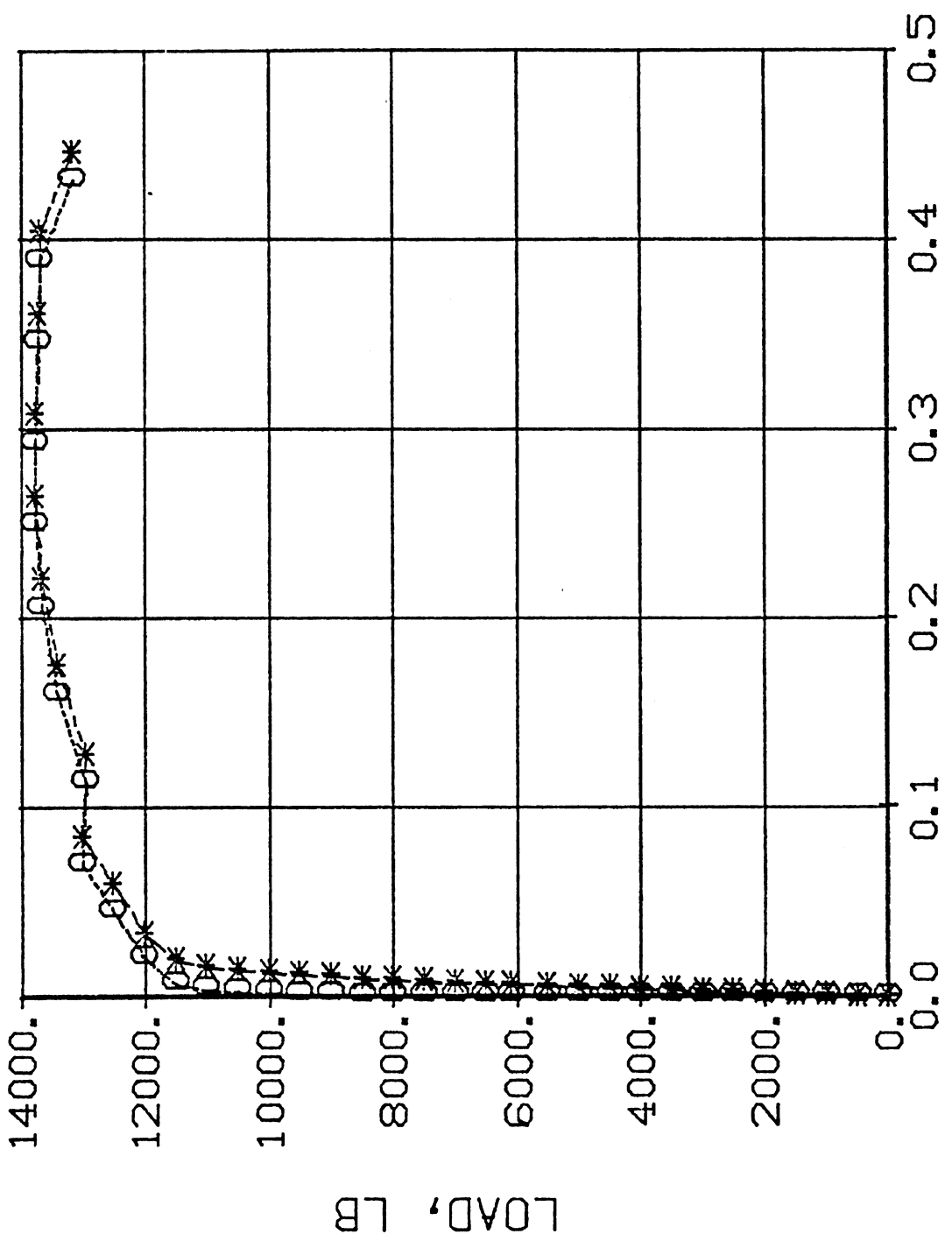




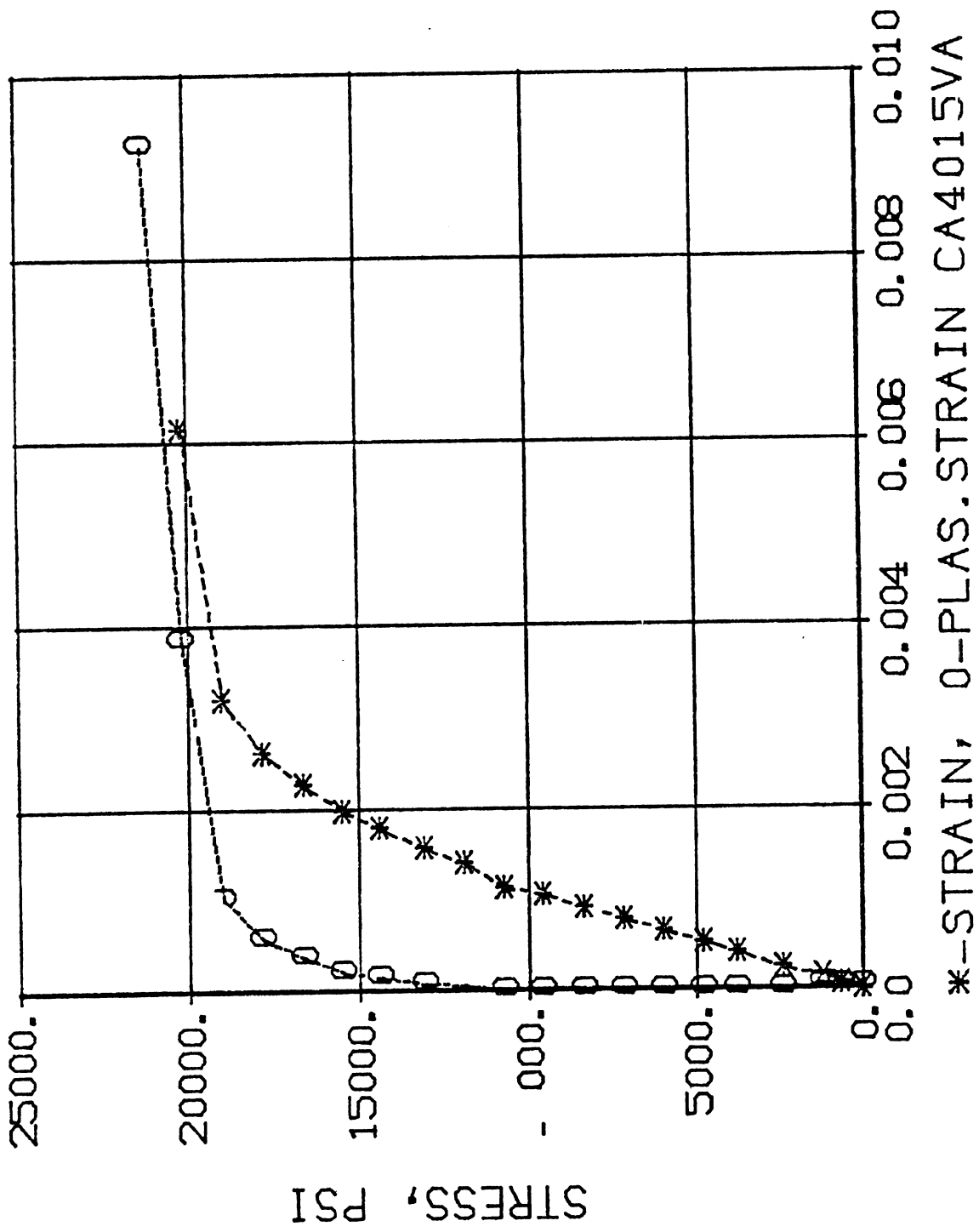


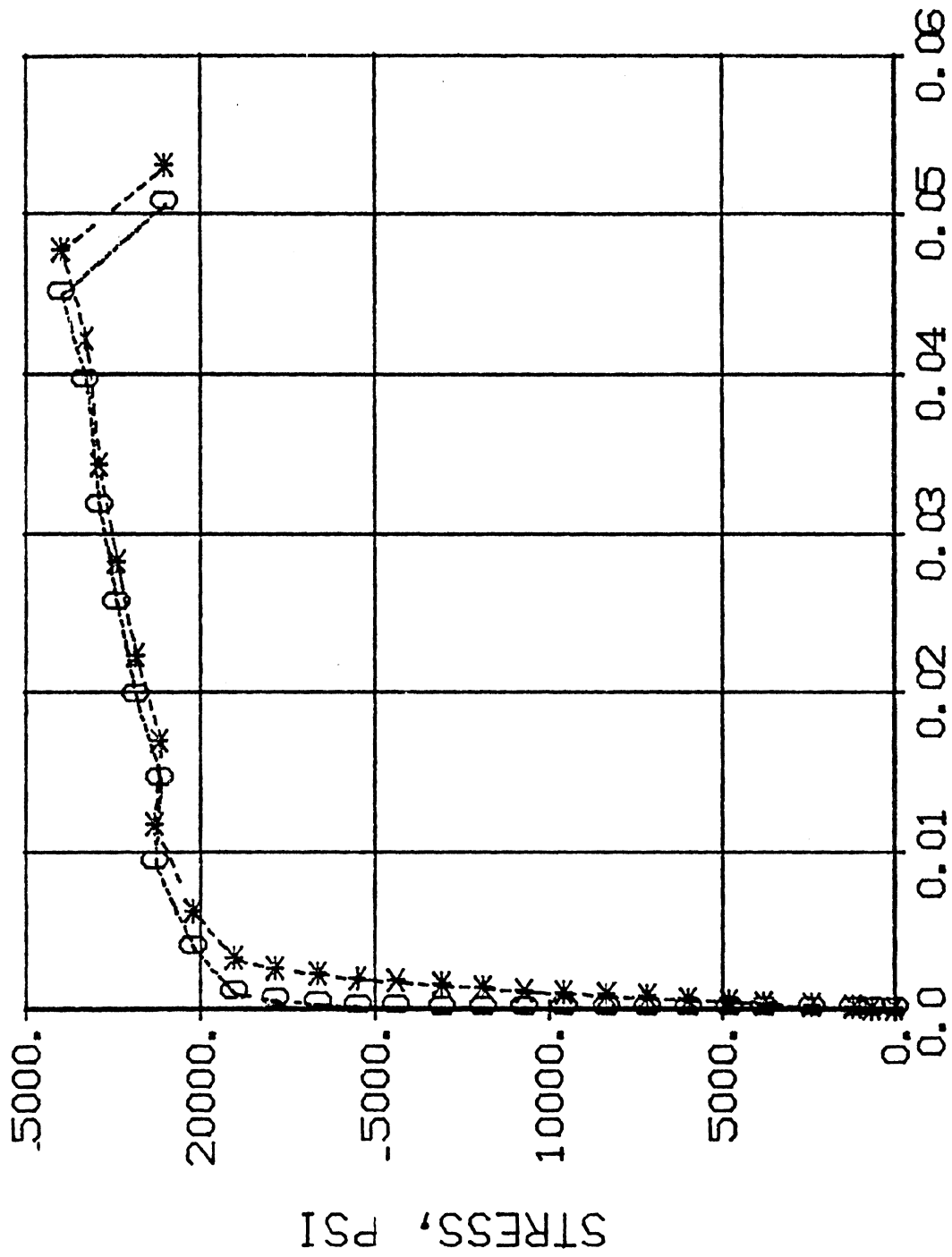




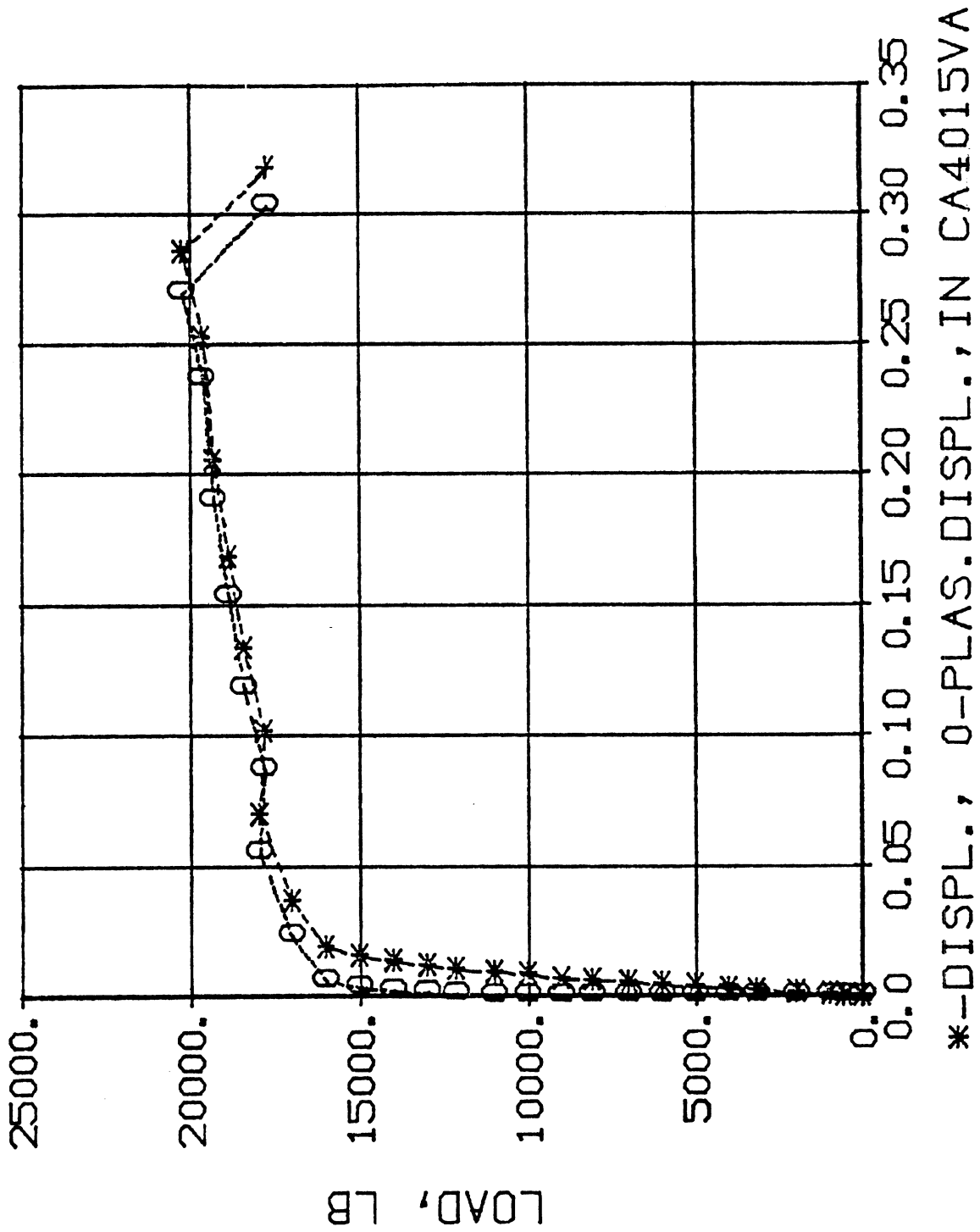


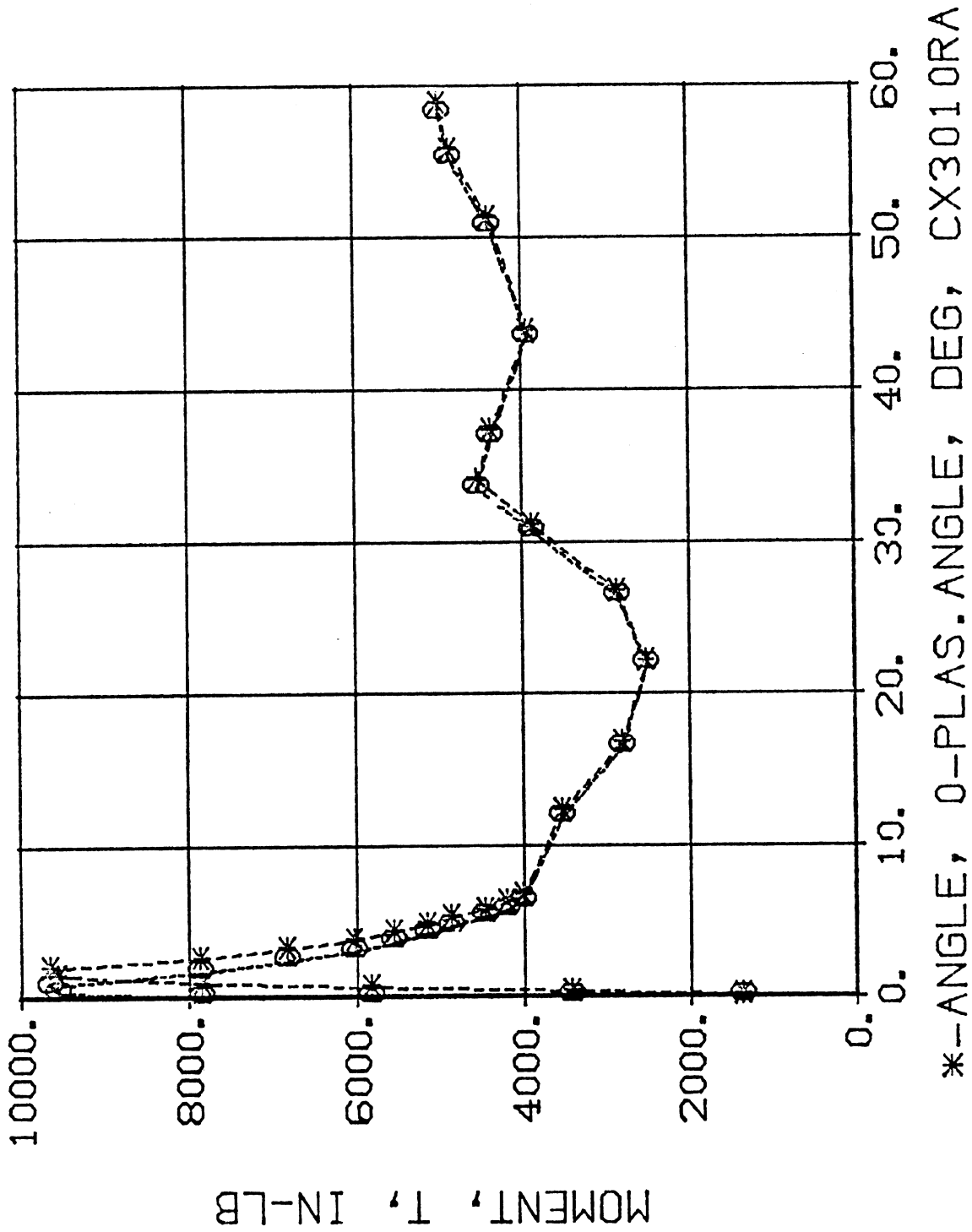
*-DISPL., 0-PLAS.DISPL., IN CA4015RA

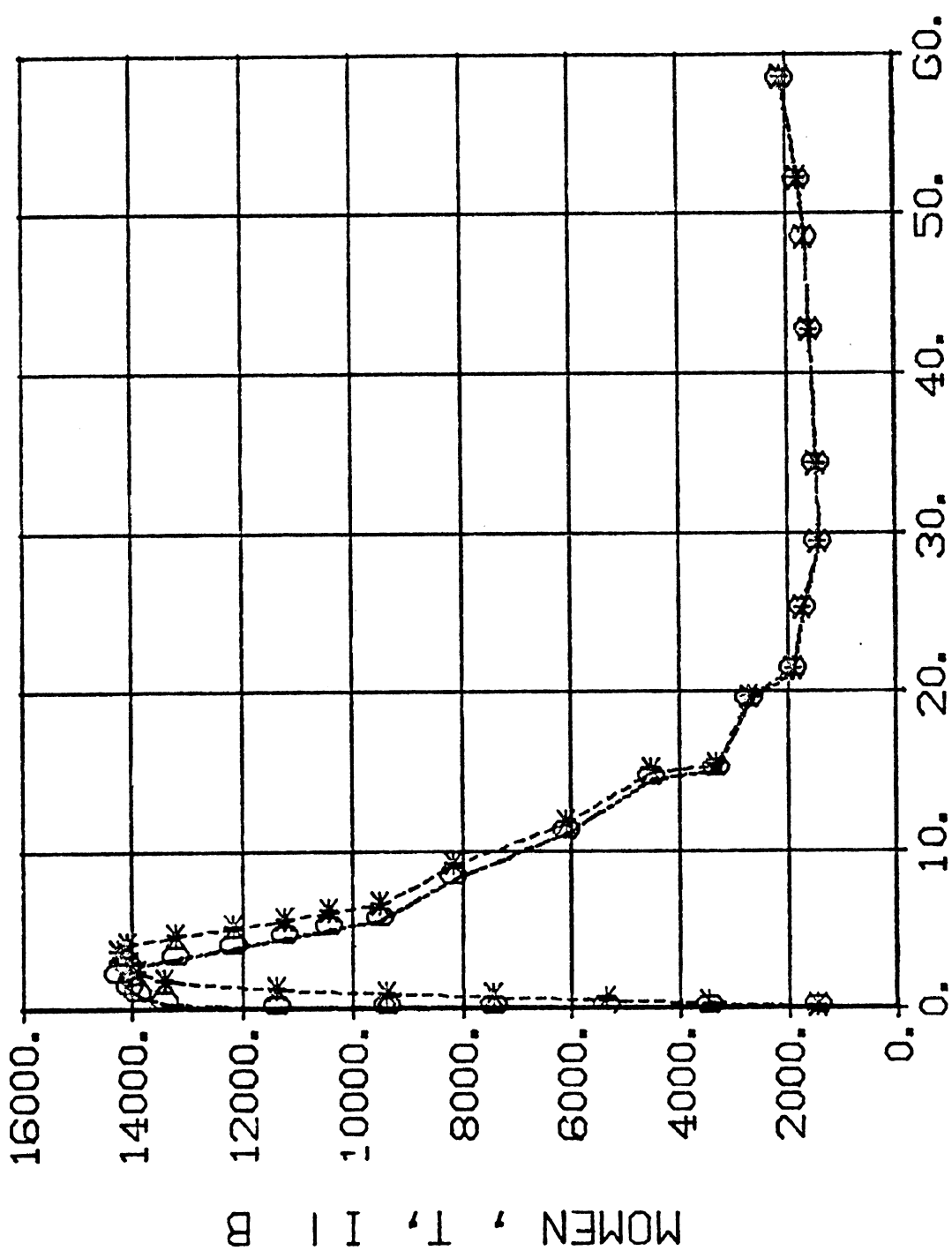




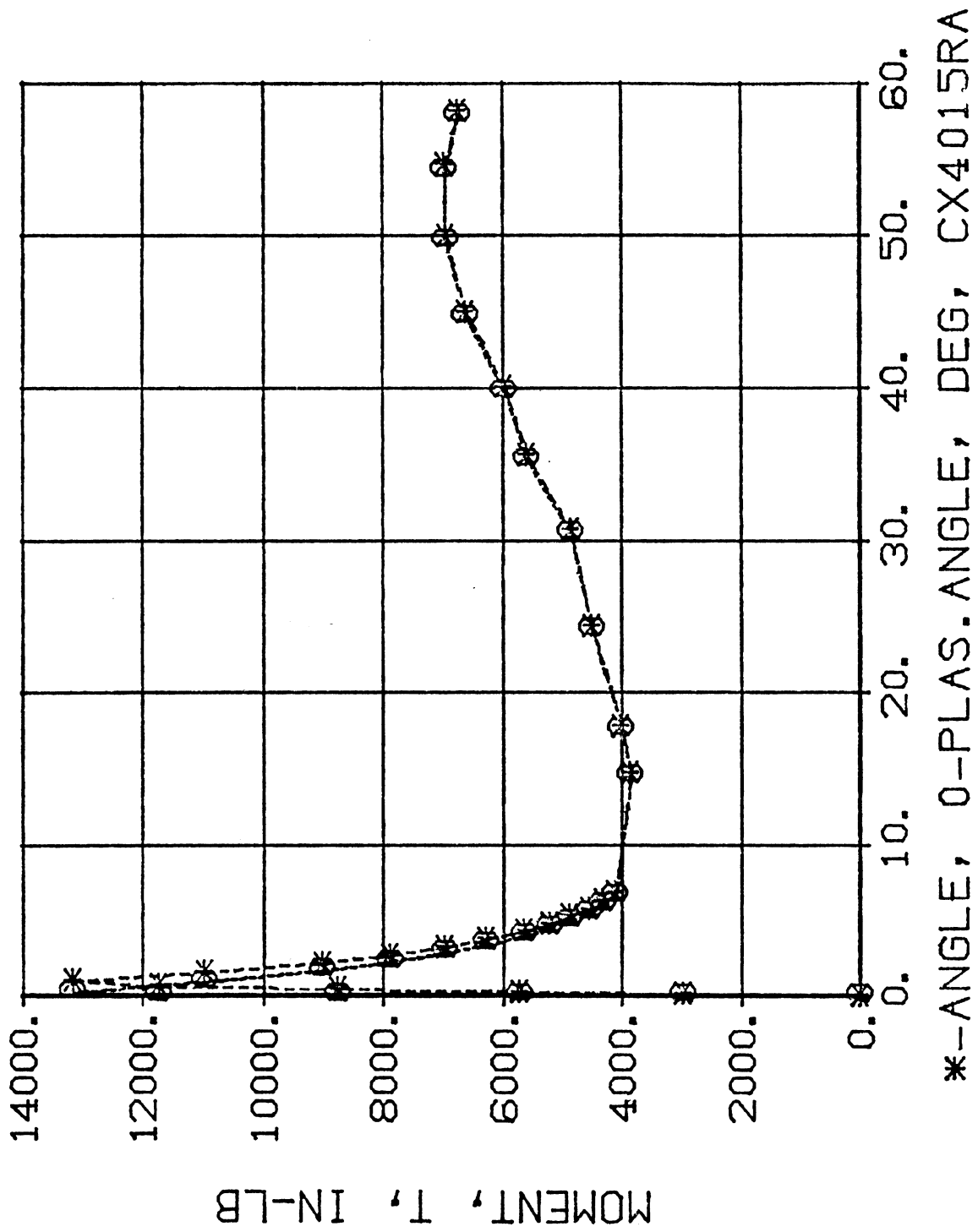
*-SIRAIN, 0-PLAS. STRAIN CA4015VA

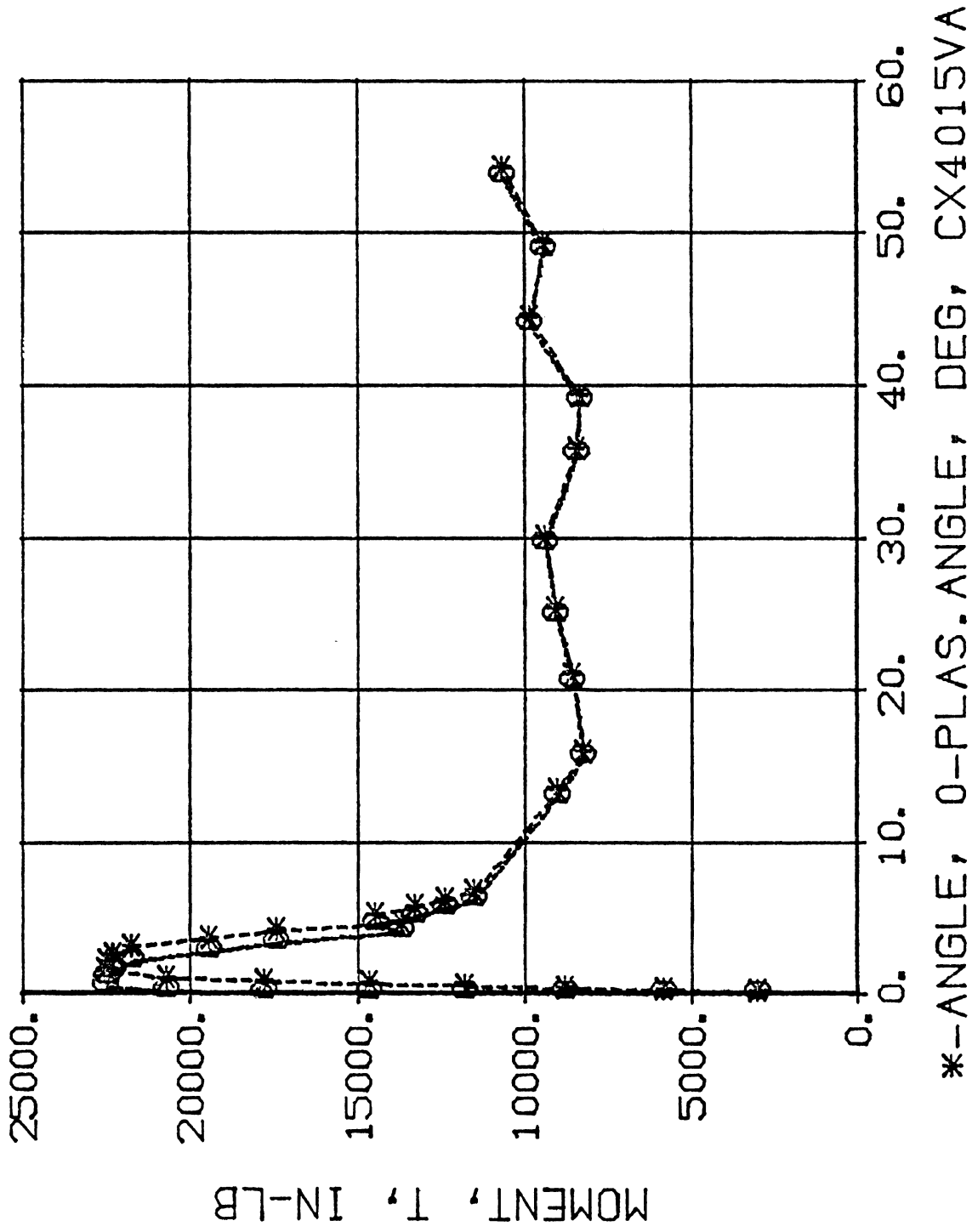


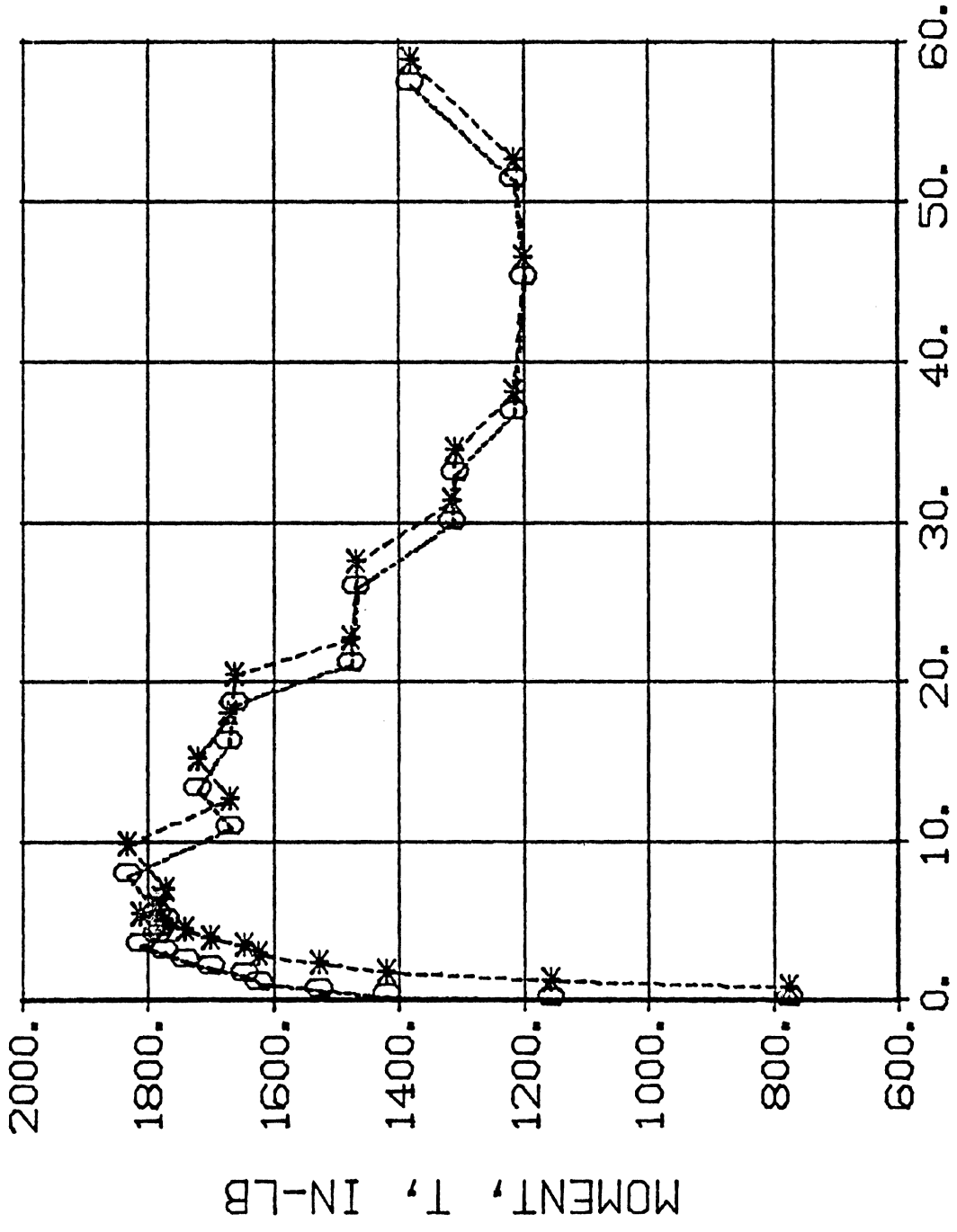




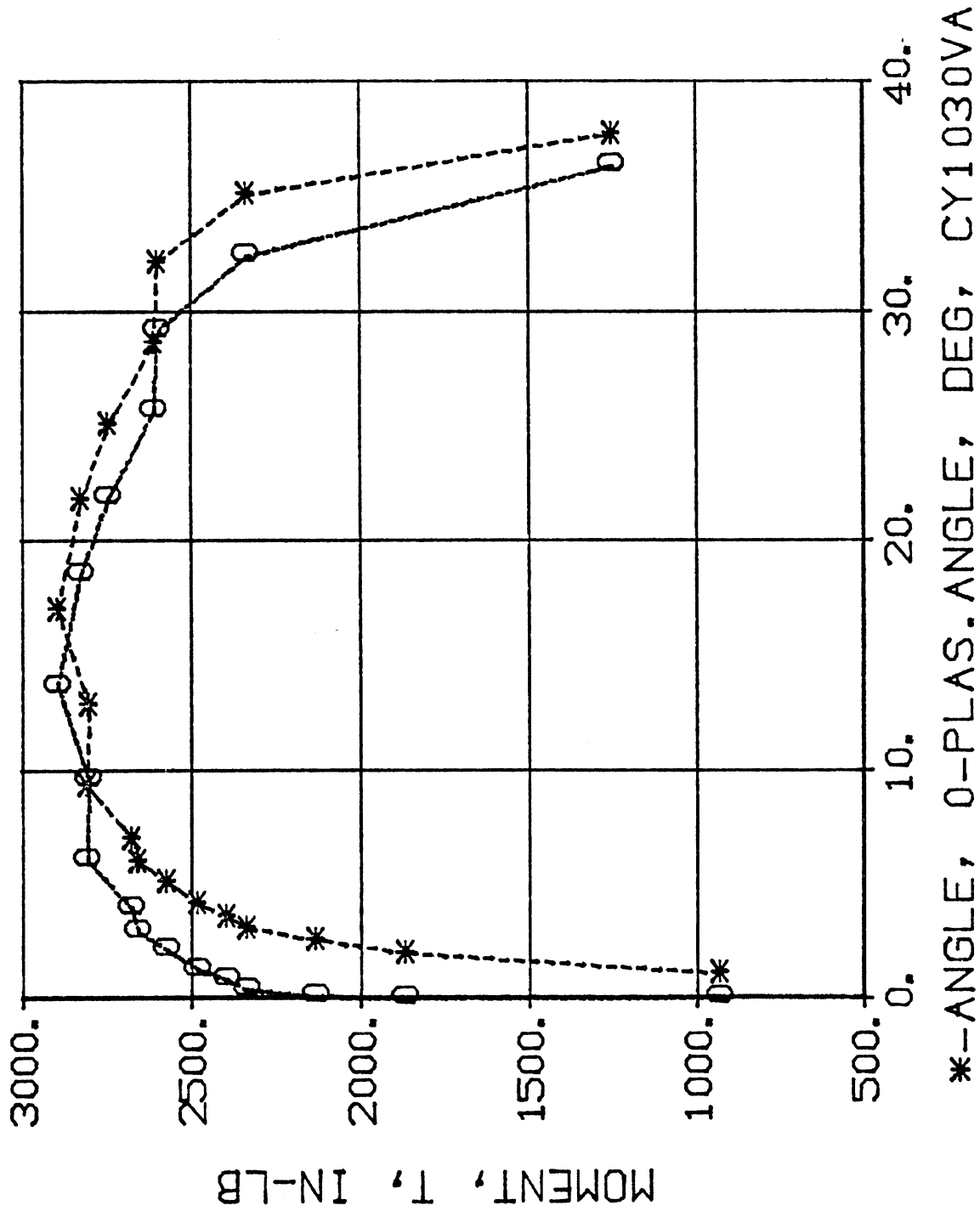
*-ANGL-, 0-PLAS. ANGLE, DEG, CX3010VA

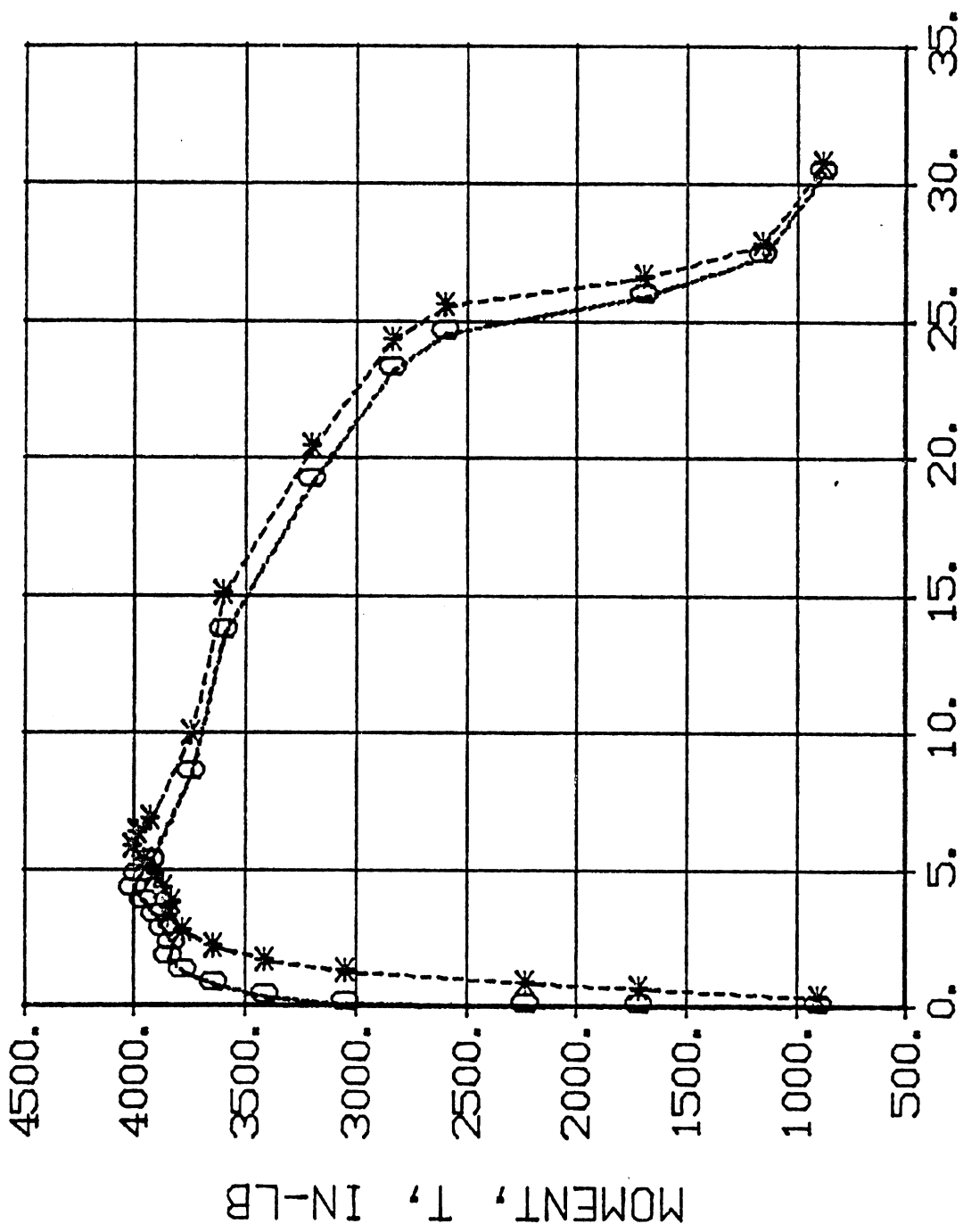




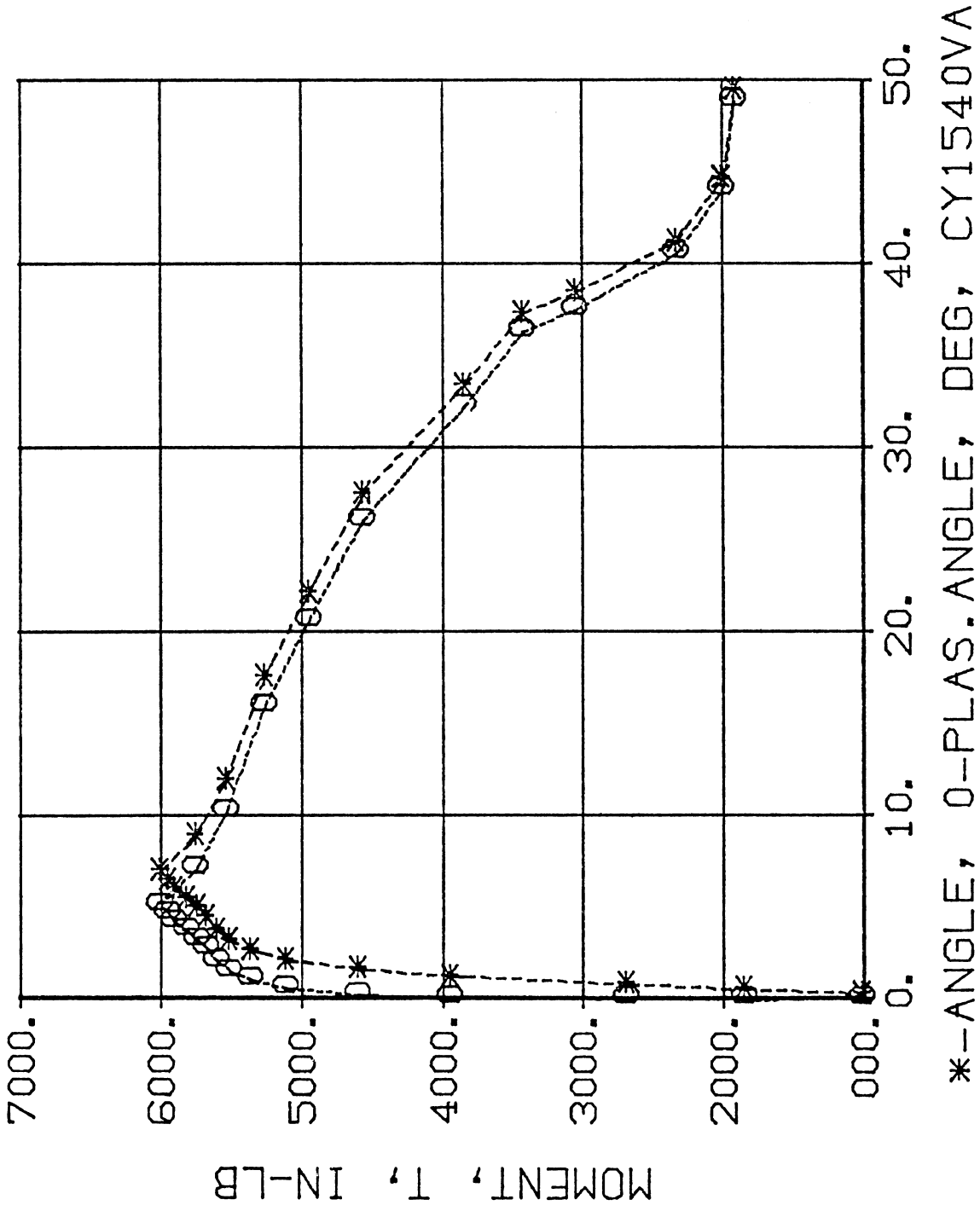


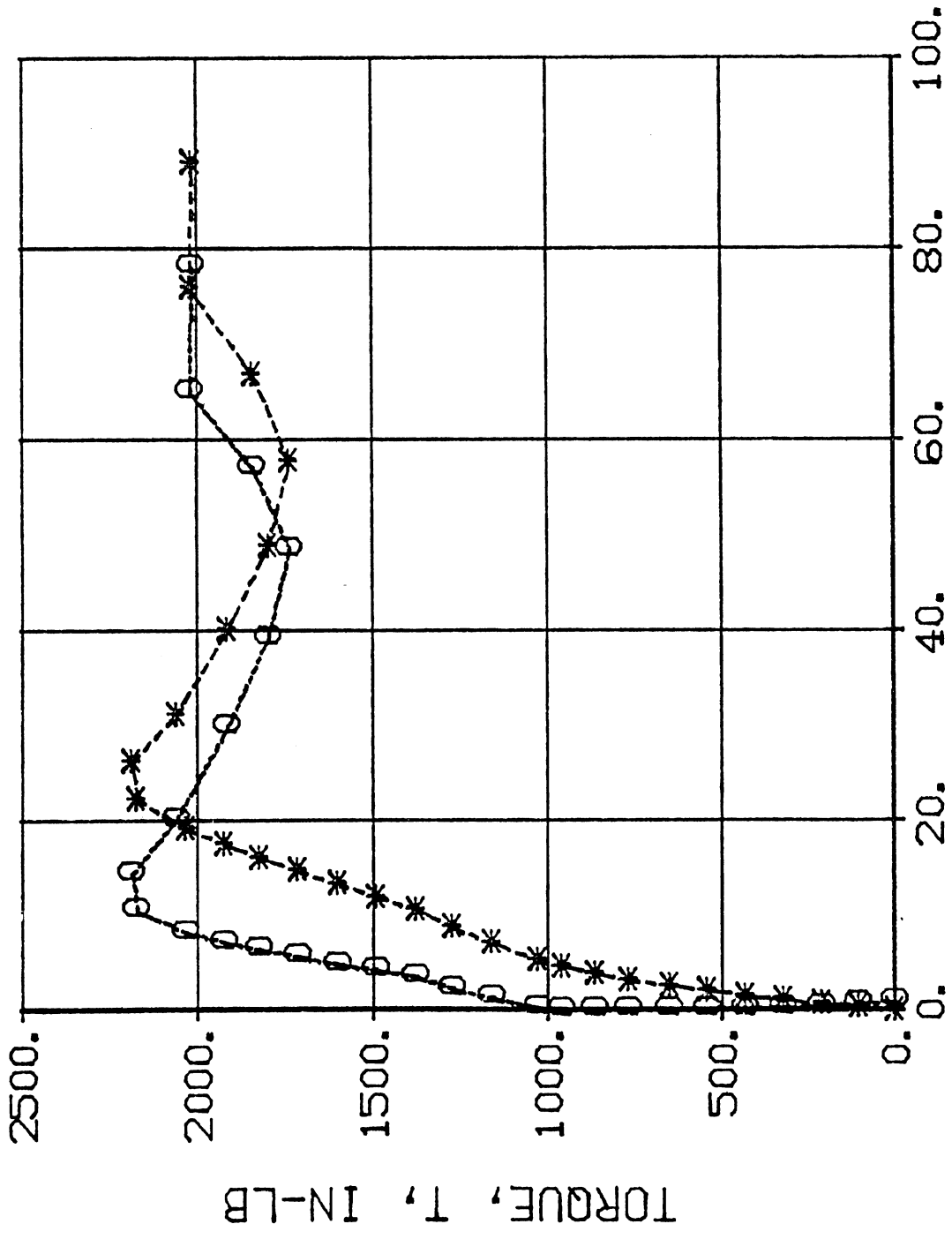
*-ANGLE, 0-PLAS.ANGLE, DEG, CY1030RA



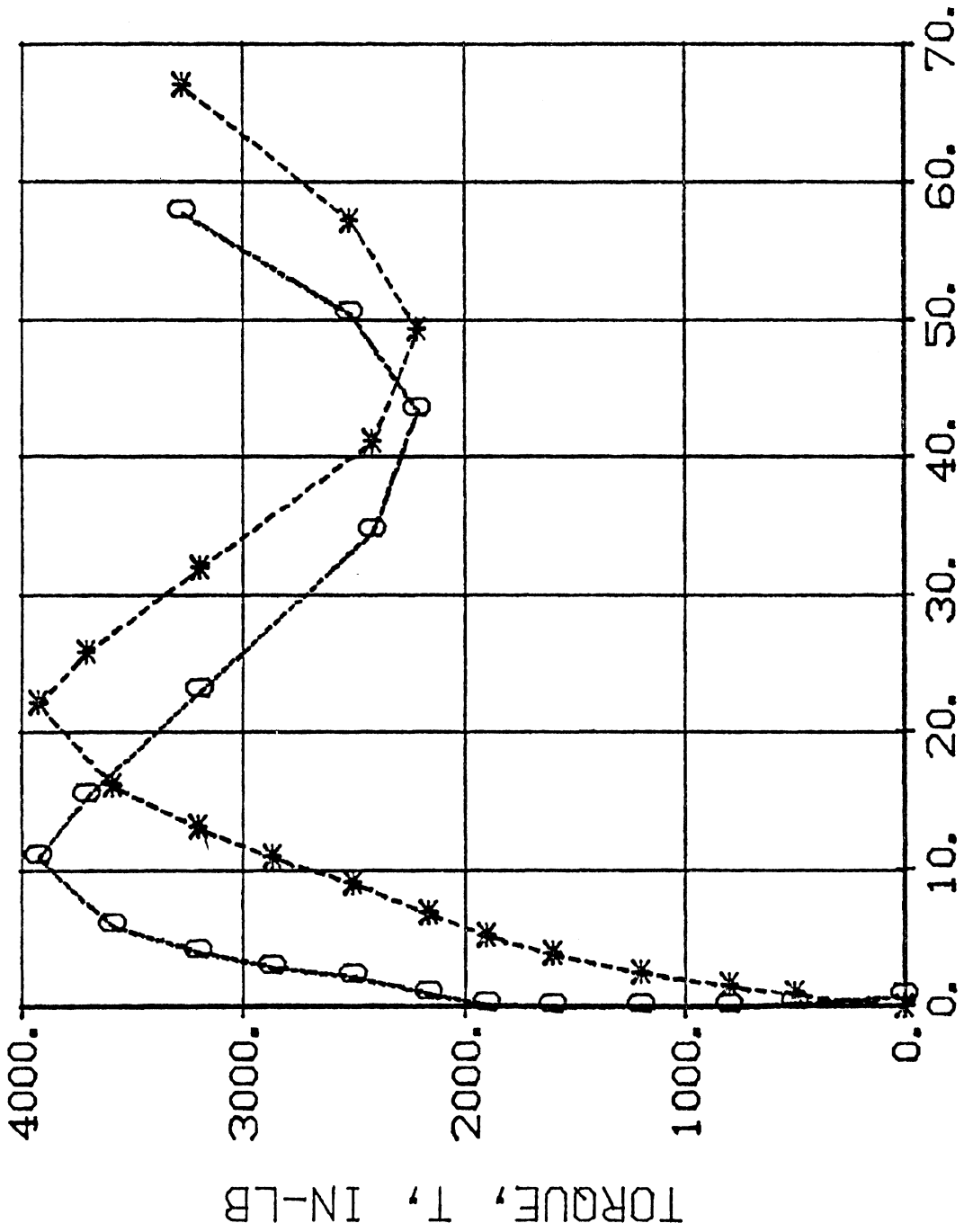


*-ANGLE, 0-PLAS.ANGLE, DEG, CY1540RA





*-ANGLE, 0-PLAS. ANGLE, DEG, CZ3010VA



*--ANGLE, 0-PLAS. ANGLE, DEG, CZ4015VA